Investigation of microbubble-cell interaction and development of an ultrasound delivery system

Raniska Tente

A thesis submitted for the degree of Doctor of Philosophy

The University of Edinburgh

2009

Declaration

I declare that this thesis has been written by myself and that the work contained within is my own. This work has not been submitted for any other degree of professional qualification.

Raniska Tente

May 2009

Acknowledgements

I would like to thank my project supervisors, Dr Rory Duncan, Prof Jim Ross and Dr Carmel Moran, for their hard work, advice and for not giving up on me during this project. I would also like to thank a number of people that helped me throughout this project with their valuable knowledge and advice. Many thanks go to: Steve Pye for all his advice on the experimental set up of this project and explaining to me concepts of physics I would otherwise be still wondering what they are, Karne McBride for all her help in performing apparatus measurements, Shonna Johnston for all her advice and help with flow cytometry, Bill Ellis for letting me use one of the ultrasound scanners employed in this project, Mourad Chennaoui from the School of Chemistry for his help with the coulter counter, Mairead Butler for all the advice and explanations that she provided for me. A huge thank you to all the members, past and present, of both TIRG and CIP groups for their continuous advice and support. Special thanks to Ian Ansell and Kathryn Sangster, without your support and encouragement I would have never made it so far! I would also like to thank Pedro, whose support; encouragement and patience were invaluable for completion of this thesis. Finally, thanks go to my parents for their endless and unconditional love and support, to them I owe everything I have accomplished in my life.

Abstract

Microbubbles have been used for several decades as ultrasound contrast agents in diagnostic ultrasound imaging. However, their application in gene therapy as delivery vehicles has only recently been realised. The presence of microbubbles in close proximity to cells during ultrasound insonation can increase the efficacy of drug or gene delivery by inducing formation of transient, non-lethal perforations in the cell membrane, a process termed sonoporation. In order to develop techniques for successful delivery of therapeutic agents, it is necessary to quantify the composition and physical characteristics of microbubbles in order to be able to determine how these affect the sonoporation process as required. Although several microbubbles are available commercially, the components of the shell of these proprietary microbubbles have not been disclosed. In order to study sonoporation and the possibility of delivering drugs and genes it became necessary to develop a formulation for in-house experimental microbubbles.

These experimental in-house microbubbles have not been previously investigated with regard to their interaction with cells, their potential for sonoporation and / or their bioeffects. Characterisation of the in-house microbubbles was necessary prior to any attempts to use them as delivery vehicles *in vitro*, or indeed, *in vivo*. Confocal laser scanning microscopy (CLSM) was used in order to determine the size distribution of both in-house microbubbles and Definity® a commercially available contrast agent. Confocal imaging and 3-D reconstruction of in-house microbubbles indicated the structure, morphology and size-distribution of these membrane-bound microbodies. Microbubbles were later separated according to size using a density gradient. It was concluded that the distribution of sizes of the

microbubbles was in part due to the multi-lamellar nature of the microbubble shell.

Cells were initially cultured in Petri dishes and insonated in the presence and absence of in-house microbubbles, in order to assess any bioeffects emerging from the application of ultrasound alone or in the presence of the microbubble constructs. Cells were cultured subsequently on an acoustically-transparent Mylar membrane, which was then "sandwiched" between two acetal homopolymer (Derlin) rings and placed in a specially designed ultrasound tank. Ultimately, cells were grown in an OptiCell™, an acoustically-transparent parallel membrane environment, where delivery of molecules of various sizes, in the presence of both in-house and Definity® microbubbles was investigated. Sonoporation was achieved with insonication of SK Hep-1 cells with a "physiotherapy machine" applying a power of 2.54 W / cm^2 for 2-3 secs in the presence of Definity® microbubbles and passage of Calcein, an impermeable molecule, into the cells was detected using flow cytometric analysis. In addition, expression of enhanced green fluorescent protein (EGFP) was also detected 24 hours after insonication of SK Hep-1 cells in the presence of Definity® microbubbles and a linearised plasmid pCS2, encoding EGFP, under the same ultrasonic conditions. Sonoporation was also investigated with the use of a diagnostic ultrasound scanner, since it is more clinically relevant. Although several acoustic and non-acoustic parameters were investigated, sufficient sonoporation was not attained using this scanner.

The bioeffects of ultrasound on cells both *in vivo* and *in vitro* have been extensively investigated. However, the exact cellular mechanisms that are affected by the application of ultrasound waves are not understood. In this study, the effects of ultrasound on a number of pathways were investigated.

Expression of Hsp70, a cell stress protein often associated with heat-shock, during application of continuous wave ultrasound, suggests that cells may undergo heat stress. During application of continuous wave ultrasound in the presence of Definity® microbubbles, expression of Hsp70 was shown to decrease compared to when ultrasound was applied in the absence of Definity® microbubbles. In addition, expression of HO-1, a protein associated with hypoxic pathways was also present during application of ultrasound in the absence of microbubbles. These results suggest that in the absence of ultrasound contrast agents, insonation can cause the expression of proteins associated with different forms of cell stress such as heat-shock and hypoxia, thus initiating the apoptotic process.

In this thesis, it has been shown that the mean size of the in-house microbubbles is comparable to that of commercially available microbubbles such as Definity®. In addition, it has been shown that sonoporation and successful delivery of small molecules in the presence of Definity® microbubbles is achievable with the equipment and the specific system which was developed. This reinforces the promising role of in-house microbubbles as delivery vehicles for therapeutic agents. Finally, an investigation on the possible bioeffects of ultrasound in the presence and absence of ultrasound contrast agents, revealed that under acoustic conditions identical to those used for achieving sonoporation, cells experience stress, instigating pathways that could potentially lead to cell death.

Table of Contents

List of Figures

List of Tables

Abbreviations

3D	3-dimensional
ANOVA	analysis of variance
BDH	2-methylpropan-1-ol
boPET	bi-axially oriented polyethylene terephthalate
BSA	bovine serum albumin
Calcein AM	acetoxymethyl ester
CLSM	confocal laser scanning microscopy
CW	continuous wave
DMEM	Dulbecco's Modified Eagle Medium
DNA	deoxyribonucleic acid
ECL	enhanced chemiluminescent reagent
EGFP	Enhanced green fluorescent protein
EIAV	equine infectious anaemia virus
FDA	U.S. Food and Drug Administration
FIV	feline immunodeficiency virus
FM 14-3	Fei Mao 14-3 (N-(3-triethylammoniumpropyl)-4-(4-dibutylamino) styryl) pyridinium diprobmide)
GAPDH	glyceraldehydes-3-phosphate dehydrogenase
GPI	Glycosylphosphatidylinositol
HIV	human immunodeficiency virus
HO-1	heme oxygenase-1
HSP	heat shock proteins
LP	long pass
MI	mechanical index

MRM	membrane-ring-membrane “sandwich”
OCT	ornithine transcarbamylase
PBS	phosphate buffered saline
PEG	polyethylene glycol
PFC	perfluorocarbons
PRF	pulse repetition frequency
PRM	revolutions per minute
PSF	point spread function
PVDF	piezoelectric polymer polyvinylidene fluoride
PW	pulsed wave
PZT	lead zirconate titanate
RIPA	Radio Immuno Precipitation Assay
SDS	sodium dodecyl (lauryl) sulfate
SDS-PAGE	sodium dodecyl (lauryl) sulphate-polyacrylamide gels
SEM	standard error of mean
SF_6	sulphur hexafluoride
SOC	Super Optimal broth with Catabolite repression
TEMED	tetramethylethylenediamine
TBS	tris buffered saline
TBST	tris buffered saline Tween
TGC	time gain compensation
TI	thermal index
v/v	volume in volume
w/v	weight in volume

Symbols

Atm	atmospheres
B	bulk modulus
C	Celsius
F	radiation force
I	intensity
ʃ	frequency
P	pressure amplitude
R	amplitude reflection coefficient
r	radius
Rc	critical molecular distance
T	period
v	speed
W	acoustic power
Z	acoustic impedance
λ	wavelength
π	pi
ϱ	density

Chapter 1

Introduction

Gene therapy

1.0 Gene therapy

1.1 Viral gene delivery

The first building blocks for gene therapy were implemented with the practice of subcloning mammalian genes into plasmids becoming a reality in the early 1980s (Terence 2007). Gene therapy was developed in order to serve as a means of restoring the normal function of genes in a large number of inherited and acquired genetic disorders (Friedman 1999). Its success relies on efficacious delivery of a therapeutic gene into a target cell, tissue or organ in the absence of any detrimental consequences (Li and Huang 2000). Such an approach requires the employment of a vector capable of gene delivery. Regardless of their type, vectors need to comply with some fundamental criteria.

Firstly, efficient production of a high volume of vectors at minimal time and at low cost is very important, for example, for clinical applications (Somia and Verma 2000; Liu 2002). This is due to the vast number of cells that need to be transduced (Somia and Verma 2000). The shelf life of the vector is also of great concern, to circulate the product to the desired locations in adequate time (Verma and Weitzman 2005).

Secondly, the size of genes may range from a few hundred to tens of thousands of base pairs. Supplementing the genes of interest with additional sequences may be at times necessary in order to maximise gene transfer and expression (Follenzi 2000; Zennou, Petit et al. 2000). Thus it is essential that vectors can accommodate genes of such large dimensions (Allocca, Doria et al. 2008).

Thirdly, targeting vectors to specific types of tissue or cells, while evading other types of tissue or cells can prove beneficial. For example, it would be desirable for vectors to avoid dendritic cells, which play a role in inducing immune responses (Fields 2000). In cases of cancer therapy,

delivery of therapeutic molecules is required only to the malignant cells. The ability of a vector to detect the target cell, tissue or organ would also assist in attaining its target and in facilitating gene transfer (Douglas 1996; Wickham 1996; Rajotte D. 1998).

Another crucial factor limiting gene therapy is the presence of immunogenic responses. The emergence of an immune response would mean arresting the activity of the vector and subsequently halting gene transfer (Somia and Verma 2000). Although immune responses are most commonly seen in the presence of viral vectors, induction of inflammatory molecules has been reported for non-viral vectors (Liu 2002). Furthermore, activation of certain immunogenic pathways modulates suppression of gene expression and tissue damage (Qin 1997; Loisel 2001; Sellins 2005).

Upon successful gene delivery, it is important that the effects of gene therapy remain present for a specified period of time or permanently, depending on the specifications of the disease (Lewis 1992; Bukrinsky 1993). This can only be ensured if the therapeutic gene is either integrated into the chromosomal genome of the target cell or settles in the nucleus of the cell and is consistently passed on to daughter cells (Kotin, Siniscalco et al. 1990; Inoue 1999; Carter 2000).

Finally, genetic therapy is required for a multitude of diseases that occur in all types of cells within the human body. It is thus of great importance that the vector can efficiently deliver genes to all types of cells regardless of whether they are dividing or non-dividing cells (Kafri 1997; Zufferey 1997).

A multitude of gene delivery studies using either viral or non-viral vectors have taken place, with both types of vectors exhibiting complications (Smith, Mehaffey et al. 1993; Setoguchi, Jaffe et al. 1994; Yang, Li et al. 1995;

Yang, Nunes et al. 1995; Jans 2000; Kircheis, Wightman et al. 2001; Lyman 2002). Throughout the millions of years of their existence, viruses have had the time to perfect their gene delivery approach thus allowing them to successfully integrate into a cell's genome without destroying the host cell (Rubanyi 2001). Hence, viral vectors are regarded as the predominant candidate for a successful gene delivery study. The main viruses employed in gene delivery studies are retroviruses, lentiviruses, adenoviruses and adeno-associated viruses (Edelstein 2008).

1.1.1 Retroviruses

Retroviruses are a group of viruses that contain RNA instead of DNA, thus they need to generate DNA before proceeding into replication of their genetic material. Retroviruses encompass certain genes that are necessary for integrating into the genome of the host cell (Monse, Laufs et al. 2006; Mousnier, Kubat et al. 2007; Montini, Cesana et al. 2009). Provided that only this set of genes is functioning, then it is possible for the virus to integrate with the host genome without replicating itself yet at the same time allowing for the gene of interest to be expressed (Kafri 1997; Zufferey 1997). The advantage of using retroviral vectors is that they are able to integrate with the host genome in a stable manner, thus resulting in a sustained gene delivery (Agosto, Yu et al. 2007; Deichmann, Hacein-Bey-Abina et al. 2007; Felice, Cattoglio et al. 2009). However, although there are currently over 300 clinical trials utilizing retroviral vectors for gene delivery, this approach still exhibits several limitations including the vectors' ability to infect only non-dividing cells, their low titres and the prospect of random insertion of viral DNA into the host genome (Nabel 1994).

1.1.2 Lentiviruses

Lentiviruses are a family of complex Retroviruses (Swanstrom 1997). They take their name (lenti = slow) from the gradual development of the infection they induce (Lever, Strappe et al. 2004). Lentiviruses were also considered as suitable vectors for gene delivery due to their ability to integrate into both dividing and non-dividing cells (Cockrell AS 2007; Edelstein 2008). Thus, a large number of lentiviruses have been studied, including, HIV-1, HIV-2, EIAV (equine infectious anaemia virus) and FIV (feline immunodeficiency virus) (Rizvi 1992; Olsen 1998; Sadaie 1998; Johnston 1999; Mitrophanous 1999; Wang 1999; Curran 2000; Mangeot 2000; Schnell 2000; Griffin 2001; Stitz 2001; Brooks 2002; Takahashi 2002; Kobayashi 2003; Loewen 2003). In addition, lentiviruses have a large packaging capacity, which enables the insertion of large sized therapeutic genes (Lever, Strappe et al. 2004). The low levels of immunogenic activity seen with lentiviruses are also advantageous (Sandrin, Russell et al. 2003; Toelen, Deroose et al. 2007). Nonetheless, immunogenic responses should be rigorously evaluated for each study as they form the main hurdle of gene delivery. On the other hand, random insertional mutagenesis, which can lead to carcinogenesis, is of major concern (Linda, Niels et al. 1986). Finally, the limited capacity of lentiviruses to diffuse through tissues creates a further obstacle in their potential role as gene delivery vectors (Lever, Strappe et al. 2004).

1.1.3 Adenoviruses

Another family of viruses amongst the list of promising vectors for gene therapy are adenoviruses. Their ability to infect both dividing and non-dividing cells and their ability to express high levels of the therapeutic gene were amidst the traits that made them favourable for gene delivery (Fields,

Knipe et al. 1996; Doetsch, Caillι et al. 1999). However, the development of immune responses by the host is one of the traits that prevented adenoviruses from fulfilling their role as gene delivery vectors. The development of severe inflammatory toxicities in several studies, following the death of a clinical trial patient with partial ornithine transcarbamylase (OTC) deficiency (Raper, Chirmule et al. 2003) dampened successful treatments and served as a reminder of the potential disastrous effects of host immune responses.

1.1.4 Adeno associated viruses

Adeno associated viruses also exhibited a number of advantages for serving as gene delivery vectors, including their ability to penetrate into various tissues due to their small size, their ability to express in numerous cell types and their ability to integrate into the host's chromosome (Lynch 1997; Chiorini 1999; Lieber, Steinwaerder et al. 1999; Xiao 1999). However, their low rates of infection, small packaging capacity and the presence of adeno associated viral antibodies in 80 % of the adult population; diminish their rate of success as gene delivering vectors (Mselli-Lakhal 1998; Lieber, Steinwaerder et al. 1999; Berkowitz 2001; Olsen 2001).

1.1.5 Viral gene therapy limitations

Although viruses have evolved mechanisms for integrating into the host cells without evoking their death, all families of viruses, such as retroviruses, adenoviruses and adeno-associated viruses, have yet to overcome a number of complications before fulfilling their role as efficient gene delivery vectors. The main concerns with employment of viral vectors for gene therapy are the potential of immunogenicity, insertion mutagenesis, oncogenesis and the presence of high levels of toxicity (Shigeru Kawakami

2008). Several clinical trials so far have resulted in the death or the development of cancer in patients, only to accentuate the extent of the problem with such an approach (Lehrman 1999; Hacein-Bey-Abina, Von Kalle et al. 2003; Check 2005). Additional predicaments associated with the use of viral vectors also include limitations to the size of gene that can be packaged into viruses and complication of their production (Bett, Prevec et al. 1993; Zufferey. R, Dull et al. 1998; McCarty, Monahan et al. 2001).

The safety concerns associated with the use of viral gene vectors have shifted the focus towards non-viral vectors for the use of gene delivery. The latter can serve as more efficient gene therapy vectors in the absence of immunogenic responses (Robbins and Ghivizzani 1998; Shigeru Kawakami 2008). In addition, non-viral vectors are easy to produce and can be adapted to fulfil specific target requirements (Behr 1994; Boussif, Zanta et al. 1996). The ease of large-scale production also serves as a motive for using non-viral vectors (Li and Huang 2000; Makiya Nishikawa 2001). Moreover, non-viral vectors fail to integrate into the cellular genome, therefore minimising the likelihood of insertional mutagenesis (Kaminski, Huber et al. 2002).

1.2 Non-viral gene therapy

Non-viral gene therapy involves the use of DNA vectors (plasmid DNA) that can be administered to patients directly by either tissue or systemic injection in order to reach the target cells and express the therapeutic gene products (Ledley 1994). Although non-viral vectors are safer to use than viral vectors in terms of toxicity and immunogenicity, a number of other hurdles have emerged. These include the negative charge of DNA and its large size that block it from crossing any unimpaired membrane boundaries (Ledley 1994). Furthermore, the presence of cellular nucleases halt cytoplasmic transport of DNA before it can reach the nucleus and get

access to the cell's reproductive machinery (Mir 1999; Rizzuto 1999; Fattori 2002). Therefore, the key to a successful non-viral gene delivery is to find the balance between inducing irreversible cell damage and obtaining nuclear entry (Cheng-Huang, Yeh et al. 2008).

1.2.1 Techniques for non-viral therapy

Several methods have been explored in order to overcome the hurdles stated above. These can be broadly categorized into (a) delivery by physical techniques and (b) delivery mediated by chemical carriers (Shigeru Kawakami 2008).

1.2.1.1 Physical techniques

Physical techniques promote entry of DNA vectors into cells via diffusion through transiently impaired cell membranes by applying a physical force on the target cell membrane (Yang 1990; Van Wamel, Kooiman et al. 2006a). The use of a gene gun, electroporation and ultrasound are amongst the most accepted physical techniques applied (Makiya Nishikawa 2001; Gao 2007; Shigeru Kawakami 2008).

One of the physical methods used for enhancing the efficiency of non-viral vectors is the employment of a gene gun. This involves coating of heavy metal particles (predominantly gold beads) with the selected DNA vector. Pressurised gas is then applied to the particles, thrusting the former towards the target cells or tissue (Gao 2007; Shigeru Kawakami 2008). The extensive force of the particles enables them to penetrate a few millimetres deep into the tissue (Yang, Burkholder et al. 1990). The DNA vectors that have been placed on the particles are thus deposited into the target cells. Efficiency of this method has been reported to range from 10 to 20 % in skin epidermal cells and from 1 to 5 % for muscle cells and lasting from 14 days up to 60

days after bombardment respectively (Yang 1990; Williams. R. S. 1991; Zelenin 1997). However, the major drawback of this approach is the shallow penetration into the target area, thus limiting this approach to superficial layers such as skin, mucosa, and skeletal muscle (Zelenin 1997). In addition, in vivo application of a gene gun in skin, liver and skeletal muscle culminates in a short lived and diminished effect (Boretti, Leutenegger et al. 2000; Oehen, Junt et al. 2000).

Electroporation (also known as electropremiabilisation) produces transient pores on the cell membrane by application of high intensity electric oscillations (Cheng-Huang, Yeh et al. 2008). DNA vectors found in close proximity to the cell membranes are thought to able to pass through the plasma membrane via electrophoresis (Liu, Heston et al. 2006). Although, the use of electroporation has been shown to increase gene expression by 100- to 1000- fold, there are several hindrances associated with this approach (Bigey 2002; Gehl 2003; Bloquel 2004; McMahon 2004). Firstly, electroporation has been mainly used in studies correlated with skin (Zhang 2002) and skeletal muscle (Mir 1999; Rizzuto 1999; Fattori 2002), since the distance between the two electrodes cannot exceed 1 cm (Vanbever, Lecouturier et al. 1994; Jaroszeski, Gilbert et al. 1999). Therefore, application of electroporation to any internal organs would necessitate a surgical procedure in order to place the electrodes in close proximity of the target area (Gao 2007). Furthermore, the high voltage applied during electroporation can lead to irreversible tissue damage due to high calcium influx and thermal heating (Gissel 2001; Durieux 2004). Finally, application of high voltages is also likely to afflict the stability of genomic DNA (Durieux, Bonnefoy et al. 2004).

Ultrasound is a modality that is already in clinical use for both diagnostic and therapeutic applications (Kremkau, Kaufmann et al. 1976;

Preston, Bacon et al. 1983; Madersbacher, Kratzik et al. 1995; Madersbacher, Padevilla et al. 1995; Harrison, Balcer-Kubiczek et al. 1996; Akiyama, Ishibashi et al. 1998; Kornbluth, Liang et al. 1998; Desser, Jeffrey et al. 1999). It is an efficient tool as it is of low cost, simple and safe (Liu 2002) . In the mid 1990s, the potential role of ultrasound in gene delivery was discovered (Shigeru Kawakami 2008). Ultrasound has since been shown to be an effective delivery method, presenting several advantages over other viral and non-viral methods such as electroporation (Pan, Zhou et al. 2005). The main advantage of ultrasound mediated gene delivery is that it exerts its effects with minimal invasiveness (Bachor, Gottfried et al. 1995; Madersbacher, Pedevilla et al. 1995; Larsen, Krasnik et al. 2002). In addition, ultrasound apparatus can effectively image as deep as 24 or more centimetres in the human body (Nelson, Perry et al. 1990). The use of ultrasound has been reported to result in a 10- to 20- fold increase in gene expression compared to that achieved by naked DNA (Lawrie, Brisken et al. 2000). Ultrasound mediated gene transfection involves acoustic cavitation, which leads to formation of transient pores on the membranes of adjacent cells (Van Wamel, Kooiman et al. 2006b). Addition of ultrasound contrast agents can further increase gene delivery efficiency (Nozaki 2003; Ogawa 2004). Ultrasound contrast agents are air filled microbubbles that oscillate during application of ultrasound, thus reducing cavitation threshold (Apfel and Holland 1991). Furthermore, ultrasound contrast agents can be used as vehicles for therapeutic molecules (Zarnitsyn and Prausnitz 2004). The proficiency of the ultrasound mediated gene delivery system is regulated by numerous parameters, including frequency, power, pressure and duration of the ultrasound wave applied, local concentration of DNA plasmid and ultrasound contrast agents (Huber 1999). Both continuous wave and pulsed

wave ultrasound have been used for intracellular delivery of molecules (Lawrie, Brisken et al. 1999; Miller and Quddus 2000). The generation of adverse effects such as mechanical and thermal damage to cells, due to prolonged exposures or high intensities of ultrasound are of concern (Barnett 1994). Although ultrasound mediated gene delivery is a promising method for gene therapy, further research is necessary in order to achieve regulated and coherent gene delivery (Zarnitsyn and Prausnitz 2004).

1.2.1.2 Chemical techniques

Chemical approaches include the establishment of DNA into naturally occurring or synthetic compounds (Gao 2007). Conventionally employed compounds include cationic liposomes and cationic polymers (Shigeru Kawakami 2008). The positive charge of such compounds enables them to interact with the negatively charged DNA thus forming a complex (Felgner, Gadek et al. 1987). The former is believed to enter the cell via endocytosis (Xu and Szoka 1996). Although, it is believed that once entering the cell as a complex, the DNA is protected from nuclease degradation (Hui, Langner et al. 1996), Cheng-Huang Su et al. (2008) report that only 1 % of the DNA is able to enter the nucleus. In addition, although *in vitro* studies with the aid of cationic compounds have been compelling (Rose 1991; Felgner, Kumar et al. 1994; Vigneron, Oudrhiri et al. 1996), a number of complications have been encountered during clinical trials, including low efficiency and toxicity (Bottega and Epand 2002; David, Marie-Laure et al. 2002; Kim, Park et al. 2005; Lv, Zhang et al. 2006).

In conclusion, although nonviral gene delivery techniques are more advantageous than viral techniques, the former also face several hurdles. The use of gene gun and electroporation are limited to superficial areas such as

the skin and skeletal muscle, while chemical techniques are characterised by low efficiencies. Therefore, ultrasound mediated gene delivery, either in the presence or absence of ultrasound contrast agents, is one of the most promising techniques since it can result in successful gene delivery into deep tissues with minimal invasion (Nelson, Perry et al. 1990; Bachor, Gottfried et al. 1995; Madersbacher, Kratzik et al. 1995; Larsen, Krasnik et al. 2002). Nevertheless, further investigation is required in order to establish the exact parameters necessary for regulated gene delivery both *in vitro* and *in vivo* (Zarnitsyn and Prausnitz 2004).

Chapter 2

Introduction

Ultrasound

2.0 Sound

2.1 Acoustic waves

Sound is a form of mechanical wave energy that can travel from waves from a source to a receiver through a medium such as air, water or tissue (O'Brien 2007). The sound wave can be defined by frequency, period, wave length, propagation speed, amplitude, intensity and attenuation (Kavic 1996). The type of wave formed when a sound wave is propagating through a medium depends on the direction of motion of the particles of the medium in relation to the direction of the wave (O'Brien 2007). When sound is emitted from a source, the particles of a medium are displaced, thus transferring to adjacent particles (Laird and Walmsley 1991). When a sound wave is propagating though a medium, there are regions where the particles experience high pressure (compression) and regions where the particles experience low pressure (rarefaction) (figure 2.1) (Hangiandreou 2003). When the particles within a medium move in the direction of the sound wave, then the sound wave is termed longitudinal (O'Brien 2007). When the particles of the medium are moving at right angles in relation to the direction of the sound wave, the latter is termed a transverse or shear wave (O'Brien 2007). While longitudinal waves can be found in all types of materials (solid, liquid, gas), shear waves can only be found in solid materials (O'Brien 2007). Therefore, in soft tissues, only longitudinal waves are of importance, whereas both longitudinal and shear waves can propagate through tissues such as bone (Humphrey 2007).

The high points (crests) and lowest points (troughs) of the wave constitute the pressure amplitude (P) of the wave and are designated as the peak compressional and rarefractional values respectively (figure 2.1) (O'Brien 2007). The pressure amplitude of a wave is measured in Pascals. The terminology peak-to-peak amplitude is also used in order to describe the

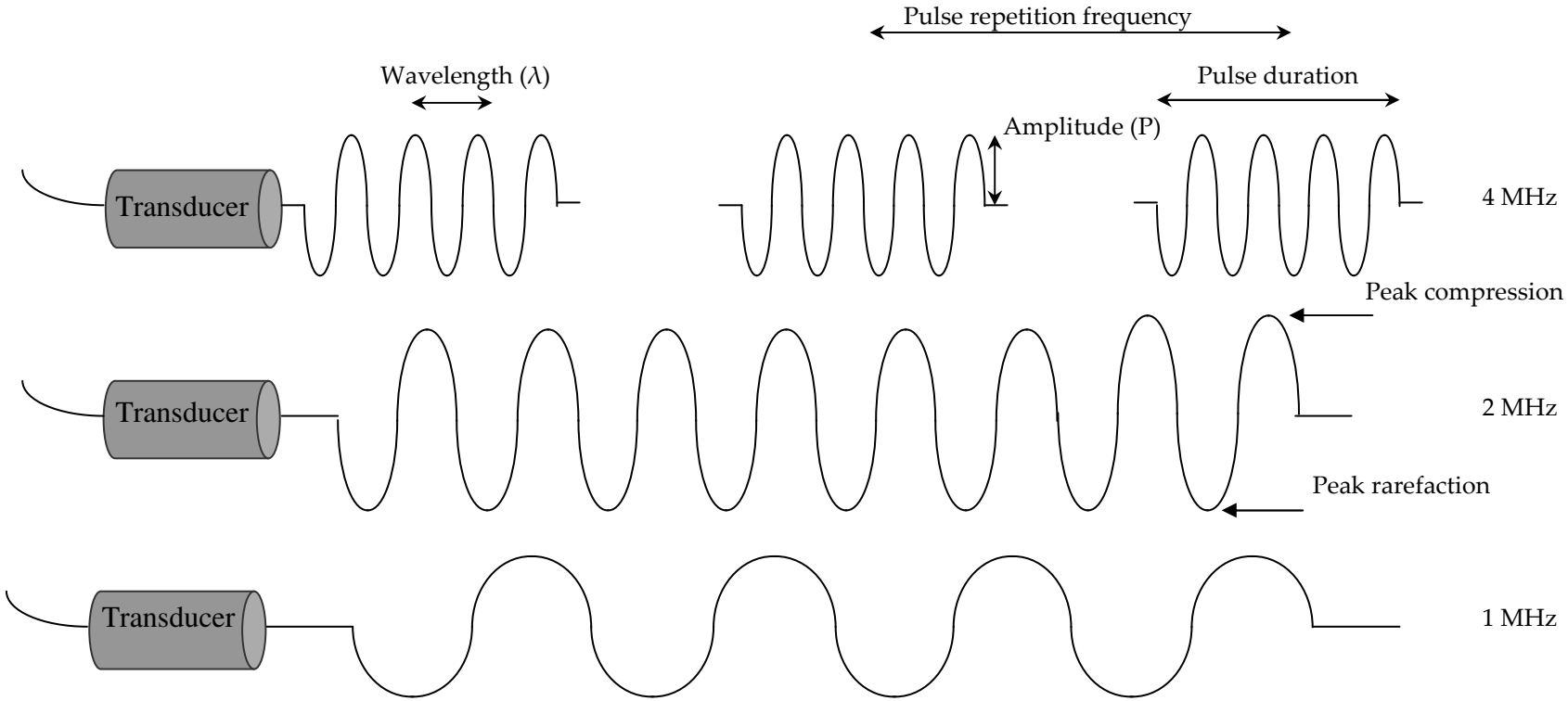

Figure 2.1 **Sound wave.** Adapted from (Hangiandreou 2003; Fischetti and Scott 2007). Acoustical energy emitted from a source travels through a medium (air, solid, liquid) in order to arrive to a receiver. The acoustical energy released is transferred through the medium by displacing adjacent particles. This creates an acoustic wave that exhibits high pressure (compression) and low pressure (rarefaction) regions. The highest points (peak compression) and lowest points (peak rarefaction) of the wave constitute the pressure amplitude (P) of the wave. The distance between repeating points of a propagating waveform is defined as the wavelength (λ) of an acoustic wave. The number of complete wave cycles per second is referred to as frequency (ʃ). The relationship between the wavelength and the frequency of an acoustic wave is inversely proportional. An acoustic wave can be emitted in short bursts (pulses). The time interval of these pulses is defined as pulse duration. Pulse repetition frequency (PRF) is the rate of sound pulses per unit of time.

magnitude of change between a crest and a trough. The time taken for the wave to complete one cycle is defined as the period (T). The speed (v) of a sound wave through a medium is dependent on density (ρ) and compressibility of the material, also known as bulk modulus (B). Thus, speed can be expressed by the following equation:

$$v = \frac{\sqrt{B}}{\rho} \qquad (1)$$

The velocity of sound in fat, liver, kidney, blood and muscle are approximately 1,460, 1,555, 1,565, 1,560 and 1,600 ms^{-1}, respectively (Zagzebski 1996). Since the velocity of sound in human soft tissues exhibits such small alterations from one tissue to another that, it is generally accepted to be around 1540 ms^{-1} (Herbener 1996; Zagzebski 1996; O'Brien 2007). The intensity (I) of an acoustic plane wave is given by:

$$I = \frac{P^2}{2\rho v} \qquad (2)$$

2.1.1 Frequency

The number of wave cycles per second is referred to as frequency (ʃ) and is measured in Hertz (1 Hertz = 1 cycle per second). Frequency is inversely proportional to the period (ʃ=1/T). Pulse repetition frequency (PRF) is the rate of sound pulses per unit of time (Fischetti and Scott 2007). The acoustic spectrum range can be classified into infrasound, audible sound and ultrasound depending on the range of frequency used (O'Brien 2007). Infrasound has a frequency range of less than 20 Hertz (Hz), while frequencies ranging between 20 and 20,000 Hertz (Hz) are within the human audible sound range (Kavic 1996; O'Brien 2007). The term ultrasound is employed for frequencies exceeding 20 kHz (Kavic 1996). Although ultrasound is inaudible to the human ear, a range of animals, including bats,

dolphins, tortoises and whales, use it in order to detect objects in the absence of light (Wade 2000). Nowadays, most ultrasound equipment serve for therapeutic and diagnostic purposes in the medical field with the former operating around 1-3 MHz and the latter operating between 2 and 15 MHz (Herbener 1996; O'Brien 2007). The selected frequency is a compromise between the depth of penetration and the spatial resolution (Herbener 1996) .

2.1.2 Wavelength

The wavelength (λ) of an acoustic wave is defined as the distance between repeating points of a propagating waveform. Wavelength depends on the velocity of sound in the medium and the frequency of the sound wave and is given by the following relationship:

$$\lambda = \frac{v}{f} \qquad (3)$$

Where λ is wavelength, v is velocity of sound and f is frequency of sound. Therefore, the higher the frequency, the smaller the wavelength will be.

2.1.3 Acoustic power

Acoustic power is defined as the rate of flow of acoustic energy per unit time and is measured in Watt (W). The acoustic intensity of a sound wave can be defined as the rate of flow of acoustic energy within a unit area and is measured in W / m^2.

2.1.4 Absorption

When an acoustic wave travels through a medium, a fraction of its energy is lost due to absorption, reflection and scattering, and it becomes attenuated (Herbener 1996).

Absorption is the conversion of acoustic energy into heat energy while passing through a medium. The absorption coefficient of many media

depends on the frequency of the acoustic wave and the composition of the medium, thus the higher the frequency, the greater the absorption (Herbener 1996).

2.1.5 Reflection and scattering

Acoustic waves act in a similar manner to light waves in that when an acoustic wave encounters an interface between two different materials, such as soft tissue and bone, at a perpendicular angle, a fraction of the wave will be reflected back to the first material, and the rest will be transmitted to the second material (Laird and Walmsley 1991; Herbener 1996). The acoustic impedance (Z) of a medium characterises how mechanical energy propagates through the medium. For a plane wave, characteristic acoustic impedance is defined by the product of the density (ρ) of the medium and the propagation speed of the acoustic wave ($Z = \rho c$). In ultrasonics, the unit of acoustic impedance is the rayl. The greater the impedance difference between two materials, the more energy is reflected back into the original material and the smaller the impedance difference between two materials, the more energy will be transmitted into the second material (Laird and Walmsley 1991). The amplitude reflection coefficient (R) is given by the ratio of the pressure amplitude reflected (Pr) to the incident pressure amplitude (Pi). So

$$R = \frac{P_r}{P_i} = \frac{Z_2 - Z_1}{Z_2 + Z_1} \qquad (4)$$

where Z_1 is the acoustic impedance of the first material and Z_2 the acoustic impedance of the second material (Zagzebski 1996). Since the amplitude reflection coefficient at air interfaces has been calculated to be nearing 1, practically most of the acoustic wave would be reflected at air / soft tissue interface (Zagzebski 1996). Agents that reduce the amplitude reflection coefficient between two interfaces (such as gel), thus enabling the

transmittance of most of the ultrasound waves are known as acoustic coupling agents (Herbener 1996; Zagzebski 1996). It should be noted at this point that if the projected beam is at a non-perpendicular angle, the reflection wave will not return to the transducer, rather it will be reflected at an angle equivalent to the angle of incidence (Hangiandreou 2003). In addition, acoustic waves that are emitted at a non-perpendicular angle will also experience refraction at the interface between two surfaces. Refraction is the change of direction of an acoustic wave that occurs when the acoustic wave strikes an interface between two media at an angle and the speed of sound of the two media on either side of the interface is different (Zagzebski 1996). The extent of refraction can be calculated by Snell's law, which is as follows:

$$\frac{\sin\theta_t}{\sin\theta_i} = \frac{v_t}{v_i} \qquad (5)$$

Where θ_i is the incidence wave angle, θ_t is the transmitted wave angle, v_i is the incident velocity of sound and v_t is the transmitted velocity of sound (figure 2.2).

If however the projected beam strikes an object of the same size as its wavelength or smaller, at a non-perpendicular angle, then the beam will be scattered (Zagzebski 1996). Scattering occurs in all directions, thus scattered echoes are not as dependent on the angle of incidence of the wave as are reflected echoes (Zagzebski 1996). In addition, scattered echoes tend to be weaker than reflected echoes (Zagzebski 1996).

2.1.6. Attenuation

Attenuation is the depletion of intensity of an acoustic wave due to absorption, reflection and scattering and can be expressed in decibels per centimetre (dB / cm). Since absorption is frequency dependent and it promotes attenuation, acoustic waves of a high frequency also

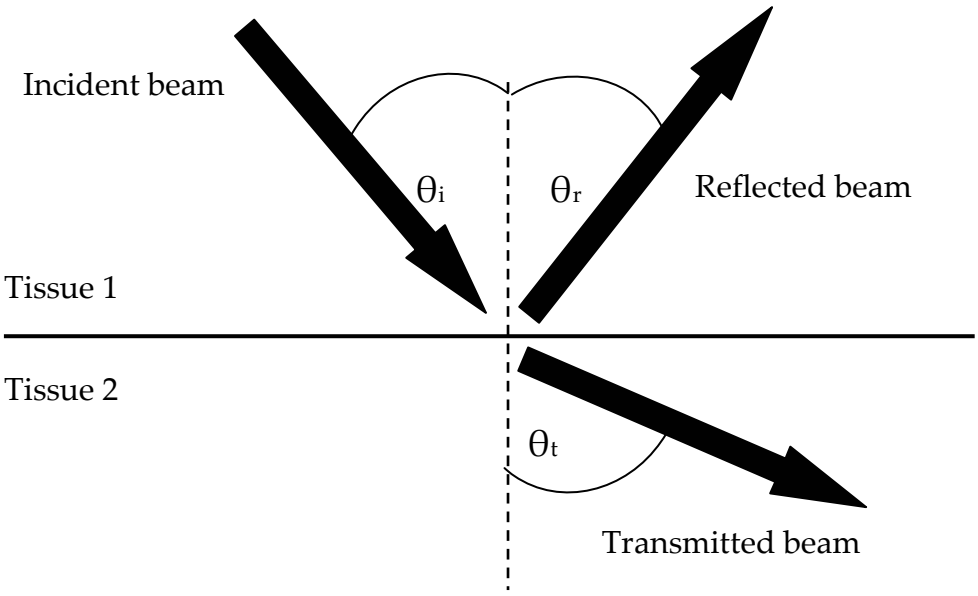

Figure 2.2 **Reflection and transmission of a beam**. When an incident beam travelling at a θ_i angle, hits an interface between two tissues, a fraction of the incident beam will be reflected at a θ_r angle, which is equal to θ_i but is travelling at an opposite direction. The rest of the beam will be transmitted through the second tissue. A difference in the acoustic impedance between the two tissues will lead to refraction of the transmitted beam, which will travel at a θ_t angle, where $\theta_t > \theta_i$. Adapted from (Zagzebski 1996).

exhibit greater attenuation (Herbener 1996). Therefore, when applying ultrasound at a higher frequency, the depth of penetration will be reduced compared to a lower frequency of insonation (Herbener 1996).

2.2 Ultrasound

The field of ultrasound was discovered by the Currie brothers, the pioneers of the piezoelectric effect in the late 19th century (O'Brien 2007). The Currie brothers observed that application of an electric field through certain materials resulted in the vibration of these materials and subsequently the development of a sound wave. Amongst the several piezoelectric materials that have been discovered, ceramics, such as lead zirconate titanate (PZT) are most commonly employed for diagnostic ultrasound (Zagzebski 1996).

Ultrasound machines send ultrasound waves through a medium and detect any echoes that return to them. Ultrasound waves are produced by an ultrasound transducer. The latter is composed of a piezoelectric crystal arranged in such as way that the overall electrical charges of the domains are evenly distributed. Application of an electrical field causes a disturbance on the electrical charges thus causing them to vibrate and produce a sound wave (Kavic 1996). The emitted ultrasound waves propagate through a medium. Upon striking a second medium, a fraction of the wave is reflected or scattered back to the transducer (due to differences in acoustic impedance), whereas the remaining wave is transmitted through the object. Since the speed of sound in soft tissue is assumed to be constant, the time it takes for the scattered / reflected echo to travel back to the transducer is proportional to the distance of the structure from the transducer. Once the ultrasound probe has emitted an ultrasound wave, it enters receive mode and any scattered or reflected waves incident on the transducer crystal generate a voltage due to the converse piezoelectric effect (Kavic 1996). This voltage is

then detected, amplified and displayed as an image on the ultrasound apparatus screen (Kavic 1996). One of the first applications for piezoelectricity unfolded during the First World War in order to produce submarine detecting sonar (Wade 2000). Following the end of the war, scientists from the medical field envisioned the use of ultrasound for diagnostic and later for therapeutic medical purposes.

2.2.1 Transducers

The simplest form of transducer is a single unfocused transducer element (figure 2.3). The piezoelectric element is placed in a plastic casing and is isolated with rubber or cork in order to avert transmission of ultrasonic energy to the plastic case (Zagzebski 1996). In addition, the casing is contained in a metal electrical shield so as to prevent interference from external electrical signals (Zagzebski 1996). The frequency at which a transducer performs optimally is termed its resonance frequency and is effected by the thickness of the piezoelectric element (Zagzebski 1996). For greater precision the thickness of the piezoelectric element is designed so as to equal half the wavelength of the desired pulse centre frequency (Whittingham 2007). Furthermore, broad bandwidth transducers have been developed, that can transmit a range of frequencies. Modern array transducers allow the user to alter the focal depth without having to interchange between transducers (Fischetti and Scott 2007).

Due to the high acoustic impedance of PZT in relation to tissue, impedance-matching layers are inserted in front of the transducer so as to achieve maximum transmission (Whittingham 2007). Ultrasound waves can be produced in two modes: continuous and pulsed. Continuous waves (CW) are formed by exciting the ultrasound transducer at a constant amplitude, whereas pulsed waves (PW) are formed by exciting the ultrasound

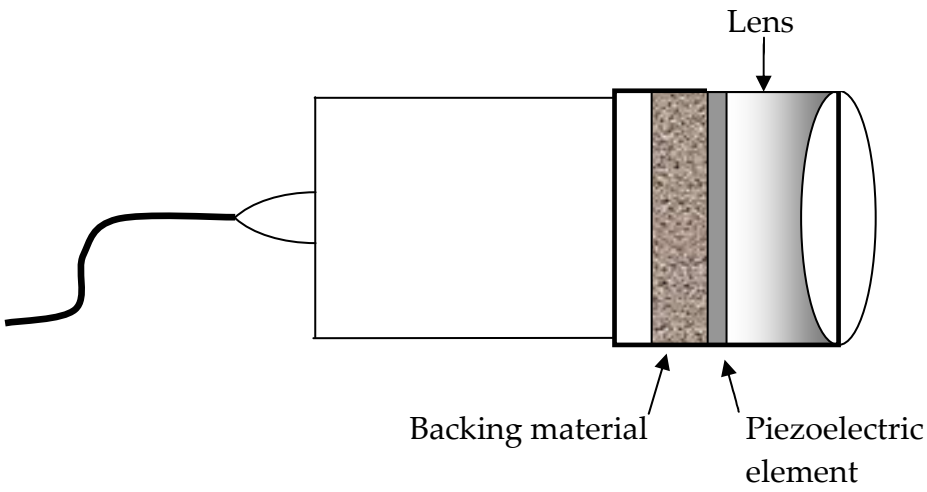

Figure 2.3 **Single element transducer.** A typical ultrasound transducer is composed of a piezoelectric element that is encapsulated in a plastic case and is isolated from electrical interference with the use of rubber or cork. The encapsulated element is then contained in a metal electrical shield so as to further prevent interference from any external electrical signals. A backing material is placed behind the piezoelectric element in order to reduce vibrations of the element immediately after emission of a wave, thus allowing for formation of short pulses. Positioning a lens in front of the piezoelectric element allows focusing of the ultrasound beam to the required distance. Adapted from (Zagzebski 1996).

transducer repeatedly for short periods of time (O'Brien 2007). In pulsed wave transducers, a backing material is placed behind the piezoelectric element in order to diminish the vibrations of the elements as soon as possible, thus forming pulses of short duration (Zagzebski 1996).

2.2.1.1 Ultrasound resolution

Spatial resolution alludes to the minimal distance that two reflectors can have before they are no longer detected as two separate media but as one (Zagzebski 1996). Spatial resolution is proportional to frequency, thus as frequency increases, spatial resolution is enhanced (Zagzebski 1996). Spatial resolution can be divided into axial and lateral resolution, signifying the resolution along the length and width of the ultrasound beam respectively (Fischetti and Scott 2007). Axial resolution depends on pulse duration and frequency of the wave whereas lateral resolution depends on the ultrasound beam width (Zagzebski 1996; Fischetti and Scott 2007). Resolution can be enhanced by focusing the beam (Fischetti and Scott 2007). Focusing can be achieved by mechanical or electronic means. Mechanical focusing involves the use of a lens or a curved piezoelectric element in order to focus the ultrasound beam to the required distance (Zagzebski 1996). The focal distance is the plane at which the ultrasound beam is at its most confined span (Zagzebski 1996). More advanced transducers achieve electronic focusing by using of an array up to 196 elements (Hangiandreou 2003). Phase array transducers function by activating all elements of the transducer with a time delay, thus allowing steering of the direction of the beam (Fischetti and Scott 2007).

2.2.2 Receivers

Following an ultrasound beam being transmitted through a medium, the receiver of the ultrasound scanner detects the reflected waves and processes them, before displaying them on the monitor (figure 2.4). Processing involves various stages, including amplification, time gain compensation (TGC), compression, demodulation and rejection (Zagzebski 1996). Since ultrasound waves are attenuated when travelling through a medium, the reflected waves that arrive at the receiver are weak. Initially, the reflected signal is amplified. The degree of amplification is termed the gain of the receiver and is the ratio of the signal amplitude produced to the signal amplitude that is acquired (Zagzebski 1996). An additional component is also used in order to amplify the reflected waves. This component is called a preamplifier and as its name indicates, it amplifies the reflected signals before they are further amplified by the receiver. A prevalent complication with amplifiers is that apart from amplifying the reflected signal they also create artificial electrical signals, termed noise (Zagzebski 1996). Reflection waves arriving at the receiver from greater distances are more attenuated, thus give weaker signals than reflection waves arriving from shorter distances. TGC is the process which compensates for such attenuation (Zagzebski 1996). Distinct components of the ultrasound scanner have different dynamic ranges, i.e. the range of signal amplitude they can detect varies (Zagzebski 1996). A reflected signal of a large dynamic range needs to be compressed before the components with lower dynamic ranges are able to display it (Zagzebski 1996). Demodulation entails the modification of a reflected signal into a single pulse (Zagzebski 1996). Finally, rejection is a function that excludes any electronic noise, such as that generated by the amplifiers (Zagzebski 1996).

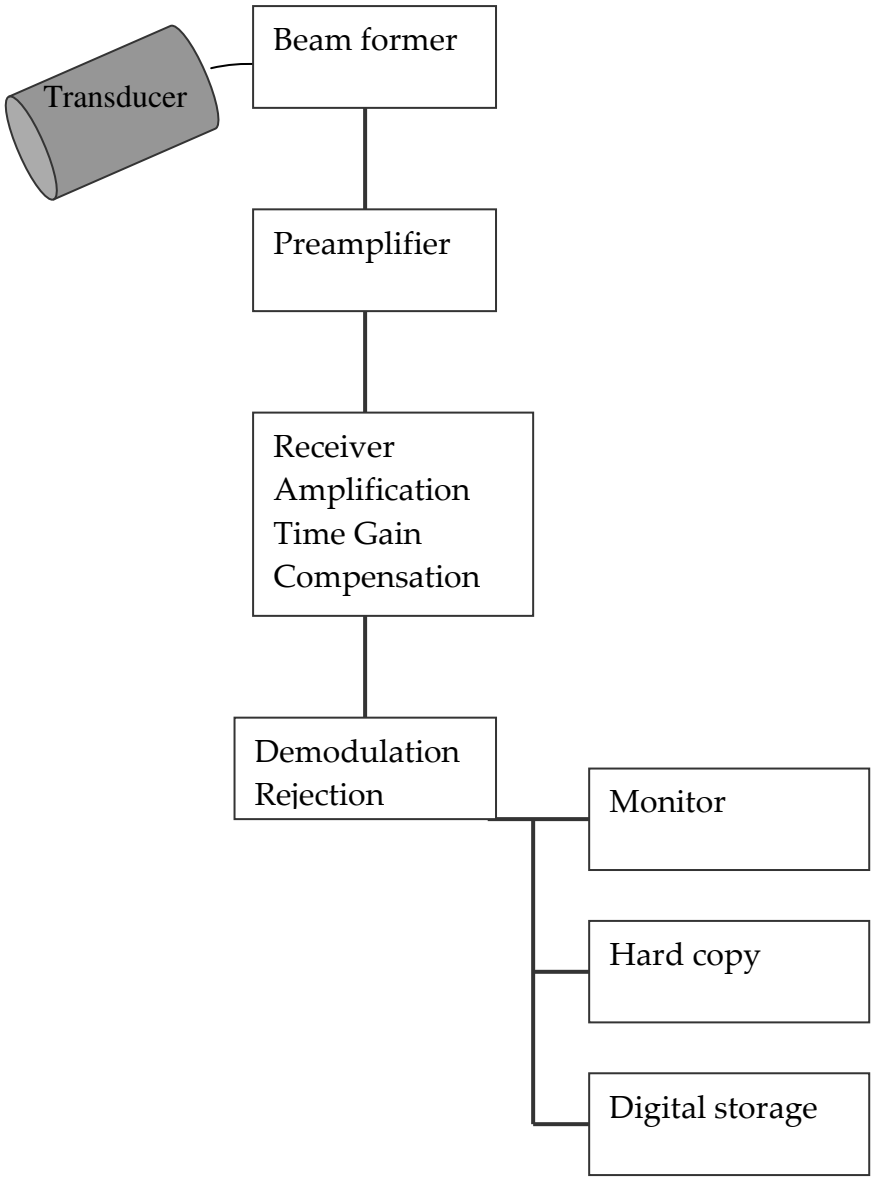

Figure 2.4 **Schematic representation of the principal components of an ultrasound imager.** Upon expulsion of an ultrasound wave from the ultrasound transducer, the latter is converter into a receiver, thus collecting the reflecting waves for further processing. Reflected signals tend to be attenuated due to their travelling through a medium, thus Initial processing necessitates amplification of the reflected signal firstly by the preamplifier and then by the amplifier. The signal then undergoes time gain compensation (TGC), compression, demodulation and rejection of any artificial electrical signal (noise) that has been created during the amplification process. The processed signal is presented at the monitor of the ultrasound imager and a copy of the image is stored in the machines memory. Adapted from (Dawson 1999).

2.2.3 Display modes

There are three main display modes used in pulsed echo ultrasonography, these are: A-mode, B-mode and M-mode (figure 2.5). A-mode (amplitude) displays the amplitude of the reflected wave versus the time it took for the reflected wave to arrive to the transducer (Zagzebski 1996). Since this time corresponds to the distance of the reflector, therefore A-mode is a display of amplitude of reflection versus distance of reflector. In addition, the PRF in A-mode is restricted so as to provide enough time for the reflected wave to decline before transmitting the next ultrasonic wave (Whittingham 2007). Factors such as propagation speed of ultrasound and distance of concern, determine the values of PRF (Whittingham 2007). A-mode is advantageous when accuracy of depth is desired (Whittingham 2007). B-mode (brightness) displays the reflected waves in pixels, which have different levels of brightness, whose position represents the amplitude of the scattered / reflected signal received at the transducer. The position of the pixel is related to the distance of the reflector from the source (Zagzebski 1996). While both A-mode and M-mode transmit the ultrasonic beam in a fixed direction, B-mode is concerned with scanning the ultrasonic beam (Whittingham 2007). M-mode (motion) displays reflector distance versus time (Zagzebski 1996). M-mode is mainly used in echocardiography and obstetrics in order to observe movement of the heart valves, heart chamber wall and embryonic heart movements respectively (Whittingham 2007).

2.2.4 Ultrasound equipment

The capacity of ultrasound to serve both for therapeutic and diagnostic purposes makes it a very effective tool (ter Haar 2007). However, the requirements for each application differ. Therapeutic applications require

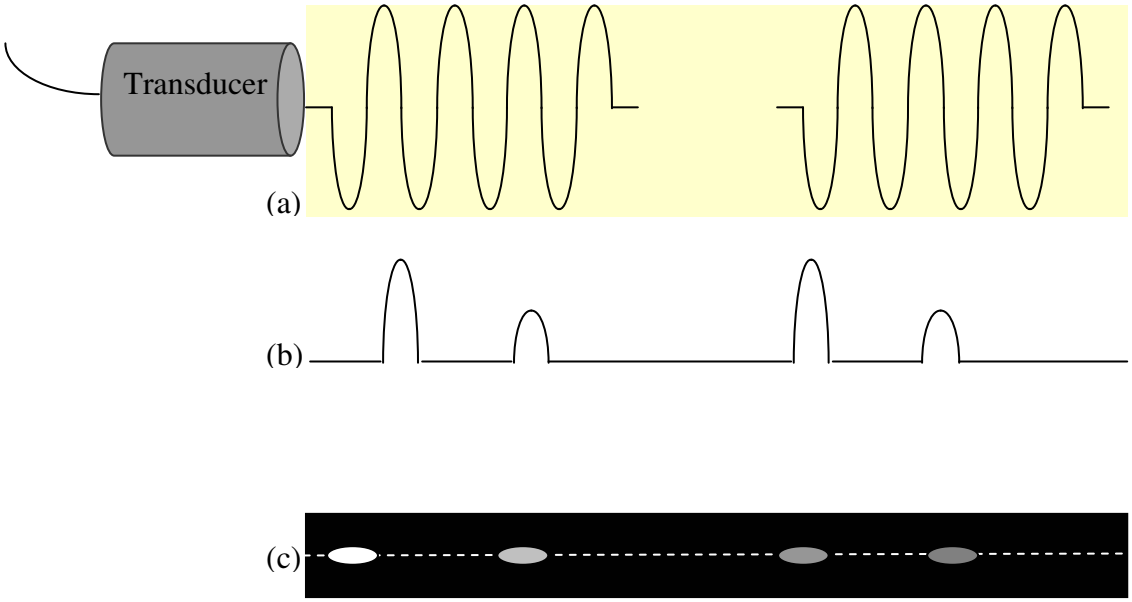

Figure 2.5 **Schematic representation of the A-mode and B-mode displays.** (a) A-mode display of a two pulse wave. This mode displays the amplitude of a reflected wave versus the time, which also corresponds to distance travelled by the reflected wave. (b) B-mode display of a two pulse wave. This mode displays the reflected wave in pixels of different brightness levels. The position of the pixel represents the amplitude of the wave, thus corresponds to the distance reflector from the source. (c) M-mode display of a two pulse wave. This mode displays the distance of the reflector versus time, thus it is useful for observing moving parts of the body. Adapted from (Dawson 1999).

induction of reversible or irreversible bioeffects, subject to the aim of the treatment, while diagnostic applications necessitate production of images with good spatial and temporal resolution (ter Haar 2007). Therapeutic applications of ultrasound include physiotherapy, transdermal drug delivery, thrombolysis, cancer treatment and bone healing (ter Haar 2002; Paliwal and Mitragotri 2009). The equipment used for each application are therefore different.

Ultrasound apparatus used for therapeutic applications, do not need to produce an image. The ultrasound beam is expelled by a non steered single disk shaped PZT element. The transducers used can transmit relatively high powers up to 10-12 Watts and emit waves of frequencies between 1-3.5 MHz. As frequency increases, penetration decreases and heating increases due to absorption (ter Haar 2007). Therefore the preference of frequency is a compromise between the maximum depth and absorption required (ter Haar 2007). The ultrasound waves delivered are of low pressures amplitudes (100-200 kPa) and can be either continuous or long pulsed waves (ter Haar 2007). Near field of transducer has complex interference pattern, i.e. local intensity varies rapidly with distance close to the transducer.

The objective of diagnostic apparatus is to provide an image with axial resolution, i.e. the ability to distinguish between adjacent tissues (Paliwal and Mitragotri 2009). In addition it is important that no adverse effects are generated (ter Haar 2007). The transducers employed in diagnostic scanners are composed of an array of many small PZT elements so as to be able to steer the ultrasound beam through the tissue in order to form a 2D or 3D image. The ultrasound beam transmitted is of low power (few mWatt to 100-200 mWatt) while frequencies used normally range between 0.2-20 MHz

depending on the depth of the tissue being imaged (ter Haar 2007). Diagnostic ultrasound scanners operate at higher frequencies than those used in therapeutic ultrasound (Miller 2007b). Typical frequencies used in diagnostic ultrasound are 3-5 MHz for abdominal and cardiac imaging, 10 MHz for superficial areas such as the neck or breast, 30 MHz for the anterior chamber of the eye and 100 MHz for the cornea of the eye (Paliwal and Mitragotri 2009). The ultrasound scanners use relatively high pressures, with peak pressure ranging between 0.5-33 MPa and relatively short pulses.

2.2.5 Bioeffects of ultrasound

As ultrasound passes through a medium, such as a biological tissue, the particles of this medium experience forces and stresses that might lead to damage of the tissue (Zagzebski 1996). Although no tissue damage has been reported so far from clinical diagnostic ultrasound application, some effects of ultrasound on biological tissue have been described and are continuously been investigated in order to obtain a clear idea of any risk factors associated with the use of ultrasound (Miller, Pislaru et al. 2002). The bioeffects seen, are predominantly caused during application of high intensities and long exposure periods (Zagzebski 1996). Ultrasound bioeffects can be separated into two categories, mechanical and thermal (BMUS 2007; ECMUS 2008). Mechanical bioeffects include acoustic cavitation, acoustic microstreaming and radiation pressure, while thermal bioeffects involves heating of the tissues (Cheng-Huang, Yeh et al. 2008).

2.2.5.1 Mechanical bioeffects of ultrasound

2.2.5.1.1 Cavitation

Ultrasonic cavitation refers to the production of microscopic gas bubbles during passage of an ultrasound beam through a medium (Patil and

Pandit 2007). The gas bubbles expand and contract with the fluctuations of the ultrasound wave (Zagzebski 1996). The occurrence of cavitation presupposes the presence of stabilized nuclei (Dalecki 2004). If the negative pressure applied to the medium compels the particles within the medium to diverge further than their critical molecular distance (Rc), then gas bubbles will be formed (Mason 1987). Gas bubbles then grow by rectified diffusion, where gas diffuses into the bubble during rarefaction and escapes during compression (Crum 1982). Since the rate of diffusion depends on the surface area of the bubble, more gas enters the gas bubble during rarefaction than escapes during compression, bringing about the growth of the bubble (Crum 1982). In theory, in order for cavitation to take place in water, a negative pressure of 100 MPa (1000 atmospheres) would be necessary (Mason 1987). However, in reality, cavitation occurs at much lower negative pressures, due to the presence of weak spots in the medium (Mason 1987). According to the crevice model, weak spots are areas of hydrophobic impurities, where gas nuclei are stabilized (Dalecki 2004). During negative pressures, the gas nuclei expand and disassociate from the impurities, thus forming gas bubbles (Dalecki 2004). In biological tissues gas nuclei are mainly present in the lungs and intestines (Dalecki 2004). The collapsed bubbles can either act as nuclei for new gas bubbles or if very small, can dissolve in the solution because of the "Laplace pressure" due to surface tension (Mason 1987; Wu and Nyborg 2008). The physical properties of the medium and the initial radius of the gas bubbles are amongst the various parameters that determine the extent of cavitation (Dalecki 2004; Patil and Pandit 2007). In addition, frequency has been shown to be inversely proportional to production of cavitation (Mason 1987). The basis for this observation can be explained in several ways. For

example, at high frequencies the time of rarefaction is so short that there is not sufficient time for the gas bubbles to grow (Mason 1987).

2.2.5.1.2 Non-inertial cavitation

Non-inertial or stable cavitation entails the oscillation of gas bubbles below the inertial cavitation threshold (Miller 2007b). Gas body behaviour models locate the inertial cavitation threshold at ultrasonic conditions of a mechanical index (MI) of about 0.4 (Miller, Averkiou et al. 2008). Non-inertial cavitation can persist for several cycles and can expand the radius of the gas bubbles to around twice their initial radius (Mason 1987; Dalecki 2004). During non-inertial cavitation, extensive oscillatory and steady fluid shear stresses develop adjacent solid surfaces (Miller, Averkiou et al. 2008). Fluid shear stresses have been shown to exert mechanical injury on cell membranes (Miller, Averkiou et al. 2008). However, non-inertial cavitation is seldom studied since the microbubbles relevant to medical ultrasound undergo transient cavitation (Miller 2007b).

2.2.5.1.3 Inertial cavitation

Above the inertial cavitation threshold, gas bubbles grow to such dimensions that they collapse violently. Inertial or transient cavitations prevail for only a few acoustic cycles and can amplify the radius of the gas bubbles to many times the initial radius before collapsing (Mason 1987). This produces severe localized effects such as the formation of free radicals, fluid jets, temperatures of up to 14,000 K, pressures of up to 10,000 Atm and sonoluminescence (Patil and Pandit 2007; Cheng-Huang, Yeh et al. 2008; Miller, Averkiou et al. 2008). The latter refers to the production of light produced by cavitation.

2.2.5.2 Thermal bioeffects of ultrasound

During transmission of an ultrasonic beam through a medium, part of the beam is absorbed and converted into heat. The degree of temperature increase is dependent on both the properties of the medium and the ultrasonic beam (Dalecki 2004).

2.2.5.3 Measuring bioeffects of ultrasound

One can appreciate the importance of monitoring the factors that cause all the bioeffects discussed above. Therefore, a number of indicators have been assigned that relate to the potential bioeffects that arise from application of ultrasound. Such indicators include the mechanical index (MI) and thermal index (TI). The mechanical index is used to describe the likelihood of occurrence of cavitation and is directly proportional to the peak rarefractional pressure in the medium and inversely proportional to the square root of the ultrasound frequency (Zagzebski 1996). The higher the value of the MI, the higher the probability of cavitation (Wu and Nyborg 2008). The thermal index is used to describe the potential increase in temperature that can happen as a result of ultrasound exposure and is defined as the ratio of the acoustical power over the power required to raise the temperature by 1 degree C (Zagzebski 1996).

2.2.6 Measurement of ultrasound probes

As the performance of ultrasound probes tends to decline over time, it is necessary to conduct frequent measurements in order to be able to employ ultrasound safely. Thus, measurement of power and pressure amplitude is essential.

2.2.6.1 Measurement of acoustic power

Ultrasonic power is routinely measured with the aid of a radiation force balance (Zeqiri 2007). Radiation force (F) is a force that is produced by an acoustic field and affects any object intercepting the field (Zeqiri 2007).The probe under investigation is placed in a water bath and held directly above a balance. The plate of the balance is composed of an acoustic absorber so as to collect the ultrasound wave generated by the probe (Zagzebski 1996). One can calculate the acoustic power that is exerted from the probe by applying the following equation:

$$F = \frac{W}{v} \qquad (6)$$

where W is the acoustic power and v is the propagation speed in water (Zagzebski 1996).

2.2.6.2 Measurement of acoustic pressure

Measurement of pressure is achieved with a hydrophone (Zagzebski 1996). A hydrophone is made from thin membranes of the piezoelectric polymer polyvinylidene fluoride (PVDF) and functions as a receiver of the ultrasonic beam generated by the probe under investigation (Zagzebski 1996; Zeqiri 2007). As it contains a piezoelectric element, it is able to transform the vibrations received from the probe into an electrical signal of comparable amplitude (figure 2.6) (Zagzebski 1996).

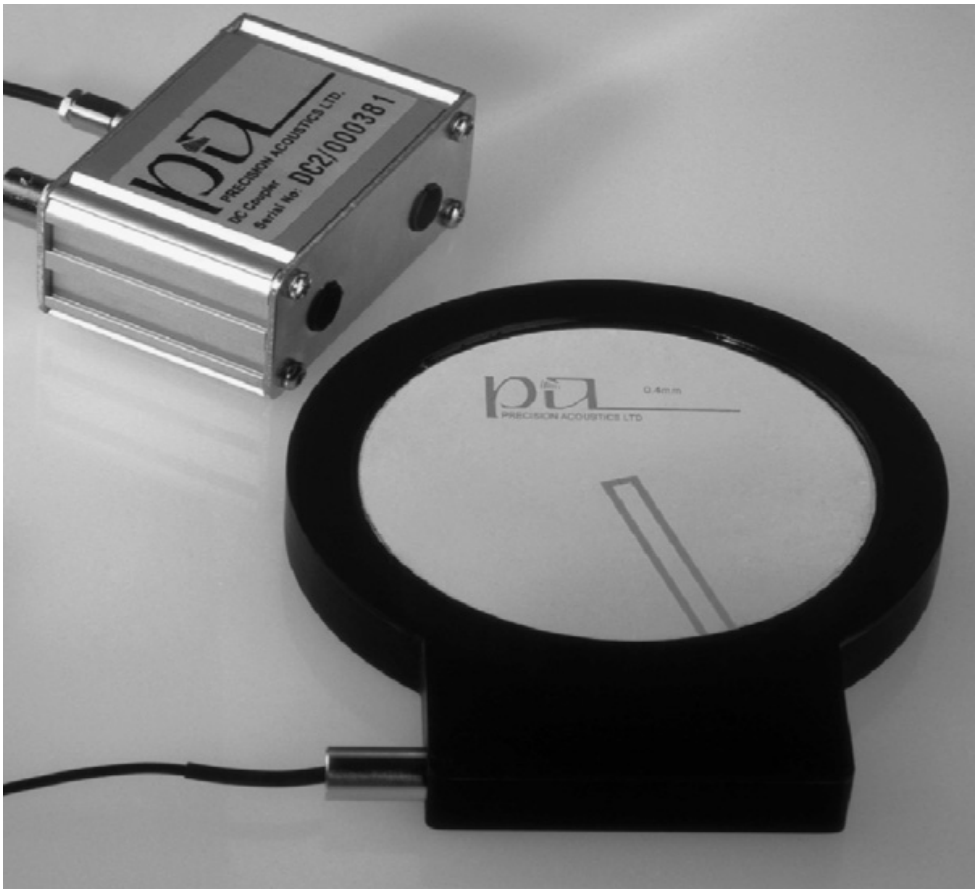

Figure 2.6 **Image of a type of hydrophone.** A membrane hydrophone is composed of thin membranes of piezoelectric polymer polynivylidene fluoride (PVDF). It operates by transforming received vibrations into electrical pulses of comparable amplitude. Such a hydrophone can be used in order to measure the acoustical pressure of an acoustic wave. Printed by permission Elsevier® (Leighton 2007b).

Chapter 3

Introduction

Microbubbles

3.0 Microbubbles

Gramiak and Shah (1968) were the first to publish the enhanced reflectivity of blood observed by Joyner (Joyner, Reid et al. 1963), while carrying out a heart ultrasound during a catheter examination (Winkelmann, Kenner et al. 1994; Dawson 1999; Nico de Jong 2002; Miller and Nanda 2004). The use of a fluorescent dye (indocyanin green) during Joyner's study was thought to be responsible for the increase in reflectivity observed (Dawson 1999). However, it was later discovered that other dyes also produced a comparable outcome and that the presence of small air filled microbubbles were responsible for these effects (Winkelmann, Kenner et al. 1994; Dawson 1999). These microbubbles were created as a result of cavitation when liquids were administered via a catheter or a small needle (Winkelmann, Kenner et al. 1994). This discovery instigated the development of a multitude of molecules with the same characteristics, including liquid-core microemulsions and nanoemulsions, colloidal suspensions, liposomes and microbubbles (de Jong, Frinking et al. 2000; Klibanov 2005). These are nowadays collectively known as ultrasound contrast agents. It should be noted at this point that the use of the term microbubble is somewhat generic. Microbubbles can be defined as spherical structures that are filled with air or gas. Liposomes can be defined as self-assembled lipid shelled microbubbles filled with an aqueous solution (Alkan-Onyuksel, Demos et al. 1996; Huang 2008). However, it has been stated that liposomes can also be filled with gas (Alkan-Onyuksel, Demos et al. 1996; Dawson 1999; Wu, Chen et al. 2006). For example, the ultrasound contrast agent Definity® can be classified either as a liposome or as it encapsulates gas, a microbubble. Further research has lead to the development of efficient microbubbles that are employed for diverse ultrasound applications. First-generation ultrasound contrast agents were air filled microspheres, such as Albunex®, Levovist® and Echovist®. Second-

generation ultrasound contrast agents, such as Optison® encompass inert high molecular gases in their cores. Finally third generation ultrasound contrast agents, such as Definity® and Sonovue®, are even more advanced with shells that are composed of several chemical components (figure 3.1) (Rubin 2004). Several of the ultrasound contrast agents developed and their relevant characteristics are listed in table 3.1.

3.1 Interaction of microbubbles with ultrasound waves

The contrast enhancing powers of the microbubbles are determined by variables such as their compressibility, their resonance frequency and their contents (Dawson 1999). Microbubbles oscillate in distinct modes depending on the frequency of the ultrasound wave applied (figure 3.2) (Dawson 1999). At a specific frequency, also known as the fundamental or resonance frequency, microbubbles demonstrate maximal oscillation (Dawson 1999). Since the scattered wave that is produced when an ultrasound beam strikes a microbubble is proportional to the sixth power of the microbubble's diameter, such large increases in its diameter account for the exceptional enhancement in reflection observed (Winkelmann, Kenner et al. 1994). The resonance frequency of microbubbles of sizes equivalent to those used for clinical purposes, lies within the range of frequencies utilised for diagnostic ultrasound, thus allowing the employment of their reflectivity for diagnostic purposes (Dawson 1999). At frequencies higher than the fundamental frequency, microbubbles contract and expand in a non-linear manner, thus producing scattered waves of both fundamental and harmonic frequencies (Dawson 1999). Although harmonic frequencies tend to decline in intensity, the second harmonic frequency can be as much as twice or three times the

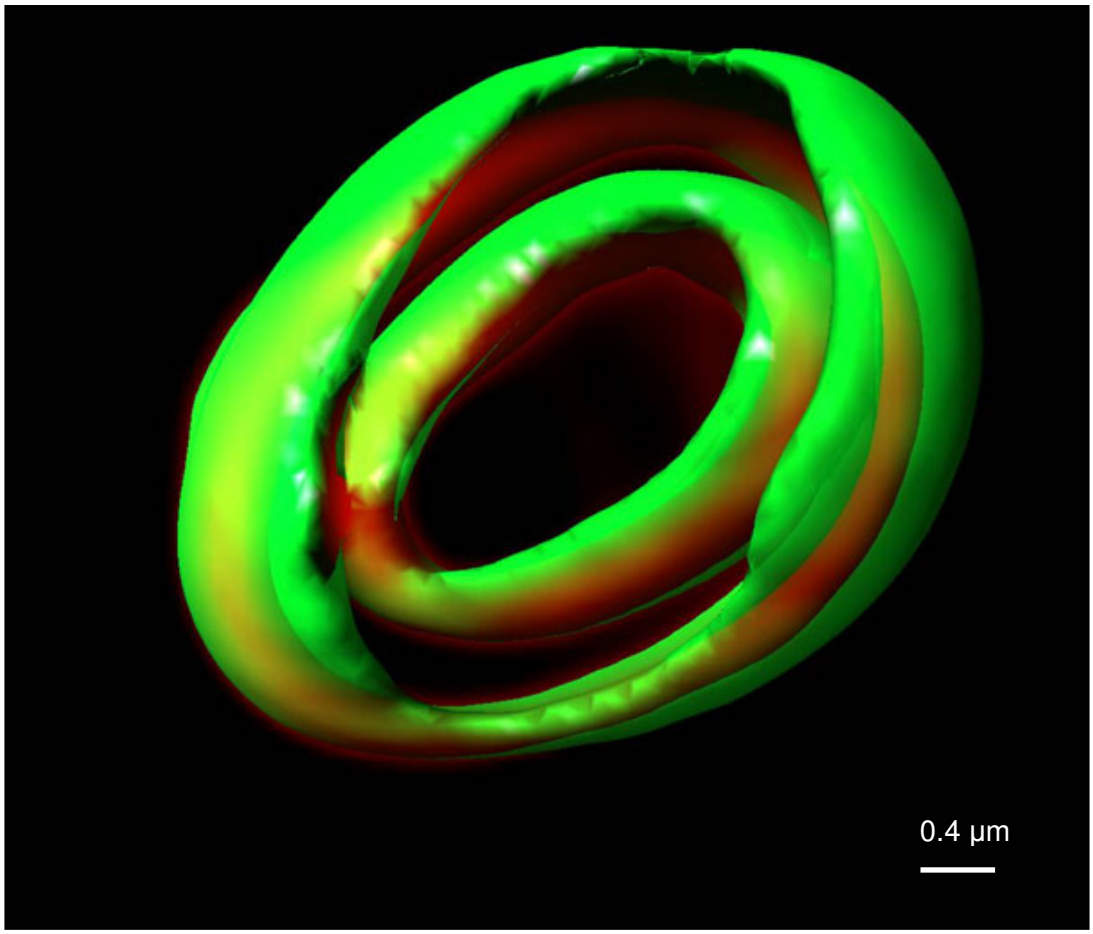

Figure 3.1 **Representation of typical microbubble.** Microbubbles are spherical structures composed of lipid shells and an air / gas core. First-generation ultrasound contrast agents were air filled microbubbles (Albunex®, Levovist® and Echovist®). Second-generation ultrasound contrast agents, encompass inert high molecular gases in their cores (Optison®). Third generation microbubbles are composed of more advanced shells, such as phospholipids (Definity® and Sonovue®). Incorporation of molecules, such as ligands, peptides, hormones or antibodies, in the microbubble shell can assist attachment of the microbubbles to target cells. Therapeutic agents, such as genes or drugs, can be incorporated in the microbubble core in order to serve as delivery systems by ultrasound induced microbubble destruction. This is an electron microscopy image of an in-house microbubble, composed of two layers of lipid shell and filled with aqueous solution. The phospholipid layers have been stained with FM-143, a molecule that emits green fluorescence once attached to phospholipids.

Name	Shell	Charge	Gas	Count	Size Mean diameter	Company
Albunex®	Albumin		Air	$7x10^8$ ml	95%<10 µm 4 µm	MBI, San Diego
Levovist® SHU 508A	Galactose Palmitic acid	Negative	Air	Varies with concentration	95%<10 µm 2-8 µm	Schering AG
Optison ® FS069	Human serum Albumin N-acetyltryptophan, Caprylic acid	Negative	Octafluoropropane	$5–8\ x10^8$ ml	93% <10 µm 2-5 µm	Amersham Health
Definity® DMP115	Dipalmatoylphosphatidic acid Dipalmatoylphosphatidylcholine Dipalmatoylphosphatidalethanolamine	Negative	Octafluoropropane	$1.2\ x10^{10}$ ml	98% <10 µm 1.1-3.3 µm	Bristol-Myers Squibb Medical Imaging Inc.
Imagent® AF0150	Dimyristoylphosphatidalcholine	Neutral	Perfluorohexane Nitrogen	$1.4\ x10^9$ ml	99.8% <10 µm 6 µm	Pharmaceuticals Inc.
Sonovue® BR1	Macrogol 4000 Distearoylphosphatidylcholine Dipalmitoylphosphatidylglycerol Sodium Palmitic acid	Negative	Sulfurhexafluoride	$1\text{-}5\ x10^8$ ml	99% <11 µm 2 µm (median)	Bracco Diagnostics Inc.

Table 3.1 **Ultrasound contrast agents.** First, second and third generation microbubbles have several different characteristics. As microbubble production evolved, certain physical parameters were changed, such as shell composition, gas content, size, polarity and concentration, in order to produce microbubbles that had a longer life in the blood stream and achieved higher sonoporation efficiencies. A list of some of the commercially available ultrasound contrast agents and their characteristics is listed in this table in order of generation. I.e. first generation microbubbles are shown at the top of the table while third generation microbubbles are shown at the bottom of the table (Alkan-Onyuksel, Demos et al. 1996; Miller and Nanda 2004; Cosgrove 2006; Junru and Nyborg 2008; Sboros 2008)

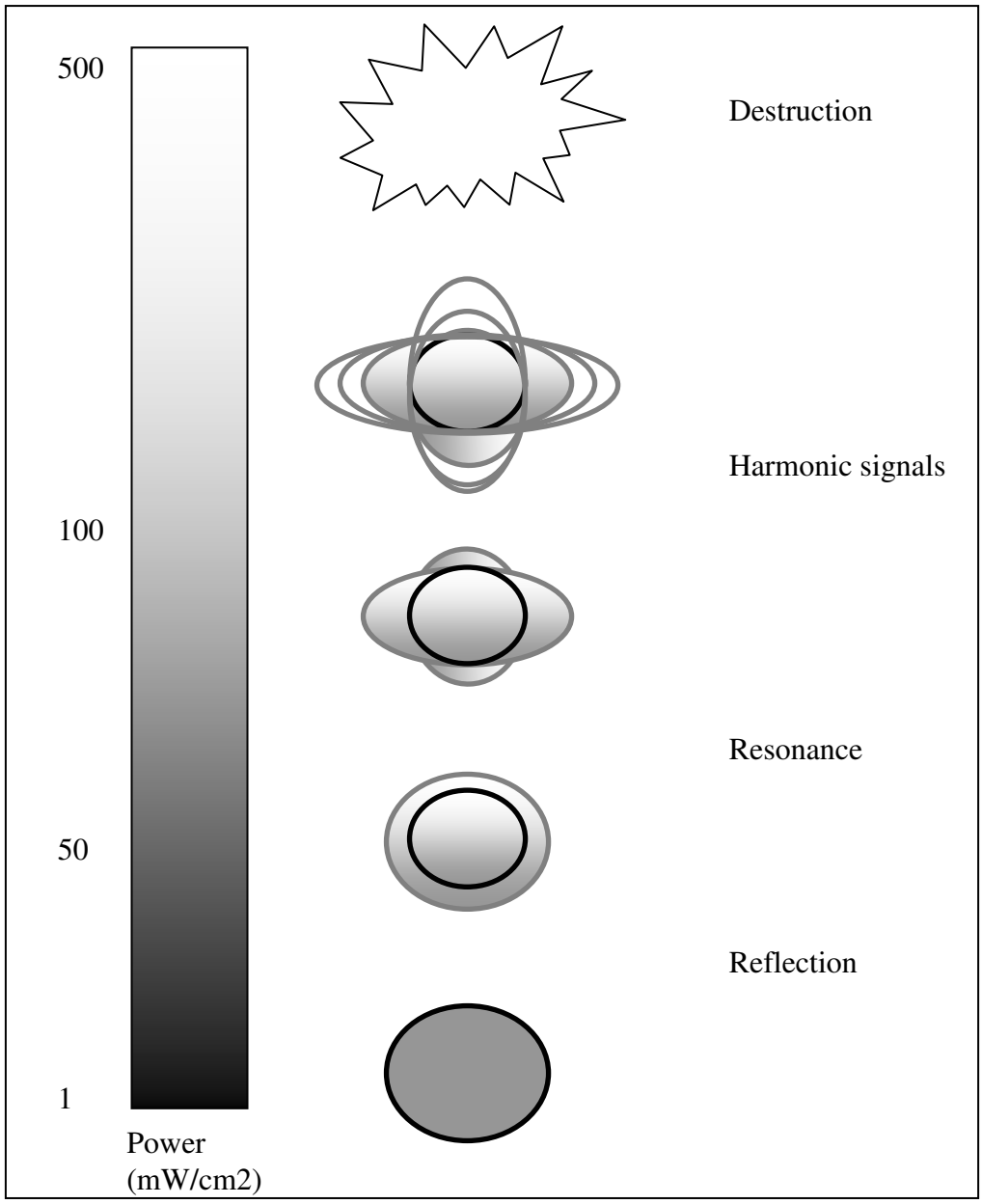

Figure 3.2 **Reflection modes of microbubbles.** Microbubbles oscillate in distinct modes depending on the frequency of the ultrasound wave applied. Upon application of an ultrasound wave, microbubbles begin to oscillate, thus producing reflective waves (reflection). At a specific frequency (resonance) microbubbles demonstrate maximal oscillation. At frequencies higher than the resonance frequency, microbubbles contract and expand in a non-linear manner, thus producing scattered waves of both resonance and harmonic frequencies (harmonic signals). At even higher frequencies, microbubbles can be destroyed, releasing their contents to the surrounding environment. Adapted from (Dawson 1999).

(Goldberg, Liu et al. 1994; Calliada, Campani et al. 1998; Dawson 1999). The harmonic response of the microbubbles is determined by the compressibility of the shell and the contents of the core (Dawson 1999). The more rigid the shell of a microbubble is, the smaller the scattered wave will be (Dawson 1999). Hence, most microbubbles are composed of either a lipid or an albumin shell in order to reduce the shell rigidity. While small free air microbubbles exposed to an ultrasound beam disintegrate and are dissolved rapidly, microbubbles filled with high molecular weight gases show prolonged persistence within the circulation due to the slower diffusion rate of such gases (Mason 1987; Dawson 1999; Klibanov 2005; Wu and Nyborg 2008). At higher acoustic powers tissues also generate harmonics (Cosgrove 2006). However, current microbubbles, composed of a phospholipid shell, generate harmonics at much lower acoustic powers than those necessary for tissues harmonics (Cosgrove 2006). One can therefore attempt to isolate the microbubble harmonics from tissue signals by separating the fundamental from the harmonic frequencies (de Jong, Frinking et al. 2000; Cosgrove 2006). Finally, at higher pressures, microbubbles can be destroyed, releasing their contents to the surrounding environment (Dawson 1999). This effect can be used clinically to study perfusion defects and has the potential to be tailored to be utilized for delivering a range of molecules, such as drugs and genes, to specific tissues (Nico de Jong 2002).

3.2 Microbubble characteristics

3.2.1 Size

Microbubbles are administered intravenously and diffuse by means of in the bloodstream to all parts of the body. It is therefore vital to attribute an upper size limit in order for the microbubbles to be able to cross the lung capillary bed (Dawson 1999; Palma and Bertolotto 1999). This denotes that

microbubbles must have comparable size to that of red blood cells, not exceeding 7 μm diameter (Palma and Bertolotto 1999; Miller and Nanda 2004). However, size limitations turn into a complex issue once echogenicity is taken into consideration. Since the echogenicity of a microbubble is proportional to the sixth power of its diameter, the bigger the size of a microbubble the greater its echogenicity. Therefore, the ideal size of a microbubble if one that takes into consideration both echogenicity and size limitations parameters. Most microbubbles nowadays have a diameter of 2-6 μm (Quaia 2007).

3.2.2 Longevity

Both the shelf life and life span of microbubbles upon administration to the patient are important. Examination of certain areas of the body, such as renal and leg arteries can take considerable amount of time, thus microbubbles need to be able to persist in the bloodstream throughout the entire length of the examination (Dawson 1999). Persistence of a microbubble is dependent on both the nature of its shell and its contents. It can be described by the equation:

$$\frac{RxP}{2DxC_s} \qquad (7)$$

where R=bubble radius, P=gas density, D=gas diffusivity and Cs= saturation constant (Raisinghani and DeMaria 2002). First generation microbubbles did not employ a shell and thus dissolved rapidly after administration to patients (Klibanov 2005). Second and third generation microbubbles employ a shell which delays diffusion of their contents (Klibanov 2005; Marcel, Alexander et al. 2009). Use of surfactants, such as palmitic acid, serum albumin, polymer, and phospholipids for shell manufacture, also extend the life span of microbubbles, as they act by reducing their surface tension (Dawson 1999;

Huang 2008). In addition, incorporation of electrostatically charged molecules, such as polyethylene glycol (PEG), hinders merging of the microbubbles (Klibanov 2005). Microbubbles containing PEG have been shown to survive many years without manifesting any decline in their echogenicity and can persist in the circulation for up to one hour after administration (Klibanov 2005). Furthermore, microbubbles can be classified as thin- or hard-shelled depending of the number of layers present (Marcel, Alexander et al. 2009). Thin-shelled microbubbles are 2-3 nm thick whereas hard-shelled microbubbles fall within the range of 20-200 nm (Dayton, Klibanov et al. 1999; Marcel, Alexander et al. 2009). The thickness of the shell affects the degree of oscillation which in turn affects the echogenicity of the microbubble (Marcel, Alexander et al. 2009).

The contents of the microbubbles also play an important role in their persistence in the circulation. First generation microbubbles, such as Albunex and Levovist, were filled with air and exhibited short persistence once injected (Miller and Nanda 2004). Gases such as perfluorocarbons (PFC) and sulphur hexafluoride (SF_6) were perceived as ideal for within the microbubbles since they have a low saturation constant, high density and they diffuse slowly (Schneider 1999; Miller and Nanda 2004). In addition, the large discrepancy in acoustic impedance between gas (4.30×10^2) and blood (1.67×10^6), contributes to the echogenicity of the microbubbles (Calliada, Campani et al. 1998; Palma and Bertolotto 1999; Pomper and Gelovani 2008). Microbubbles containing such gases include Optison® (Amersham Health), Definity® (Bristol-Myers Squibb Medical Imaging Inc.), Imagent® (Pharmaceuticals Inc.) and Sonovue® (Bracco Diagnostics Inc.) (Miller and Nanda 2004). The presence of high molecular weight gases improves the

longevity of the microbubbles, since they have a slower diffusion rate than air.

In addition to their capacity as ultrasound contrast agents, research into the potential use of microbubbles as delivery vehicles to target tissues is ongoing. In such cases, an equilibrium needs to be reached between adequate microbubble longevity and obliteration of microbubbles upon application of ultrasound waves of a specific frequency (Miller and Nanda 2004).

Finally, a number of precautions can be taken that can extend the shelf life of microbubbles. These include avoiding extreme temperatures and administering microbubbles at a steady rate so as to avoid high pressurization and shear stress in the needle, which can lead to microbubble destruction (Dawson 1999; Barrack and Stride 2009).

3.2.3 Safety

As an ultrasound beam strikes microbubbles, the latter encounter a force that propels them away from the source of the beam. This force is known as acoustic radiation force. The latter can project microbubbles through distances of a fraction of a micron with each acoustic cycle, at a speed of 5-10 cms^{-1} (Dawson 1999; Ferrara, Pollard et al. 2007). In addition to this primary radiation force, microbubbles also endure a secondary radiation force, which can result in their coalescence (Dawson 1999; Ferrara, Pollard et al. 2007). When a microbubble is positioned adjacent to another echogenic surface, the radiation force of the microbubble is echoed back to itself. Thus the microbubble effectively receives its own radiation force, which leads to it being attracted to the echogenic surface in the same manner that two microbubbles are attracted to each other by secondary radiation forces (Dawson 1999). This can explain the attraction of microbubbles to cells in suspension during ultrasound application (Dawson 1999). Microbubbles

experiencing primary radiation forces, collide with cells at such high speeds and can cause severe impairment to cells, so much as to induce cell death (Dawson 1999). However, it is believed that this is not true for high cell concentrations where microbubbles are attracted to the cells and do not have enough distance to accelerate to such high speeds (Dawson 1999).

As with any clinical application, safety is of utmost importance. Extensive investigations have been implemented in order to examine the possible bioeffects that can arise from the use of ultrasound in the presence of microbubbles, leading to the establishment of guidelines and good clinical practise recommendations for contrast enhanced ultrasound (Claudon, Cosgrove et al. 2008). Although bioeffects in animals have been observed, including haemolysis, platelet aggregation and endothelial damage, they are deemed negligible (Cosgrove 2006; Quaia 2007). Furthermore, bioeffects in humans are sparse, moderate and mainly temporary (Raisinghani and DeMaria 2002; Cosgrove 2006; Quaia 2007). These include dyspnea, chest pain, hypo-hypertension, nausea and vomiting, taste alterations, headaches, vertigo, warm facial sensation, and rashes (Cosgrove 2006; Quaia 2007). While, *in vitro* bioeffects include haemolysis, sonoporation and cell death (Claudon, Cosgrove et al. 2008). However, in response to a small number of reported cardiopulmonary events in high risk patients, the U.S. Food and Drug Administration (FDA) issued an alert to healthcare professionals, recommending monitoring of high risk patients for at least 30 min post administration of Definity® and Optison® contrast agents (FDA 2008). Ultrasound contrast agents are now treated as pharmaceuticals and require more stringent clinical trials than previously. In the same report, the FDA included a balancing comment, claiming that the clinical benefits of

ultrasound contrast agent use can outweigh the risk of severe reactions, even in high risk patients (FDA 2008).

3.3 Clinical applications

Microbubbles were initially discovered and developed for their capability to enhance echoes, thus serving as contrast agents for ultrasound diagnostic applications. Since then it has become evident, through several studies, that microbubbles can also be exploited for therapeutic purposes (figure 3.3) (Everbach and Francis 2000; Miller 2000; Unger, Matsunaga et al. 2002; Dijkmans, Juffermans et al. 2004; Mitragotri 2005; Hernot and Klibanov 2008; Marcel, Alexander et al. 2009).

3.3.1 Diagnostic applications

Two of the most prominent diagnostic applications of ultrasound contrast agents are liver and heart imaging. Although the reasons behind this effect continue to be ambiguous, it has been well established that microbubbles are taken up by the liver and spleen (Blomley, Cooke et al. 2001). Ultrasound contrast agents can assist with visualisation of small (under 1 cm in diameter) liver lesions such as metastases and hepatocellular carcinomas (figure 3.4) (Blomley, Cooke et al. 2001).

Microbubbles are widely used in echocardiography. Enhancement of the left ventricular cavity and the endocardial border of the heart are amongst the areas employing ultrasound contrast agents (Blomley, Cooke et al. 2001). Microbubbles are also employed for evaluating microvascular perfusion in various organs within the body (Lindner and Sanjiv Kaul 2001).

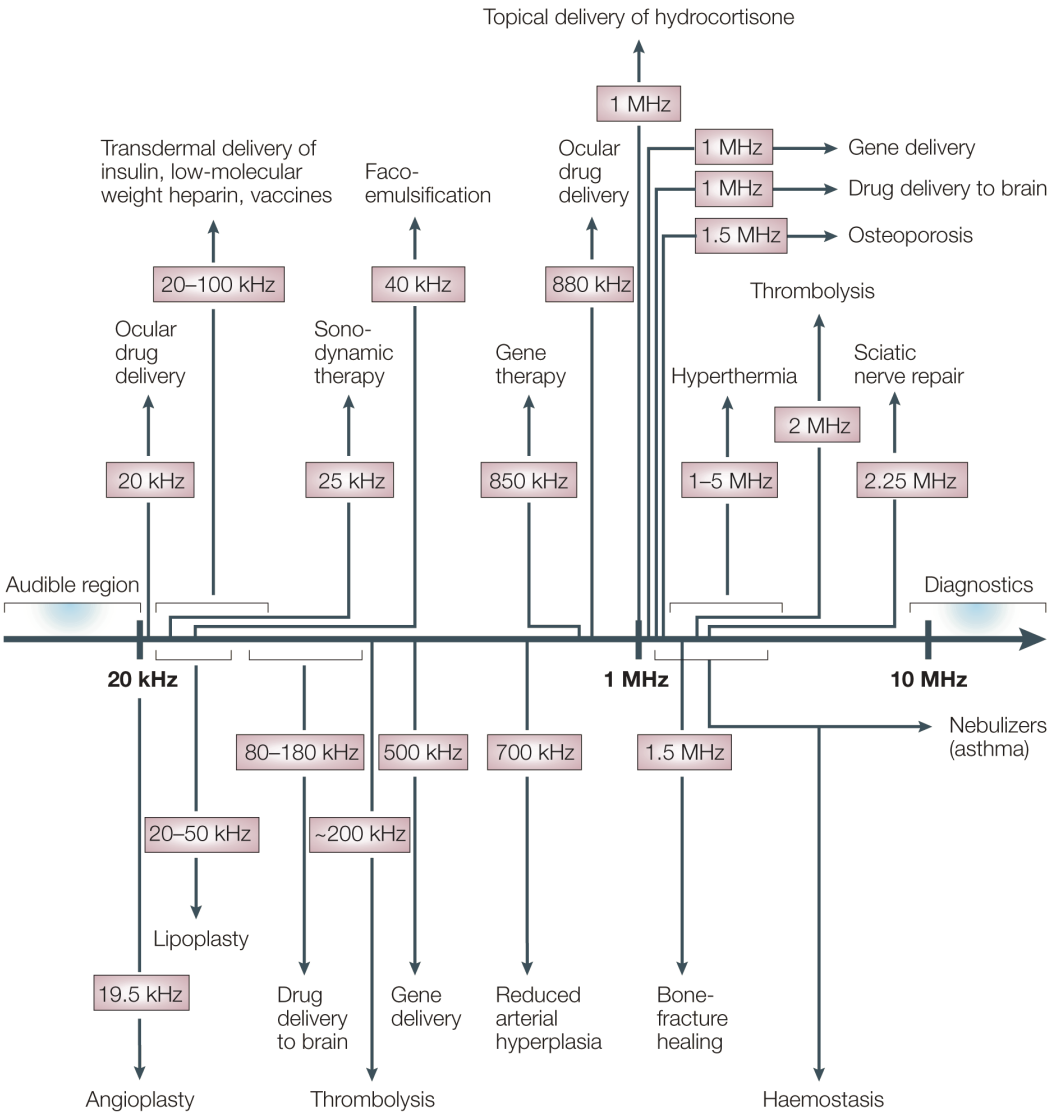

Figure 3.3 **Ultrasound applications.** A number of medical applications of ultrasound amongst many are shown in this figure. The optimal frequencies at which they are applied are also shown. A considerable amount of these applications are achieved at 1 MHz. Printed by permission Elsevier® (Mitragotri 2005).

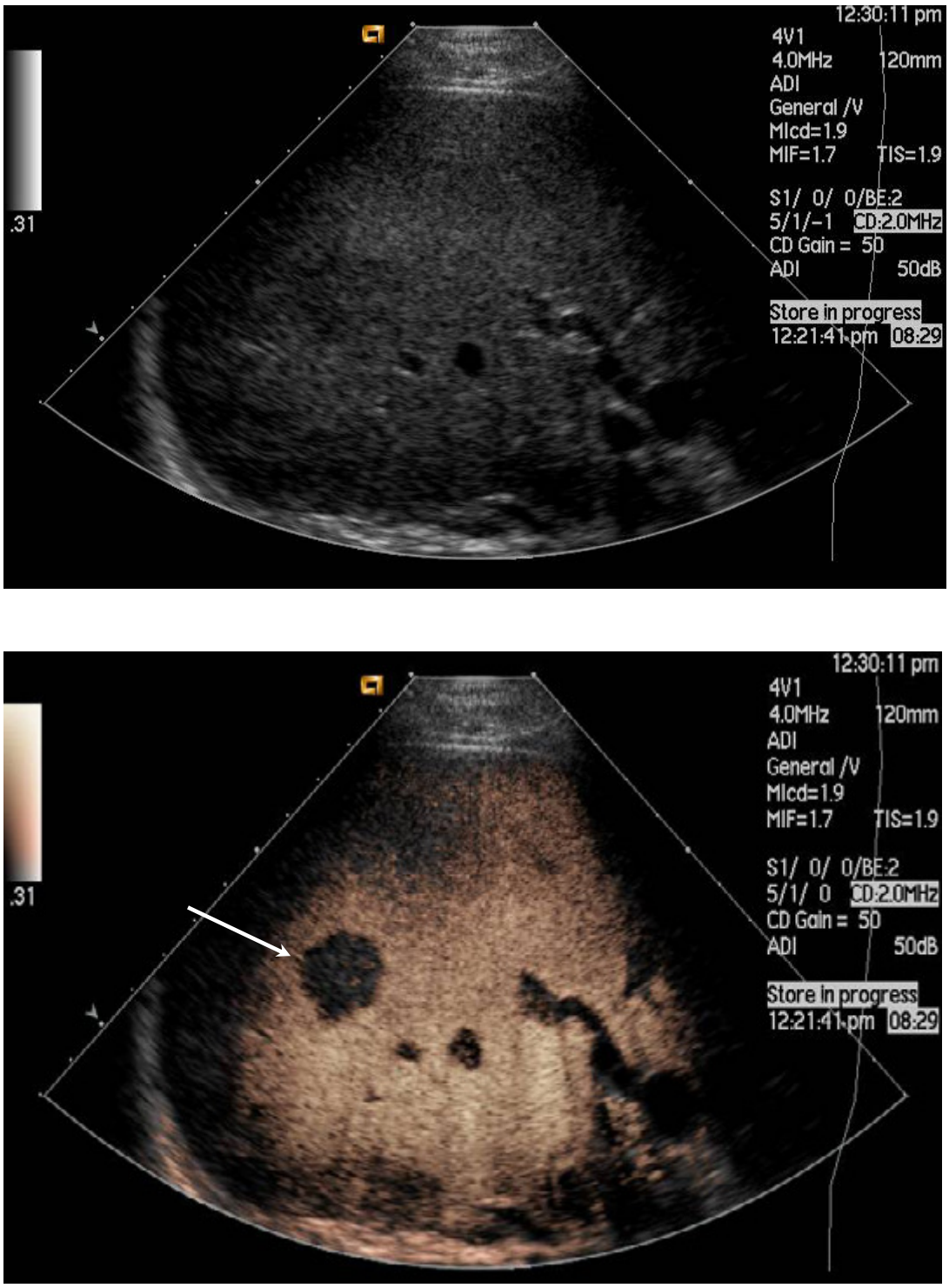

Figure 3.4 **Ultrasound contrast agents.** Ultrasound liver scans in the absence (a) and in the presence (b) of ultrasound contrast agent, depicting metastasis. Ultrasound contrast agents increase the contrast from reflected images, thus making it possible to detect previously undetectable lesions. White arrow is pointing towards the lesion that can only be detected in the presence of ultrasound contrast agents. Printed by permission Elsevier® (Blomley, Cooke et al. 2001).

3.3.2 Therapeutic applications

The utilization of ultrasound contrast agents as a therapeutic tool has been increasing rapidly and may ultimately develop into a more prominent role than as a diagnostic tool (Miller 2000). Therapeutic uses of microbubbles amongst others include thrombolysis, vascular permeability, tissue healing, soft tissue stimulation, bone regeneration tumour suppression, arteriogenesis, lithotripsy and haemostasis (Everbach and Francis 2000; Miller 2000; Unger, Matsunaga et al. 2002; Dijkmans, Juffermans et al. 2004; Mitragotri 2005; Hernot and Klibanov 2008; Marcel, Alexander et al. 2009). A particularly significant use of microbubbles involves the delivery of a therapeutic agent (gene or drug) by ultrasound targeted microbubble destruction (Bekeredjian, Grayburn et al. 2005).

Chapter 4

Introduction

Ultrasound contrast agent mediated gene delivery

4.0 Ultrasound contrast agent mediated delivery

4.1 Sonoporation

Successful drug / gene delivery and targeting to specific organs or tissues is still one of the main impediments of gene therapy (Shohet, Chen et al. 2000). Delivery of a therapeutic agent can be achieved by loading microbubbles with the desired agents or by co-administration of drugs and microbubbles (figure 4.1) (Hernot and Klibanov 2008). This notion consists of two parts. Firstly, as mentioned earlier, the application of ultrasound of a sufficiently high pressure can bring about the destruction of microbubbles, thus causing outward dispersion of their contents. Microbubbles can act as carriers of genes or drugs that are incorporated into their cores and releasing them at the target area upon their destruction. This would result in a build up of their local concentration, which in turn would allow administration of lower drug doses (Bekeredjian, Grayburn et al. 2005). On the other hand, the amount of drugs that can be incorporated into microbubbles is limited due to the size and the thickness of their shell (Marcel, Alexander et al. 2009). Alternatively, one can attach the drugs on the outer surface of the microbubble shell (Marcel, Alexander et al. 2009).

Cell membranes are arranged in a phospholipid bilayer, embedded with integral proteins (Singer and Nicolson 1971). They form a barrier between the cell and the outside environment. Cell membranes thus present an obstruction to large molecules such as drugs and particularly genes (Huang 2008). Application of ultrasound in the presence of microbubbles has been shown to lead to the formation of transient non-lethal perforations, a phenomenon termed sonoporation (Blomley, Cooke et al. 2001). During sonoporation, perforations up to 75 nanometers are formed permitting diffusion of small molecules across the cell membrane (Mehier-Humbert, Bettinger et al. 2005a). Formation of these pores has been reported to last

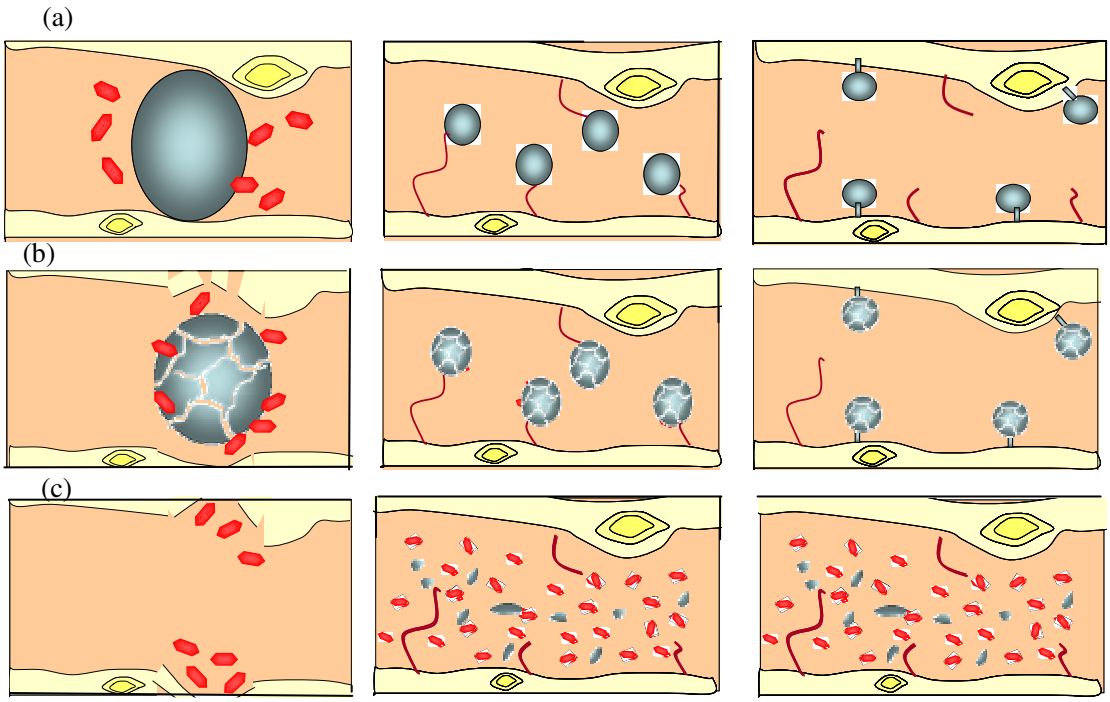

Figure 4.1 **Methods of drug / gene delivery.** (a) Therapeutic agent is co-administered with microbubbles. Microbubbles destruction occurring upon insonification results in the formation of pores on the cell membrane. Therapeutic agents located in the vicinity can diffuse into the cell due to disparities in local concentration. (b) Therapeutic agent is incorporated into microbubbles. Upon microbubble destruction, the agent is released in the region of interest. (c) Microbubbles are attached to target tissues via cell surface receptors. Destruction of the microbubbles will release the therapeutic agent in the area of interest thus increasing its local concentration. Adapted from (Lindner and Sanjiv Kaul 2001).

milliseconds, sealing almost instantaneously after sonication, thus halting movement of drug / gene molecules across the plasma membrane (figure 4.2) (Mehier-Humbert, Bettinger et al. 2005a). However, certain ultrasonic conditions such as high pressures and prolonged exposure can induce irreparable damage to the cell membrane and therefore lead to cell death (Miyake and McNeil 1995; Ferrara, Pollard et al. 2007).

A reduction in cell size is also observed after sonoporation, on account of the leakage of the cytosolic fluid through the pores formed (Mehier-Humbert, Bettinger et al. 2005a). Morphological changes on the cell membrane have also been reported, whereby cell surface receptors such as CD19 (a Glycosylphosphatidylinositol (GPI) anchored cell surface receptor) are dislodged due to insonification (Brayman, Coppage et al. 1999; Mehier-Humbert, Bettinger et al. 2005a). Moreover, nuclear membrane permeability seems to be impervious to insonification (Duvshani-Eshet, Baruch et al. 2005; Mehier-Humbert, Bettinger et al. 2005a).

Although sonoporation has also been shown to occur in the absence of microbubbles, the level of acoustic power required is substantially higher than that used in clinical imaging (Lawrie, Brisken et al. 1999; Blomley, Cooke et al. 2001; Bekeredjian, Grayburn et al. 2005). The presence of microbubbles significantly reduces the energy threshold for sonoporation within the authorised ranges (Blomley, Cooke et al. 2001; Duvshani-Eshet, Baruch et al. 2005; Hernot and Klibanov 2008; Huang 2008).

4.1.1 Mechanisms of sonoporation

Several means have been proposed for the increase of cell permeability, yet the precise mechanism is poorly understood. One of the most accepted mechanisms is inertial cavitation, which is associated with severe localized effects such as formation of free radical, high temperatures

and pressures, sonoluminescence, microjets and microstreaming (Gerard and Junru 1998; Ward, Wu et al. 2000; Patil and Pandit 2007; Cheng-Huang, Yeh et al. 2008). Microstreaming occurs as a result of cavitation and can be described as the high shear currents in the liquid that originate around oscillating gas bubbles in an acoustic field (Nyborg and Miller 1982; Wu, Ross et al. 2002; Dijkmans, Juffermans et al. 2004). There have been reports demonstrating that the shear stress created by microstreaming is correlated with sonoporation (Wu, Ross et al. 2002; Marcel, Alexander et al. 2009). Other reports suggest that the formation of free radicals, in particular H_2O_2, can cause sonoporation without impinging on cell viability (Juffermans, Dijkmans et al. 2006). The high temperatures produced during insonification, may modify the fluidity of the cell membrane, thus changing its permeability (Dijkmans, Juffermans et al. 2004). While it has been suggested that high temperatures may be a parameter of sonoporation, other reports detected changes in cell permeability in the absence of an increase in temperature (Miller, Pislaru et al. 2002; Duvshani-Eshet, Baruch et al. 2005). Mechanisms such as endocytosis and fusion of microbubble shell with the cell membrane have also been suggested (Dijkmans, Juffermans et al. 2004). Finally, an investigation using a high frame camera proposed that sonoporation occurs due to the mechanical force applied by oscillating microbubbles on the surface of the cells, thus putting forward stable cavitation as the basis for sonoporation (figure 4.3) (Van Wamel, Kooiman et al. 2006b).

4. 2 Targeting

Efficient delivery of the contents of a microbubble can be reinforced with the persistence of the microbubbles in the bloodstream and more specifically at the target area (Lindner and Sanjiv Kaul 2001). Radiation forces acting upon the microbubbles are able to displace them

towards the target area, thus increasing their concentration and in effect their contents' local concentration (Dayton, Klibanov et al. 1999; Ferrara, Pollard et al. 2007). Further direction can be achieved by targeting the microbubbles to the areas of interest. One of the tactics developed, is making use of the intrinsic electrostatic attributes of microbubbles (Lindner and Sanjiv Kaul 2001). However, as electrostatic bonds are not highly specific, other mechanisms have been developed, which are based on stronger chemical interactions (Ferrara, Pollard et al. 2007). These include adhering particular ligands or antibodies to the surface of the microbubble, which would then aim at specific surface markers embodied in the target cells (Lindner and Sanjiv Kaul 2001; Marcel, Alexander et al. 2009). While small molecules such as peptides and hormones can be incorporated within the microbubble shell during its preparation, larger and more unstable molecules such as antibodies are attached to a preassembled microbubble shell (Klibanov 2005; Ferrara, Pollard et al. 2007). The latter can be attained by attaching a biotinylated ligand with a biotinylated microbubble via an avidin link (figure 4.4) (Lindner and Sanjiv Kaul 2001; Klibanov 2005; Ferrara, Pollard et al. 2007). The avidin link is used in order to prevent binding between microbubbles (Klibanov 2005).

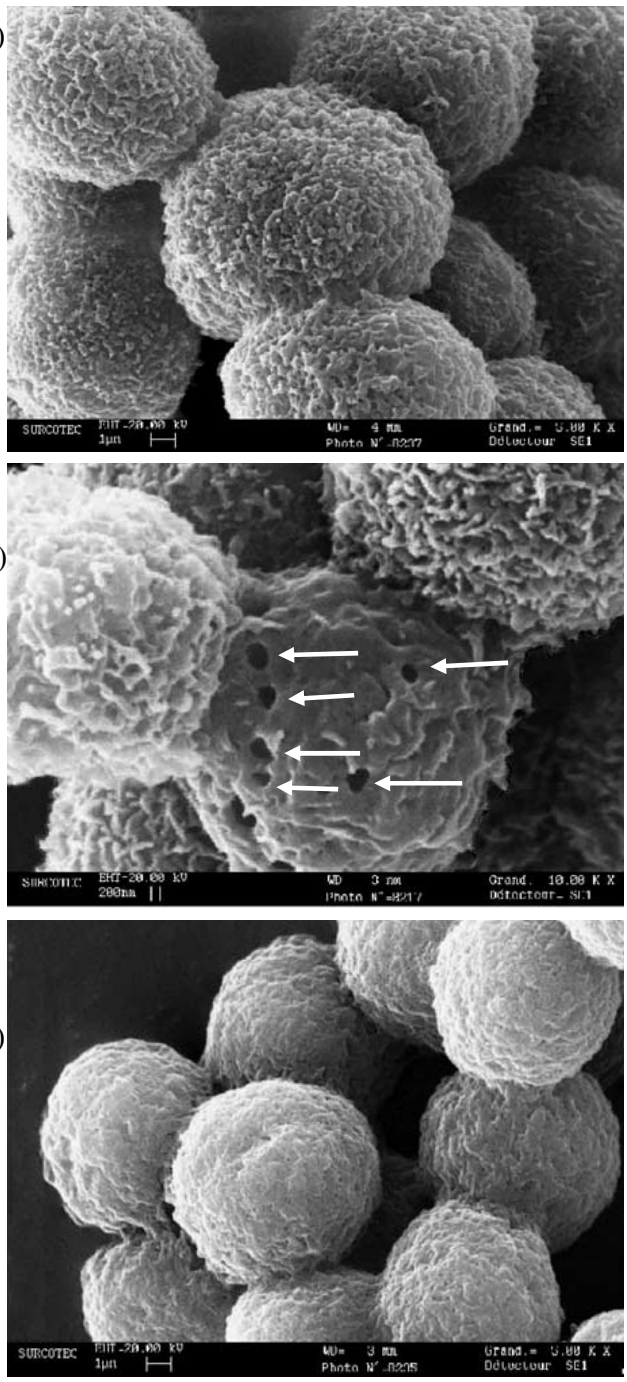

Figure 4.2 **Scanning electron microscopy micrographs.** SEM images of Rat mammary carcinoma cells (MAT B III). (a) Cell morphology before insonification (scale bar represent 1 µm). (b) Perforations formed during insonification are shown with arrows (scale bar represent 200 mm). (c) Cell morphology after insonification, were perforations have been sealed (scale bar represent 1 µm). Printed by permission Elsevier® (Mehier-Humbert, Bettinger et al. 2005a).

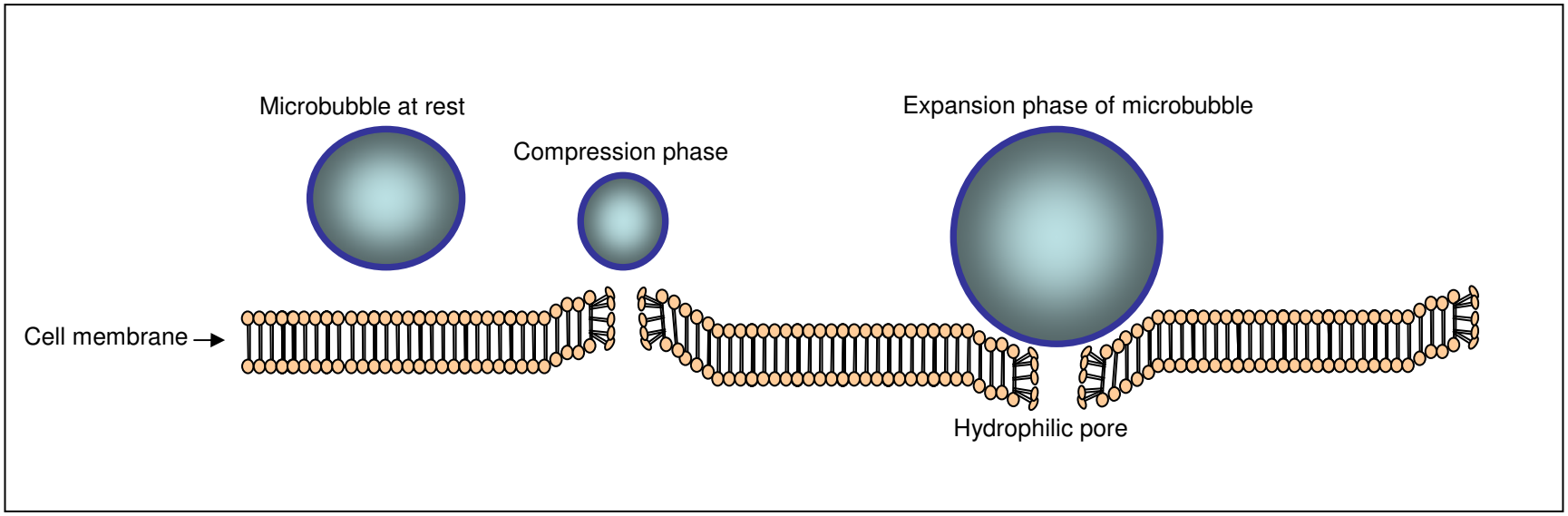

Figure 4.3 **Schematic diagram showing the proposed model for sonoporation.** During insonification, microbubbles experience cavitation, a cycle of expansion and contraction phases in response to the ultrasound waves present. During its expansion phase, the microbubble applies a mechanical force on the cell membrane which can lead to formation of pores on the cells membrane. Adapted from (Van Wamel, Kooiman et al. 2006b).

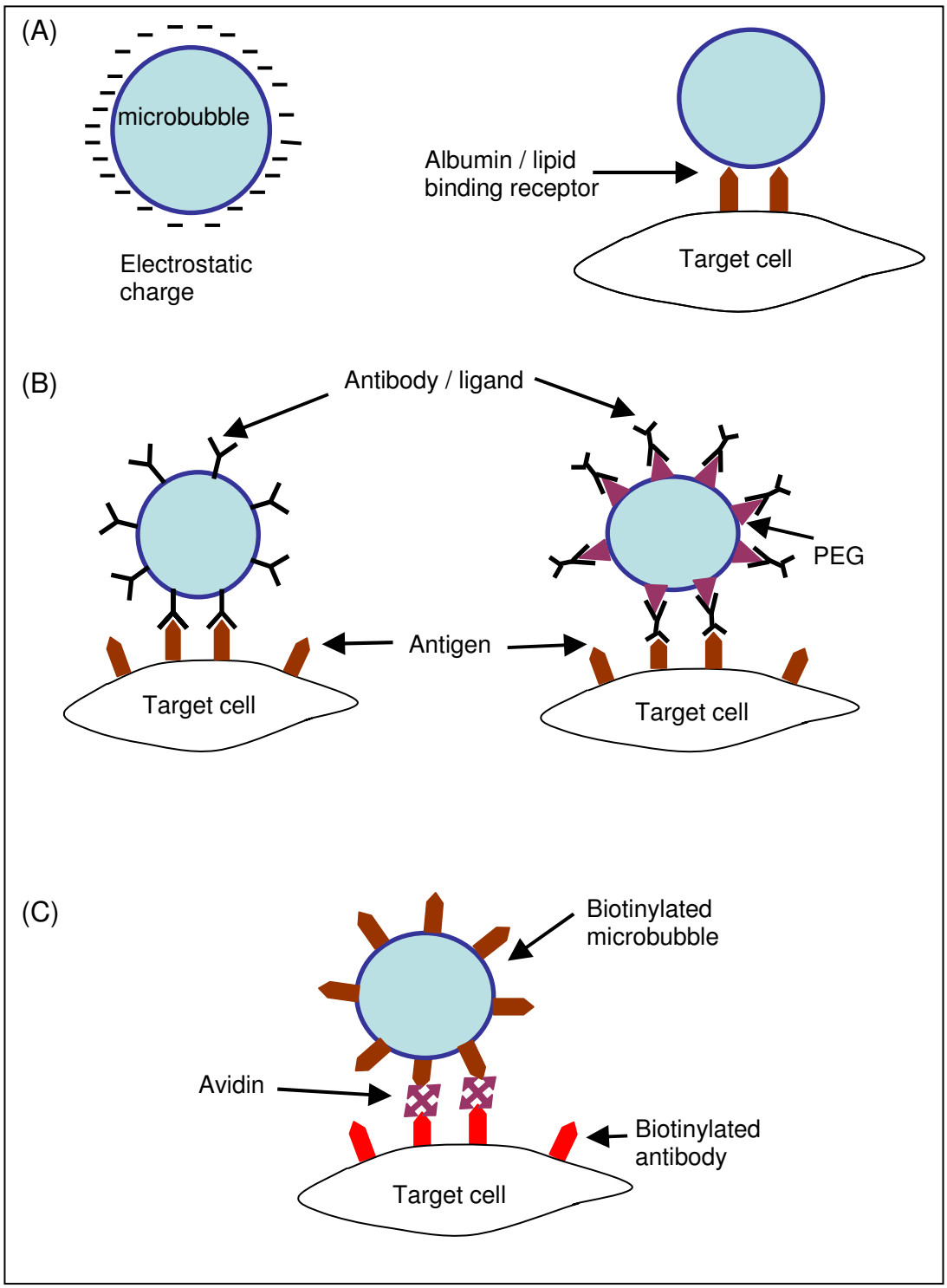

Figure 4.4 **Mechanisms for attaching microbubbles to targets cells**. (a) Microbubbles can be attached to target cells via electrostatic interactions. (b) Microbubbles containing a ligand on the outer surface of their shell can attach to target cells via antibody-antigen interactions with the aid of polyethylene glycol (PEG). (c) For unstable molecules, such binding can also take place with the aid of an avidin linker molecule. Adapted from (Lindner and Sanjiv Kaul 2001).

Chapter 5

Introduction

Microscopy

5.0 Microscopy

Conventional microscopy is a useful tool for visualising biological samples. However, a few obstacles emerge with the use of conventional fluorescence microscopy that limit the quality of the images acquired. Fluorescence microscopy images are often accompanied by an out of focal flare. This phenomenon is due to the presence of scattered light from objects not in the focal plane (McNally, Karpova et al. 1999; Piston 1999; Cahalan, Parker et al. 2002). Furthermore, the high numerical aperture objective lenses employed for conventional fluorescence microscopy limit the depth of image field. Finally, the prolonged use of excitation light when examining living specimens, can cause photodamage to the cells and bleach the fluorescent dye (McNally, Karpova et al. 1999; Cahalan, Parker et al. 2002). Confocal microscopy provided a partial solution to this problem. It has an advantage over conventional fluorescent microscopy in that a pinhole is placed in front of the detector. This pinhole allows the collection of excitation light from the focal plane while concurrently rejecting any out of focus light coming from below or above the focal plane (McNally, Karpova et al. 1999; Piston 1999; Cahalan, Parker et al. 2002). Confocal microscopy can, therefore, be used for 3 dimensional (3D) reconstruction of a sample by acquiring a series of optical slices along the z axis (Cahalan, Parker et al. 2002), while precluding any bleaching of the fluorescent dyes.

5.1 Deconvolution

Any image obtained by microscopy is distorted compared to the original object. Deconvolution, is an image data restoration technique that has been developed in order to characterise the distortion and restore an image to its original object (McNally, Karpova et al. 1999). Deconvolution can be applied to any microscope data, although a wide field or bright

microscope would produce an image with greater distortion than that of a confocal microscope. Deconvolution methods attempt to establish the amount of light that is expected to be acquired from out of focus plane and then attempt to reallocate this light back to its points of origin in the sample (McNally, Karpova et al. 1999). The out of focus light calculation is based on the 2D image of a point of source of light, accordingly named point spread function (PSF). The PSF can be determined both theoretically and experimentally. For a PSF to be calculated theoretically specific information must be provided, such as the numerical aperture of the objective lens, working distance of the objective lens, wavelength of the emitted light, XYZ dimensions of the PSF, size of pixel, spacing between Z slices and refractive index of the immersion medium (McNally, Karpova et al. 1999). A number of commercially available software packages are then able to determine the theoretical PSF. The experimental PSF can be determined with the use of a fluorescent microsphere of known size, ideally of diameter one third of the resolution size limit expected (McNally, Karpova et al. 1999). A 3D image should be acquired using the same parameters as for the real sample. Once the experimental PSF has been obtained, 3D images of the sample can also be acquired and then undergo deconvolution in order to restore the original sample. The final product should be an object with sharper edges than that of the initial image.

5.2 Two-photon microscopy

Although confocal microscopy rejects any excitation light derived from out of focus plane, laser light is still emitted both above and below the focal plane, consequently, even though large regions of the sample are not being visualised; they are still predisposed to photodamage (Piston 1999). Therefore, confocal microscopy is still limited for long-term imaging of living

specimens. Maria Goppert-Mayer was first to introduce the concept of two photon excitation in her doctoral presentation in 1931 (Goppert-Mayer 1931, German). Two photon microscopy offers similar 3D resolution as confocal microscopy, in addition to providing an even deeper image field, as much as two to three times deeper, and negligible photodamage and photobleaching (Piston 1999; Cahalan, Parker et al. 2002). Two-photon microscopy is based on the physical principle that the energy of a photon is inversely proportional to its wavelength (λ) (Piston 1999). Therefore, a single photon, of a specific wavelength should result in the same fluorescent emission as two photons of twice the wavelength. For example, a fluorophore that normally absorbs light at 350 nm can also be excited by two photons at 700 nm. Since this principle is valid only if two photons are absorbed simultaneously, that is within 10^{-18} seconds from each other, fluorescent emission is enhanced in proportion to the square of the excitation intensity (Cahalan, Parker et al. 2002). In other words, the probability to obtain two absorption events at any one time is equal to the product of individual probabilities of obtaining a single photon absorption event (figure 5.1). Thus for very improbable events, the probabilities improve as the number of single events increases. Such an approach can be achieved by sending the photons in batches, i.e. using pulsed beams (White and Errington 2005). Pulse lasers send a high peak power beam for every 80 femtoseconds wide, with a repetition rate of 80 MHz, thus increasing the photon density for a limited amount of time while keeping the average laser power lower than that of the conventional laser. The probability of generating considerable amount of two photon absorption events is very high only at the focal point, whereas it drops to nearly zero at distances less than 1 μm above or below the focal point (Piston 1999; Cahalan, Parker et al. 2002). Since excitation in two-

photon microscopy is confined exclusively to the focal point, the presence of a pinhole is no longer required. The Titanium Sapphire femtosecond laser is the most commonly used pulse laser system, providing pulses of wavelengths λ=700 to 1000 nm (Cahalan, Parker et al. 2002).

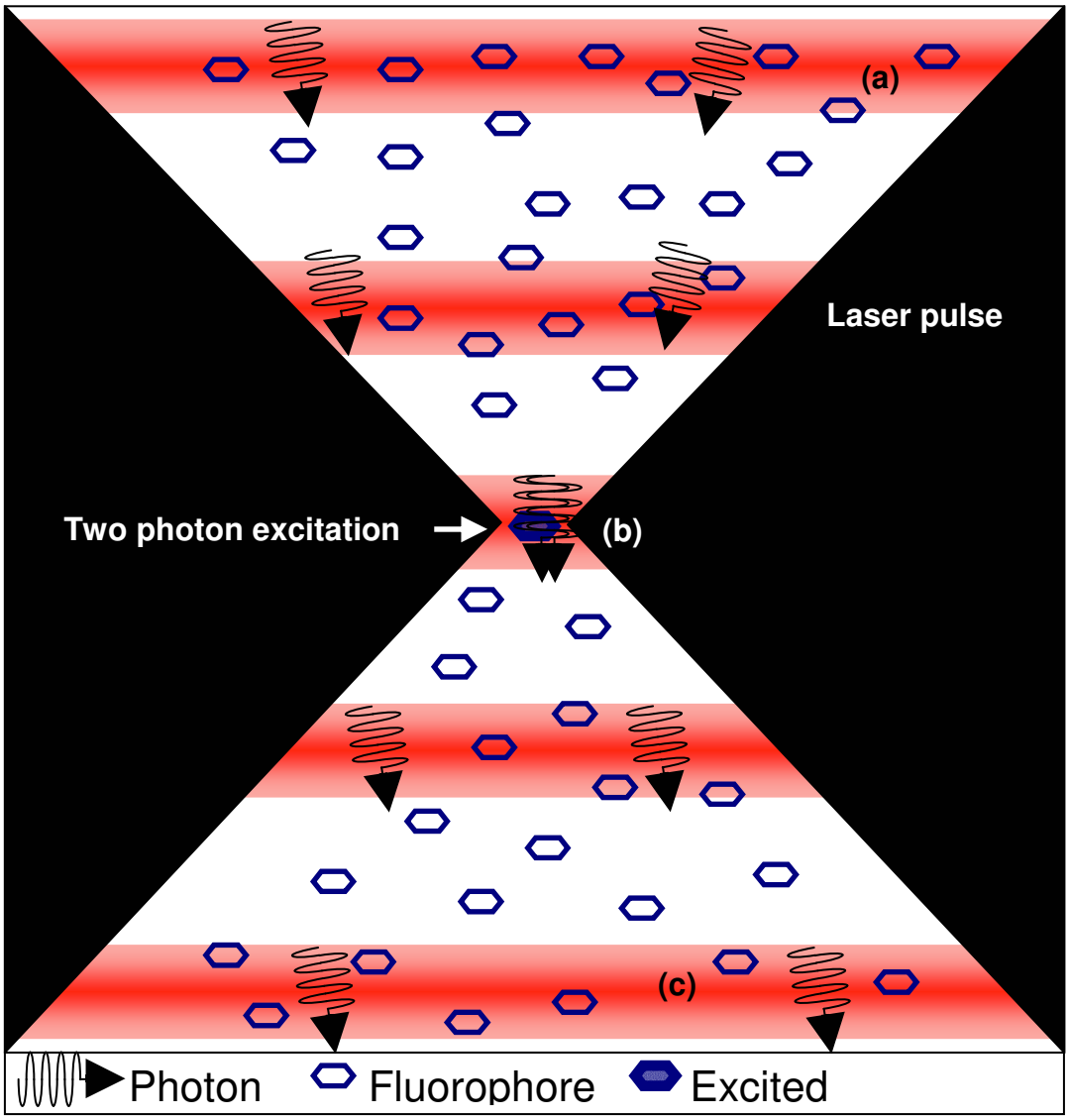

Figure 5.1 **Two photon microscopy**. The probability of generating a two photon event falls to nearly zero outside the focal point (a) & (c). However, it is feasible at the focal point due to the high photo density (b). Thus, exciting the fluorophores (blue hexagon) only at the focal point prevents prolonged exposure of sample to laser light, thus minimising photodamage. Adapted from (Piston 1999).

Chapter 6

Introduction

Cellular responses

6.0 Cellular responses

6.1 Stress response

Ritossa (1962) was the first to observe that an elevation in temperature above physiological levels leads to upregulation of certain genes, which in turn results in expression of a number of proteins. It was later comprehended that in addition to elevated temperatures, a number of other environmental stresses, such as UV radiation, hypoxia, heavy metals, radiation, glucose deprivation, environmental pollutants, inflammation and virus infection could also provoke production of these proteins (Santoro 2000; Robert 2003; Horvath, Multhoff et al. 2008). Although these proteins have vital functions during non stressful settings, they have been termed heat shock proteins due to the circumstances in which they were first discovered (Benjamin and McMillan 1998). Heat shock proteins serve as a protective mechanism against stimuli that attempt to shift cell homeostasis (Santoro 2000). The term stress response was thus conceived in order to describe cell reaction to stressful stimuli. Stress response is universal and the proteins produced are highly conserved (Lindquist 1986).

6.1.1 Heat shock proteins

Although heat shock proteins are also referred to as stress proteins, the later term also includes glucose regulated proteins and ubiquitin (Moseley 2000). Heat shock proteins are classified in six groups in accordance to their molecular weights (Sontag and Kruglikov 2009). The most abundant heat shock proteins are Hsp40, Hsp60, Hsp70, and Hsp90. Heat shock proteins are also termed molecular chaperones, since they play an important role in assisting in protein folding and in preventing aggregation of denatured proteins (Benjamin and McMillan 1998; Walther and Stein 2009). A large number of diseases have been associated with misfolding or

aggregation of proteins due to malfunction of heat shock proteins, including, Alzheimer's, Parkinson's and Huntington's disease diseases (Broadley and Hartl 2009). Heat shock proteins also have several other functions, including regulating apoptotic events and engaging in antigen formation (Horvath, Multhoff et al. 2008). Heat shock proteins are found in all intracellular compartments of a cell, while some are constitutively expressed whereas others are stressed inducible (Robert 2003). However, expression of heat shock proteins is upregulated, even those that are constitutively expressed (Robert 2003). Heat shock proteins have also been found in the extracellular environment, were they are believed to regulate immunity (Multhoff 2007). Under normal physiological conditions, heat shock proteins are expressed in low levels in the cytoplasm and are attached to a set of proteins termed heat shock factors (Kiang and Tsokos 1998). When cells experience a stressful stimulus, heat shock proteins release heat shock factors, which are then phosphorylated, trimerised and translocated into the nucleus, where they promote heat shock protein expression by binding on promoter regions of the heat shock factor genes (Kiang and Tsokos 1998). Newly manufactured heat shock proteins act as a self inhibitory mechanism by binding to heat shock factors, thus repressing further production of heat shock proteins (figure 6.1) (Kiang and Tsokos 1998).

6.1.2 Heat shock protein 70

Heat shock protein 70 (Hsp70) is one if the best characterized families of heat shock proteins. Its structure is found to be highly conserved throughout evolution, thus signifying its vital role for cell survival (Santoro 2000). Hsp70 proteins perform a range of chaperone functions, including stabilizing unfolded proteins, transferring proteins between intracellular departments, assisting in protein folding and preventing formation of

protein aggregates (Becker and Craig 1994). The Hsp70 family encodes for heat shock proteins that are both constitutively expressed (Hsc70) or are induced upon stressful environmental conditions (Hsp70, Hsp72) (Santoro 2000). All proteins belonging to the Hsp70 family are composed of two conserved domains, an N-terminal and a C-terminal domain, that bind to ATP and to target proteins respectively (Benjamin and McMillan 1998; Robert 2003).

6.1.3 Heme oxygenase-1

Heme oxygenase-1 (HO-1) also known as heat shock protein 32 (Hsp32) is a stress protein. Its expression is induced in the presence of environmental stresses such as hypoxia, UV light, heavy metals and hydrogen peroxide (Benjamin and McMillan 1998; Otterbein and Choi 2000). Although termed a heat shock protein, its expression is not linked with hyperthermia, yet its name was attributed due to its expression during elevated temperatures in the rat (Morse and Choi 2005). HO-1 has been shown to be involved with degradation of heme, thus releasing carbon monoxide, free iron and biliverdin (Morse and Choi 2005). The latter is then converted to bilirubin (figure 6.2). All the products of this reaction fulfil essential cellular functions, for example carbon monoxide is a effective second messenger, biliverdin and bilirubin are antioxidants, while iron regulates oxidative stress levels (Morse and Choi 2005; Sontag and Kruglikov 2009). Over-expression of HO-1 has been associated with several human disorders including hypertension, arteriosclerosis and acute renal failure (Sontag and Kruglikov 2009). Although there are three isoforms of heme oxygenase, only HO-1 is inducible by stressful stimuli, while HO-2 and HO-3 are constitutively expressed (Otterbein and Choi 2000). In addition, the high

conservation of HO-1 molecules amongst distinct species, serves as an indicator to its vital role in cell survival (Morse and Choi 2005).

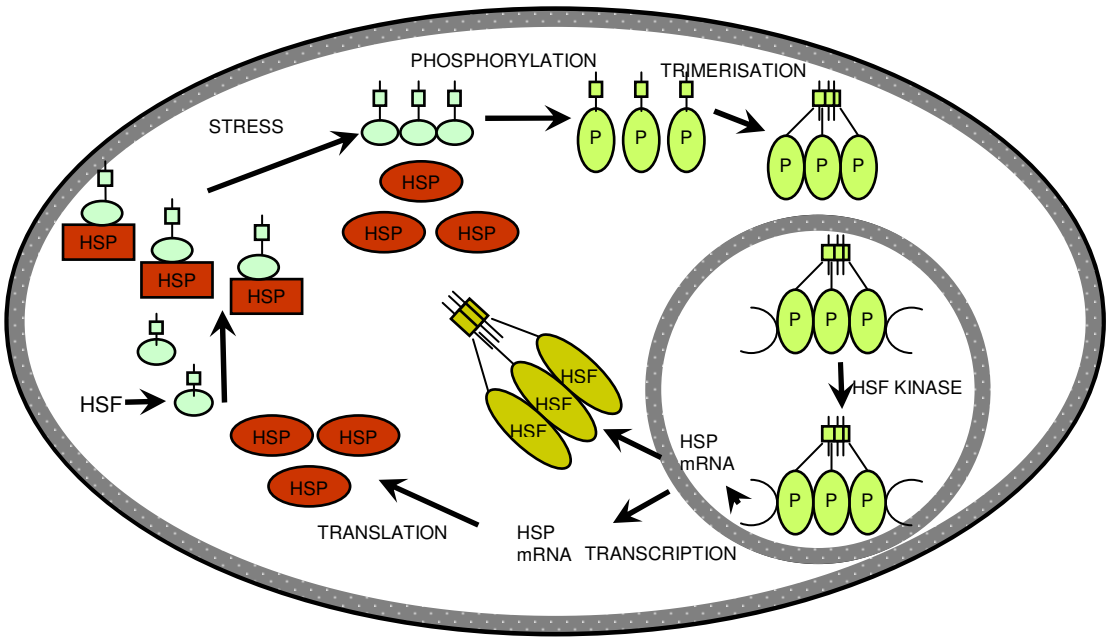

Figure 6.1 **Mechanism of heat shock protein induction in humans.** Heat shock protein factor (HSF) is found in the cytosol, bound by a heat shock protein (HSP). Upon application of a stress stimulus, HSPs disassociate from the HSFs, who are then phosphorylated and trimerized, prior to entering the nuclear compartment. In the nucleus, HSFs bind to the promoter region of the HSPs, thus initiating their transcription. Newly synthesized HSPs translocate to the cytosol where they inhibit further production of HSP molecules by binding to HSFs. Printed by permission Elsevier® (Kiang and Tsokos 1998).

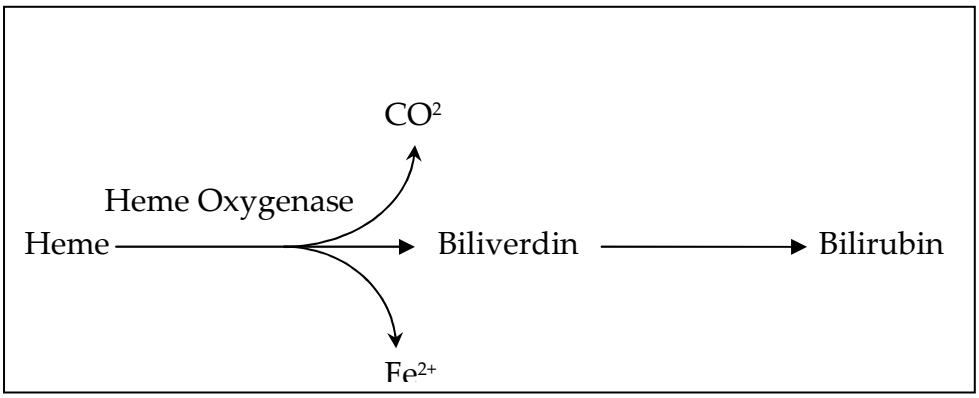

Figure 6.2 **Heme oxygenase reaction.** Heme degradation into Biliverdin, carbon monoxide and free iron is catalysed by heme oxygenase. Adapted from (Morse and Choi 2005).

Chapter 7

Materials and methods

7.0 Materials and methods

7.1 Microbubble techniques

7.1.1 Preparation of in-house microbubbles

The constituent materials (Table 7.1) were placed in a glass flask and 4 ml of 0.9 % (v/v) saline were added into the flask for every 100 mg of lipid mixture made. The lipid mixture was then allowed to hydrate at room temperature for 2 hours while stirring continuously. The flask was then placed in a heating bath and heated at 70-80 °C for 1 hour while stirring continuously. A condenser was fitted to prevent evaporation. The mixture was then removed from the heating bath and allowed to return to room temperature with continuous stirring for 16-24 hours.

Constituents	PC	CHOL	PE	PG
Amount	56 mg	30mg	11 mg	3 mg

Table 7.1 **Constituent materials of in-house microbubbles.** Quantities of constituents are per 4 ml of saline. PC= Phosphatidyl Choline (Sigma Aldrich Company Ltd), CHOL= Cholesterol (Sigma Aldrich Company Ltd), PE= Phosphatidylethanolamine (Sigma Aldrich Company Ltd), PG= Phosphatidyl Glycerol (Sigma Aldrich Company Ltd).

7.1.2 Commercial microbubbles

The commercial microbubbles used for the purposes of some experiments were Definity® (Bristol-Myers Squibb).

7.1.3 Sizing of microbubbles

Both commercial and in-house microbubbles were fed through a LS230 coulter counter (Beckman) in order to obtain a size distribution graph. Two latex beads differing in diameter were used in order to confirm the minimum and maximum ranges of the coulter counter. The latex beads used were P.V.T. latex (Coulter electronics Ltd) and Nanosphere™ size standards (Duke scientific corporation) with a diameter of 2 μm and 300 nm respectively.

7.1.4 In-house microbubble counting

The concentration of in-house microbubbles was determined with a haemocytometer. An aliquot of a 1 in 100 dilution of in-house microbubble solution was mixed with 4 % (w/v) Trypan blue providing a 1 in 2 dilution. The solution was placed in a counting chamber of a haemocytometer and viewed under the microscope. The number of microbubbles within all 4 squares present in the haemocytometer is counted. This is then divided by 4 in order to provide an average count. In order to calculate the concentration of microbubbles within the sample, an equation is applied that takes into consideration the dilution factor, the area of each square on the haemocytometer and total volume of the microbubble suspension. The equation is as follows: Number of in-house microbubbles per ml = (total count of in-house microbubbles / 4) * dilution factor * 10^4 * volume of suspension.

7.1.5 Density Gradient Centrifugation

1 ml of in-house microbubbles was placed at the bottom of a centrifuge tube. Different densities of 2 ml Nycoprep (Axis-Shield) were stacked on top of each other, ranging from 50 %, 30 %, 20 %, 10 % and 5 %

(figure 7.1). Samples were then centrifuged at a Beckman L8-55 ultracentrifuge using a SW42 swing rotor, at 30,000 rpm for 30 min. Each fraction was collected at the end of the centrifugation with the use of a pipette and visualised using CLSM.

7.1.6 Microbubble sorting

Crude and fractionated in-house microbubble samples were taken for cell sorting. Crude samples correspond to the original in-house microbubble samples produced without any further manipulations. Cell sorting was performed by a FACS Vantage SE cell sorter, equipped with a dual output 351 nm / 488 nm laser and a 633 nm laser, using FACSDiva software (Becton Dickinson) at the Centre of Inflammation Research, Little France, Edinburgh, UK.

7.2 Microscope techniques

7.2.1 Immunofluorescence

The in-house microbubble preparation was diluted 1 in 1000. A drop of the diluted sample was placed on a 9 mm coverslip and then placed in the microscope chamber. 1 μl of 1 mM FM 1-43 (Invitrogen) dye was added to the drop of microbubbles. Fluorescence of FM 14-3 was measured at 488 nm, with a long pass (LP) at 505 nm on a Zeiss LSM 510 inverted microscope.

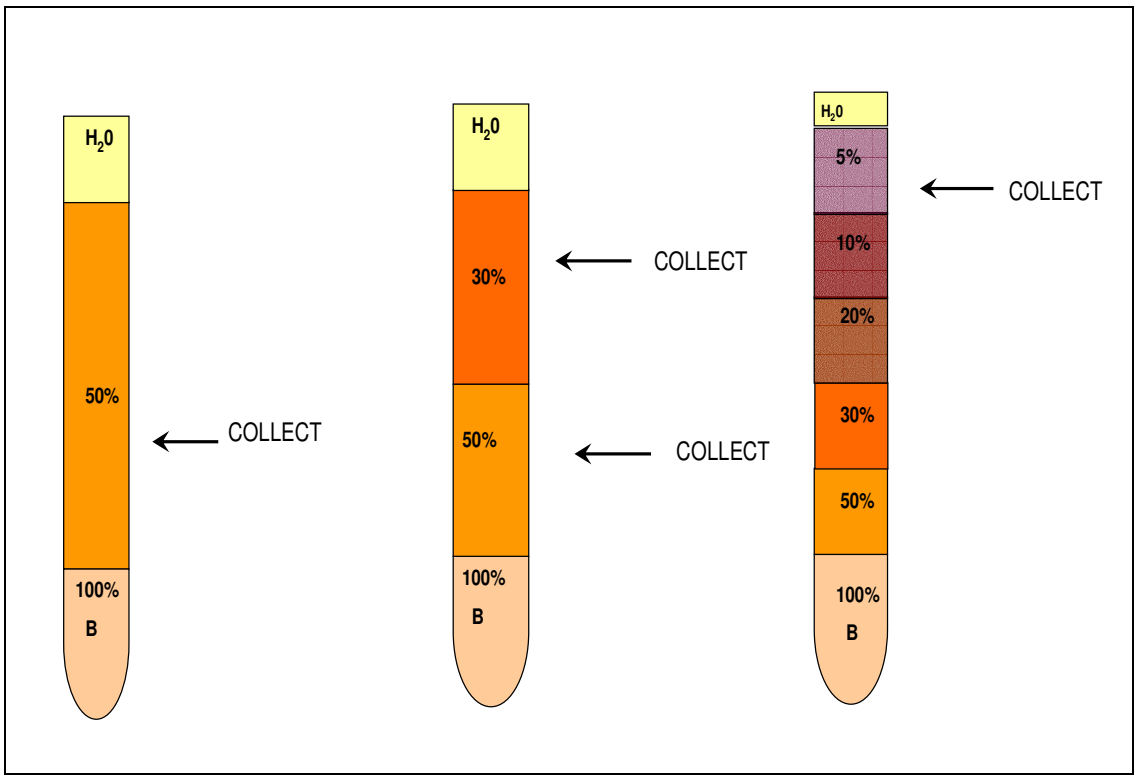

Figure 7.1 **Nycoprep separation.** Microbubble preparations were mixed with different densities of Nycoprep solution and placed on top of each other in a centrifuge tube. The densities of Nycoprep used were 50 %, 30 %, 20 %, 10 % and 5 %. The top fraction of each tube was collected using a pipette and the microbubbles in that fraction were imaged under a microscope.

7.2.2 Confocal microscopy

Confocal microscopy images were obtained by using a Zeiss LSM 510 inverted microscope, which equipped with four types of lasers, 488 nm Argon, 543 nm and 633 nm He-Ne and a MIRA NIR pulsed Titanium Sapphire multiphoton laser. Parameters such as detector gain, laser power and scan zoom were adjusted so as to acquire data within the dynamic range of the instrument. All live cell imaging was conducted in the microscope at 37 °C, 5 % (v/v) CO_2 and 95 % (v/v) air.

7.2.3 Imaging processing and analysis

The data collected from the microscope were deconvoluted using the Huygens II package (Scientific Volume Imaging, Netherlands) to remove the out-of-focus haze, which is characterized by the microscope's point spread function (PSF). The PSF, optical aberration and threshold levels were determined in advance using 200 nm and 15 nm diameter fluorescent latex beads (490 nm excitation / 517 nm emission; Molecular Probes). Image data were analysed using the Volocity software package (Improvision, Coventry), which allows visualisation and manipulation of image data. Therefore, 3D data describing each microbubble underwent a series of algorithms in order to reconstruct a 3D image. Further manipulation of these images provided essential information such as diameter, volume and surface area of in-house microbubbles.

7.2.4 Cell viability assay

Cells were seeded in 60 mm Petri dishes containing sterile 9 mm coverslips. This permitted the transfer of cells adhered to the coverslip to the microscope chamber. Several densities were seeded ranging from 2×10^5 to 1×10^6 cells / ml. 24 hours after seeding, the coverslips were transferred into

microscope chambers and covered with 1 ml of DMEM (Gibco BRL). 3 μl of 1 mM Propidium Iodide (Molecular Probes) and 3 μl of 1 mM Calcein AM (Molecular Probes) were added into the chamber. Calcein AM is a molecule that transverses the plasma membrane, where it is hydrolysed by intracellular esterases in order to emit a green fluorescence. Propidium iodide is a red fluorescent molecule that cannot transverse the plasma membrane, unless it has been compromised, thus staining cells which are dead or whose membrane has been compromised. The fluorescence of Calcein AM and Propidium Iodide were measured at 488-543 nm. The number of live (Calcein positive) and dead (Propidium Iodide positive) cells within each image was measured with the aid of Imaris software package (Bitplane AG, Zurich). Imaris software allows visualisation of images and identification of objects within images, based on several parameters, such as morphology, intensity and size. The total number of live and dead cells within each image of interest was counted automatically according to size. The figures collected were then used to determine cell viability, which was calculated as the number of viable cells divided by the total number of cells present (live and dead) and expressed as a percentage.

7.2.5 Cell / microbubble toxicity assay

Cells were seeded in 60 mm Petri dishes containing sterile 9 mm coverslips at a density of 2 x 10^5 cells / ml. After 24 hours, 300 μl of in-house microbubble preparations, either in PBS or saline, were added to the cells. Cells were then examined using a CLSM after 1-48 hours. 3 μl of 1 mM Propidium Iodide and 3 μl of 1 mM Calcein AM were added into 1 ml of DMEM in the microscope chamber. The fluorescence of Calcein AM and Propidium Iodide were measured at 488-543 nm. Data collected were analysed using Imaris software package (Bitplane AG, Zurich).

7.3 Mammalian cell culture

7.3.1 Mammalian cells

All mammalian cells used in this study (European Collection of Animal Cell Cultures, Public Health Laboratory Service Centre for Applied Microbiology and Research, Porton Down, UK) were cultured in DMEM (Gibco BRL) supplemented with 10 % (v/v) foetal calf serum (Gibco BRL), 1 % (v/v) penicillin / streptomycin (Gibco BRL) and 1 % (v/v) L-glutamate (Gibco BRL). Passage of cells was prepared by removing the media washing the cells with PBS. 1 ml/75 cm^2 of trypsin-EDTA was added to the cells and was incubated was 1-3 min at 37 ºC. The cells were then collected from the dish with DMEM. Cells were cultured at 37 °C in 5 % (v/v) CO_2, 95 % (v/v) air and used between passage numbers 1 and 20.

7.3.2 Cell counting

The concentration of cells of interest was determined with a haemocytometer. An aliquot of cell suspension was mixed with 4 % (w/v) Trypan blue providing a 1 in 2 dilution. The solution was placed in a counting chamber of a haemocytometer and viewed under the microscope. The number of cells within all 4 squares present in the haemocytometer is counted. This is then divided by 4 in order to provide an average count. In order to calculate the cell concentration within the sample, an equation is applied that takes into consideration the dilution factor, the area of each square on the haemocytometer and total volume of the cell suspension. The equation is as follows: cell concentration (cells / ml) = (total count of cells / 4) * dilution factor * 10^4 * volume of suspension.

7.3.3 Transfection of mammalian cells

SK Hep-1 cells were transfected with pCS2 plasmid (figure 7.2) using ExGen 500 (Fermentas Life Sciences) and the manufacturer's protocol was followed. Cells to be transfected were cultured in six well tissue culture dishes and examined with a FACSCalibur analytical flow cytometer (Bector Dickinson) 24 hours after transfection.

7.4 Flow cytometry techniques

7.4.1 Examining cell viability assay

Cells were trypsinised immediately after ultrasound exposure in order to detect the effect of ultrasound waves on cell viability. Calcein AM and Propidium Iodide were used in order to detect live and dead cells respectively. A cell suspension containing SK Hep-1 (human hepatocarcinoma) cells exposed to ultrasound waves was passed through a FACSCalibur analytical flow cytometer (Bector Dickinson). The fluorescence of Calcein AM and Propidium Iodide was detected by the FACSCalibur and cells were assessed as positive / negative for Calcein AM and / or Propidium Iodide.

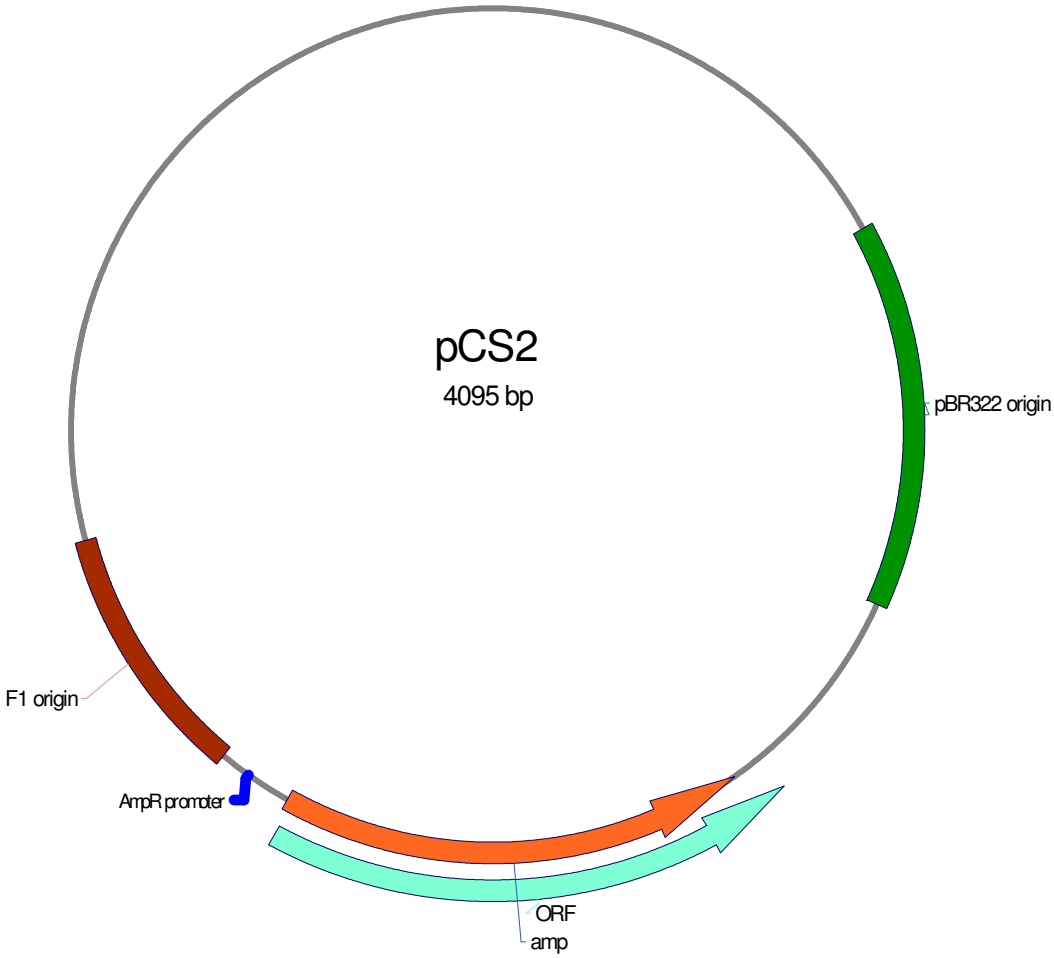

Figure 7.2 **PCS2 plasmid map**. Schematic representation of pCS2 plasmid used for acquiring DNA delivery in to cells during sonoporation and subsequent expression of genes of interest.

7.4.2 Examining for sonoporation

Cells were trypsinised immediately after ultrasound exposure in the presence or absence of microbubbles and / or enhanced green fluorescent protein (EGFP), in order to detect sonoporation. Cell impermeable Calcein or EGFP were used in order to detect transfer of these molecules into the cells through pores formed during ultrasound exposure (sonoporation). These specific molecules were used as they differ enormously in size and would perhaps provide an indication of pore size. Propidium Iodide was used in order to detect dead cells. A cell suspension of the cells exposed to ultrasound waves was passed through a FACSCalibur analytical flow cytometer (Bector Dickinson). The fluorescence of cell impermeable Calcein or EGFP and Propidium Iodide were detected by the FACSCalibur and cells. were assessed as positive / negative for cell impermeable Calcein or EGFP and Propidium Iodide respectively.

7.4.3 Examining gene expression

Cells were trypsinised 24 hrs and / or 48 hrs after ultrasound exposure in the presence or absence of microbubbles and plasmid DNA pCS2 (Centre of Cardiovascular Sciences, Little France, Edinburgh). The pCS2 plasmid contains the gene encoding EGFP. This experiment was performed in order to detect pCS2 delivery into the cells and subsequent expression of EGFP in the cells. The fluorescence of EGFP and Propidium Iodide were used in order to detect gene expression and dead cells respectively. A cell suspension of the cells exposed to ultrasound waves was passed through a FACSCalibur analytical flow cytometer. The fluorescence of EGFP and Propidium Iodide were detected by the FACSCalibur and cells were assessed as positive / negative for EGFP and / or Propidium Iodide.

7.5 Ultrasound techniques

7.5.1 Ultrasound equipment

7.5.1.1 "Physiotherapy machine"

The aim of this experiment was to calibrate the waveforms emitted by the physiotherapy machine, using a right angled PZT needle hydrophone-type NP10-390A (Dapco Inc). The signal emitted by the "physiotherapy machine" was captured by a Tektronix 2211 digital storage oscilloscope. In addition it was essential to calibrate the actual head size of the transducer, in order to be able to calculate the actual power emitted by the scanner accurately. Nominal measurements of the intensities and the head size values are provided by the manufacturer but do not always correspond to reality. We attempted to calculate the actual values and compare them to the nominal values so as to make sure that the scanner was providing adequate amounts of power for future use in our experiments.

A balance was used in order to calculate the intensity of the ultrasound waves emitted by the "physiotherapy machine". As the waves hit an absorbable object, the object becomes heavier. This change in weight could then be interpreted into power (Watts). It is also known that an increase in weight of 69 mg = 1 Watt of power. While measuring the change in weight the fact that the absorbable object became more buoyant as it absorbed the ultrasound waves, had to be taken into consideration. So the weight of the object was noted a few seconds after applying the ultrasound waves and just after turning the ultrasound scanner off. This provided a negative number that corresponded to the buoyancy of the object due to its absorbance of ultrasound waves. We then added the two figures in order to calculate the actual weight change.

Several different intensities were examined on the "physiotherapy machine" ranging from 0.5, 1.0, 1.5, 2.0, 2.5 W / cm^2 and at different

frequencies (1 MHz & 3 MHz). The nominal power was calculated in Watts by multiplying the nominal intensities with the nominal head size which is 4.42 cm^2 at 1 MHz and 3.67 cm^2 at 3 MHz. Multiplying the nominal power with 69 mg provided the nominal weight change expected. Actual weight changes were recorded and transformed to actual power by dividing with 69 mg. Actual intensity was calculated by dividing with the actual head size which is 3.68 for both 1 MHz and 3 MHz calculated in W / cm^2 (table 7.2). The hydrophone was used in order to calculate the actual head size of the transducer. Several apertures of different diameters ranging from 6 mm to 30 mm while keeping the intensity and frequency constant at 1.0 W / cm^2 and 1 MHz / 3 MHz.

7.5.1.2 Ultrasound scanners

Ultrasound experiments were conducted with a Therasonic 1032 ultrasound scanner (Electro-Medical supplies), using a range of intensities from 0.01-2.54 W / cm^2 at a frequency of 1 or 3 MHz. A number of experiments were also conducted with either a Sono 5500 (Hewlett Packard) or an ATL ultrasound B-mode scanner DHI3500 (Philips) operating at a frequency between 1 and 2 MHz and 2 to 4 MHz respectively. The transducer used with Sono 5500 was a phased array S3 (33 MHz) (Philips Medical Systems, Andover), while the transducer used with DHI3500 was P4-2 phased transducer (2-4 MHz) (Philips Medical Systems, Andover).

The waveforms emitted by the ultrasound scanners used in this study were examined with the aid of a membrane hydrophone with a 0.4 mm active element (Precision Acoustics). The signal emitted by the scanners was captured by a Tektronix 2211 digital storage oscilloscope, calibrated by the National Physics Laboratory in 2007. The peak to peak pressures of the ultrasound wave were calculated by measuring a range of acoustic powers.

Nominal Intensity (W/ cm^2)	Nominal Power (W)	Nominal weight change (mgs)	Actual weight change (mgs)	Actual Power (W)	Actual Intensity (W/ cm^2)
1MHz					
0.5	2.21	152.49	230.25	3.34	0.91
1	4.42	304.98	452	6.55	1.78
1.5	6.63	457.47	659	9.55	2.60
2	8.84	609.96	867.5	12.57	3.42
2.5	11.05	762.45	1028	14.90	4.05
3 MHz					
0.5	1.83	126.61	166	2.41	0.65
1	3.67	253.23	372	5.39	1.47
1.5	5.50	379.84	590	8.55	2.32
2	7.34	506.46	839.5	12.17	3.31
2.5	9.17	633.07	1056.5	15.31	4.16

Table 7.2 **Calculation of power output of physiotherapy machine**. Nominal power was calculated by multiplying the nominal intensities with the nominal head size which is 4.42 cm^2 at 1 MHz and 3.67 cm^2 at 3 MHz. Multiplying the nominal power with 69 mgs provided the nominal weight change expected in mgs. Actual weight changes recorded were transformed to actual power output by dividing with 69 mgs. Actual intensity was calculated by dividing with the actual head size which is 3.68 for both 1 MHz and 3MHz.

7.5.2 Ultrasound investigations

7.5.2.1 Bench-Petri Dish set up

Initial experiments involved the application of ultrasound on cells attached to a 60 mm Petri dish. The dish was then placed on the microscope stage and an image of the cells was acquired. The fluorescence of Calcein AM and Propidium Iodide were measured at 488-543 nm. The dish was then transferred onto the bench were ultrasound waves were applied. The probe of the scanner was submerged in the cell media and was held by hand at a 90° angle for the required length of time. The dish was then returned on to

the microscope stage in order to re-examine the original field of view. Data collected were analyzed using Imaris software package (Bitplane AG).

7.5.2.1.1 Investigations of cell viability in the absence of microbubbles

Cells were seeded in 60 mm Petri dishes at a density of 2 x 10^5 cells / ml. 24 hours after seeding; 3 µl of 1 mM Calcein AM and 3µl of 1mM Propidium Iodide (Molecular probes) were added into the Petri dish. The dish was then transferred on to the bench for application of ultrasound. Images of the cells were taken before and after application of ultrasound waves using a Leica DMIRB inverted microscope. Furthermore, a cross was drawn with a marker pen at the bottom of the Petri dish in order to be able to return the dish to the same field of view following any movement (figure 7.3). The fluorescence of Calcein AM and Propidium Iodide were measured at 488-543 nm. Data collected was analyzed using Imaris software package (Bitplane AG).

7.5.2.1.2 Investigations of cell viability in the presence of microbubbles

Cells were seeded in 60 mm Petri dishes at a density of 2 x 10^5 cells / ml. 24 hours after seeding, 5 different concentrations (12.5 µl, 25 µl, 50 µl, 75 µl) of 1.2 x 10^{10} Definity® microbubbles / ml were added into the Petri dish in addition to 3 µl of 1 mM Calcein AM and 3 µl of 11 mM Propidium Iodide (Molecular probes). Furthermore, each area exposed to ultrasound waves was marked. Smaller areas within the marked area, corresponding to the field of view of the microscope were also marked at the bottom of the Petri dish in order to be able to return the dish to the same field of view following any movement (figure 7.3). The dish was then transferred on to the bench for

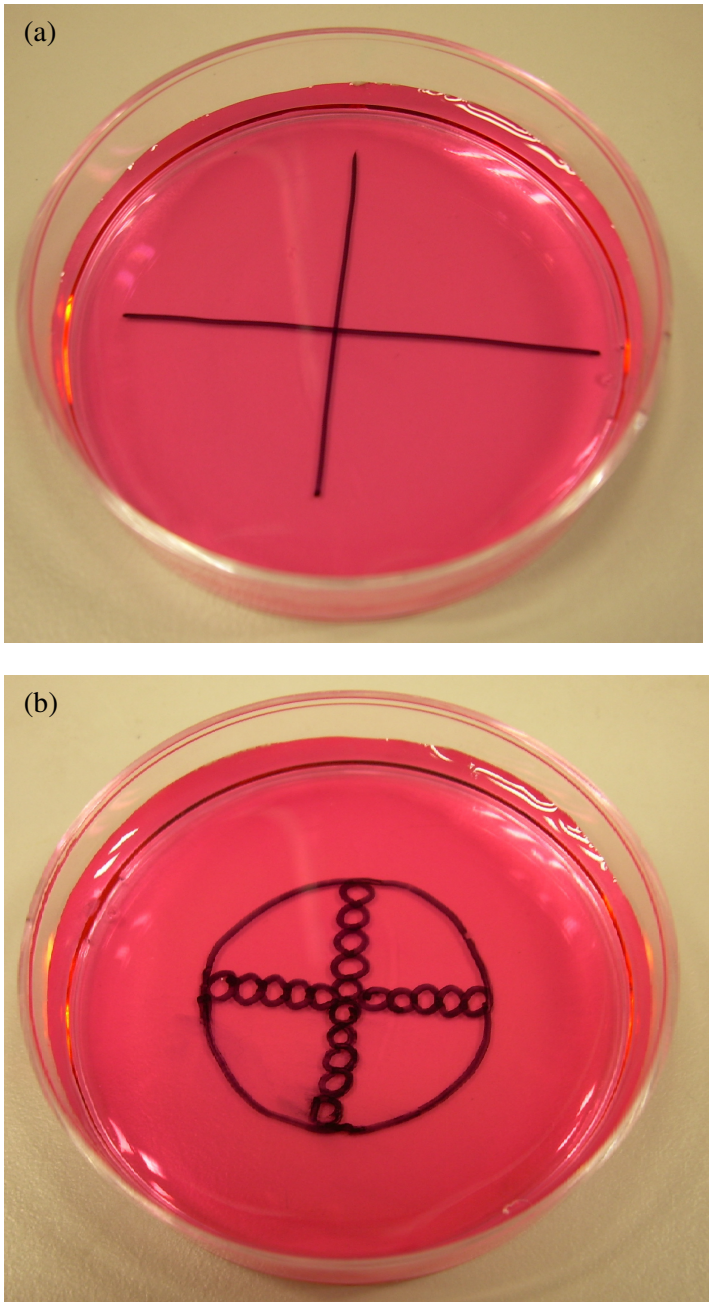

Figure 7.3 Marking of Petri Dishes. Petri dishes were placed on the microscope stage and an image was taken. The Petri dish was then transferred on the bench were ultrasound waves were applied. The Petri dishes were place back on the microscope stage and a second image was taken. The marking on the Petri dishes allowed for repositioning them on the microscope stage at the original field of view. Initial markings (a) involved just a cross, where one image was taken. Subsequent marking (b) involved viewing a number of areas, thus each field of view was marked separately.

application of ultrasound of different intensities, ranging from 0.2-1 W / cm^2. Images of the cells were taken before and after application of ultrasound waves using a Leica DMIRB inverted microscope. The fluorescence of Calcein AM and Propidium Iodide were measured at 488-543 nm. Data collected was analyzed using Imaris software package (Bitplane AG).

7.5.2.2 Ultrasound tank

Further experiments were carried out in an ultrasound tank constructed at the departmental workshop (figure 7.4). The tank was made out of Perspex and its bottom was covered with an acoustic absorber APTflexF28 (Precision Acoustics Ltd.).

7.5.2.3 Mylar membrane set up

A bi-axially oriented polyethylene terephthalate (boPET) polyester film (Mylar® membrane, Preservation Equipment) of 12 μm thickness was coated with 100 μl of rat tail collagen 1 mg / ml (Roche Applied Sciences) and left to dry. Two acetal homopolymer (Derlin) rings were constructed in the departmental workshop in such a way so that one could fit inside the other. A Mylar® membrane was placed between the two Derlin rings (figure 7.5). The membrane-ring-membrane (MRM) "sandwich" was partially submerged into the ultrasound tank and was held into position by a custom made holder (Departmental workshop).

The ring-membrane-ring (MRM) "sandwich" was then UV treated for 30 min. Cells were seeded on the membrane at a density of 2 x 10^5 cells / ml. 24 hours after seeding; 5 μl of 1 mM Calcein AM and 5 μl of 1 mM Propidium Iodide were added into the MRM "sandwich". The MRM "sandwich" was then transferred into the ultrasound tank. Images of the cells were taken before and after application of ultrasound waves. The

fluorescence of Calcein AM and Propidium Iodide were measured at 488-543 nm with a Leica DMIRB inverted microscope. Data collected were analyzed using Imaris software package (Bitplane AG).

7.5.2.4 OptiCell™ set up

OptiCell™ (Anachem) is a chamber enclosed between two optically-clear gas-permeable membranes that permit diffusion of O_2 and CO_2 across the membrane for promoting cell growth. Cells were grown on one of the membranes. The OptiCell™ has two self-sealing outlets that provide access to the interior of the chambers. The chamber provides a growth surface area of 100 cm^2. Cells were seeded in OptiCell™ chambers at a density of 2 x 10^5 cells / ml. Which enable the cells to grow in a controlled and stable environment prior to insertion into the tank for insonation. If sonoporation occurred, cell impermeable Calcein would traverse the cell membrane and the cells would have cell impermeable Calcein within their cytoplasm. The OptiCell™ was placed in a custom-made ultrasound tank, which allowed easy and precise manipulation of the ultrasound field relative to the OptiCell™.

7.5.2.4.1 Investigations of cell viability

For each OptiCell™ chamber, two areas were used for applying ultrasound. Prior to ultrasound exposure, a range of volumes of Definity® (Bristol Myers Squib) were injected into the OptiCell™, which was subsequently inverted several times in order to achieve an even distribution. The volumes of Definity® added to the OptiCell™ were 5 μl, 300 μl, 600 μl and 900 μl corresponding to a cell to microbubble ratio of 1 in 30, 1 in 1800, 1 in 3600 and 1 in 5400. The in-house microbubble volumes added to the OptiCell™ were 0.9 ml, 1.8 ml, 3 ml, 6 ml, corresponding to 1 in 300, 1 in 600,

1 in 1000 and 1 in 2000. In addition, 10 μl of 1 mM of Calcein AM and 10 μl of 1 mM of Propidium Iodide were added into each OptiCell™. Furthermore, areas corresponding to the field of view were marked just as previously done on Petri dishes (figure 7.6). These markings provided information on the viability of cells and therefore the intensities of ultrasound waves across the whole area of the probe. A custom made holder (Departmental workshop) allowed the OptiCell™ to float in the ultrasound tank at a distance of 2 cm above the acoustic absorber. This holder could also slide across the tank, thus allowing the movement of the OptiCell™ towards and away from the microscope. The fluorescence of Calcein AM and Propidium Iodide were measured at 488-543 nm and an image was taken with a Leica DMIRB inverted microscope. The OptiCell™ was then slided of the microscope stage across to the opposite side of the tank, where ultrasound waves were applied. The OptiCell™ chamber was then transferred back on to the microscope stage where another image of the cells was acquired. Data collected were analyzed using Imaris software package (Bitplane AG).

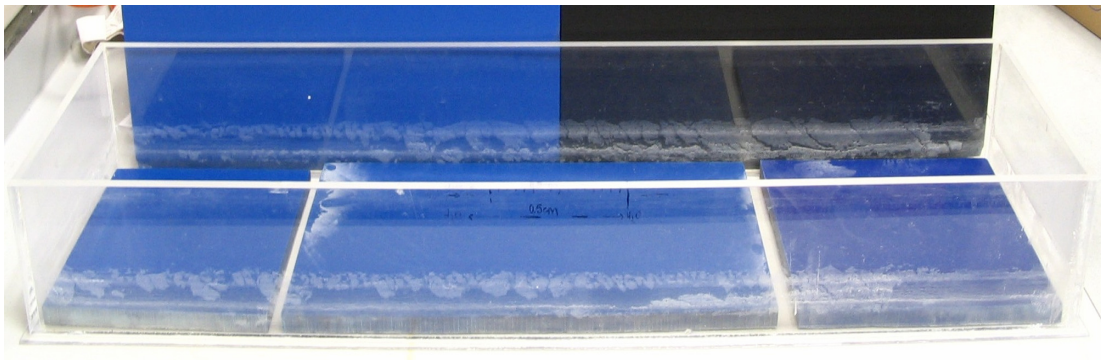

Figure 7.4 **Ultrasound tank.** The ultrasound tank was made out of Perspex and a piece of acoustic absorbing material was placed at the bottom of the tank to absorb and backscatter produced during insonation.

Figure 7.5 **Membrane-ring-membrane (MRM) "sandwich".** A thin, acoustically transparent membrane was placed between to Derlin rings so as to form a compartment where cells could be grown.

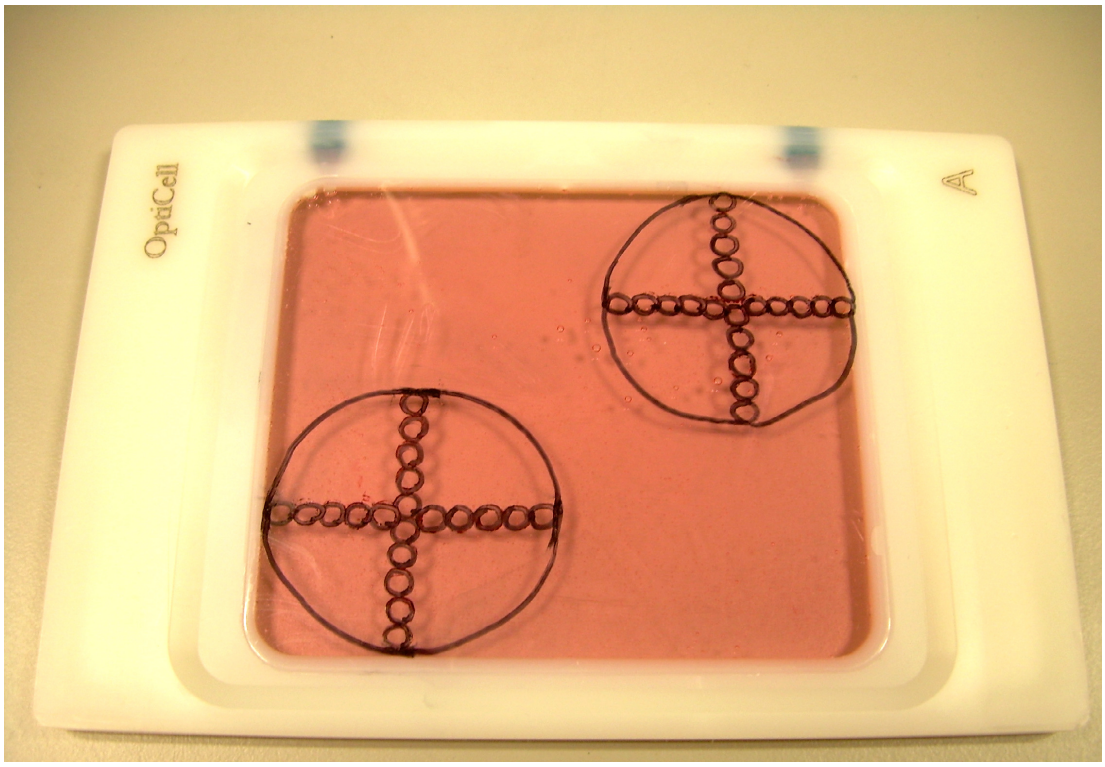

Figure 7.6 Markings on OptiCell™. The OptiCells™ used in viability assays were marked as shown. The OptiCell™ was placed under the microscope stage and an image of each field was taken. The OptiCell™ was then slided across the other side of the tank so as to allow for application of ultrasound. The OptiCell™ was finally slided back to its original position and images of the original fields of view were taken based on the markings. The markings on the OptiCell™ also provided information about the intensities of the ultrasound waves at different regions of the OptiCell™. A total of 40 images were taken for each OptiCell™.

7.5.2.4.2 Investigation of sonoporation

The OptiCell™ was placed in the ultrasound tank and was held in position by a custom made holder (Departmental workshop). Prior to ultrasound exposure, a range of volumes of Definity® (Bristol Myers Squib) or in-house microbubbles were added to the OptiCell™. The OptiCell™ was submerged into the ultrasound tank and held in place by a custom-made holder (departmental Workshop). The volumes of Definity® added to the OptiCell™ corresponded to a cell to microbubble ratio of 1 in 30, 1 in 1800, 1 in 3600 and 1 in 5400. Whereas the volumes of in-house microbubbles added to the OptiCell™ corresponded to a cell to microbubble ratio of 1 in 300, 1 in 600 and 1 in 2000. In addition, 100 μl of 10 μM of cell impermeable Calcein (Molecular Probes) and 3 μl of 1 mM of Propidium Iodide were added into each OptiCell™. The ultrasound probe was placed at a 37° angle while taking care not to trap any air bubbles between the probe and the OptiCell™ membrane. The probe was slided across and down the OptiCell™ until the whole surface area was exposed to ultrasound waves. The ultrasound probe was moved at a very slow rate; exposing the cells to ultrasound waves for 2-3 sec. Cells were trypsinised and washed with PBS three times. The fluorescence of cell impermeable Calcein and Propidium Iodide were detected within half an hour by flow cytometry.

7.5.2.4.3 Investigation of gene expression

Experiments investigating the expression of EGFP were conducted in a similar manner to the ones described in section 7.5.2.4.2; apart from emitting cell impermeable Calcein. However, in these experiments, OptiCells™ were placed in an incubator following exposure to ultrasound. The fluorescence of EGFP and Propidium iodide was detected 24 hours later by flow cytometry.

7.6 Molecular techniques

7.6.1 Transformation of Escherichia coli

Vectors were transformed using One Shot TOP10 competent cells (Invitrogen). 5 μl of the pCS2 vector was added to a 50 μl aliquot of competent cells in a pre chilled tube. Samples were chilled on ice for 20 min and then heat shocked at 42 °C for exactly 30 seconds, before returning them on ice for another 2 min. 450 μl of SOC medium (Invitrogen) was then added to the cells before they were incubated at 37 °C for 1 hour while shaking vigorously (350 rpm). 10 μl and 100 μl of the transformed cells were plated, at room temperature, on L Broth agar plates (Appendix 1) containing 0.1 mg / ml of the appropriate antibiotic. The L Broth agar plates were incubated upside down at 37 °C overnight.

7.6.2 Plasmid preparations

Following transformation, a number of colonies were picked from the L Broth agar plates. Each individual colony was placed in 3 ml of Terrific Broth (Appendix 1) containing the appropriate antibiotic and incubated at 37 °C overnight. The next day, each sample was transferred into 500 ml of L Broth (Appendix 1) containing the appropriate antibiotic and incubated at 37 °C overnight. Large scale plasmid preparations were performed using the PureLink™ HiPure Plasmid Filter Purification Kit according to manufacturer's instructions (Invitrogen).

7.6.3 Quantification of plasmid DNA

The concentration of plasmid DNA and DNA deoxyoligonucleotides was established by the A260 / 280 ratio in a spectrophotometer (Ultrospec 2000, Pharmacia Biotech).

7.6.4 Restriction endonuclease digests

Purified DNA plasmids were digested with the appropriate restriction enzymes (Promega) in order to become linearised. The linearised vectors were used for acquiring DNA delivery in to cells during sonoporation and subsequent expression of genes of interest. 1 μl of restriction enzyme was added to 1 μg of DNA solution. Then 1 μl of 10 x enzyme buffer and 1 μl of 10 mg / ml BSA (Appendix 1) were also added. The solution was then made to a final volume of 10 μl by addition of sterile distilled H_2O. The samples were allowed to incubate for 1 hour at 37 °C. Following the completion of digestion, DNA sample was separated using agarose gel electrophoresis.

7.6.5 Agarose gel electrophoresis

Digested DNA plasmids were run in an agarose gel so as to evaluate whether the DNA sample had been linearised during the digestions performed**.** A 1 % (w/v) agarose gel solution was prepared in 1 x TAE buffer (Appendix 1) by boiling. After allowing for the solution to cool down, 0.02 μg / ml of ethidium promide (EtBr) (Invitrogen) was added and the solution was then poured into a gel rack with the appropriate gel comb. Loading dye of appropriate volume was dded to the DNA samples, prior to their loading on the agarose gel. A 1 Kb DNA marker (Invitrogen) was also added in one of the wells. The agarose gel was then covered with 1 x TAE buffer and run at 100 V until adequate separation was observed under a UV light source.

7.6.6 DNA extraction

Following visualisation with agarose gel electrophoresis, the linearised DNA samples were purified using a QIAquick gel extraction kit (Qiagen, UK) and following the manufacturer's instructions.

7.7 Protein biochemistry techniques

7.7.1 Preparations of cell lysates

Cell lysates were prepared from SK Hep-1 cells grown in OptiCells™. The media was removed and the cells were washed twice with phosphate buffered saline (PBS) (Appendix 1). 1 ml of RIPA buffer containing the appropriate protease inhibitors was inserted into the OptiCell™ through its outlets. The cells were incubated for a few minutes. The top membrane of the OptiCell™ was cut with a scalpel and the solution was aspirated into an eppendorf tube and placed on ice. The samples were centrifuged at 10,000 rpm for 5 min at 4 °C and the supernatant was collected into a new eppendorf tube. Samples serving as positive controls were placed in a hypoxic incubator for 1 hour (hypoxia control) or in a heated incubator for 1 hour (heat shock control) prior to collecting the cell lysates.

7.7.2 Protein assay

A protein assay was used in order to measure the concentration of total protein present in cell extracts. The BioRad DC Protein Assay Kit was used according to manufacturer's instructions. A standard curve was made from a known standard of bovine albumin (BioRad). The cell extracts were measured on a Dynatech plate reader (Dynex MRX II, Dynatech) and the protein concentrations were calculated by comparison to the standard curve.

7.7.3 Electrophoretic separation of proteins

SDS polyacrylamide gels (SDS-PAGE) were used for the separation of proteins, using the protocol of Laemmli (1970). The mini-protean® 3 cell apparatus (Bio Rad) was used for casting gels. A 10 % separating gel (Appendix 1) was poured between glass plates to the appropriate level and then was overlaid with 2-methylpropan-1-ol (BDH) and left to polymerise. Once polymerised the 2-methylpropan-1-ol was removed and the gel was rinsed with water before the 4 %

stacking gel (Appendix 1) was poured, followed by insertion of a comb allowing wells to form before the gel polymerised. The protein samples were prepared by addition of 5x sample loading buffer (Appendix 1) and denatured by heating to 95 °C for 5 min. Once the stacking gel had polymerised the tank was filled with electrophoresis buffer (Appendix 1). The comb was then carefully removed and the samples loaded. A potential of 200 V was then applied until the dye front reached the bottom of the gel.

7.7.4 Immunoblotting

The transfer of proteins from a polyacrylamide gel to a membrane was achieved by electrophoretic elution (Towbin, Staehelin et al. 1979). The method used in this study was semi dry transfer. A gel sandwich was made using 3 pieces of blotting paper, gel, membrane and 3 pieces of blotting paper. The membrane was pre-soaked in transfer buffer (Appendix 1) for 10 min. The gel sandwich placed in a Pharmacia Novablot semi dry transfer cell (Bio Rad) and a current of 80 mA / cm^2 was applied for 1 hour. The membrane used was pure nitrocellulose membrane (Bio Rad).

7.7.5 Marking & Blocking

Complete transfer of the proteins was established by fully immersing the membrane in Ponceau Red (Sigma). Once the protein bands were visible, the membrane was rinsed with 1x TBS. The membrane was then fully immersed in 5 % (w/v) Marvel in TBS containing 0.5 % (v/v) Tween-20 (TBST) (Appendix 1) for 1 hour at room temperature, in order to prevent any non-specific binding of the antibody.

7.7.6 Antibody incubations

After the blocking solution was removed the membrane was washed 3 times over 5 min in TBST (Appendix 1)followed by incubation in the primary antibody, diluted appropriately depending on the antibody (Appendix 1), for 1 hour at room temperature or usually overnight at 4 °C. The primary antibody was then removed and the membrane was washed three times over 5 min in TBST. The membrane was then incubated with the secondary antibody for 30 min. The membrane was then washed twice over 5 min in TBST and once over 5 min in TBS.

7.7.7 Antibodies

Rabbit polyclonal antibodies were directed against Hsp70 (Bioquote Limited, cat no: SPA-812) and Anti-Heme-Oxygenase-1 (Bioquote Limited, cat no: SPA-896). Mouse monoclonal antibodies were directed against beta Actin (Abcam, cat no: ab6276) and GAPDH (Abcam, cat no: ab9385).

7.7.8 Enhanced cheminoluminescence

The detection of the protein of interest used enhanced chemiluminescent reagent (ECL) (Western blotting detection reagents, Amersham biosciences), which involved incubating the membrane for 1 min using 2 solutions in a 1:1 ratio, ECL solution 1 and ECL solution 2. Following this the protein bands were visualised by exposing the membrane to Konica x-ray film for an appropriate length of time, depending on how much protein is on the membrane, typically 1-5 min. The film was then developed (Optimax film developer). Analysis of immunoblotting was performed with image J 1.41 software (National Institute of Health, USA).

7.8 Statistical analysis

For each experiment, a minimum of three replicate samples was examined unless stated otherwise. The mean and standard error of mean (SEM) was calculated for each experiment. A student's t test was used in order to compare two treatments. A one-way ANOVA test was used to compare several treatments while a two-way ANOVA test was used to compare combinations of treatments. A significant difference between samples was considered when $p<0.05$, unless otherwise stated. Trend lines were added to some figures to show trends of samples, with the R^2 indicating how well the samples goodness of fit within this trend line.

Chapter 8

In-house microbubble characterisation

8.0 Introduction

Characterisation of in-house microbubbles was an important part of this study. Since cavitation is thought to be the main mechanism associated with sonoporation and it is dependent on microbubble size, it was speculated that the size of the microbubbles could become a limiting factor when attempting to achieve sonoporation (Lentacker, De Smedt et al. 2006). Thus, it was important to attain the size distribution of in-house microbubble preparations before attempting to perform sonoporation. In addition, the contents of the microbubbles used, are also known to affect their efficiency in instigating sonoporation (Wang, Liang et al. 2005). Initially, attempts to produce microbubbles resulted in lipid shelled microbubbles with an aqueous solution core (Huang 2008). As it was later established that the oscillation mode of microbubbles and thus their ability to cause sonoporation, are also affected by their contents, production of microbubbles was focused encompassing initially air and later high molecular gases (Li, Tachibana et al. 2003).

The aim of this investigation was to characterise the in-house microbubbles in order to obtain valuable information, such as microbubble size and contents. This information would assist in setting some of the parameters for designing sonoporation experiments in the presence of the in-house microbubbles. The size distribution of the in-house microbubbles was established with the aid of several methods, including confocal and two-photon microscopy, cell sorting and coulter counter acquisition. All three methods confirmed the size distribution of the in-house microbubbles. Direct comparison of the size distribution of in-house microbubbles to that of commercially available microbubbles, such as Definity® and Sonovue® was also performed. As commercial microbubbles have already been shown to be involved in the sonoporation process, this would further substantiate the

ability of the in-house microbubbles to instigate sonoporation. In addition, cell sorting provided an indication as to the contents of the in-house microbubbles. Finally, the information obtained from this section will allow formation of accurate parameters for designing a delivery system with the aid of ultrasound in the presence of in-house microbubbles.

8.1 Results

8.1.1 Imaging

Confocal and two-photon imaging provided information about the size and shape of the microbubbles. Microbubbles were stained with FM 14-3 dye, which is fluorescent when intercalated into phospholipid membranes and emits fluorescence at 488 nm. A number of stacks in the z plane were acquired for each microbubble and were then put together with Volocity software package, to provide a three dimensional (3-D) image. It was essential to image a large sample of microbubbles in order to be certain that we had an accurate representation of the size distribution within the microbubble preparations. Over one hundred images of in-house microbubbles were acquired in total (figure 8.1). As can be seen from figure 8.1, there is a high fluorescent background present. Volocity image analysis (Improvision, Coventry) and 3-D rendering software provided information such as the surface area of the microbubbles. With the aid of this software, we were able to plot a surface area distribution graph (figure 8.2). Further experiments were performed in order to investigate the cause of this high background fluorescence. Coverslips imaged in the absence of microbubbles confirmed that the glass of the coverslips was not responsible for the fluorescence seen. Next, it was decided to image commercially available microbubbles (Definity®, Bristol Mayer Squibb) in order to examine if high

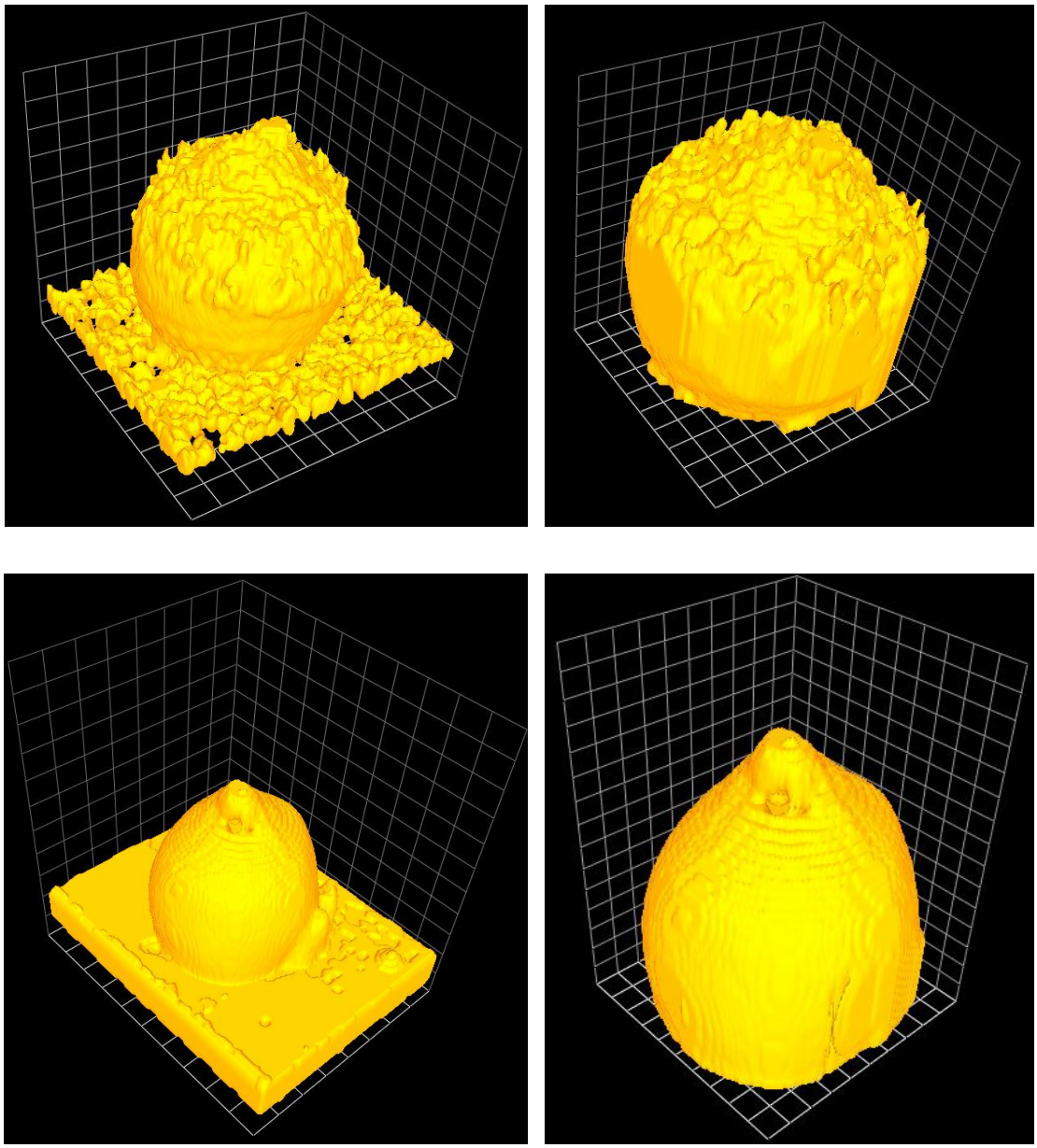

Figure 8.1 **3-D images of crude in-house microbubbles.** In-house microbubbles were stained with FM 14-3 dye. A number of stacks in the z plane were acquired with two photon microscopy for each microbubble and were then put together with Volocity software package, to provide a three dimensional (3-D) image. Original images of crude in-house microbubbles can be seen on the left hand side. Images on the right hand side are after manually subtracting the background. The units for the images are from top left clockwise 1.3 µm, 0.8 µm, 0.8 µm and 1.1 µm.

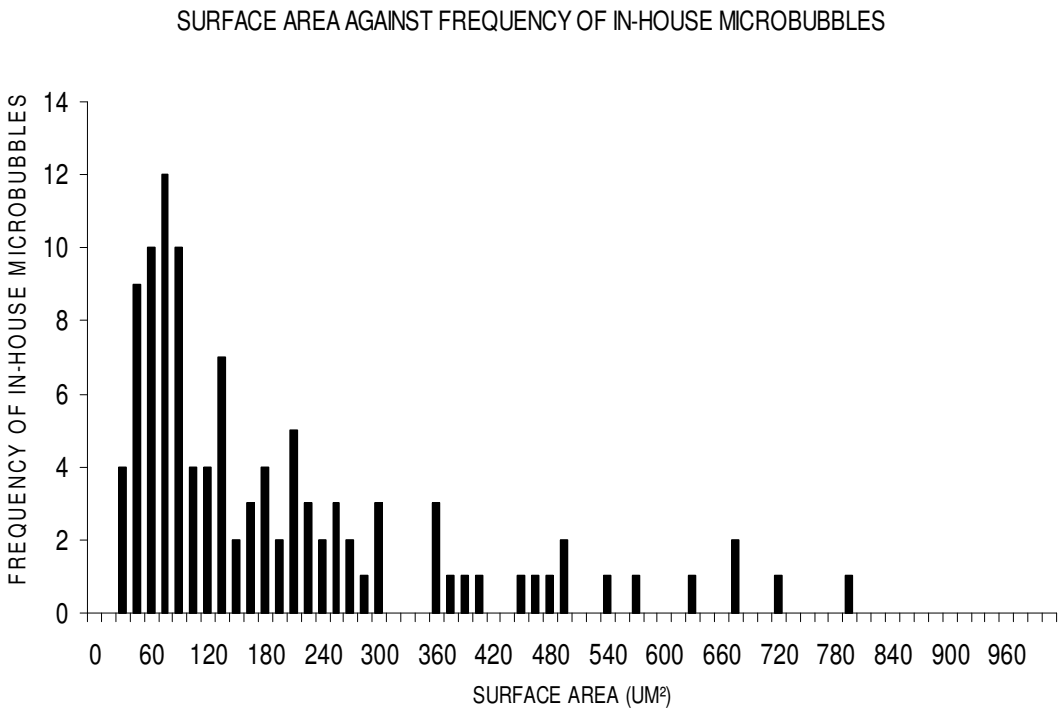

Figure 8.2 **Surface area plotted against frequency of in-house microbubbles.** A number of stacks in the z plane were acquired for each in-house microbubble and were then put together with Volocity software package, to provide a three dimensional (3-D) image. Volocity image analysis (Improvision, Coventry) and 3-D rendering software provided information such as the surface area of the microbubbles, thus allowing for plotting a surface area distribution graph.

fluorescent background would be still an issue. A total of four hundred and eighty eight images of Definity® were acquired (figure 8.3) and the data were processed as before (figure 8.4).

We then attempted to separate the apparent phospholipid residues from the microbubble preparations by density gradient centrifugation. Microbubbles were added to a gradient of different densities (50 %, 30 %, and 5 %) of Nycoprep solutions, layered on top of each other. Samples of the centrifuged microbubbles were imaged using confocal microscopy as before in order to calculate their size distribution. Again, a large number of microbubbles were imaged (one hundred and seventy three for 50 % fraction, one hundred and eighty five for the 30 % fraction and one hundred and ninety six for the 5 % fraction) so as to obtain a valid representation of the population (figure 8.5, 8.6 and 8.7 respectively).

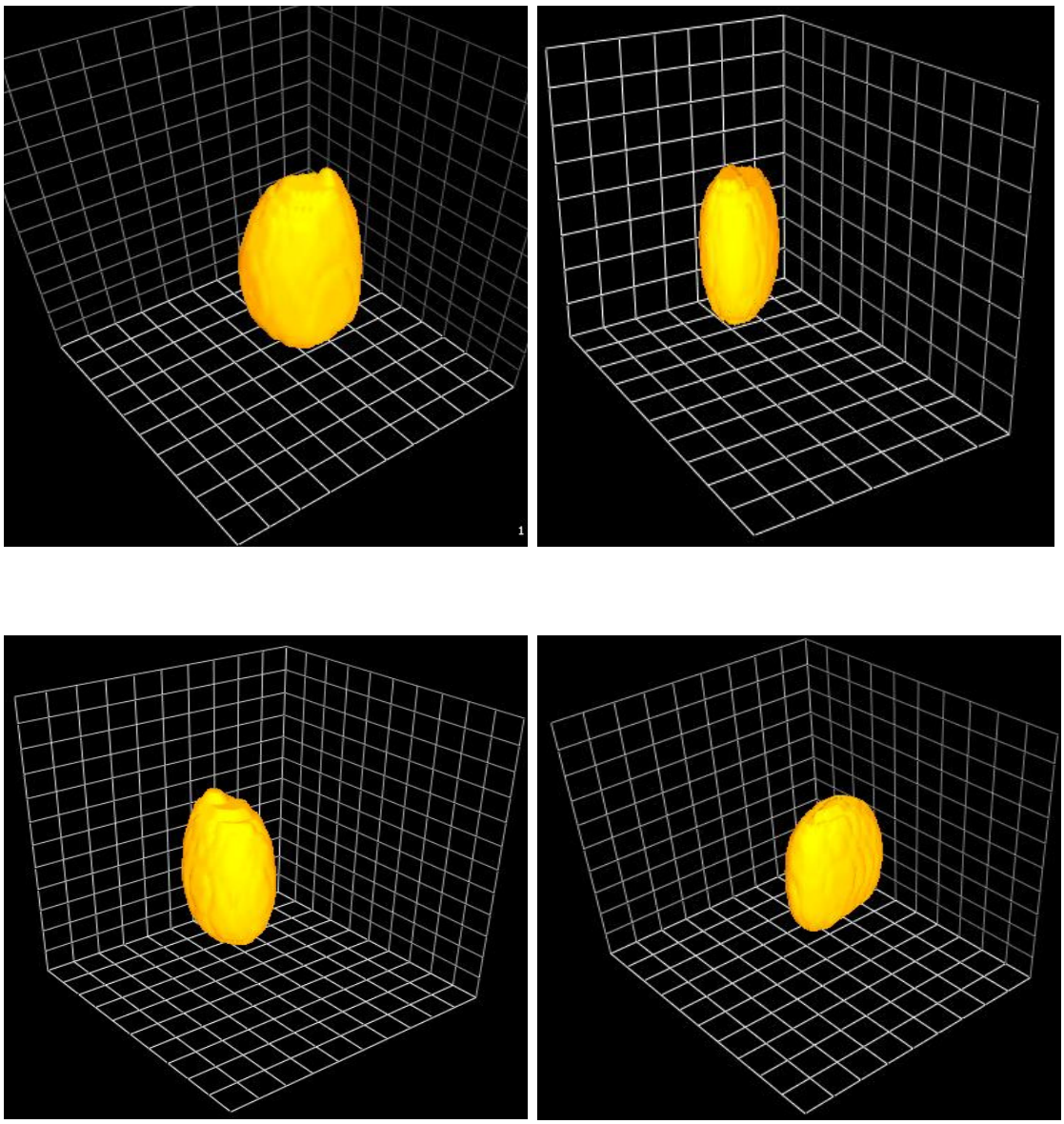

Figure 8.3 **3-D images of Definity® microbubbles.** Definity® microbubbles were stained with FM 14-3 dye. A number of stacks in the z plane were acquired with two photon microscopy for each microbubble and were then put together with Volocity software package, to provide a three dimensional (3-D) image. The units for the images are from top left clockwise 0.4 µm, 0.6 µm, 0.4 µm and 0.4 µm.

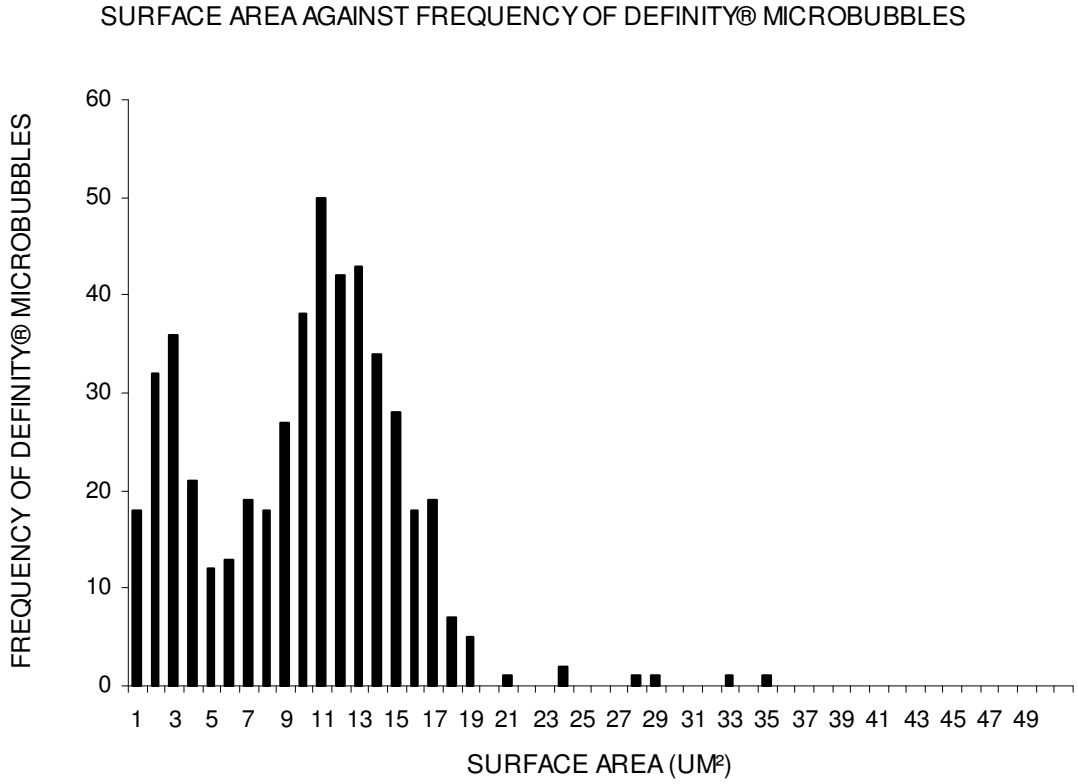

Figure 8.4 **Surface area plotted against frequency of Definity® microbubbles.** A number of stacks in the z plane were acquired for each Definity® microbubble and were then put together with Volocity software package, to provide a three dimensional (3-D) image. Volocity image analysis (Improvision, Coventry) and 3-D rendering software provided information such as the surface area of the microbubbles, thus allowing for plotting a surface area distribution graph.

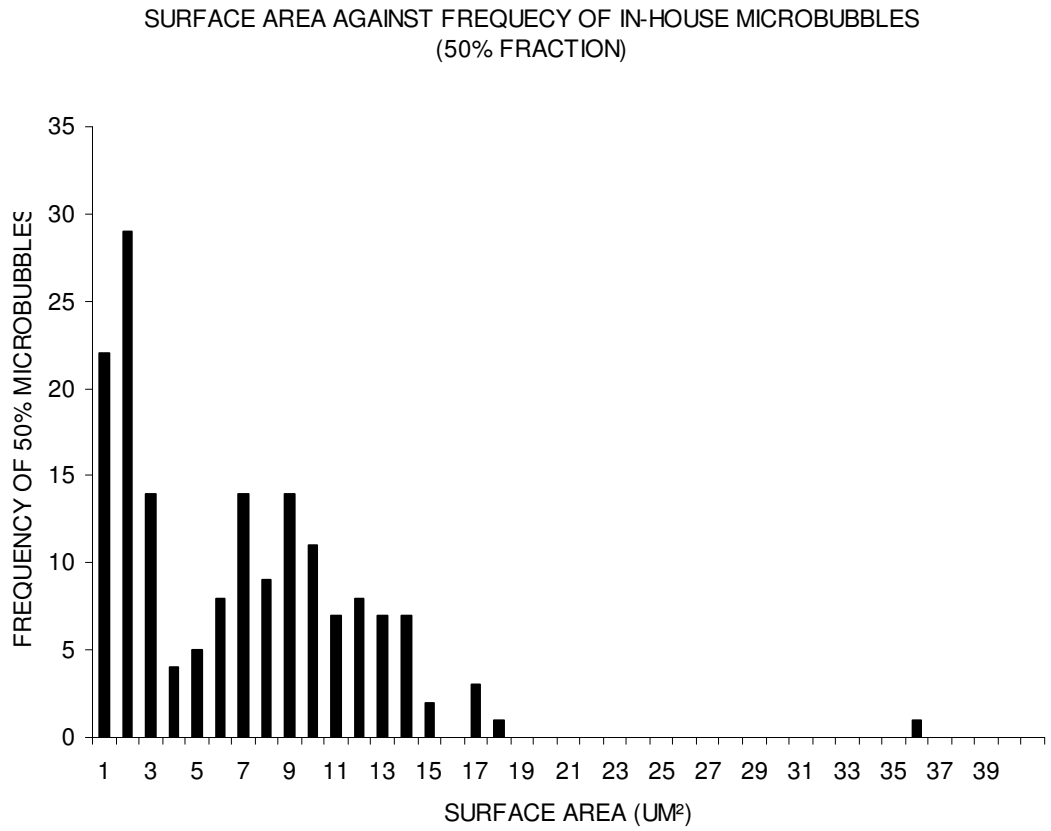

Figure 8.5 **Surface area plotted against frequency of in-house (50% fraction) microbubbles.** In-house microbubbles were separated according to size by placing them in different density Nycoprep solutions and centrifuging them. Fractionated microbubbles (50 % fraction) were then stained with FM 14-3 dye and a number of stacks in the z plane were acquired with two photon microscopy for each microbubble. The z stacks were put together with Volocity software package, to provide a three dimensional (3-D) image**.** Volocity image analysis (Improvision, Coventry) and 3-D rendering software provided information such as the surface area of the microbubbles, thus allowing for plotting a surface area distribution graph.

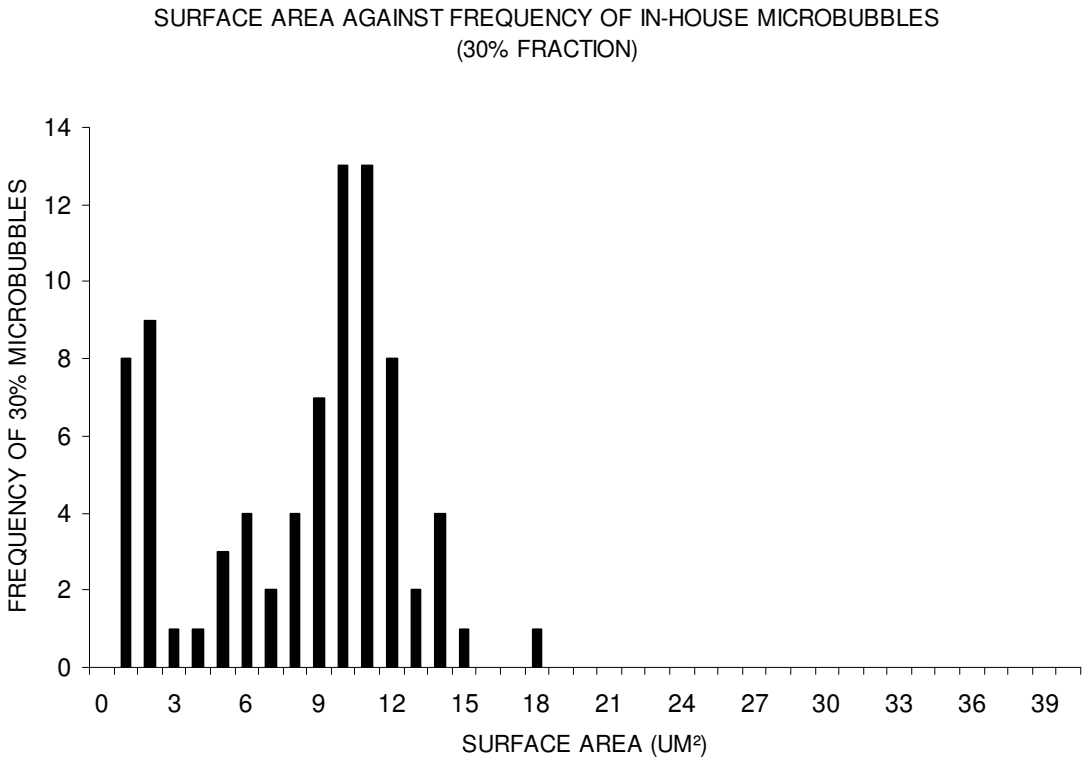

Figure 8.6 **Surface area plotted against frequency of in-house (30% fraction) microbubbles.** In-house microbubbles were separated according to size by placing them in different density Nycoprep solutions and centrifuging them. Fractionated microbubbles (30 % fraction) were then stained with FM 14-3 dye and a number of stacks in the z plane were acquired with two photon microscopy for each microbubble. The z stacks were put together with Volocity software package, to provide a three dimensional (3-D) image**.** Volocity image analysis (Improvision, Coventry) and 3-D rendering software provided information such as the surface area of the microbubbles, thus allowing for plotting a surface area distribution graph.

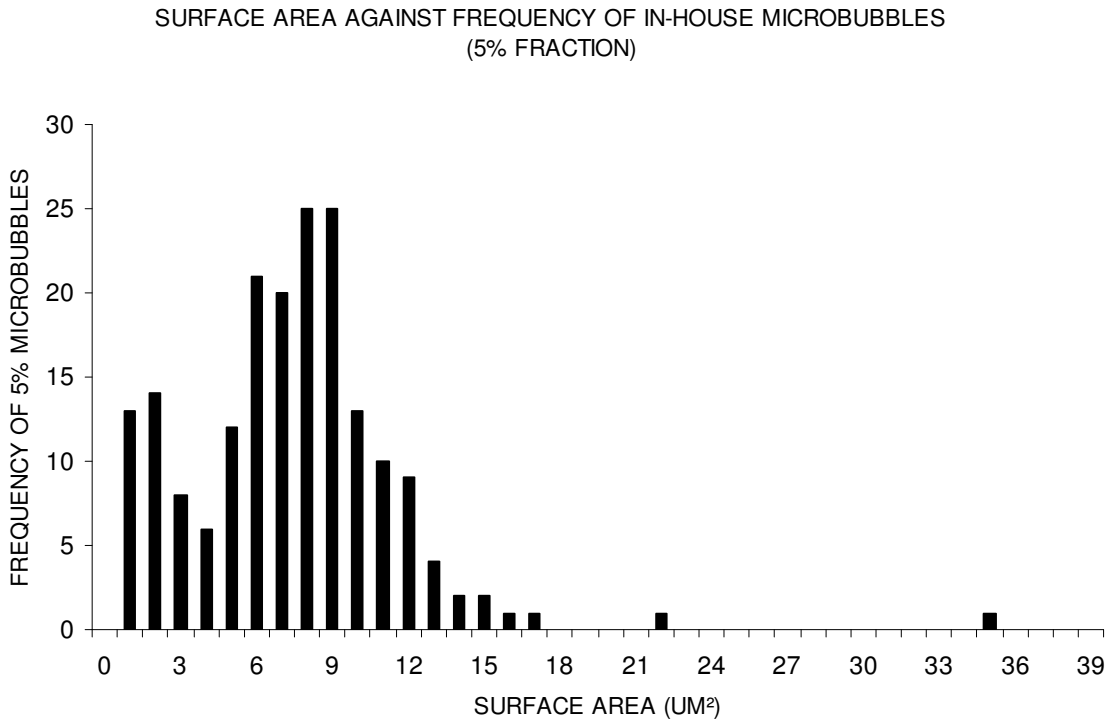

Figure 8.7 **Surface area plotted against frequency of in-house (5% fraction) microbubbles.** In-house microbubbles were separated according to size by placing them in different density Nycoprep solutions and centrifuging them. Fractionated microbubbles (5 % fraction) were then stained with FM 14-3 dye and a number of stacks in the z plane were acquired with two photon microscopy for each microbubble. The z stacks were put together with Volocity software package, to provide a three dimensional (3-D) image**.** Volocity image analysis (Improvision, Coventry) and 3-D rendering software provided information such as the surface area of the microbubbles, thus allowing for plotting a surface area distribution graph.

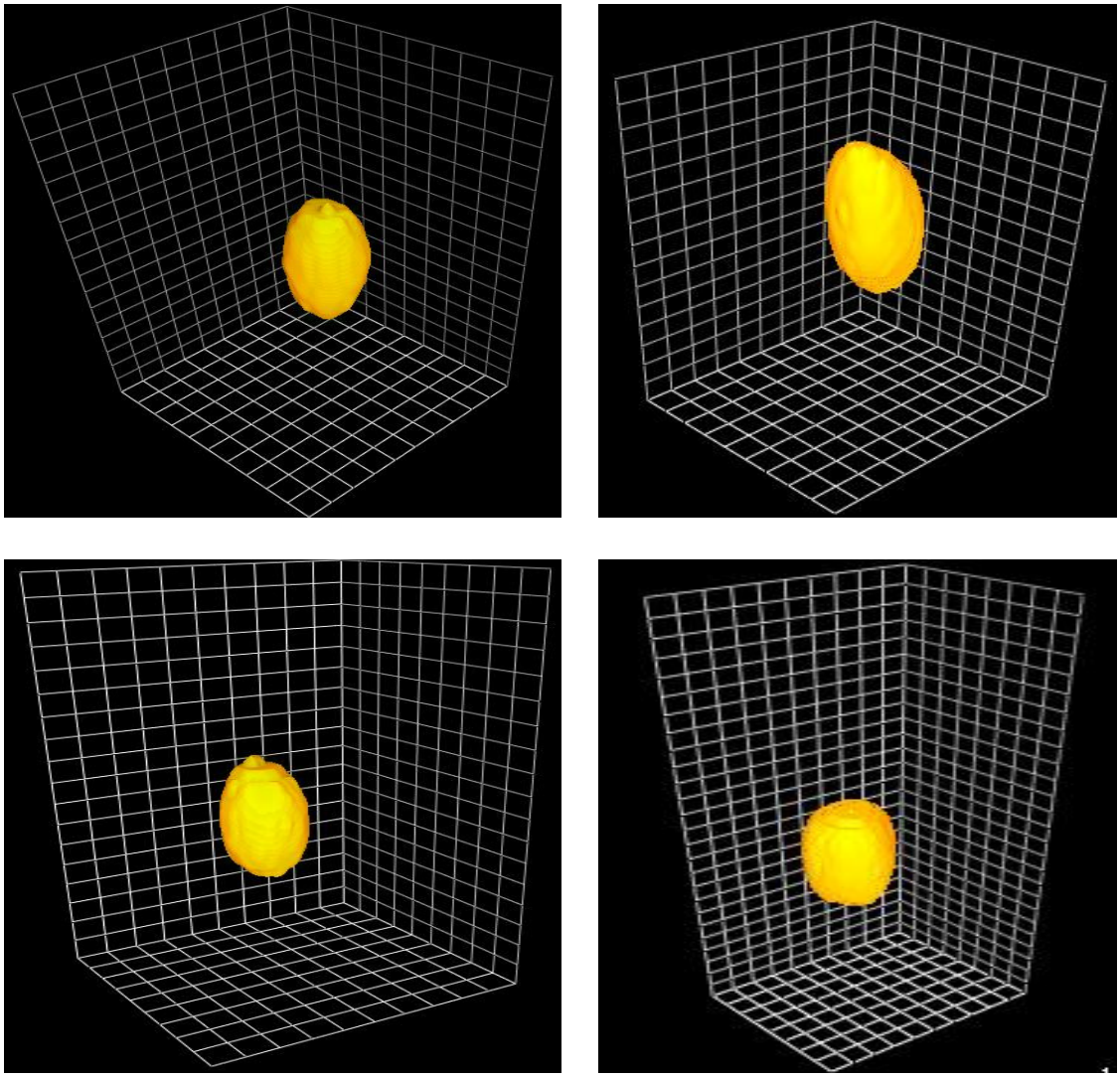

Figure 8.8 **3-D images of fractionated in-house microbubbles.** Microbubbles were separated according to size by placing them in different density Nycoprep solutions and centrifuging them. Fractionated microbubbles were then stained with FM 14-3 dye and a number of stacks in the z plane were acquired with two photon microscopy for each microbubble. The z stacks were put together with Volocity software package, to provide a three dimensional (3-D) image. Images of fractionated in-house microbubbles can be seen. The units for the images are from top left clockwise 0.4 µm, 0.4 µm, 0.6 µm and 0.5 µm.

8.1.2 Size sorting

Crude in-house and fractionated samples were passed through a cell sorter in order to validate the size distribution results, obtained by imaging and density gradient separation, with a different method. Scatter plots from the in-house microbubbles showed that around 73 % of the crude samples were within 2-3 μm in diameter (figure 8.9). We then calculated the surface area of crude in-house microbubble samples by using Volocity (figure 8.10) and chose 40 images that fell within the two standard deviation of the mean. The diameter of these 40 representative microbubbles was measured manually. The calculated (nominal) and measured (actual) diameters of the selected microbubbles were plotted against surface area provided by Volocity. Furthermore, when the size distribution histograms from the crude and 5 % fractionated samples were overlaid on top of each other (figure 8.11) a very small shift towards the smaller sizes was observed.

In-house microbubbles were fed through a coulter counter to examine their size distribution (figures 8.12-8.14). Two latex beads with a diameter of 22 μm and 300 nm were also used in order to verify the detection range of the Coulter counter. Figure 8.12 demonstrates that most of the in-house microbubbles fall within a small range of 4-10 μm, with a small fraction containing larger microbubbles.

(a)

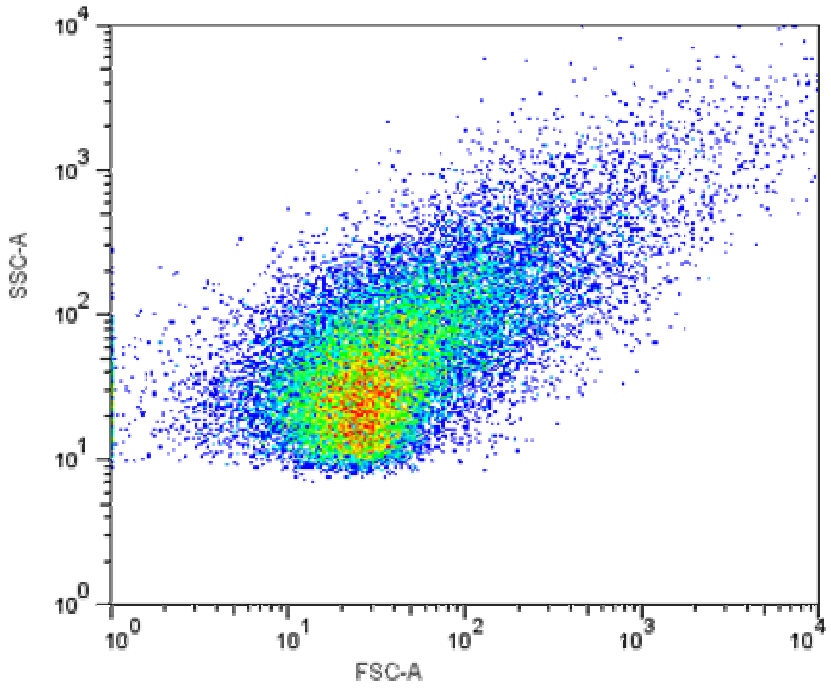

(b)

Tube: log bubbles

Population	#Events	%Parent	%Total
All Events	30,000		100.0
P1	39	0.1	0.1
P3	303	1.0	1.0
P4	21,972	73.2	73.2

(c)

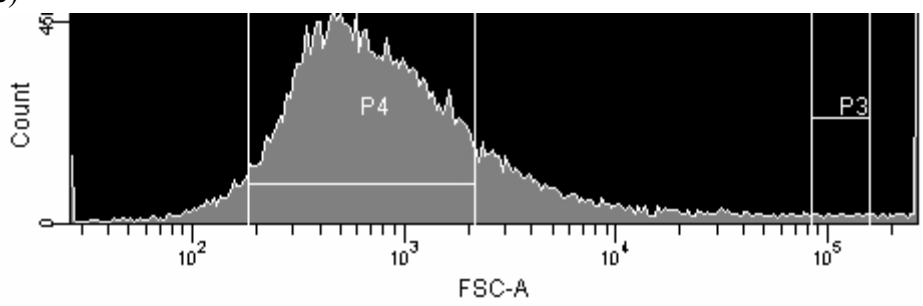

Figure 8.9 **Scatter plot of crude in-house microbubbles**. Crude in-house microbubbles were passed through a cell sorter in order to validate their size distribution. (a) Scatter plot from the microbubble sample showing population distribution. FSC-A is the forward scatter emitted, representing microbubble size, while SSC-A is the side scatter emitted, representing microbubble morphology. (b) Statistical analysis of data. A total of 30,000 events were recorder, while the population falling within two standard deviations from the mean was gated (P_4) and calculated to be 73 % of total population. (c) Population distribution graph, showing the P_4 gated events within the total microbubble population.

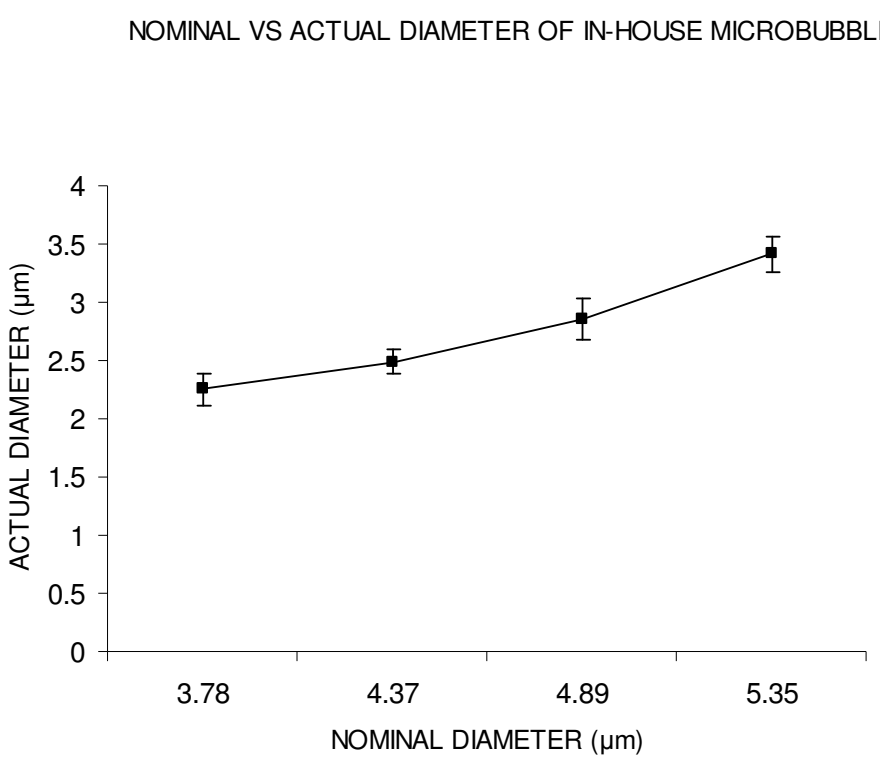

Figure 8.10 **Nominal versus actual diameter of in-house microbubbles**. 40 microscope images of crude microbubbles were chosen, that fell within the two standard deviation of the mean microbubble surface area distribution according to Volocity (figure 8.2). The nominal and actual diameters of these microbubbles were obtained by Volocity and manual calculations respectively.

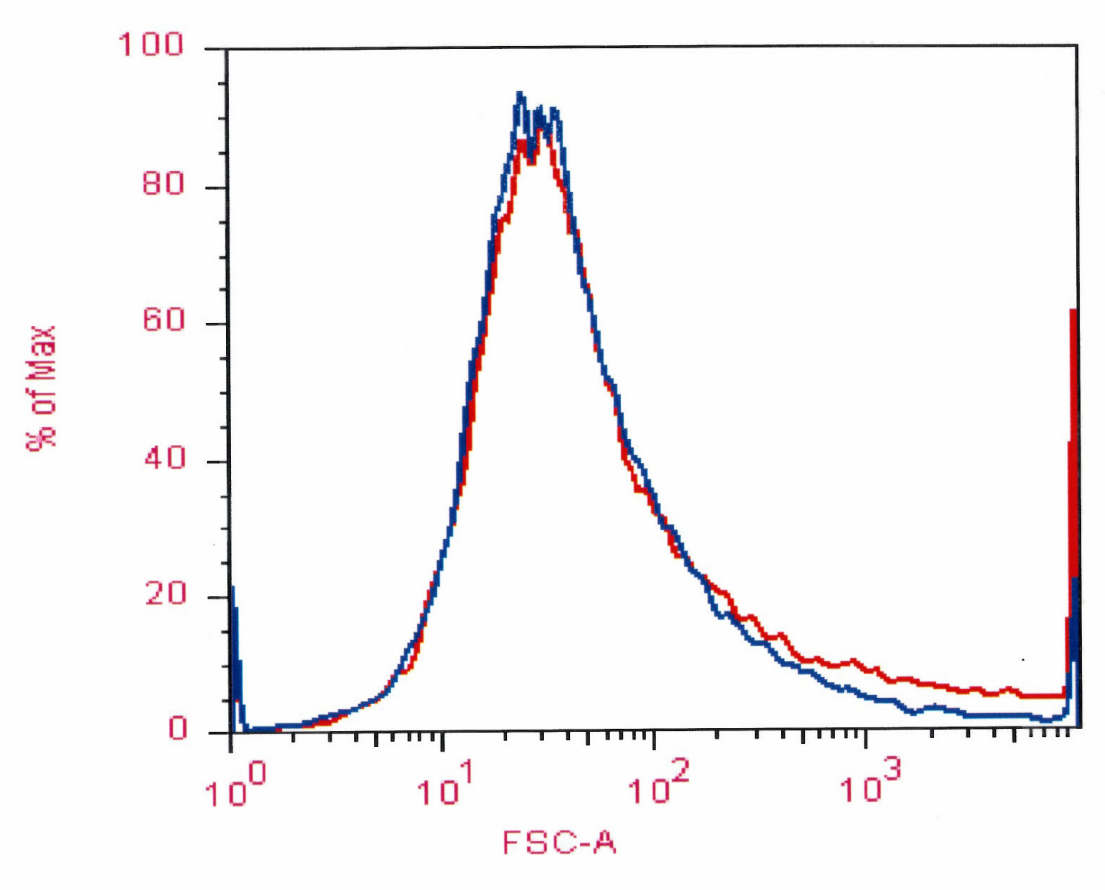

Figure 8.11 **Histogram of crude and 5% fractionated microbubbles.** Size distribution histograms for crude (red) and 5 % fractionate microbubble (blue) samples were overlaid on top of each other to show the shift in size distribution between the two samples. The small shift towards the smaller microbubbles indicates that only a small number of large microbubbles were extracted from the 5 % fraction.

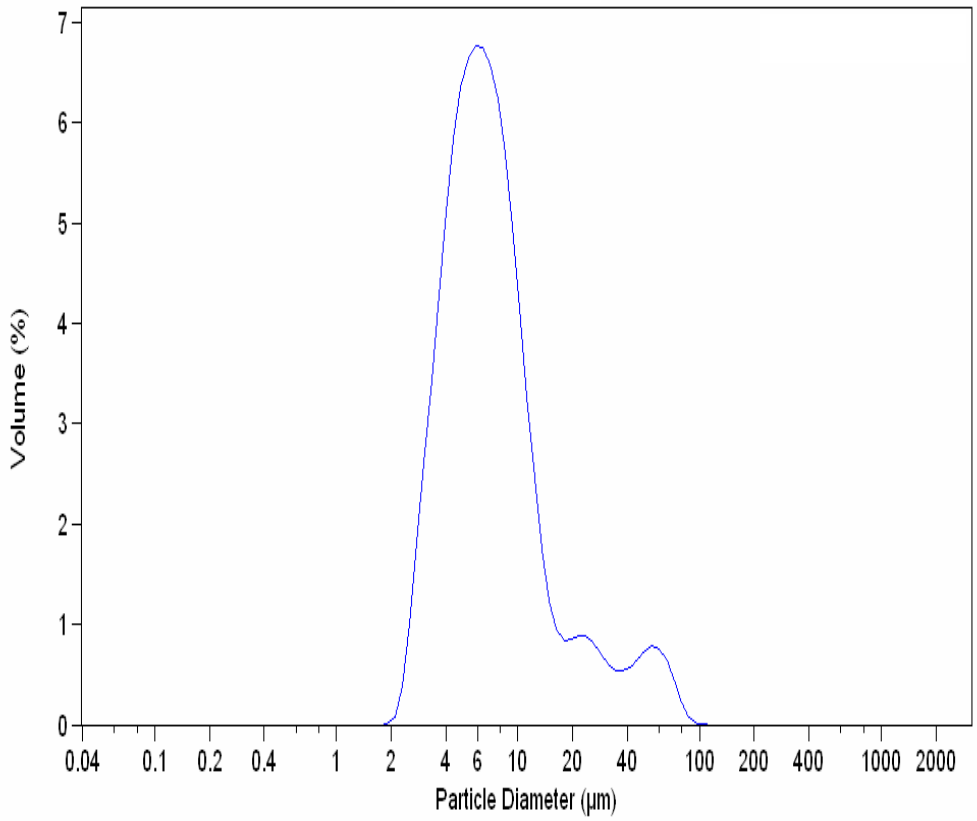

Figure 8.12 **Coulter counter histogram of in-house microbubbles.** As the size of microbubbles plays a crucial role in achieving sonoporation, it was necessary to define the size of the in-house microbubbles used. The microbubbles were therefore passed through a coulter counter in order to obtain a size distribution graph. The results show three distribution curves. The main curve contains microbubbles of an average size of 6 µm, while the other two smaller curves contain microbubbles of larger sizes.

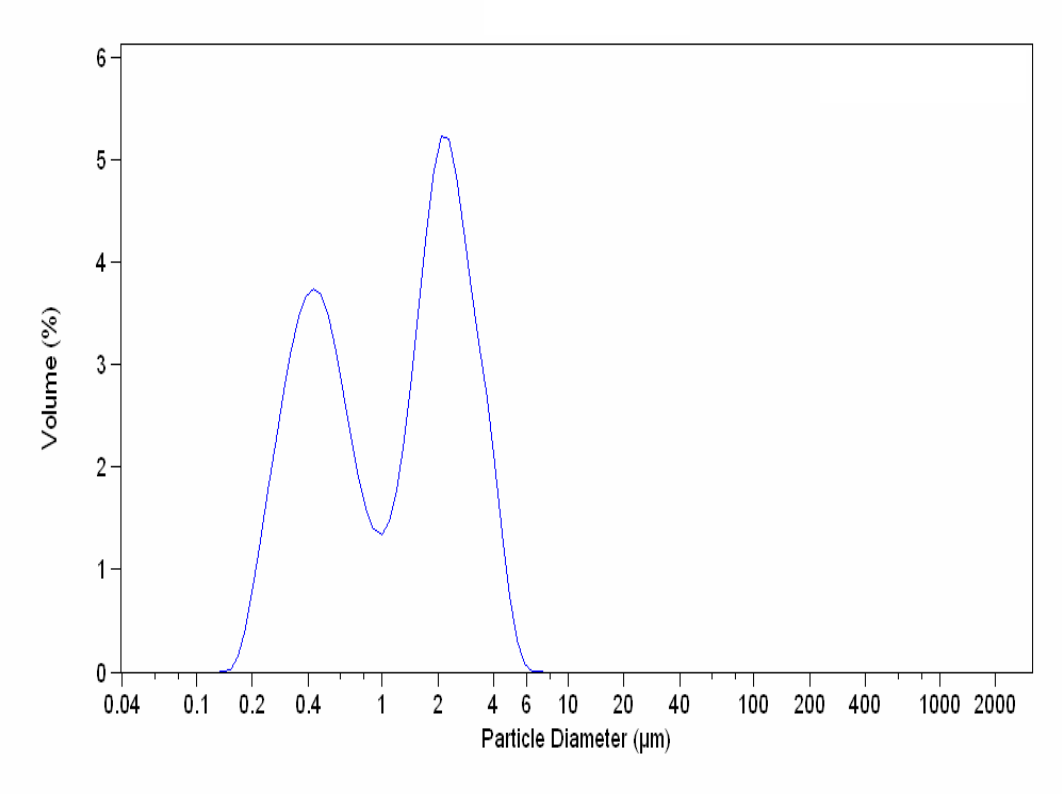

Figure 8.13 **Coulter counter histogram of Definity® microbubbles.** Obtaining the size distribution of other commercially available microbubbles such as Definity® was equally important as they have been shown to be capable of achieving sonoporation Definity® microbubbles were therefore passed through a coulter counter in order to obtain a size distribution graph. The results show two distribution curves. The first one has an average microbubble of 0.4 µm, while the second one has an average microbubble of 2 µm.

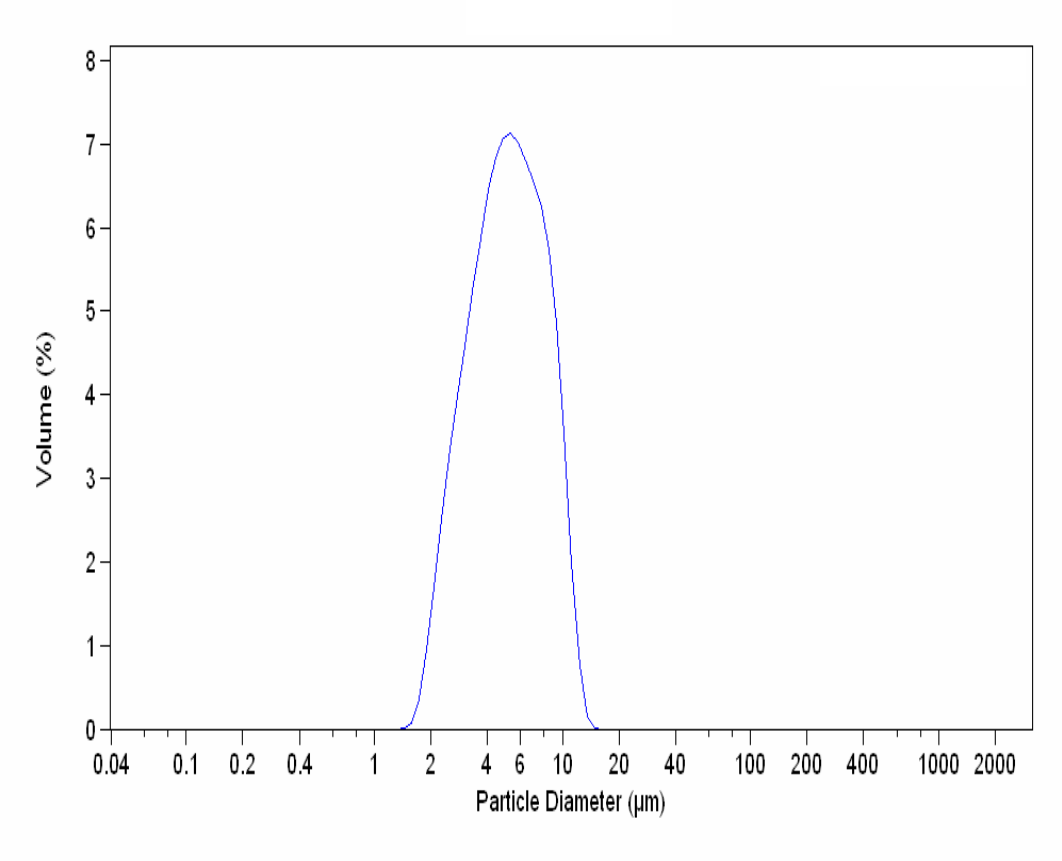

Figure 8.14 **Coulter counter histogram of Sonovue® microbubbles.** Obtaining the size distribution of other commercially available microbubbles such as Sonovue® was also important as they have been shown to be capable of achieving sonoporation Sonovue® microbubbles were therefore passed through a coulter counter in order to obtain a size distribution graph. The results show a normal distribution curve with an average microbubble size of 5 µm.

8.2 Discussion

As previously mentioned the size of the microbubbles plays an important role in achieving sonoporation. Thus, confirming that the size distribution of in-house microbubbles falls within a similar range to that of microbubbles used for sonoporation in other studies was a significant part of this study. Characterization of in-house microbubbles was achieved, from the experiments described in this section. Three separate methods were used in order to evaluate the size distribution of the in-house microbubbles (a) two photon microscopy (b) cell sorting and (c) coulter counting.

Confocal and two-photon imaging provided information about the size and shape of the microbubbles (figure 8.1). Volocity image analysis (Improvision, Coventry) and 3-D rendering software provided information such as the surface area of the microbubbles. With the aid of this software, we were able to plot a surface area distribution graph (figure 8.2). Volocity software was informed for the sake of the calculation that the microbubbles were spherical and applied the mathematical equation for calculating surface area of a sphere ($4\pi r^2$, where r is the radius of the sphere). However, from the images obtained, it can be seen that the microbubbles were apparently not spherical (figure 8.1), since Volocity software analysis was unable, understandably, to distinguish between the high fluorescent background present and the microbubbles.

Further experiments were performed in order to investigate the cause of this high background fluorescence. Images taken in the absence of microbubbles on coverslips, confirmed that the glass of the coverslips was not the cause of the fluorescence observed. As the FM 14-3 dye used for staining the microbubbles is only fluorescent inserted in phospholipid bilayers found in the sample, another possible explanation could be that some of the phospholipids used for microbubble production did not

incorporate themselves into the microbubbles, thus residues of these phospholipids would be accumulated on the coverslip surface and could explain the fluorescence seen.

Examination of commercially available microbubbles (Definity®, Bristol Mayer Squibb) could assist to establish as to whether the high fluorescent background seen was present with all microbubbles or only in-house microbubbles. As seen from figure 8.4, the population present was of much smaller size than that of the in-house microbubbles. In addition, the background fluorescence was much lower than that seen with in-house microbubbles, which suggested that the Definity® samples had fewer impurities (due to unincorporated lipids) than the in-house microbubbles.

Two approaches were taken in order to eliminate the fluorescent lipidic "background" seen to be able to measure accurately the diameter of the in-house microbubbles. First, we attempted to "cut off" the fluorescent background of the in-house microbubbles manually using tools available in Imaris software. While there was now no fluorescence remaining in the sample data on the coverslip surface, the microbubbles were still not spherical since the cutting tools only allowed us to cut a straight line , so the bottom surface of the microbubbles was flat. However, this may reflect reality, since the phospholipid membrane of the microbubbles is most likely deformable, thus their own weight could actually result in a flat surface were they touch the coverslip surface. Nevertheless, once again the mathematical equation applied for calculating the surface area of the microbubbles by Volocity is assumed to be invalid, since the microbubble shape is not spherical. Secondly, we attempted to separate the apparent phospholipid residues from the microbubble preparations by density gradient centrifugation. Nycoprep consists of Nycodenz, a high density solution.

When microbubbles within the different density Nycoprep solutions were centrifuged, they separated according to size into the different density solutions. Therefore, any phospholipid residues present in the solution should be separated from the fully formed microbubbles. This experiment would also provide information about the contents of the microbubbles i.e. if the microbubbles were filled with air, then the smaller ones should sink to the bottom of the tube, however if the microbubbles were filled with saline, then the smaller ones should float to the top of the tube. Separation of microbubbles by density would also be useful for future experiments, if certain sizes of microbubbles prove to be toxic or more or less efficient in sonoporation, when introduced into cell cultures.

Samples of the centrifuged microbubbles were imaged using confocal microscopy as before in order to calculate their size distribution. The images produced three types of information. First, as can be seen from figures 8.5-8.7 the fractionated microbubbles were separated according to size and smaller microbubbles seem to accumulate at the top 5 % layer. If microbubbles were filled with saline, then smaller microbubbles would move towards the lower density fraction while larger microbubbles would move towards higher density fraction. The opposite would be true if microbubbles were filled with air, since larger microbubbles would be more buoyant than smaller ones, due to the density of air. Accumulation of smaller microbubbles at the top 5 % layer was an indication that in-house microbubbles were most probably filled with saline. Secondly, the fluorescent "background" had now been largely removed, presumably because of its difference density to the microbubbles (figure 8.8). Although this is not a direct proof that the background fluorescence was due to non-incorporated phospholipids, this speculation is plausible from the outcome of these results. Thirdly, a

comparison between the fractionated in-house and Definity® microbubbles (figure 8.4-8.7) confirmed that their surface area distribution was similar.

Crude in-house and fractionated samples were passed through a cell sorter in order to validate the size distribution results obtained by imaging and density gradient separation, with a different method. Scatter plots from the in-house microbubbles showed that 73 % of the crude samples were within the 2-3 μm in diameter. It was decided to cross examine these results with those obtained from microscope imaging and Volocity measurements. 40 microscope images of crude microbubbles were chosen. Selected images fell within the two standard deviation of the mean microbubble surface area distribution according to Volocity (figure 8.2). The diameter of these 40 microbubbles was then manually calculated. The nominal diameter of these microbubbles that were calculated by Volocity, were plotted against the actual diameters that were calculated manually (figure 8.10). Data from figure 8.10 provide two pieces of information. Firstly it can be deduced that actual microbubble diameters fall within the range of 2-3 μm. Secondly, the actual diameters of microbubbles do not agree with the nominal diameter calculations according to Volocity. Thus it can be postulated that the method for calculating microbubble surface area with Volocity was not valid.

Size distribution histograms from the crude and 5 % fractionated samples were overlaid on top of each other in order to verify whether fractionation had indeed separated microbubbles into fraction of different sizes (figure 8.11). The results indicate that fractionated sample has been slightly shifted towards smaller sizes. This suggests that only a small number of large microbubbles were extracted from the 5 % fraction. If however we take into consideration that most of the crude samples fall within the 2-3 μm

range (figure 8.10), then we can assume that there were not many large microbubbles in the original sample.

Finally, in-house microbubbles were fed through a coulter counter to further validate their size distribution with a different method. Figure 8.12 demonstrates that most of the microbubbles fall within a small range of 4-10 μm, with a small fraction containing larger microbubbles. Although the results from the coulter counter show a microbubble population of a larger size than that observed with confocal imaging or cell sorting, data from commercially available Definity® and Sonovue® microbubbles demonstrate that in-house microbubbles have similar size distribution to that of microbubbles used for attaining sonoporation (figure 8.13 and 8.14).

8.3 Conclusion

From the methods used in this section, it can be concluded that the size distribution of in-house microbubbles ranges from 2-10 μm with 73 % of the population falling within the 2-3 μm range and a smaller fraction containing larger microbubbles. These values are of comparable to microbubbles such as Definity® (mean 1.1-3.3 μm), (Miller and Dou 2009), Sonovue® (median 2 μm) (Rahim, Taylor et al. 2006a) and Optison® (mean 2-5 μm) (Kinoshita and Hynynen 2007), that are used in sonoporation studies.

Furthermore, cell sorting provided a possible indication that the in-house microbubble core is filled with aqueous solution rather than air. Subsequent research was focused on establishing the parameters necessary for achieving sonoporation in the presence of in-house microbubbles. Induction of sonoporation would allow development of a system for ultrasound mediated gene delivery in the presence of in-house microbubbles and possible gene expression.

Chapter 9

Investigation of ultrasound mediated sonoporation *in vitro*

9.0 Introduction

Cavitation is thought to be one of the main mechanisms for obtaining sonoporation (Van Wamel, Kooiman et al. 2006b). Several reports suggest that inertial cavitation and the phenomena associated with it, such as free radical formation, microstreaming, generation of high temperatures and pressures can be accountable for sonoporation (Gerard and Junru 1998; Ward, Wu et al. 2000; Dijkmans, Juffermans et al. 2004; Juffermans, Dijkmans et al. 2006; Patil and Pandit 2007; Cheng-Huang, Yeh et al. 2008). On the other hand, other studies have demonstrated that sonoporation takes place as a consequence of stable cavitation (Van Wamel, Kooiman et al. 2006b). Regardless of the type of cavitation that leads to sonoporation, its manifestation is strongly associated with the presence of microbubbles (Greenleaf, Bolander et al. 1998; Wu, Ross et al. 2002; Zhou, Cui et al. 2008). It has also been demonstrated that cell viability and molecular uptake are proportional to cell density and inversely proportional to bubble concentration (Ward, Wu et al. 2000; Guzmán, McNamara et al. 2003). It is therefore safe to assume that sonoporation entails a cell-bubble synergy. Thus, the cell-to-bubble ratio could function as a useful non-acoustic parameter (Guzmán, McNamara et al. 2003). The cell-to-bubble ratio reflects the distance between cells and microbubbles. However, previous studies reporting sonoporation use a wide range of cell to bubble ratio from 1:1 to 1:1000 (Brayman, Coppage et al. 1999; Ward, Wu et al. 1999; Kirosoglou, Hardt et al. 2006; Wu, Pepe et al. 2006; Van Wamel, Kooiman et al. 2006a). The use of such a broad range of cell to bubble ratio, and a large variation in published acoustic and non-acoustic parameters, has resulted in the publication of a vast spectrum of sonoporation efficiencies (Appendix 2) (Guzmán, McNamara et al. 2003).

The aim of this section was to establish both the acoustic and non acoustic parameters necessary for achieving ultrasound mediated sonoporation in the presence of microbubbles. Deciding on the initial parameters of this study was difficult due to the vast number of acoustic and non acoustic parameters involved in such an investigation. In order to decrease the number of initial parameters investigated, ultrasound induced sonoporation was examined in the presence of Definity® microbubbles, since they have been shown to induce sonoporation under certain ultrasonic conditions (Han, Ikegami et al. 2007; Zhou, Cui et al. 2008; Zhou, Shi et al. 2008). Once the acoustic parameters for achieving sonoporation were established, experiments were repeated in the presence of in-house microbubbles. This course of action allowed for investigation initially of acoustic parameters, followed by investigation of non acoustic parameters. In addition, the use of three different ultrasound pieces of equipment necessitated the establishment of the acoustic parameters for each separate apparatus. Therefore, experiments in this section can be divided into three sections:

(a) Acoustical measurements

When an ultrasound beam strikes upon an interface, a fraction of the wave will be reflected, leading to the generation of backscattered waves. Backscattered waves tend to move in the opposite direction of the original ultrasound wave, thus creating a standing wave (Wu and Nyborg 2008). Standing waves are characterized by areas called nodes, where no displacement takes place, and antinodes, where maximum displacement takes place (Wu and Nyborg 2008). Thus, the acoustic pressure along the length of a standing wave changes dramatically from one area to another. It is therefore important to eliminate the production of any backscatter and

hence any standing waves during insonation of cells. Although all studies provide information about the parameters of the ultrasound wave applied to their samples, such as intensity, only a handful of them take into consideration standing waves that might be present, thus failing to calculate the actual power delivered to the cells (Rahim, Taylor et al. 2006a; Kinoshita and Hynynen 2007). In addition, although ultrasound machines are calibrated by manufacturers, a discrepancy arises with time, between nominal and actual values obtained. Moreover, several studies perform their experiments in polystyrene or glass culture tubes without taking into consideration any backscatter waves produced at the medium / polystyrene or glass interface, due to the large discrepancy in their acoustic impedances (Rahim, Taylor et al. 2006a). Furthermore, acoustic pressure is critical to microbubble behaviour and thus for achieving sonoporation. The scarcity of precise recording of acoustic pressures during sonoporation studies, has made it difficult to reproduce experiments or to compare observations among studies (Rahim, Taylor et al. 2006a).

Although all precautions were taken in this study to eliminate the presence of any backscatter and standing waves, it was necessary to confirm this by measuring the exact acoustic field arriving at the cells of interest during each experimental set up. Therefore, measurement of the power outputs and pressure amplitudes of all the ultrasound equipment used was performed in order to accurately express the acoustic parameters used in sonoporation experiments.

(b) "Physiotherapy machine"

Although ultrasound imaging does not utilize ionizing radiation, a number of studies have reported some adverse bioeffects. For example, cell surface molecules have been shown to detach from cells after ultrasound

exposure (Mehier-Humbert, Bettinger et al. 2005a). Microvascular leakage was also observed after exposure to ultrasound in the presence of ultrasound contrast agents (Li, Cao et al. 2003; Miller 2007a). On the other hand several studies have examined the possible harmful effects resulting from ultrasound application and have not found any detrimental effects (Bekeredjian, Chen et al. 2005). It was therefore important to investigate whether both the acoustic (acoustic pressure & intensity) and non acoustic parameters (optimal cell concentration & potential microbubble toxicity) used in this study had any adverse effects that could compromise cell viability.

(c) Ultrasound scanner

Physiotherapy machines, as their name suggests are used for therapeutic purposes while ultrasound scanners are used for clinical imaging and diagnostic purposes. Therefore, the waveforms that are produced by each type of machine differ in a number of parameters. Since sonoporation was established with the aid of a physiotherapy machine, it was decided that further investigation of sonoporation should be carried out with the aid of an ultrasound scanner since that would be clinically relevant.

Furthermore, throughout the investigation of ultrasound induced sonoporation the following issues were examined:

- Transport of different size molecules across plasma membrane
- Transport and expression of DNA molecule across plasma membrane
- Effect in sonoporation efficiencies amongst three different cell lines
- Effect in sonoporation efficiencies between different culture methods
- Sonoporation in the presence of in-house and Definity® microbubbles with the aid of a “physiotherapy machine” and an ultrasound scanner

Finally, a number of experiments have been conducted in this study with the use of either a "physiotherapy machine "or an ultrasound scanner, in order to investigate sonoporation. Each experiment is normally an adaptation of the previous experiment with only one or two parameters changing. In order to make this chapter easier to follow, each experiment has been assigned a number and a schematic representation of the parameters used in each one is shown in Appendix 3.

9.1 Experimental set up

9.1.1 Petri dish

During initial ultrasound experiments cells were seeded in a Petri dish and were placed on a bench, since similar studies investigating sonoporation had used Petri dishes or other culture dishes of similar material (Greenleaf, Bolander et al. 1998; Brayman, Coppage et al. 1999; Wu, Ross et al. 2002; Duvshani-Eshet, Baruch et al. 2005; Feril, Ogawa et al. 2005). Some studies took into consideration the acoustic pressure transmission coefficient (acoustic pressure measured outside the tube divided by the acoustic pressure measured inside the culture tube), which was found to be 0.77 (Wu, Ross et al. 2002) while other studies reported that over 95 % of the ultrasound waves passed through the bottom of a Petri dish (Zhou, Shi et al. 2008).

9.1.2 Mylar membrane

While placing the cells in the ultrasound tank would significantly diminish the backscatter arising from the passing of ultrasound waves from the Petri dish to the air, the polystyrene, which the Petri dishes are made of, would still reflect a fraction of the ultrasound wave. The use of a Mylar membrane, which is acoustically transparent, would lessen the reflections produced, thus allowing for more accurate measurements of the acoustic

field. The Mylar membrane was wedged between two Derlin rings in order to eliminate any creases (ring-membrane-ring (MRM) "sandwich").

9.1.3 OptiCell™

A small number of studies investigating sonoporation have used OptiCells™ as the sample chamber for applying ultrasound (Rahim, Taylor et al. 2006b; Van Wamel, Kooiman et al. 2006b). Subsequent experiments were performed with the use of OptiCells™, which are chambers enclosed between two acoustically transparent gas-permeable membranes. Such chambers provided a stable environment for the cells in order to survive for the length of time necessary to perform the ultrasound experiments (maximum 60 min). In addition, due to the closed environment provided with the use of OptiCells™, no bacterial contaminations were observed. Furthermore, since the membranes of the OptiCell™ were permeable only to gas, the OptiCell™ could be submerged into the tank, thus allowing for a greater distance between the transducer and the cells, which would decrease the likelihood of reflections generated from the base of the tank.

9.1.4 Development of experimental rig

In order to be able to measure accurately the acoustic field incident on the cells, it is essential to diminish the possibility of any backscattered ultrasound. An ultrasound tank was designed so as to minimize generation of any backscatter. This was mainly achieved by increasing the distance between the cells and the bottom of the tank to 2 cm compared to almost none when the experiment was performed on the bench. Hence, ultrasound waves were allowed to travel further before reaching the Petri dish (polystyrene / air interface) thus reducing any backscatter waves. However, the distance between the transducer and the cells, was kept constant (~0.5

cm). Since the ultrasound tank set up minimized the possibility of backscatter, there was no reason to change the distance between the transducer and the cells. Increasing the transducer-cell distance would alter the power of ultrasound wave received by the cells, thus making comparison with previous experiment not possible. Some studies attempted to minimise the likelihood of reflection waves by placing a rubber absorber below the culture dish (Brayman, Coppage et al. 1999; Duvshani-Eshet, Baruch et al. 2005). However, it should also be taken into account that once the ultrasound waves have passed through the bottom of the culture dish they would first encounter air, which would result in generation of reflection waves, before arriving at the rubber absorber. In another study, cells were seeded in a 6 well dish and insonated from below (Feril, Ogawa et al. 2005). Although a transmitting gel was used between the transducer and dish interface in order to reduce the reflected waves, the reflection waves generated at the medium / air interface, were not taken into consideration. During subsequent experiments, an acoustic absorber was therefore placed at the bottom of the tank, prior to an air interface, in order to further minimise the possibility of any backscatter. Furthermore, turning the transducer at a 37° angle ensured that any backscatter still present would be guided away from the cells. The ultrasound tank set up also allowed for the cells to be placed on the microscope stage and then to be moved away from the stage so that ultrasound could be applied and returned back to the identical position on the microscope stage (figure 9.1-9.2).

The presence of air bubbles can act as potential cavitation nuclei, thus augmenting any effect the ultrasound might have on the cells (Dalecki 2004). However, Ward, Wu et al. (1999) did not detect any significant difference in the outcome of their experiments with the use of air-saturated or degassed

water at room temperature. In addition, a study investigating sonoporation with a range of temperatures reported maximum sonoporation efficiency at 37 °C (Zarnitsyn and Prausnitz 2004). Therefore it was decided to fill the ultrasound tank with boiled water and leave it to settle for 30 min, so as to minimise the presence of air bubbles and at the same time keep the temperature of the water as close to 37 °C as possible.

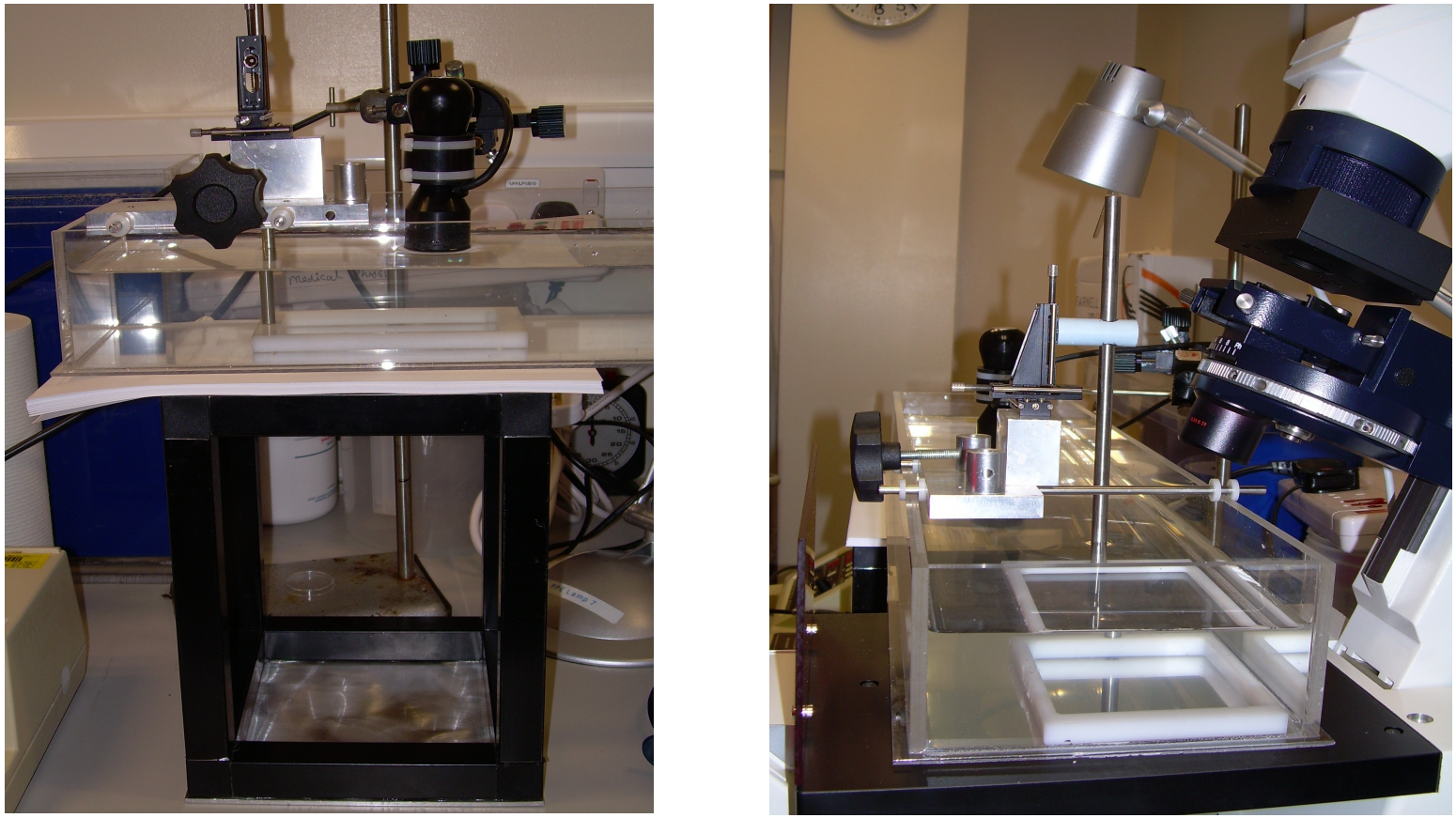

Figure 9.1 **Ultrasound tank setup.** The tank was placed on a base so as to be the same level as the microscope. Cells grown in an OptiCell™ were submerged in the tank and held into position with the aid of a custom made holder. The holder also allowed for the cells to slide on to the microscope stage after insonation which enabled images at the same field of view as that observed prior to insonation.

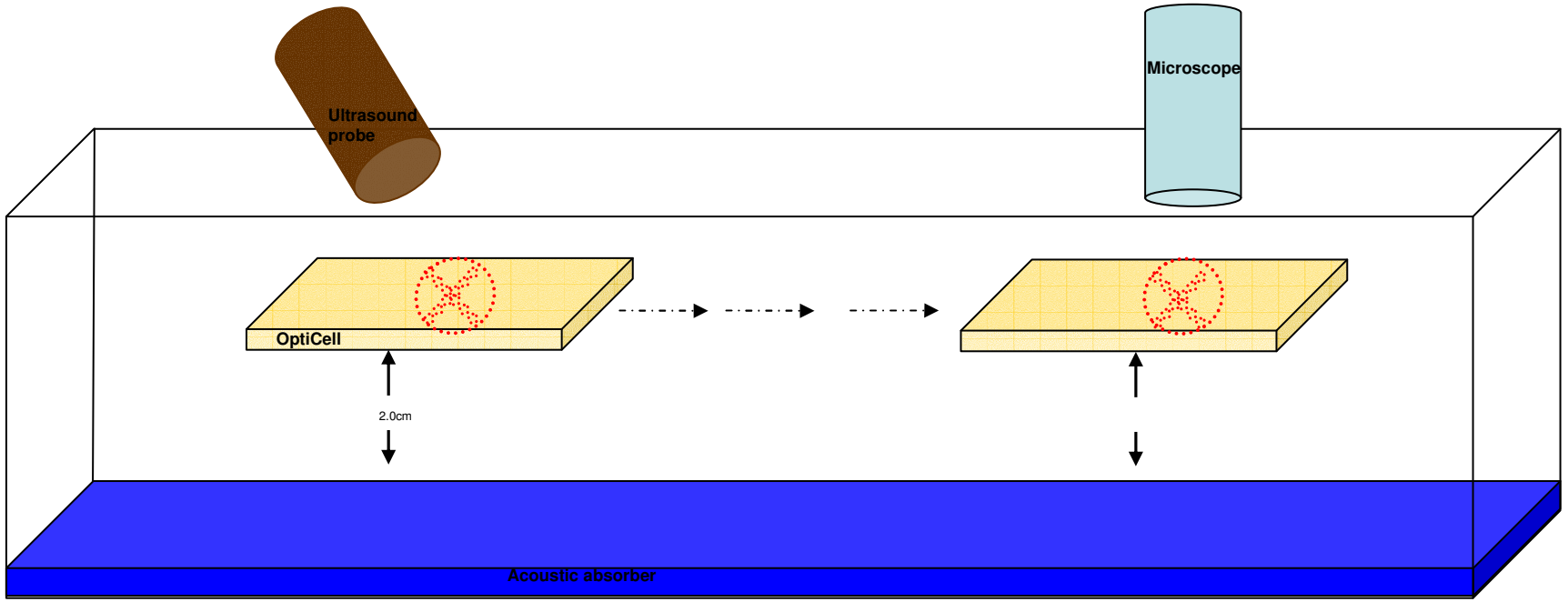

Figure 9.2 **Schematic representation of ultrasound tank set up.** Cells grown in an OptiCell™ were submerged in the tank and held into position with the aid of a custom made holder. The holder also allowed for the cells to slide on to the microscope stage after insonation which enabled images at the same field of view as that observed prior to insonation (image not drawn to scale).

9.2 Results

9.2.1 Ultrasound fields

9.2.1.1 Measurements of the ultrasound field of the "physiotherapy machine"

The peak to peak pressure of the ultrasound wave of the "physiotherapy machine" used in this study was investigated with the aid of a hydrophone (figure 9.3). The electrical interference observed in both images (a) and (b) of figure 9.3 is due to the presence of harmonics generated by the transducer. As can be seen from figure 9.4 the nominal and actual intensity of the ultrasound wave emitted from the "physiotherapy machine", measured with the aid of a radiation force balance, differ significantly. The acoustic pressure for ultrasound waves of 1 MHz and 3 MHz were measured for increasing intensities, with the aid of an oscilloscope (figure 9.5).

9.2.1.2 Measurements of the ultrasound field of the ultrasound scanners

9.2.1.2.1 Acoustic pressure in the presence of OptiCells™

A Philips Sono 5500 ultrasound scanner was used for conducting initial experiments. The acoustic pressure of the ultrasound beam was measured in the presence and absence of an OptiCell™ in order to confirm that the membrane of the OptiCell™ is acoustically transparent (figure 9.6). The acoustic pressure was measured at three different frequencies (1.59, 1.62, 2 MHz). Statistical analysis (student's t test, $p=0.005$, $n=3$) of the data indicated that there is no significant difference in the acoustic pressure of an ultrasound wave in the presence and absence of OptiCell™ for a range of frequencies. This experiment confirmed that the OptiCell™ is acoustically transparent.

Subsequent experiments were preformed with HDI3500 scanner as it became available for use. Peak to peak pressures were calculated at a frequency of 2-4 MHz with a centre frequency of 3 MHz, with the aid of a

hydrophone and the negative peak pressure were found to be 2.19 μPa while the positive was 5.74 μPa (figure 9.7).

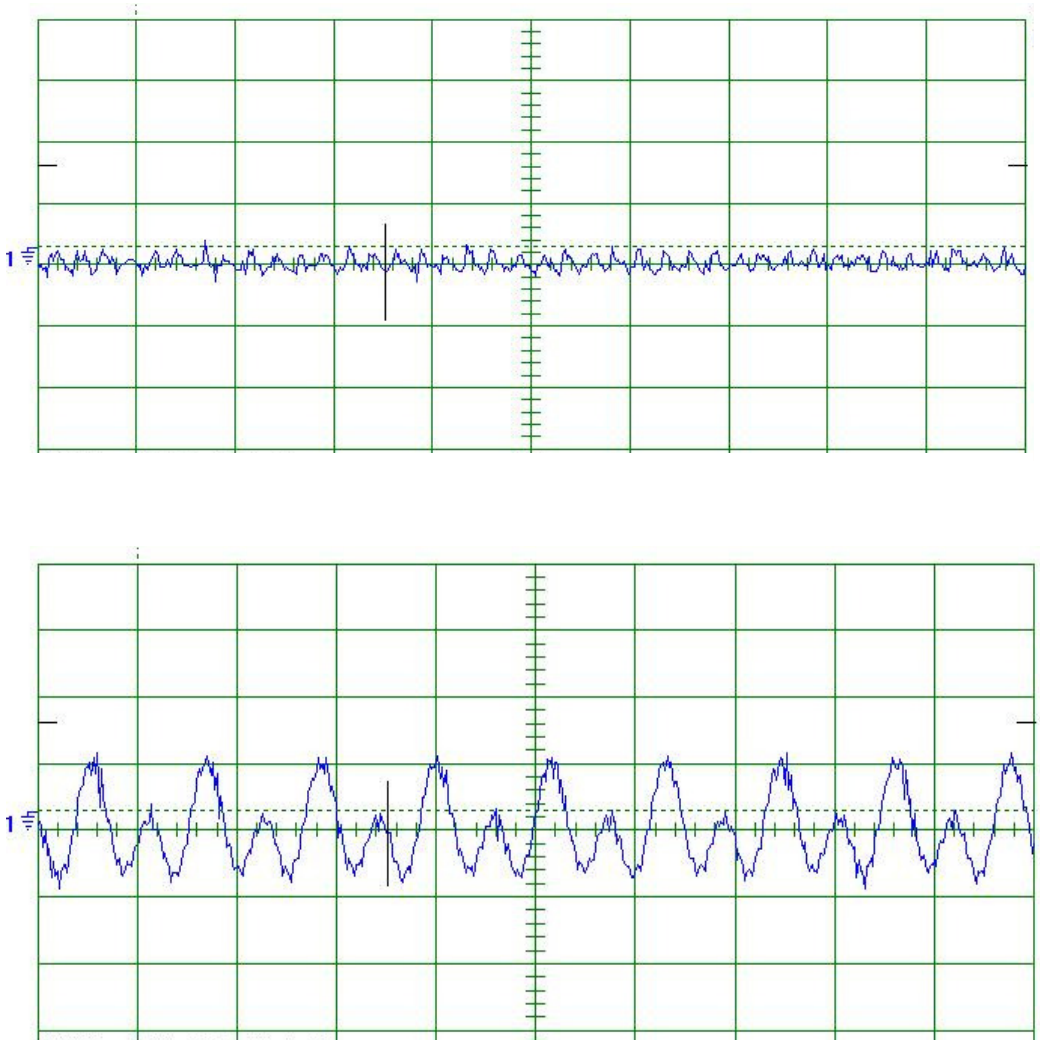

Figure 9.3 **Peak to peak pressure measurements of "physiotherapy machine" for 1MHz (a) and 3 MHz (b).** (a) X- axis is 100ns per division and Y-axis is 10 mV per division, (b) X- axis is 250ns per division and Y-axis is 10 mV per division. Peak to peak pressure for 1 MHz is 0.3 MPa and for 3 MHz is 0.79 MPa. The electrical interference observed in both images (a) and (b), is due to the presence of harmonics generated by the transducer.

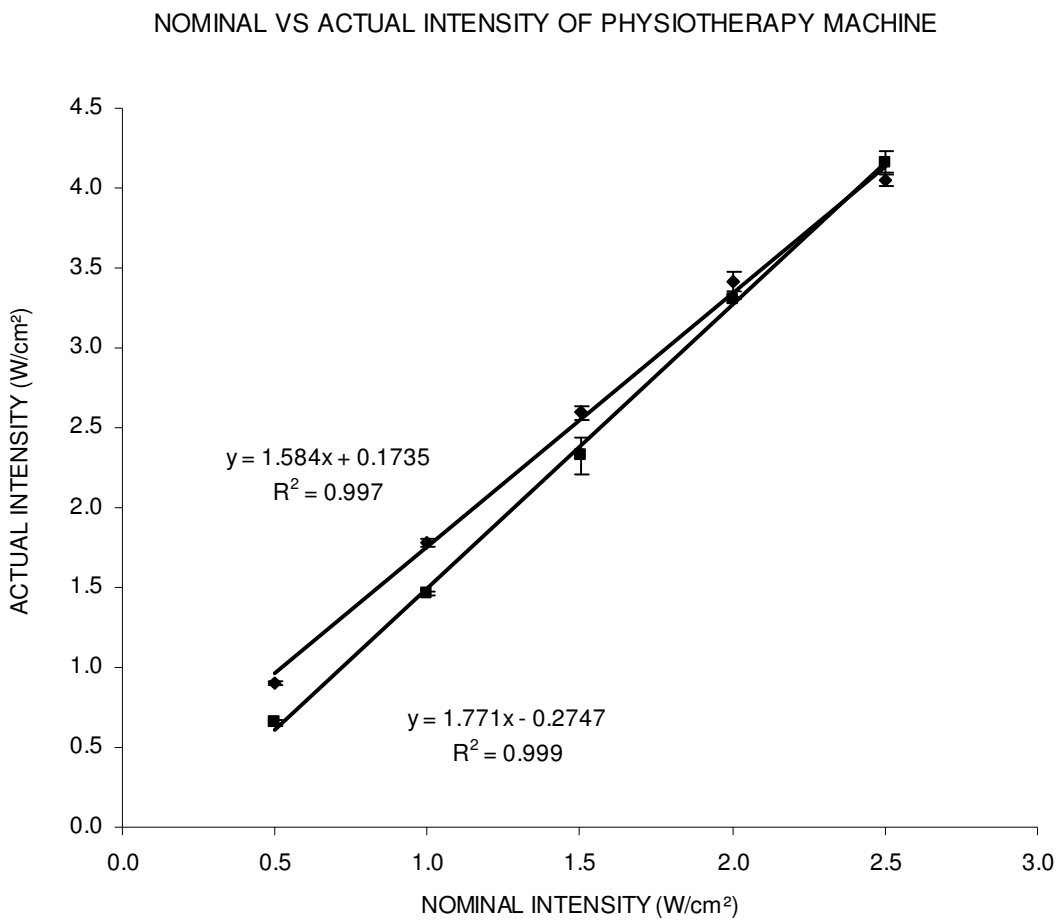

Figure 9.4 **Intensity of "physiotherapy machine".** The nominal and actual intensities of ultrasound wave of the "physiotherapy machine" used in this study were investigated with the aid of a hydrophone. The differences between the nominal acoustic intensity outputs for 1 MHz (■) and 3 MHz (▲) and the actual acoustic intensity outputs are shown in the graph.

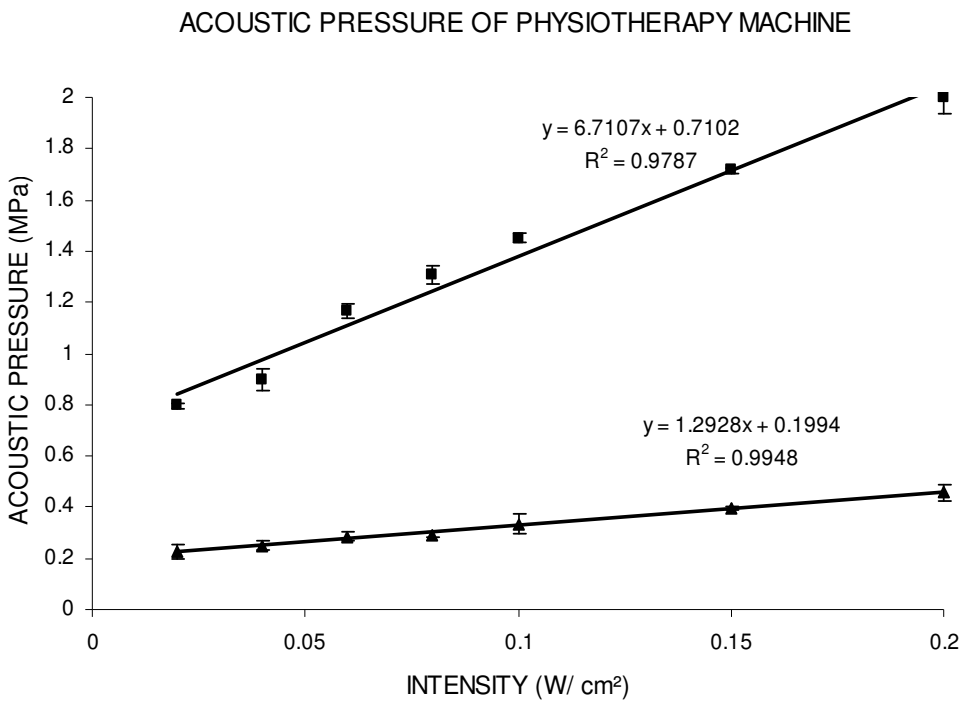

Figure 9.5 **Acoustic pressure of "physiotherapy machine".** As actual and nominal values for acoustic intensity of the "physiotherapy machine" were shown to differ significantly, it was necessary to calculate the actual acoustic pressure for ultrasound waves of 1 MHz (▲) and 3 MHz (■) for a range of intensities. These measurements were taken with the aid of an oscilloscope.

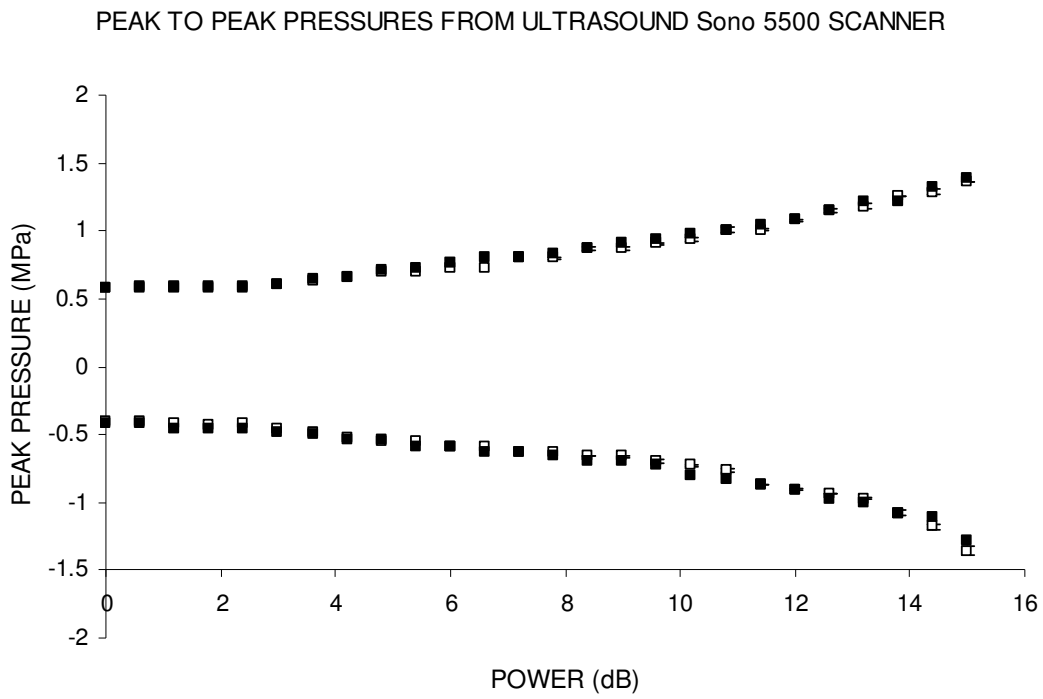

Figure 9.6 **Peak to peak pressure from the Sono 5500 scanner.** A Philips Sono 5500 ultrasound scanner was used for conducting initial sonoporation experiments. The acoustic pressure of the ultrasound beam was measured in the presence (□) and absence of an (■) OptiCell™ in order to confirm that the membrane of the OptiCell™ is acoustically transparent.

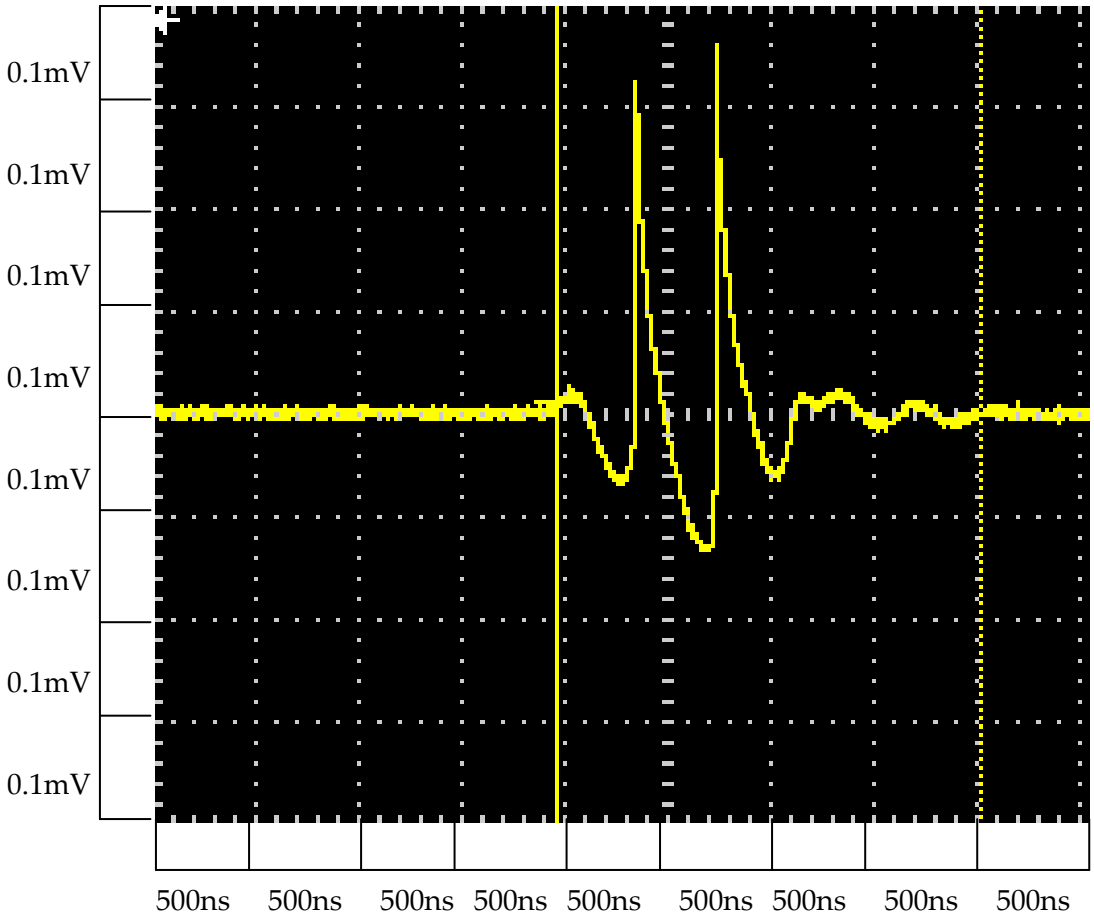

Figure 9.7 **Peak to peak pressure from the HDI3500 scanner**. Peak to peak pressure measurements of the HDI3500 scanner were performed with the aid of a hydrophone, in order to establish the actual pressure output exerted by this scanner. The figure depicts the graphical representation of the amplitude of the acoustic wave plotted against time. X- axis is 500ns per division and Y-axis is 0.1 mV per division. The negative peak pressure was found to be 2.19 µPa and the positive peal pressure was found to be 5.74 µPa for a centre frequency of 3 MHz.

9.2.1.2.2 Mechanical index in the presence of OptiCells™

Since the use of an ultrasound scanner provides an ultrasound beam with parameters that differ significantly from those applied with physiotherapy machines, it was essential to investigate cell viability in OptiCell™ during insonation with the ultrasound scanner HI3500. The mechanical index (MI) value is equal to the peak rarefractional pressure divided by the square root of the centre frequency of the beam (Church 2005). Therefore, any potential mechanical bioeffects are related to the peak negative pressure that has been measured. The mechanical and thermal (TI) indexes were recorded as they provide valuable information about the likelihood of cavitation or maximum temperature occurring, respectively. In addition, the lower the frequency the higher the likelihood of mechanical effects, hence the reason as low a frequency as possible was used with the system (3 MHz).

Cell viability assays were performed using ultrasound waves of increasing MI (0.2, 0.5, and 1.1). While in previous experiments, the transducer was placed in close proximity to the OptiCell™, during experiments with the use of the ultrasound scanner the OptiCell™ was placed 2.5-3 cm below the probe so that the cells were situated at the focal point of the ultrasound beam (figure 9.8). In order to minimise the amount of OptiCells™ used, the transducer was placed in three areas within each OptiCell™. Each of these areas was applied with ultrasound of the same MI. In addition, a fourth area was also examined within each OptiCell™, which served as an internal control. Control OptiCells™ were also used, where no ultrasound was applied. The OptiCells ™ were placed under the microscope and 10 images were taken for each of these areas before and after insonation (figure 9.9). Furthermore, the transducer was placed at a 90° angle. As can be

seen from figure 9.10, cell viability is not affected significantly for the MIs examined. This was also confirmed with statistical analysis (one-way ANOVA, $p=0.04$, $n=3$) of the data.

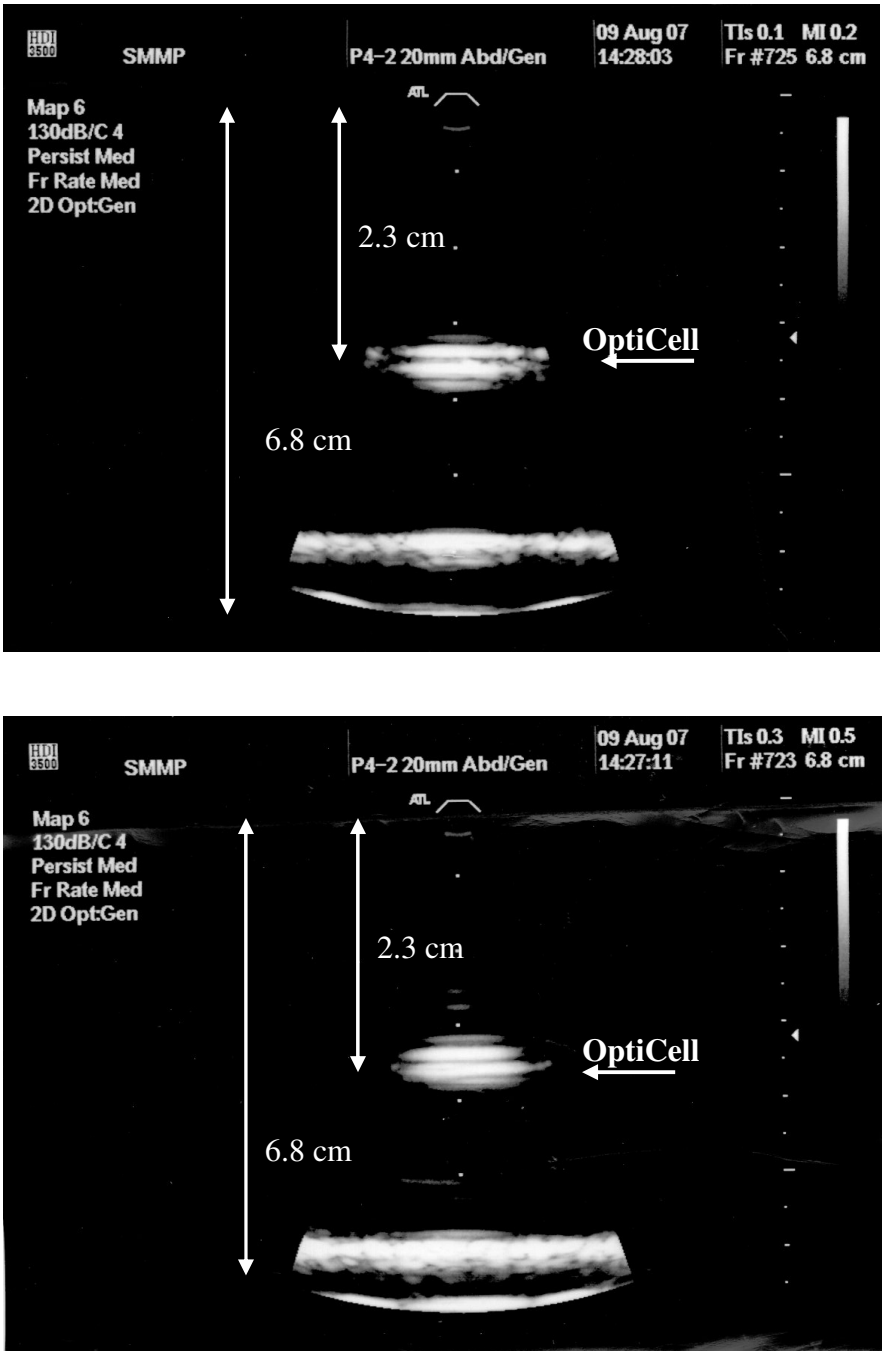

Figure 9.8 **Representation of monitor from ultrasound scanner HDI3500**. During sonoporation experiments with the ultrasound scanner, OptiCells™ were placed at the focal point of the beam, shown by the small arrow on the right hand side of the image. Distance from probe to bottom of the tank is 6.8 cm, while the focal point is around 2.5-3 cm below the probe. A range of mechanical and thermal indexes were used in order to establish sonoporation of cells. Top image MI=0.2, TI=0.1 and bottom image MI=0.5, TI=0.3.

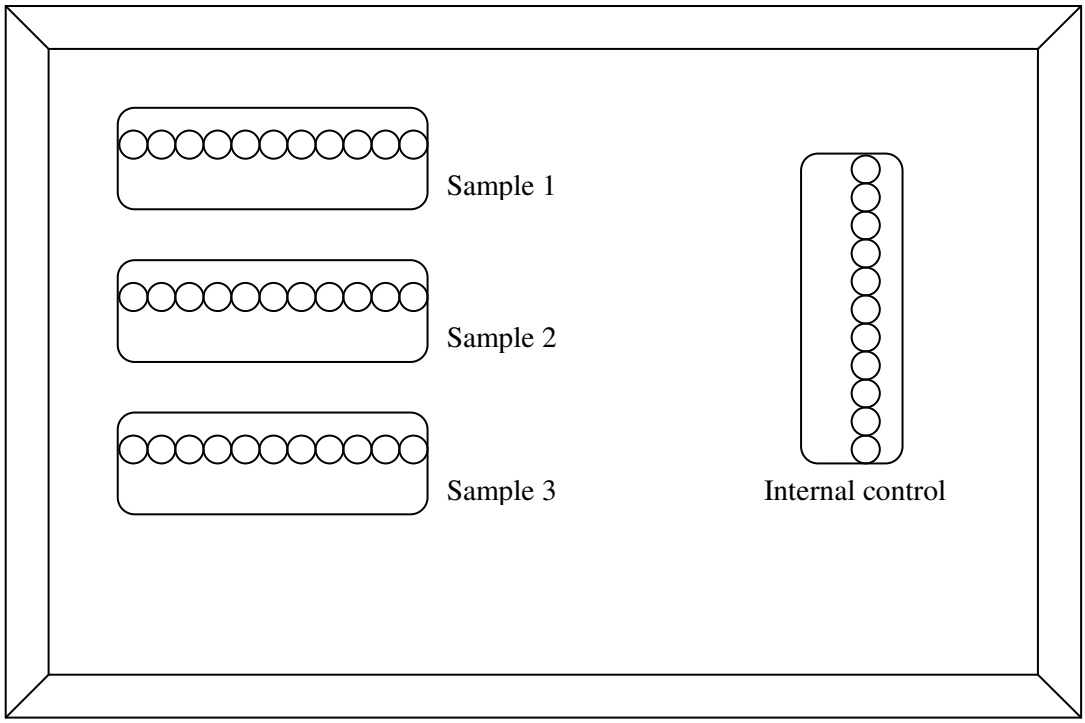

Figure 9.9 **Representation of application of ultrasound via transducer P4-2 to OptiCell™.** During investigation of the effect of mechanical index on cell viability, three areas within each OptiCell™ were exposed to ultrasound of the same MI value. A fourth area was also used as an internal control. Each circle within the areas, represents a field of view under the microscope, thus 10 images were taken before and after insonation in order to confirm cell viability (image not to scale).

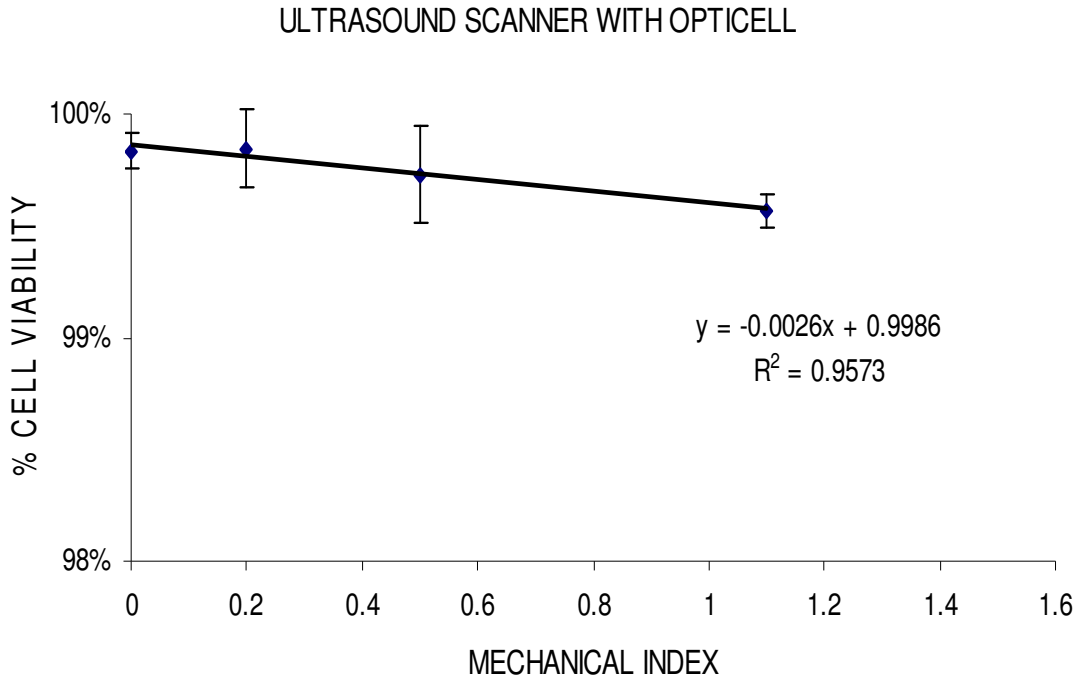

Figure 9.10 **Effects of ultrasound scanner on cell viability**. Experiments were conducted in order to determine the likelihood of any adverse bioeffects with the acoustic pressure and intensity emitted from the ultrasound scanner HDI 3500. As the peak rarefractional pressure is directly proportional to the mechanical index, the latter can provide an indication of bioeffects. Cells were thus insonated with a range of mechanical indexes in order to determine the likelihood of any adverse bioeffects occurring on cells during sonication. The mechanical indexes examined (0.2, 0.5, 1.1) correspond to acoustic pressures of 0.35 MPa, 0.87 MPa and 1.91 MPa respectively.

9.2.2 "Physiotherapy machine" experiments

9.2.2.1 Investigation of non acoustic parameters

One of the essential factors necessary to examine was the viability of the cells used in this study at different concentrations. Cells viability assays were performed on SK Hep-1 cells in order to find the optimum seeding densities. Five different seeding densities were examined, ranging from 2 x 10^5 to 1 x 10^6 cells / ml. Cell were stained with Calcein AM and Propidium Iodide 24h hours after seeding in order to measure the ratio of live to dead cells in the culture. For each seeding density, fifteen images from three separate Petri dishes were taken. The percentage of viabilities of each density along with the standard error of the mean (SEM) are plotted in figure 9.11. Cell viability was calculated as the number of viable cells after insonation divided by the number of viable cells before insonation and expressed as percentage. Statistical analysis of the data (one-way ANOVA, p=0.03, n=3) showed no significant difference between the different densities. Thus, it was decided to use the lower density of 2 x 10^5 cells / ml, as cells had to survive a further 2-3 days post seeding, so as to allow the cells to reach a concentration of approximately 4 x 10^5 cell / ml when used for sonoporation experiments.

As the microbubbles intended to be used in sonoporation experiments with in-house microbubbles, it was also essential to assess any potential toxicity. Therefore, crude in-house microbubbles were added to SK Hep-1 cells. Cells were then incubated for 1-48 hours, before carrying out a cell viability assay as described earlier. Such a prolonged period of incubation was necessary in order to evaluate cell survival during gene expression experiments. While planning these experiments, it was hypothesised that the 0.9 % (v/v) saline in which microbubbles were made in could be toxic to the cells. To test this hypothesis, in-house microbubbles that were prepared with phosphate buffered saline (PBS) were also incubated with cells. Figure 9.12

gives an indication of cell viability for different times of incubation with crude in-house microbubbles. Statistical analysis (one-way ANOVA, $p=0.03$ (saline), $p=0.01$ (PBS) $n=3$) showed no significant difference between different incubation times in the presence of microbubbles prepared in saline or in PBS. In addition, there is no significant difference between PBS and saline prepared microbubbles. Therefore, the results indicate that in-house microbubbles are not toxic to SK Hep-1 cells, regardless of the use of saline or PBS.

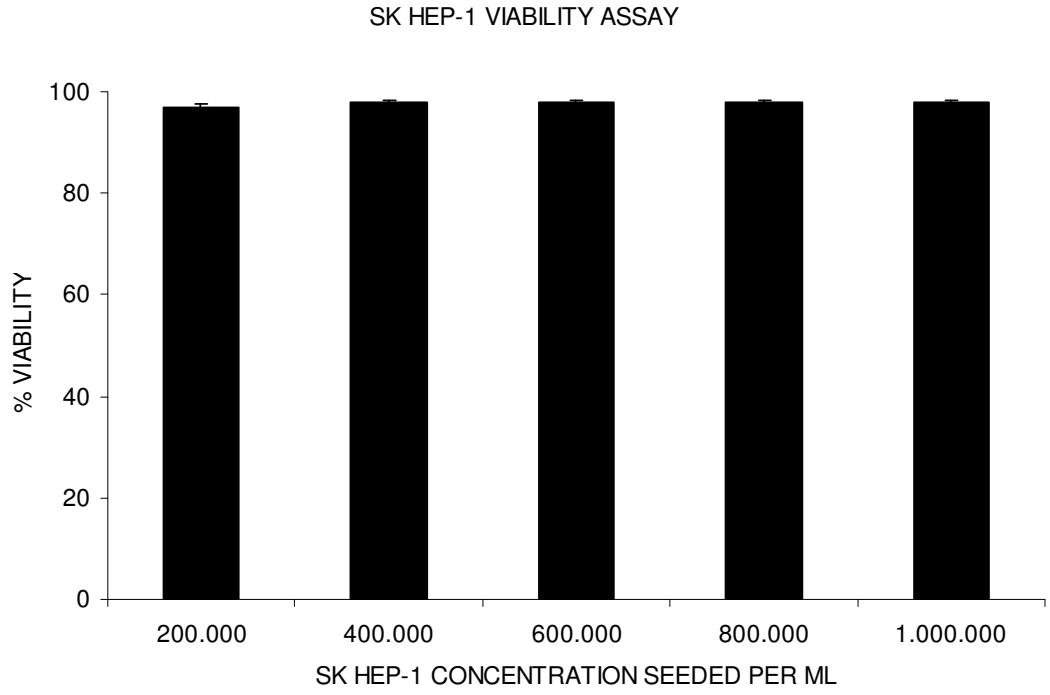

Figure 9.11 **SK Hep-1 viability assay**. Cells were seeded in a Petri dish in different concentrations in order to determine optimal seeding concentration. Cell viability was determined with the use of Calcein AM and Propidium Iodide. Error bars represent standard error of means. Statistical analysis showed no significant difference between different concentrations seeded.

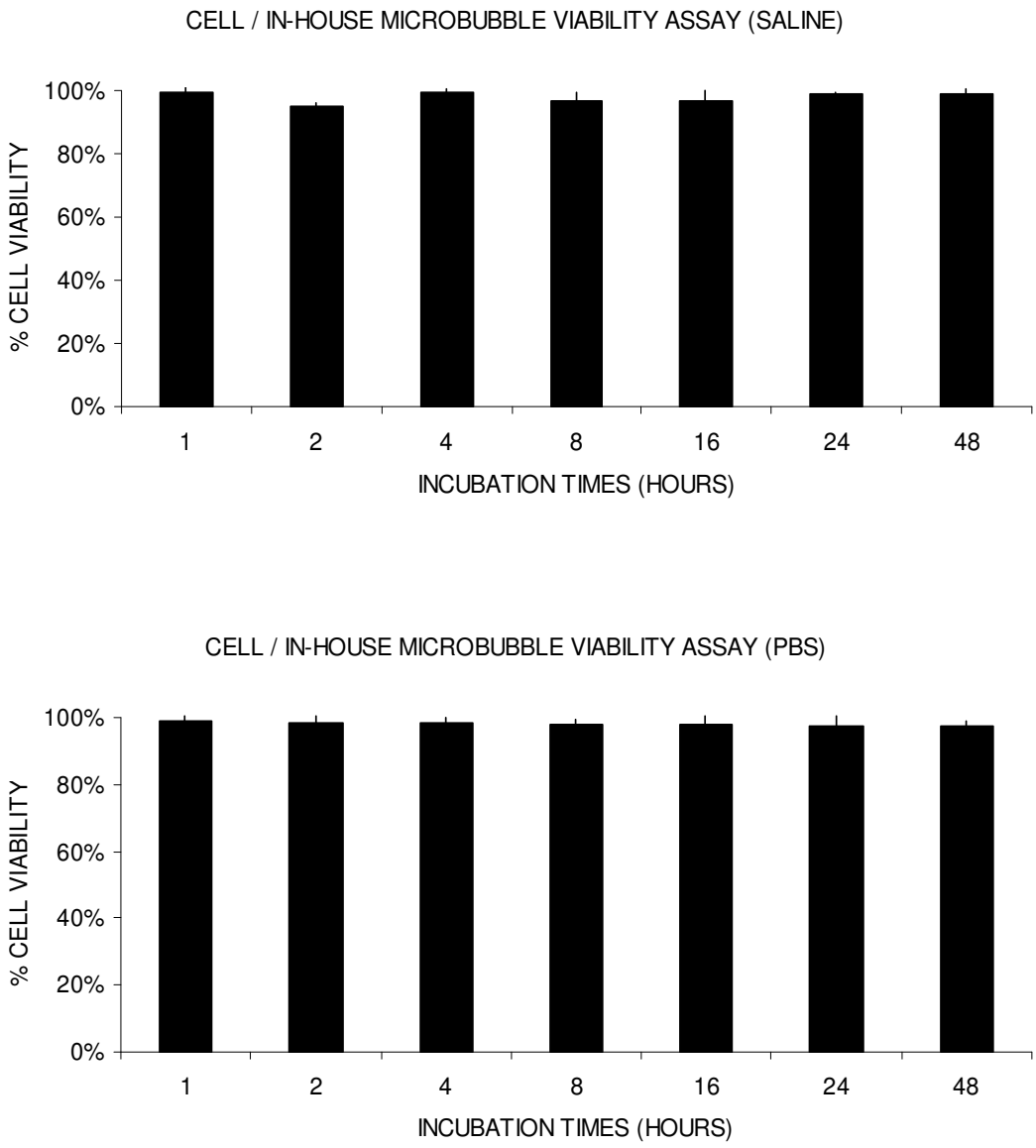

Figure 9.12 **Cell / in-house microbubble viability assays.** In-house microbubbles were incubated with SK Hep-1 cells in order to examine microbubble toxicity. Microbubbles were manufactured in the presence of saline (top graph) or in the presence of PBS (bottom graph). Microbubbles were added to the Petri dish containing SK Hep-1 cells and were left to incubate from 1 to 48 hours. Microbubble toxicity was assessed in terms of cell viability, which in turn was determined with the use of Calcein AM and Propidium Iodide.

9.2.2.2 Investigation of acoustic parameters

9.2.2.2.1 Investigation of acoustic parameters in the presence of a Petri dish

As previously mentioned, the parameters used in each study in order to achieve sonoporation vary immensely; it was therefore believed that the use of an ultrasound contrast agent previously reported to cause sonoporation could assist in setting the initial parameters necessary for sonoporation. Once all the acoustic and non-acoustic parameters were established in the set up used in this study, sonoporation of in-house microbubbles could be then investigated. Initial experiments were thus performed with Definity® microbubbles, as they are commercially available ultrasound contrast agents and have been previously shown to bring about sonoporation (Han, Ikegami et al. 2007; Zhou, Cui et al. 2008; Zhou, Shi et al. 2008).

Cells were seeded in a Petri dish and then insonified with the ultrasound waves of different intensities (0.1, 0.2, 0.3, 0.4, 0.6, 0.8 W / cm^2) in the presence and absence of Definity® microbubbles (figure 9.13). A range of microbubble concentrations was used (12.5, 25, 50, 75 μl) in order to assure that increasing amounts of microbubbles did not have any adverse effects on cell viability (Exp. 1). As can be seen from figure 9.14, cell viability is inversely proportional to intensity of ultrasound. In addition, higher concentrations of in-house microbubbles lead to decreased cell viability. Statistical analysis (two-way ANOVA, p=0.0001, n=9) of the samples confirmed that there is a significant difference in cell viability between different amounts of in-house microbubbles at a specific ultrasound intensity and between different intensities investigated. As can be seen from figure

9.14, maximum cell death (50.27 %) occurred at 0.8 W / cm^2 in the presence of 75 µl of Definity® microbubbles.

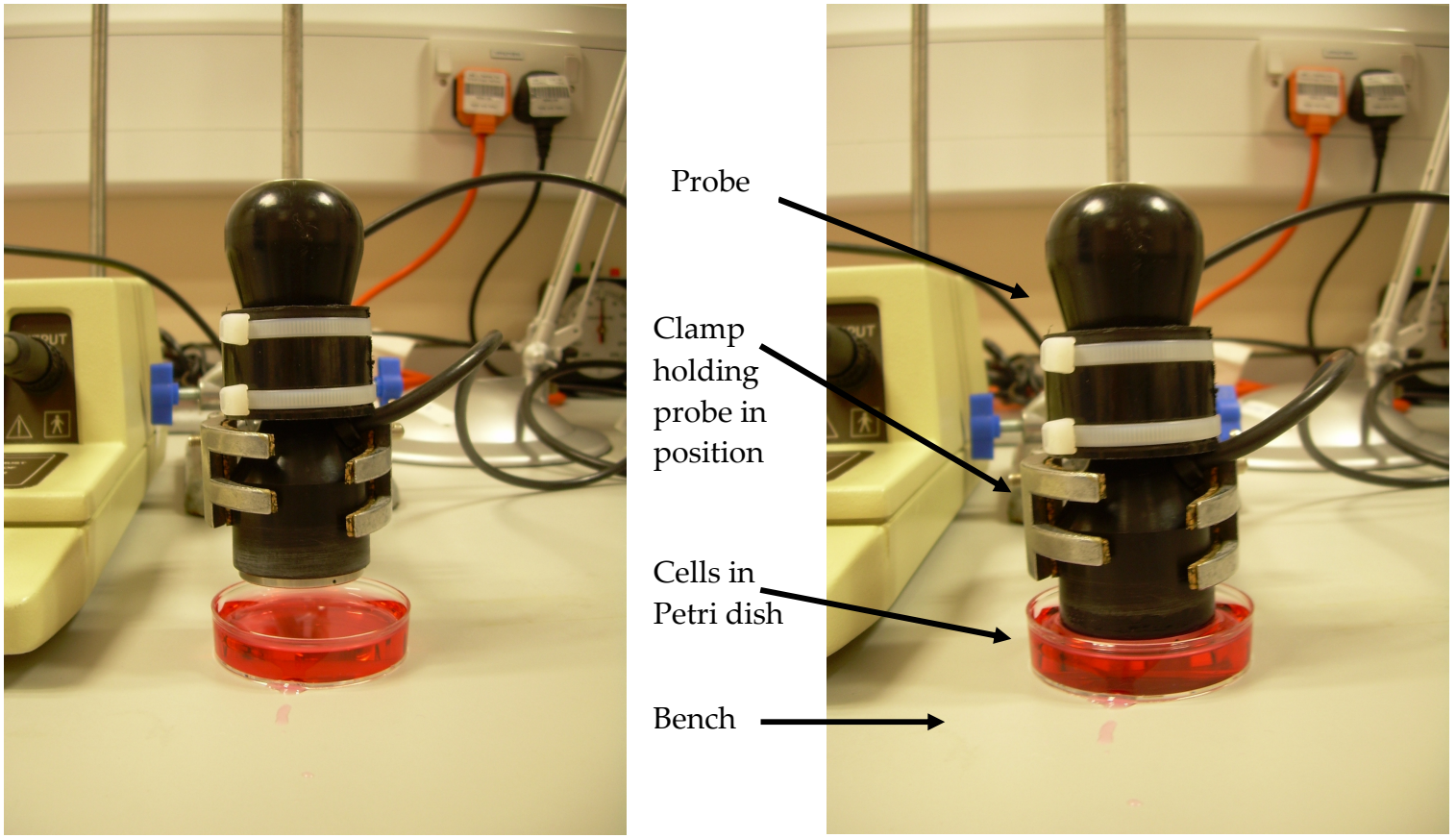

Figure 9.13 **Experimental set up for cell viability assays**. Cell viability was examined for a number of non acoustic parameters such as cell concentration and microbubble toxicity. Cells were seeded in a Petri dish 24 hours prior to insonation. The following day, cells were placed on a bench (a), where they were insonated with the "physiotherapy machine" (b). Cells were then transferred to the microscope where their viability was examined with the aid of Calcein AM and Propidium Iodide.

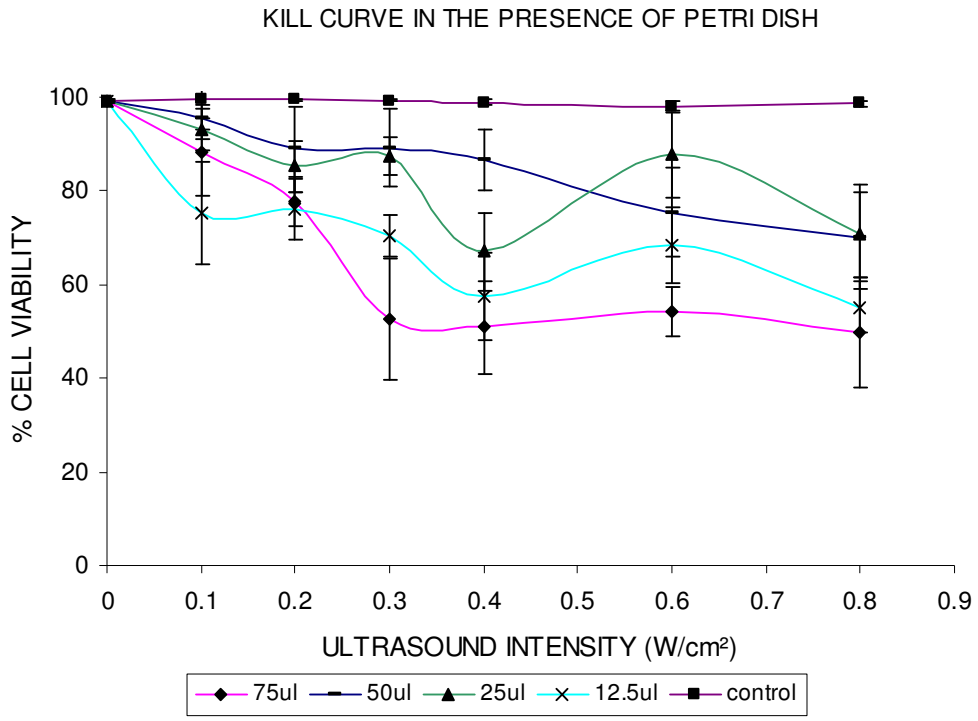

Figure 9.14 **Kill curve in the presence of Petri dish**. Cell toxicity was examined in relation to increasing ultrasound intensity and increase. Four different concentrations of Definity® microbubbles were added into the Petri dish, (◆) 75 µl, (-) 50 µl (▲) 25 µl, (x) 12.5 µl and (■) control (n=9). Cells were insonated with ultrasound waves of varying intensities (0.1, 0.2, 0.3, 0.4, 0.6 and 0.8 W / cm^2). Following insonation, cells were transferred to the microscope were their viability was assessed with the aid of Calcein AM and Propidium Iodide.

9.2.2.2.2 Investigation of acoustic parameters in the presence of a Mylar membrane (MRM) "sandwich"

During experiments with the MRM "sandwich", cell fatality was considerable even in the absence of ultrasound application, mainly because cells were exposed to non-regulated environment. Exposure of the cells to the air in the room where the experiments were conducted, affected the pH of the cellular environment. This was confirmed by the change in colour of the medium (DMEM) used to culture the cells. The DMEM contains phenol red, which is pH sensitive and changes colour accordingly; high pH values turn the medium into a bright pink colour. In addition, because cells were exposed to a non-sterile environment for a period of time, bacterial contamination was frequent. Experiments with the MRM "sandwich" were therefore not continued, since increased cell death was present in all samples, including the controls.

9.2.2.2.3 Investigation of acoustic parameters in the presence of an OptiCell™

Initial experiments with the use of OptiCells™ involved investigation of cell viability in the presence of microbubbles during sonication (Exp. 2). The viability of cells was examined in the presence of Definity® microbubbles using a range of ultrasound intensities similarly to those previously described in section 9.2.2.2.1. The microbubbles were injected into the OptiCell™ that was inverted several times in order to achieve an even distribution. Preliminary data (n=3) showed no change in cell viability with the intensities previously used (0.1, 0.2, 0.4, 0.6, 0.8 W / cm^2) (figure 9.15). It was believed that backscatter waves present in the initial (Petri dish) set up, were eliminated due to the use of OptiCells™, which are acoustically transparent unlike Petri dishes, which are highly reflective. This could

explain the absence of any effects on cells viability during insonation. Thus, subsequent experiments were performed with increased levels of intensity (2.54 W / cm^2). Two different concentrations of Definity® microbubbles were examined, while cells where sonicated for either 1 min or 3 min (Exp. 3). Figure 9.16 demonstrates the effects of different periods of sonication in the presence of Definity® microbubbles. As can be seen, the optimal cell survival was observed during application of ultrasound wave of 2.54 W / cm^2 intensity, for 1 min, in the presence of 100 μl of Definity® microbubbles. These results suggest that the presence of higher concentrations of microbubbles during sonication has a detrimental effect on cell viability.

At that point, an acoustic absorber was placed at the bottom of the tank in order to further minimise the possibility of any backscatter. At the same time, the transducer was turned at a 37° angle so that any backscatter still present would be guided away from the cells (figure 9.17). Therefore, the previous experiment was repeated in the presence of the acoustic absorber and transducer at a 37° angle. In addition, the area of cells exposed to ultrasound was marked on one of the membranes of the OptiCell™. Smaller areas within the marked area, corresponding to the field of view of the microscope were also marked as previously described in section 7.5.2.4.1. Therefore it was possible to map out the effects of ultrasound on different areas of the OptiCell™, in the presence and absence of microbubbles. Ultrasound of 2.54 W / cm^2 intensity was applied to cells for either 1 min or 3 min in the absence of microbubbles (figure 9.18), followed by 100 μl or 300 μl of Definity® microbubbles for each time period (figure 9.19-9.20). In addition to the cells being examined immediately after sonication, cells were also examined 24 hours after sonication (figure 9.21) (Exp. 4). The observations of this experiment have been plotted as percentage of cell viability. A colour

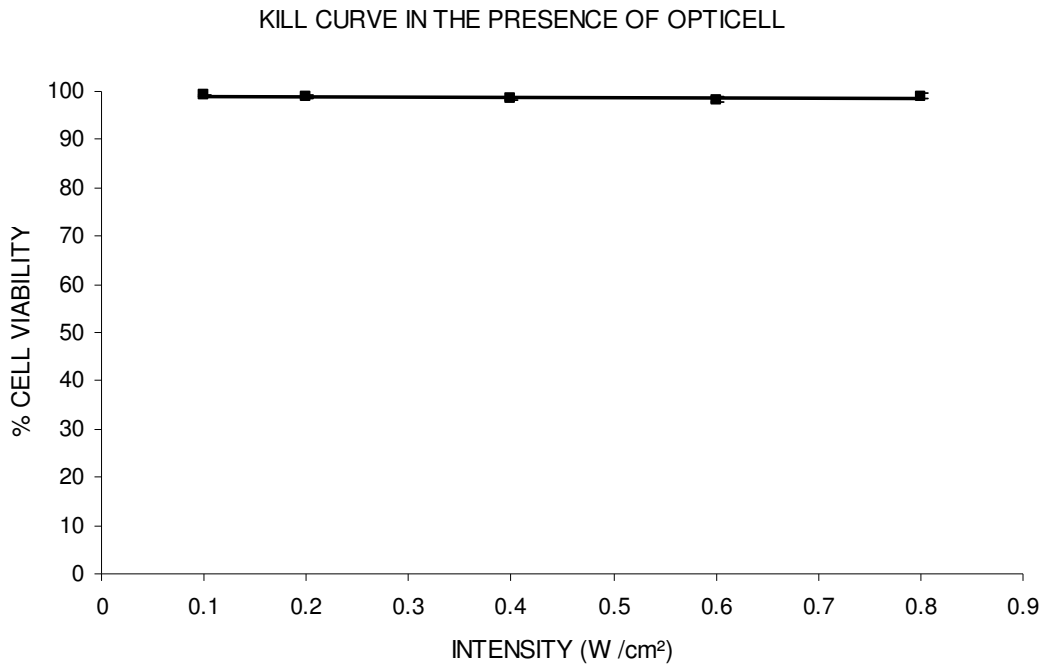

Figure 9.15 **Kill curve in the presence of OptiCell™**. During sonoporation experiments cells were seeded in acoustically transparent OptiCells™. Toxicity of the parameters established so far was examined prior to carrying out any sonoporation experiments. 100 µl of Definity® microbubbles were injected into the OptiCell™ and inverted several times in order to achieve even distribution. Cells were then insonicated with ultrasound waves of varying intensities (0.1, 0.2, 0.4, 0.6 and 0.8 W / cm^2). Following insonation, cell viability was assessed under the microscope with the aid of Calcein AM and Propidium Iodide.

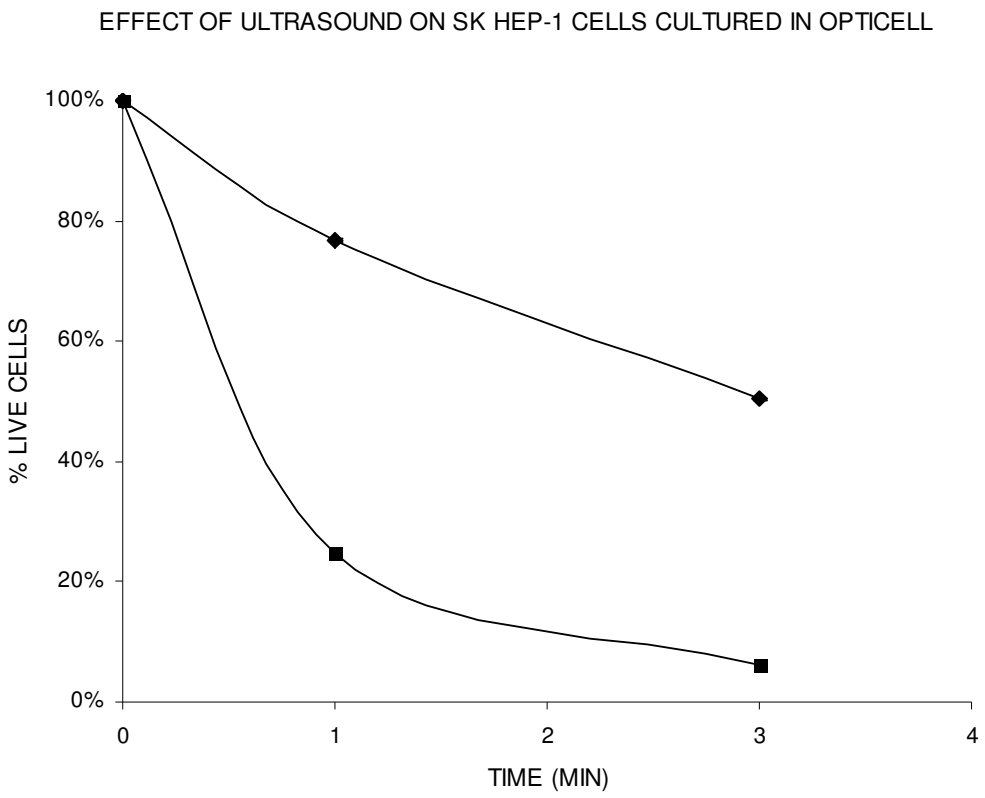

Figure 9.16 **Effect of ultrasound on SK Hep-1 cells cultured in an OptiCell™.** Cells were sonicated with an ultrasound wave of 2.54 W / cm^2 for different time periods (1min, 3 min) in the presence of 100 µl (◆) or 300 µl (■) of Definity® microbubbles. Following sonication, cells viability was examined under a microscope with the aid of Calcein AM and Propidium Iodide.

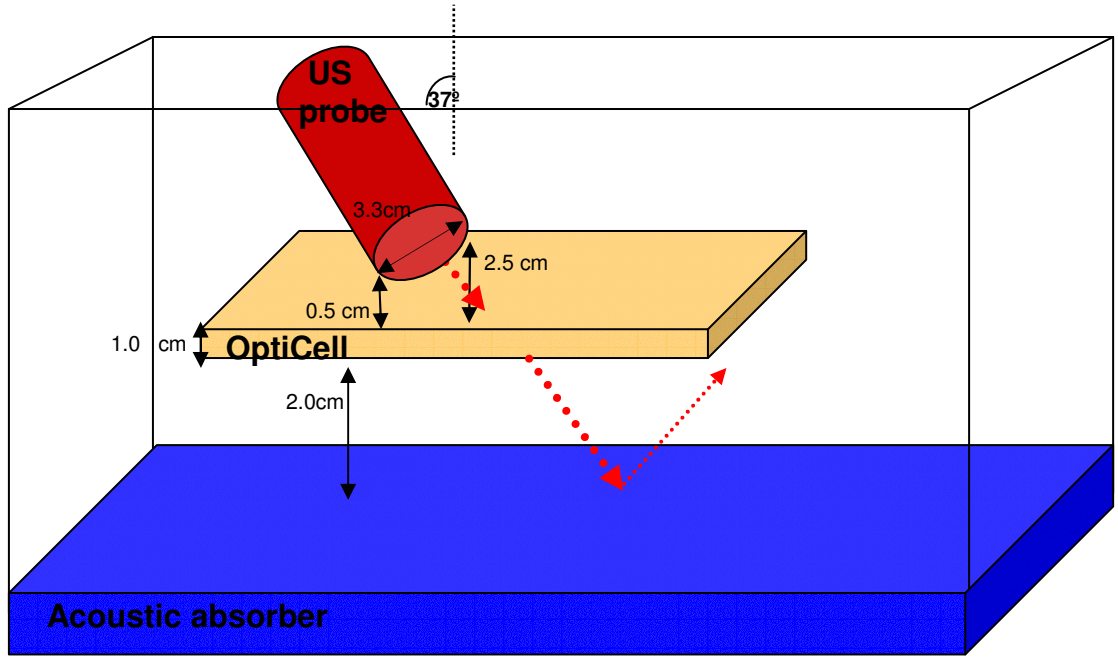

Figure 9.17 **OptiCell™ in ultrasound tank.** The OptiCell is placed in the ultrasound tank and is held at approximately 2.5 cm above the bottom of the tank so as to minimise any backscatter waves. In addition, the ultrasound probe is held in a 37 ºC angle so any backscattering waves that have not been absorbed by the acoustic absorber, will be guided away from the OptiCell (image not drawn to scale).

scale has been was devised, with each colour representing a 10 % decrease in cell viability i.e. bright red areas represent cell viability of 90-100 %, whereas bright blue areas represent cell viability of 0-10 %. Although from the data shown in figures 9.19-9.21 it visually appears that cell viability was greater during 3 min of sonication in the presence of 100 μl of Definity® microbubbles compared to all other parameters examined (3 min sonication in the presence of 300 μl of Definity® microbubbles and 1 min sonication in the presence of 100 μl and 300 μl of Definity® microbubbles), statistical analysis (two-way ANOVA, $p=0.006$, $n=3$) showed no significant difference between the different concentrations of microbubbles used or the amount of time ultrasound was applied (two-way ANOVA, $p=0.006$, $n=3$). As a result, it was decided to continue with the parameters that would minimise the probability of any bioeffects and / or cell death (minimum sonication in the presence of 100 μl of Definity® microbubbles).

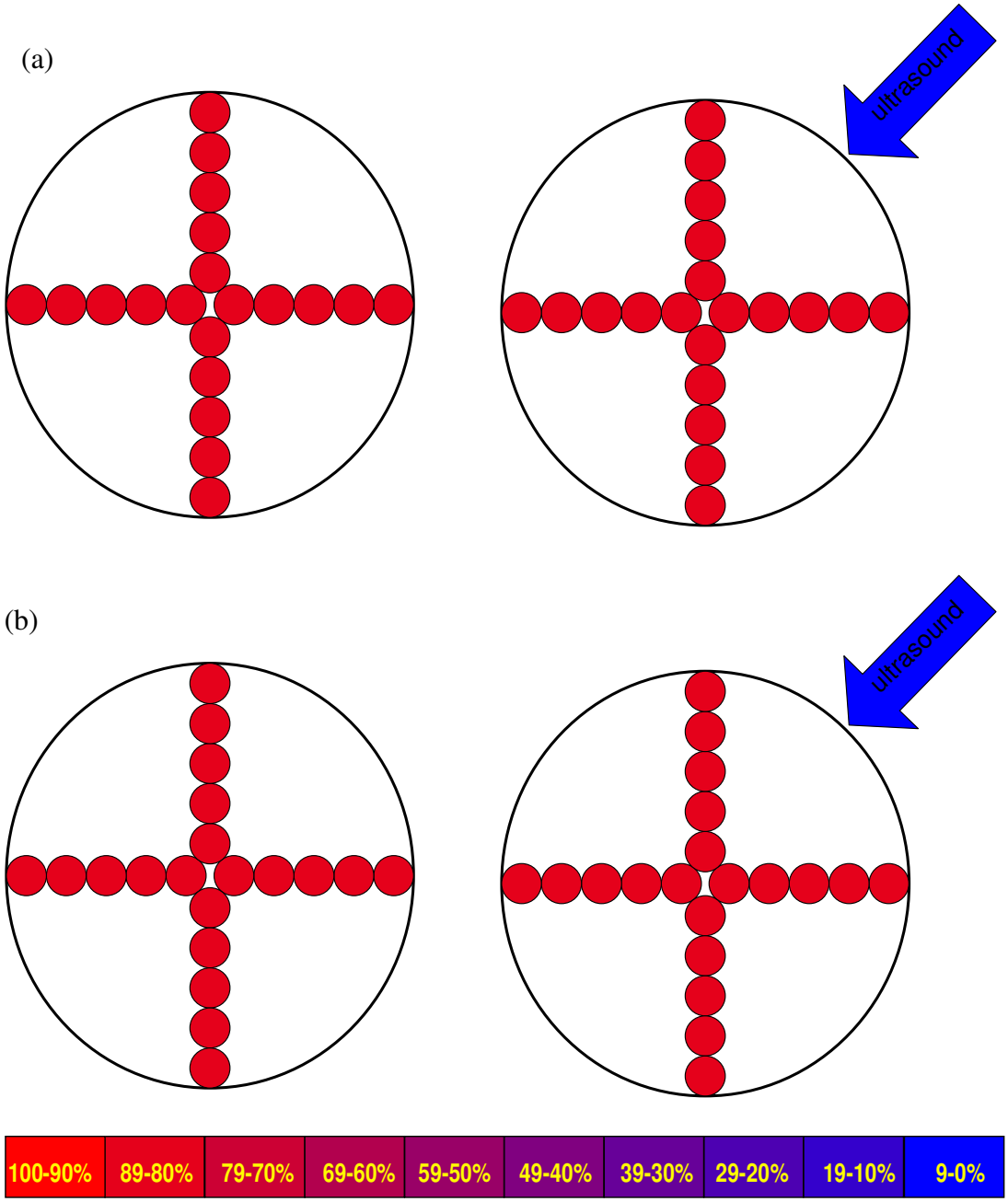

Figure 9.18 **Effects of ultrasound on SK Hep-1 cells in the absence of microbubbles.** Cells were sonicated for 1 min (a) and 3 min (b) with an ultrasound wave of 2.54 W / cm^2 intensity. Each large circle represents the area where ultrasound was applied. The circle on the left is before ultrasound and the circle on the right is after ultrasound application. Bright red areas represent cell viability of 90-100 %, whereas bright blue areas represent cell viability of 0-10%.

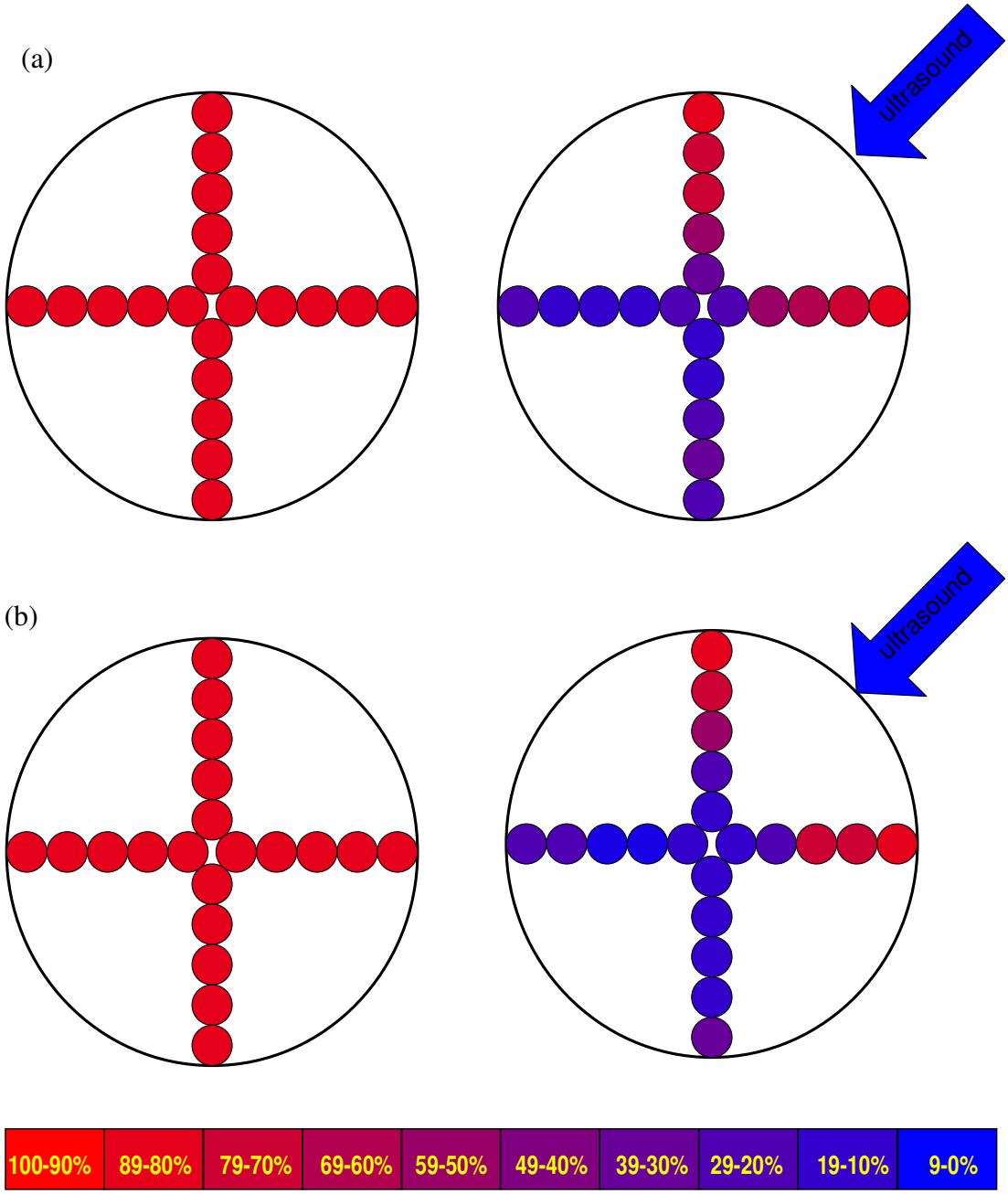

Figure 9.19 **Effects of ultrasound on SK Hep-1 cells in the presence of microbubbles.** Cells were sonicated with an ultrasound wave of 2.54 W / cm^2 intensity, for 1 min with either 100 µl (a) or 300 µl (b) of microbubbles. Each large circle represents the area where ultrasound was applied. The circle on the left is before ultrasound and the circle on the right is after ultrasound application. Bright red areas represent cell viability of 90-100 %, whereas bright blue areas represent cell viability of 0-10%.

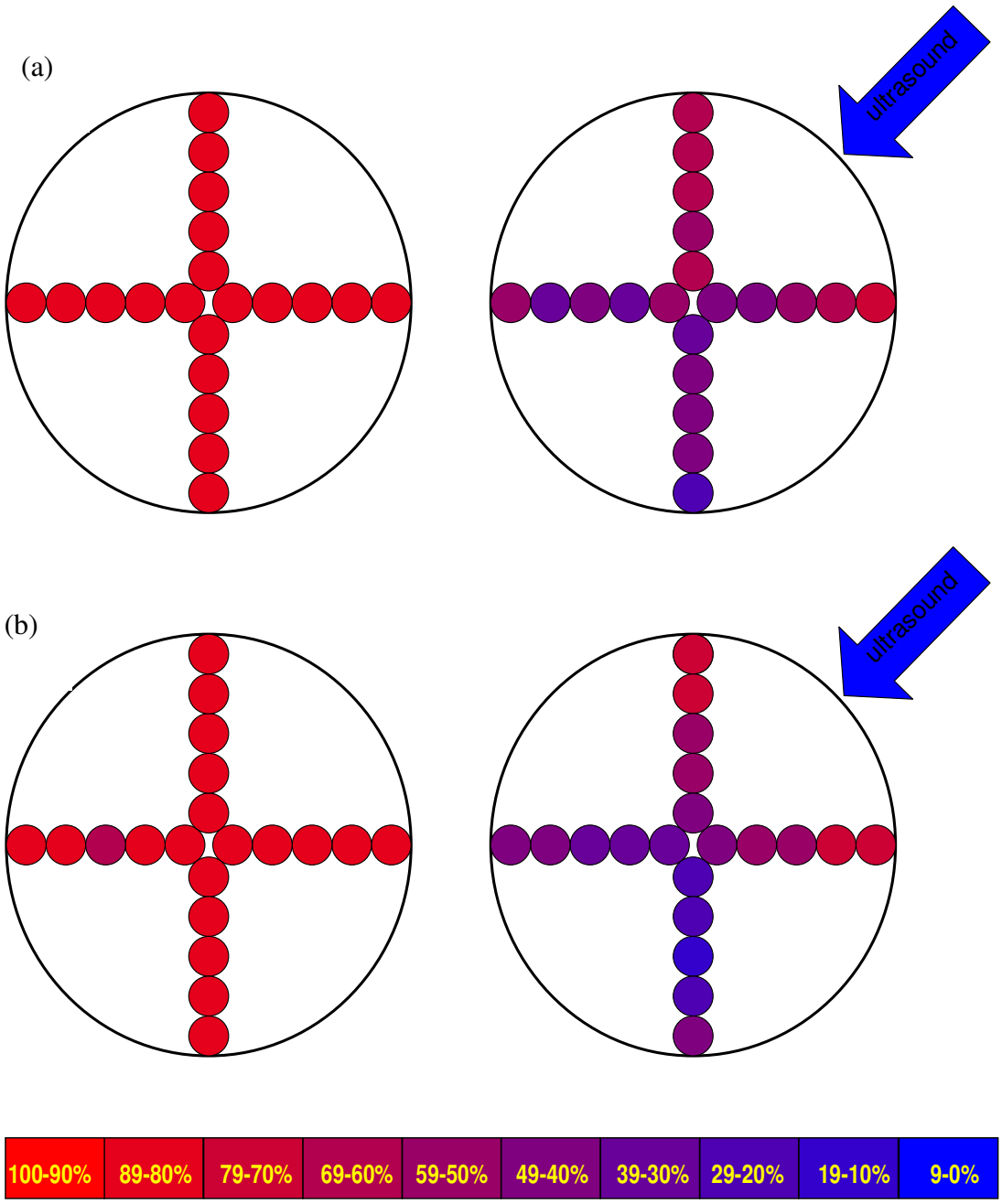

Figure 9.20 **Effects of ultrasound on SK Hep-1 cells in the presence of microbubbles.** Cells were sonicated with an ultrasound wave of 2.54 W / cm^2 intensity, for 3 min with either 100 µl (a) or 300 µl (b) of microbubbles. Each large circle represents the area where ultrasound was applied. The circle on the left is before ultrasound and the circle on the right is after ultrasound application. Bright red areas represent cell viability of 90-100 %, whereas bright blue areas represent cell viability of 0-10%.

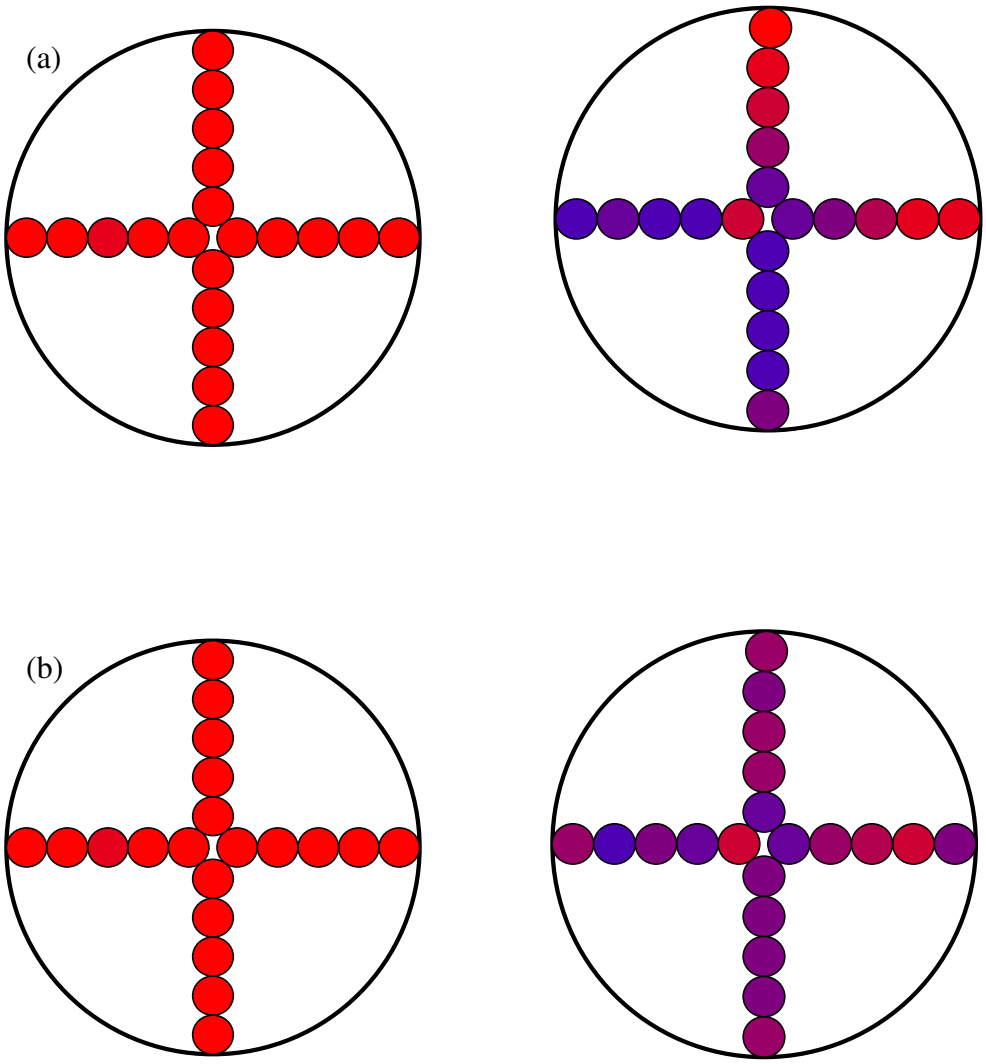

Figure 9.21 **Effects of ultrasound on SK Hep-1 cells in the presence of microbubbles 24 hours after insonation.** Cells were sonicated with an ultrasound wave of 2.54 W / cm^2 intensity, for 1 min with either 100 µl (a) or 300 µl (b) of microbubbles. Each large circle represents the area where ultrasound was applied. The circle on the left is before ultrasound and the circle on the right is after ultrasound application.

9.2.2.3 Sonoporation in the presence of Definity® microbubbles

9.2.2.3.1 Cell impermeable Calcein

Completion of initial experiments led to establishing a number of parameters necessary for achieving sonoporation. SK Hep-1 cells were therefore seeded in OptiCells™ and were sonicated for 2-3 sec with ultrasound waves of 2.54 W / cm^2 intensity in the presence of 100 μl of Definity® microbubbles. Two different concentrations of pCS2 plasmid (0.1, 0.3 μg / ml) were used in order to demonstrate occurrence of sonoporation. Successful sonoporation would allow the pCS2 plasmid to enter the cytoplasm and express EGFP, a green fluorescent protein. Expression of EGFP was examined 24 hours later, via electron fluorescence microscopy (Exp. 5). The results from this experiment suggested that sonoporation had not taken place. A possible explanation could be that sonoporation had taken place but the size of the pores formed, were too small for the plasmid to pass through. To determine if this was the case, cells were transfected with a transfection agent (ExGen 500) with the same amounts of pCS2. Although transfection uses a completely different pathway for attaining DNA entry in to the cells, the purpose of this experiment was to demonstrate that the quantities of DNA used for sonoporation experiments were capable of expressing EGFP once in the cell cytoplasm and could be detected. Increasing amounts of pCS2 plasmid during transfection showed to be correlated with increasing transfection rates. As can be seen from figure 9.22, the highest transfection rate (52.25 %) is achieved with the use of 1.5 μg / ml of pCS2.

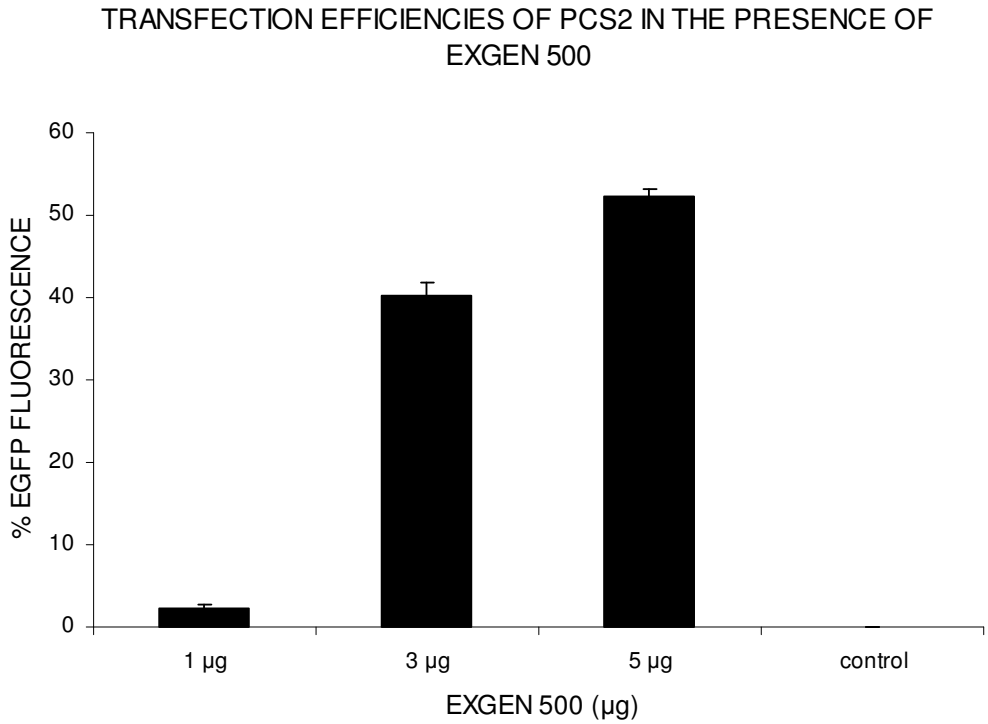

Figure 9.22 **Transfection efficiencies in the presence of ExGen 500.** SK Hep-1 cells were transfected with pCS2 plasmid in the presence of varying amounts of ExGen 500. Transfection efficiency was evaluated with EGFP fluorescence, which was measured by flow cytometry and was detected at a 515-545 broad band.

However, since the total amount of media in an OptiCell™ is 10 ml, an immense quantity of pCS2 plasmid would be required for the sonoporation experiments. Since smaller amounts of pCS2 plasmid (0.3 μg / ml) also resulted in successful transfection, it was decided to carry out sonoporation experiments with the smallest amount of pCS2 possible (0.1 and 0.3 μg / ml). In addition, it was thought that low rates of sonoporation would be difficult to detect using a fluorescence microscope, therefore subsequent experiments were examined via flow cytometry.

Sonoporation has been shown to form transient pores with an upper size limit of 75 nm for nanospheres and 464 kDa for dextran (Mehier-Humbert, Bettinger et al. 2005a). It was therefore hypothesised that the lack of EGFP expression during sonoporation experiments was due to the size of pores being smaller than the size of the pCS2 plasmid (149 kDa). In addition, it has been shown that there is an inverse correlation between the size of a molecule and its cellular uptake (Mehier-Humbert, Bettinger et al. 2005a). Thus, even if plasma membrane permeability was increased, only a small number of larger molecules would pass through the plasma membrane, which would be very hard to detect. In order to verify this hypothesis, sonoporation experiments were performed in the presence of cell impermeable Calcein, a much smaller molecule of 623 kDa (d=1.2 nm) (Exp. 6). Flow cytometry data, shown in figure 9.23, show that sonoporation was achieved during sonication of SK Hep-1 cells in the presence of several different concentrations of Definity® microbubbles. Statistical analysis (one-way ANOVA, p=0.001, n=3) of the data revealed that there is a significant difference between all the samples. In addition, the samples with the highest amounts of microbubbles (300 μl, 600 μl & 900 μl) were significantly different from controls (student's t-test, p=0.001 (300μl), p=0.007 (600μl), p=0.004

(900μl), n=3), whereas the lowest amount of microbubbles used (5 μl) was not significantly different from the controls (student's test, p=0.5, n=3). As can be seen from figure 9.24, maximum sonoporation (8.37 % efficiency) was achieved in the presence of 900 μl of Definity® microbubbles, which corresponds to a cell to bubble ratio of 1 in 5400. Nevertheless, lower amounts of microbubbles, such as 300 μl, also resulted in sonoporation (4.97 % efficiency).

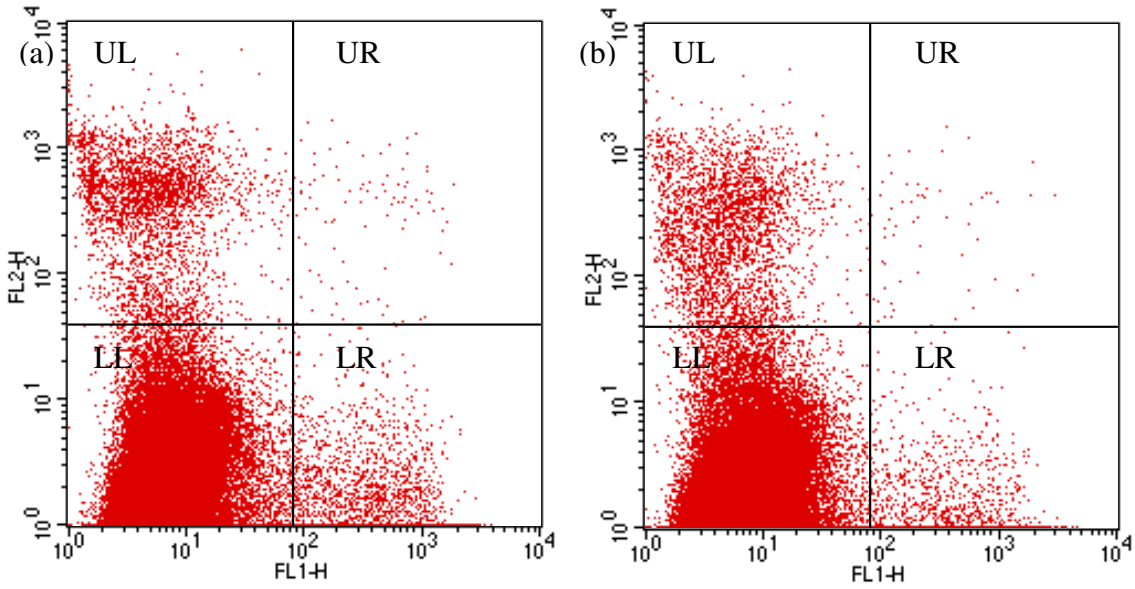

Sample ID:
Gate: G1
Gated Events: 100000
Total Events: 107652

(c)

Quad	Events	% Gated	% Total
UL	3195	3.19	2.97
UR	95	0.10	0.09
LL	90171	90.17	83.76
LR	6539	6.54	6.07

Sample ID:
Gate: G1
Gated Events: 100000
Total Events: 108996

(d)

Quad	Events	% Gated	% Total
UL	2954	2.95	2.71
UR	58	0.06	0.05
LL	92934	92.93	85.26
LR	4054	4.05	3.72

Figure 9.23 **Sonoporation in the presence of cell impermeable Calcein.** Representation of data collected via flow cytometry, during application of ultrasound (a) & (b). Cells were fed through a flow cytometer and emission of Calcein (green) and PI (red) fluorescence were detected. A 2D histogram was plotted with the x- axis (FL1-H) representing the Calcein fluorescence and the y-axis (FL2-H) representing the PI fluorescence. The histogram can thus be divided into 4 quadrants with 4 distinct populations. The lower left (LL) quad is Calcein and PI negative, i.e. cells are alive but have not been sonoporated. The Upper left (UL) quad is Calcein negative and PI positive, i.e. cells are dead and were not sonoporated. The lower right (LR) quad is Calcein positive and PI negative, i.e. cells were sonoporated and are still alive. The upper right (UR) quad is Calcein and PI positive, i.e. cells were sonoporated but died. A total of 100,000 cells were examined per sample and the statistics for each histogram is shown in (c) and (d).

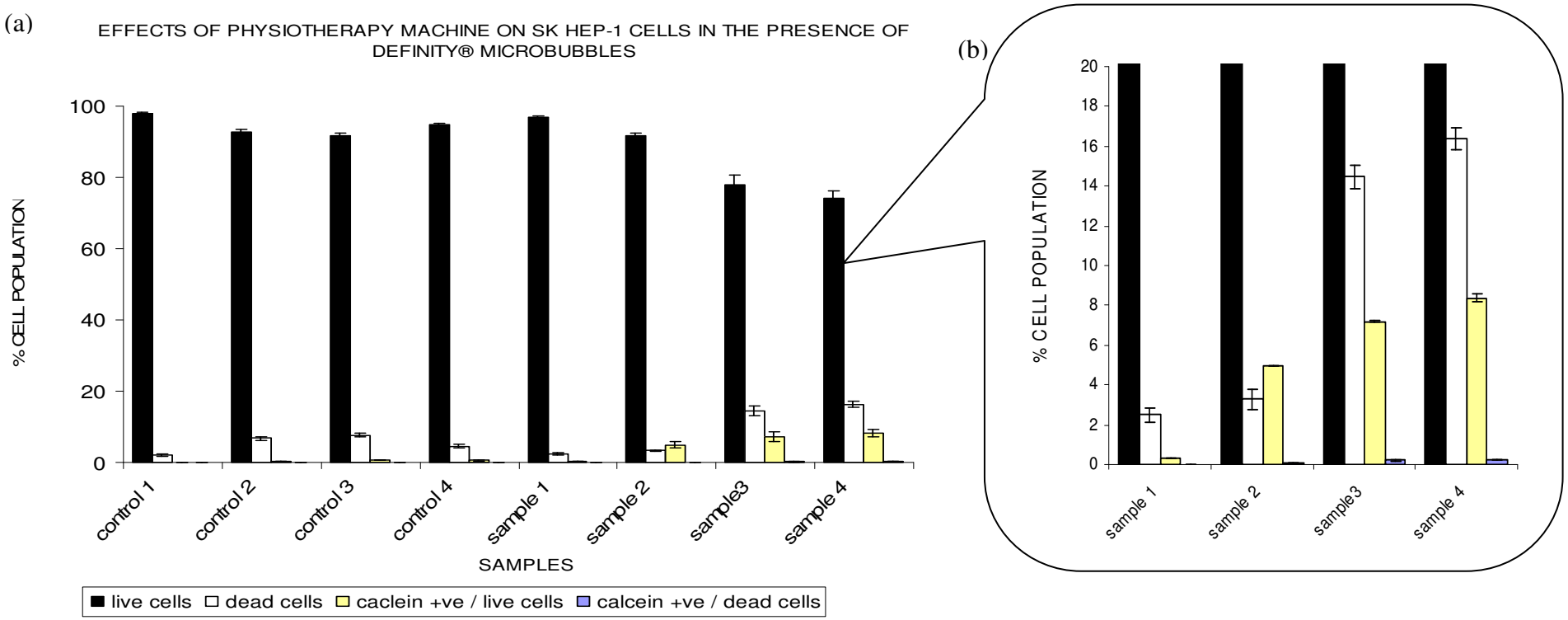

Figure 9.24 **Sonoporation in the presence of cell impermeable Calcein.** (a) Ultrasound was applied at a nominal intensity of 2.54 W / cm^2 for 2-3 secs, in the presence of 5 µl (sample1), 300 µl (sample 2), 600µl (sample3) & 900 µl (sample 4) of Definity® microbubbles (1.2 x 10^{10} / ml), in order to detect attainment of sonoporation. After sonoporation cells underwent flow cytometry, where the presence of Calcein and viability of cells were assessed. Successful sonoporation should lead to transport of Calcein into the cytoplasm of a viable cell (yellow bars). Control 1= no treatment, control 2 = only Calcein, control 3 = 5 µl of Definity® microbubbles and Calcein, control 4= ultrasound and Calcein. Samples 1-4 have been magnified (b) so as to be able to see all 4 columns corresponding to each sample.

9.2.2.3.2 EGFP expression in SK Hep-1 cells

Detection of cell impermeable Calcein in the cell cytoplasm confirmed the hypothesis that under the specific ultrasonic conditions used in this study, sonoporation had taken place. As mentioned previously a possible explanation for the absence of EGFP expression could be the large size of pCS2 plasmid. It was therefore hypothesised that linearization of pCS2 plasmid would decrease its 3D size enabling it to pass through the pores formed during insonation (Exp. 7). In the experiments in the previous section sufficient sonoporation was achieved with as low as 300 μl of Definity® microbubbles. It was decided to use only this amount of Definity® for subsequent experiments for two reasons. Firstly, the cell to bubble ratio with such an amount was 1 in 1800, which is closer to those reported in other studies. Secondly, each vial of Definity® contained 3 ml, thus it was important to use it economically. Samples were placed in an incubator following insonation and were examined 24 hours later. However, no expression of EGFP was detected during these experiments. During transfection experiments with transfection reagents, it is common practise to use serum free media. It has been reported that serum interferes with DNA-cell interaction by binding to the transfection reagent-DNA complexes (Nchinda, Überla et al. 2002). It was therefore hypothesised that the serum present in the cell media could also inhibit uptake of pCS2 plasmid during sonoporation. The sonoporation experiments were repeated in the absence of serum, as described in section 9.2.2.3.1 and expression of EGFP was detected as shown in figure 9.25-9.26 (Exp. 8).

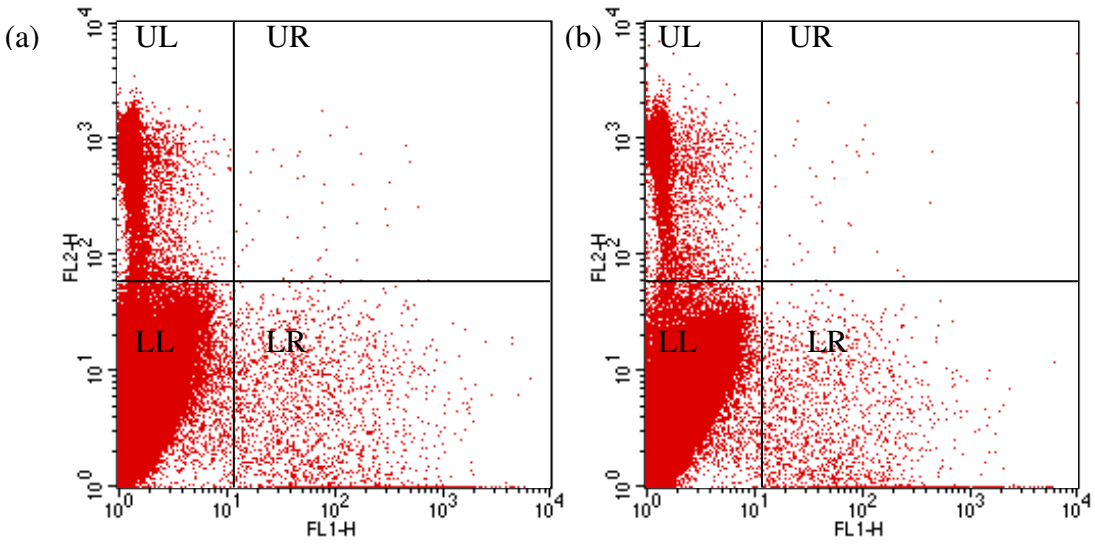

(c)

Sample ID:
Gate: G1
Gated Events: 100000
Total Events: 110570

Quad	Events	% Gated	% Total
UL	10979	10.98	9.93
UR	49	0.05	0.04
LL	86731	86.73	78.44
LR	2241	2.24	2.03

(d)

Sample ID:
Gate: G1
Gated Events: 100000
Total Events: 109463

Quad	Events	% Gated	% Total
UL	7447	7.45	6.80
UR	41	0.04	0.04
LL	90651	90.65	82.81
LR	1861	1.86	1.70

Figure 9.25 **Sonoporation in the presence of linearised pCS2.** Representation of data collected via flow cytometry, during application of ultrasound (a) & (b). Cells were fed through a flow cytometer and emission of Calcein (green) and PI (red) fluorescence were detected. A 2D histogram was plotted with the x- axis (FL1-H) representing the Calcein fluorescence and the y-axis (FL2-H) representing the PI fluorescence. The histogram can thus be divided into 4 quadrants with 4 distinct populations. The lower left (LL) quad is Calcein and PI negative, i.e. cells are alive but have not been sonoporated. The Upper left (UL) quad is Calcein negative and PI positive, i.e. cells are dead and were not sonoporated. The lower right (LR) quad is Calcein positive and PI negative, i.e. cells were sonoporated and are still alive. The upper right (UR) quad is Calcein and PI positive, i.e. cells were sonoporated but died. A total of 100,000 cells were examined per sample and the statistics for each histogram is shown in (c) and (d).

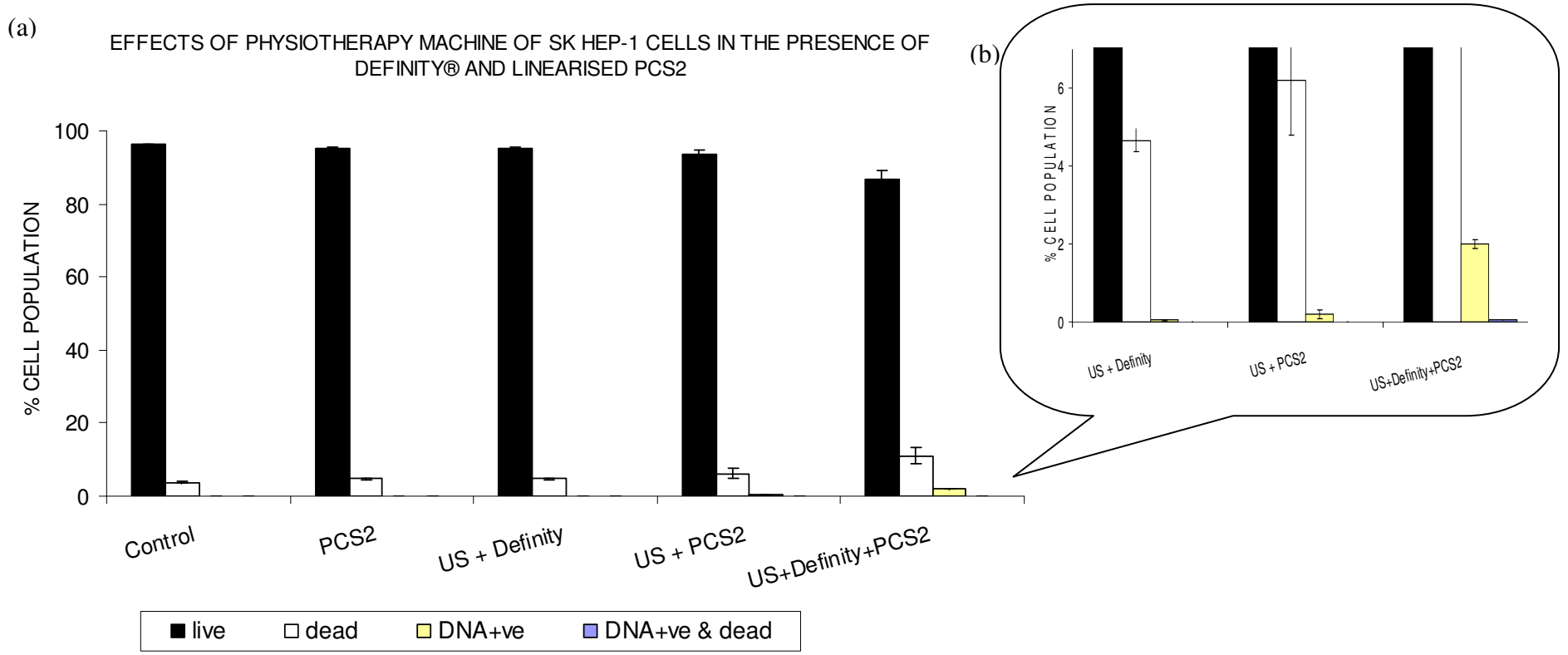

Figure 9.26 **Sonoporation in the presence of linearised pCS2.** Ultrasound was applied at a nominal intensity of 2.54 W / cm^2 for 2-3 secs, in the presence of 300 µl of (1.2 x 10^{10} / ml) Definity® microbubbles, in order to detect attainment of sonoporation. After sonoporation cells underwent flow cytometry, where the presence of Calcein and viability of cells were assessed. Successful sonoporation should lead to transport and expression of DNA into the cytoplasm of a viable cell (yellow bars). Control = no treatment. The last three samples have been magnified (b) so as to be able to see all 4 columns corresponding to each sample.

9.2.2.3.3 Pore size formation during sonoporation

Previous studies have shown that the pores formed during sonoporation have an upper limit of 75 nm yet with the molecular size being inversely proportional to the rate of their uptake (Mehier-Humbert, Bettinger et al. 2005a). In order to confirm the upper size limit of the pores formed during the sonoporation experiments of this study, EGFP, which is 4.2 nm in length and 2.4 nm in diameter, was added into the culture medium (Exp. 9) (Pawley 2006). A range of EGFP concentrations (final concentration 70 μM, 700 μM & 700 mM) were investigated in the presence of 300 μl of Definity® microbubbles. No EGFP was detected in the cells after insonation, suggesting that the pores formed during sonoporation were not large enough for the protein to pass through.

9.2.2.3.4 Sonoporation of different cell lines

Sonoporation experiments were repeated with two other cell lines (ACHN (human renal adenocarcinoma) & HUH7 (human hepatic carcinoma) in the presence of Definity® microbubbles, as previously described in section 9.2.2.3.2. The purpose of these experiments was to establish whether sonoporation efficiency was affected by the use of different cell lines (Exp. 10). As can be seen in figures 9.27-9.28 sonoporation was not achieved. However, a decrease in cell viability is observed after cell insonation. Statistical analysis (student's t test, $p=0.00004$ (ACHN), $p=0.0001$ (HUH7), $n=3$) of the data confirmed that there is a significant difference between insonated and non-insonated samples for both ACHN and HUH7 cells lines. Figure 9.29 shows the effect of ultrasound on cell viability for all three cell lines examined in this study, under identical experimental conditions. Statistical analysis (one-way ANOVA, $p=0.0002$, $n=3$) confirmed that there is a significant difference in cell viability amongst the three cells lines used in

this study.

9.2.2.4 Sonoporation in the presence of in-house microbubbles

Since the parameters necessary for sonoporation were established with the aid of Definity® microbubbles, sonoporation in the presence of in-house microbubbles was subsequently investigated. A range of in-house microbubble volumes were investigated leading to cell-bubble ratios of 1:300, 1:600, 1:1000, and 1:2000 (Exp. 11). Cells were insonated with acoustic parameters identical to those used for achieving sonoporation in the presence of cell impermeable Calcein (section 9.2.2.3.1). The results shown in figure 9.30 demonstrate that sonoporation was not achieved.

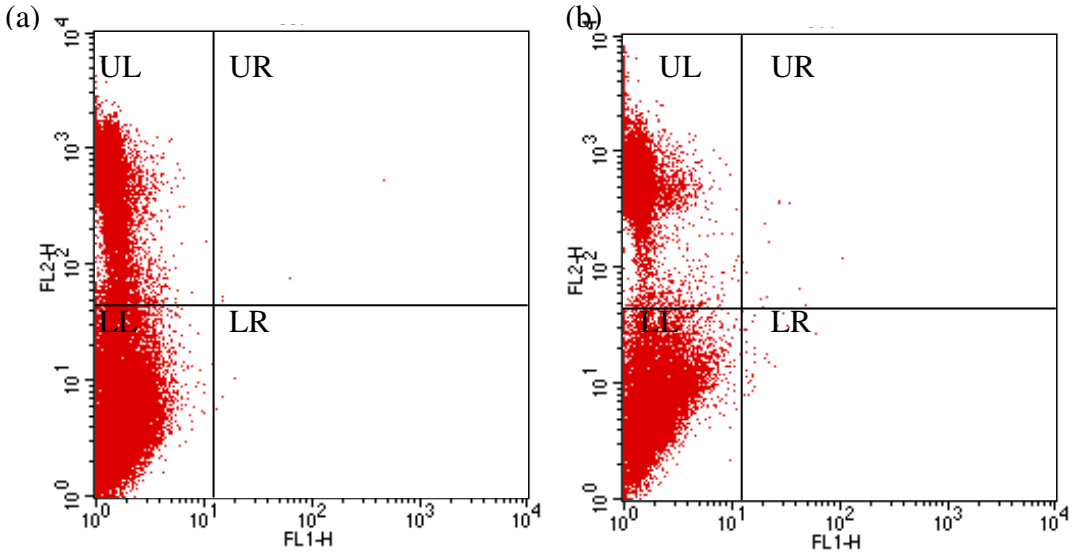

(c)

Sample ID:
Gate: G1
Gated Events: 50682
Total Events: 90030

Quad	Events	% Gated	% Total
UL	24750	48.83	27.49
UR	4	0.01	0.00
LL	25925	51.15	28.80
LR	3	0.01	0.00

(d)

Sample ID:
Gate: G1
Gated Events: 40182
Total Events: 53310

Quad	Events	% Gated	% Total
UL	27026	67.26	50.70
UR	12	0.03	0.02
LL	13116	32.64	24.60
LR	28	0.07	0.05

Figure 9.27 **Effects of "physiotherapy machine "on ACHN & HUH7 cell lines in the presence of Definity® microbubbles and linearised pCS2.** Representation of data collected via flow cytometry, during application of ultrasound (a) & (b). Cells were fed through a flow cytometer and emission of Calcein (green) and PI (red) fluorescence were detected. A 2D histogram was plotted with the x- axis (FL1-H) representing the Calcein fluorescence and the y-axis (FL2-H) representing the PI fluorescence. The histogram can thus be divided into 4 quadrants with 4 distinct populations. The lower left (LL) quad is Calcein and PI negative, i.e. cells are alive but have not been sonoporated. The Upper left (UL) quad is Calcein negative and PI positive, i.e. cells are dead and were not sonoporated. The lower right (LR) quad is Calcein positive and PI negative, i.e. cells were sonoporated and are still alive. The upper right (UR) quad is Calcein and PI positive, i.e. cells were sonoporated but died. A total of 100,000 cells were examined per sample and the statistics for each histogram is shown in (c) and (d).

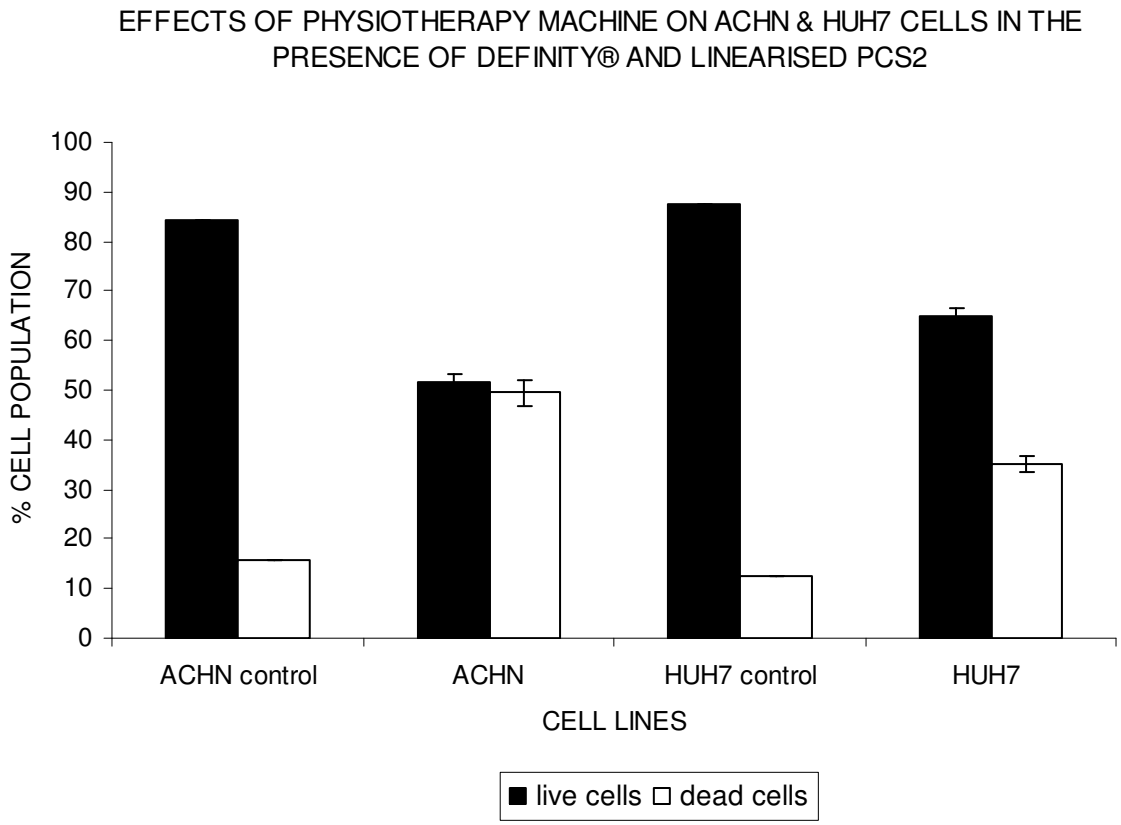

Figure 9.28 **Effects of "physiotherapy machine" on ACHN & HUH7 cell lines in the presence of Definity® microbubbles and linearised pCS2.** An experiment was conducted with ACHN and HUH7 cells, using identical conditions as those used for achieving sonoporation in SK Hep-1 cells. Ultrasound was applied to ACHN and HUH7 cells, at a nominal intensity of 2.54 W / cm^2 for 2-3 secs, in the presence of 300 µl of (1.2 x 10^{10} / ml) Definity® microbubbles, control = no treatment (n=1). Although no sonoporation was detected, this graph shows the effect of sonication on cell viability of ACHN and HUH7 cells.

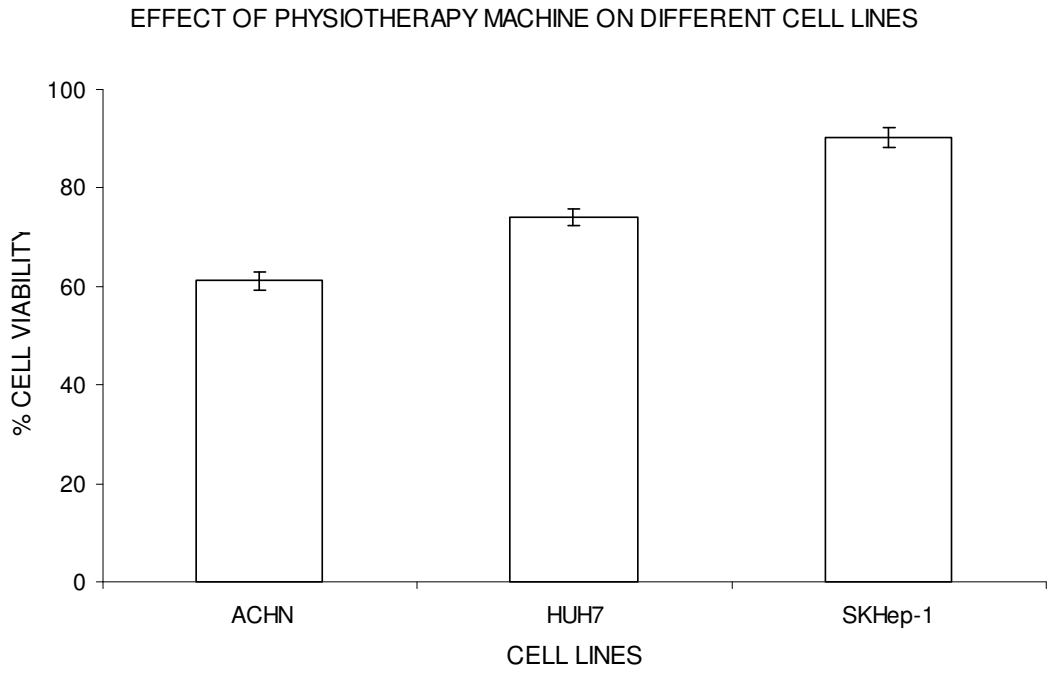

Figure 9.29 **Effects of "physiotherapy machine" on ACHN, HUH7 & SK Hep-1 cell lines in the presence of linearised pCS2.** All three cells lines were treated under identical conditions in order to achieve sonoporation. Ultrasound was applied at a nominal intensity of 2.54 W / cm^2 for 2-3 secs, in the presence of 300 µl of (1.2 x 10^{10} / ml) Definity® microbubbles. The graph presents the effect of sonication on viability of each separate cell line.

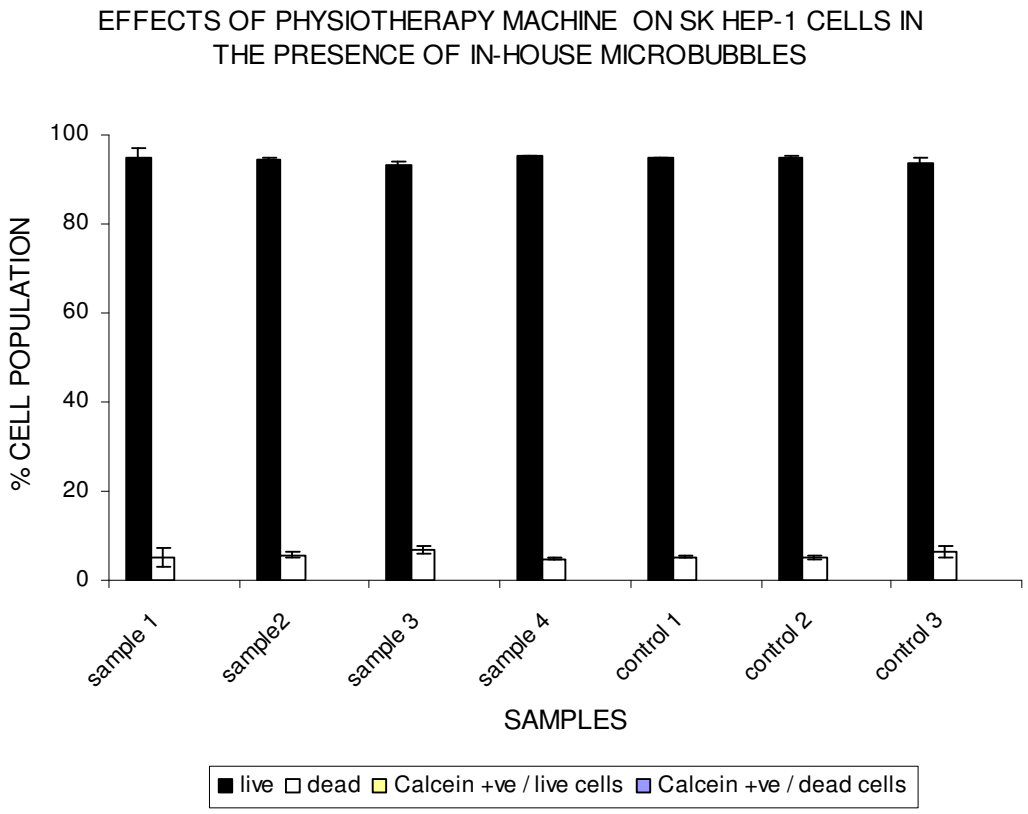

Figure 9.30 **Effects of "physiotherapy machine" in the presence of in-house microbubbles and cell impermeable Calcein.** Cells were treated in the presence of in-house microbubbles with identical conditions to those used to achieve sonoporation in the presence of Definity® microbubbles. Ultrasound was applied at a nominal intensity of 2.54 W / cm^2 for 2-3 secs, in the presence of 0.9 ml (sample 1), 1.8 ml (sample 2), 8 ml (sample 3) & 5.97 ml (sample 4) of in-house microbubbles (6.7 x 10^8 / ml). Control 1= no treatment, control 2 = only Calcein, control 3 = ultrasound and Calcein. In the presence of in-house microbubbles no sonoporation was detected.

9.2.3 Ultrasound scanner experiments

9.2.3.1 EGFP expression in SK Hep-1 cells

A set of experiments were performed in order to achieve sonoporation with the aid of the ultrasound scanner. Since the acoustic parameters used in these experiments in comparison with those performed with the "physiotherapy machine "were different, a range of Definity® microbubbles, MIs and DNA plasmid concentrations were investigated (Exp. 12). Therefore, cells were insonated with ultrasound wave of MI 0.2-0.5-1.1, in the presence of a range of concentrations of linearised pCS2 plasmid (0.1μg / ml, 1 μg / ml & 5 μg / ml) and two different amounts of Definity® microbubbles (100 μl and 300 μl). In addition, cells were insonated in the presence / absence of serum for the reasons described in section 9.2.2.3.2. Furthermore, since the ultrasound wave produced by the scanner is of a much lower pressure (peak to peak pressure 0.3 MPa) than that produced by the "physiotherapy machine "(peak to peak pressure 3 MPa), the duration of insonation was increased to 10 secs. The probe was held at a 90° angle, while being moved 0.5 cm across the OptiCell™ and then moved 0.5 cm downwards, thus swiping the entire surface of the OptiCell™ (figure 9.31). Following sonication, samples were placed in an incubator and examined 24 hours later by flow cytometry. Results from these experiments suggested that sonoporation had not taken place. It was therefore hypothesised that cells might require more time in order to express EGFP. Therefore, experiments were repeated and samples were examined 48 hours after insonation, however, no EGFP expression was detected (Exp. 13). A possible explanation for this could be that a higher concentration of DNA was necessary in order for sufficient amounts of EGFP to be detected. Therefore, subsequent experiments were performed with increased amounts of linearised pCS2 plasmid (20, 30 μg / ml) (Exp. 14). Results from these experiments, collected

24 and 48 hours after insonation, showed no EGFP expression. Even when the MI was further increased to 1.3, no EGFP expression was detected.

Microbubble concentration could be another possible factor limiting sonoporation. Therefore, experiments were repeated with increased amounts of Definity® microbubbles (1 ml) in the presence of 20 μg of pCS2 plasmid (Exp. 15). Cells were insonated with ultrasound of MI=1.3. During these experiments, it was observed that addition of such large amounts of microbubbles formed a white layer above the cells.

All the experiments in this study, up to this point, were performed with cells grown in a monolayer fashion, as this best reflects the way cells are organised in tissues within the human body. It was thus decided to investigate the possibility of sonoporation for both adherent and suspension in cells. Therefore, sonoporation experiments were repeated as described earlier in this section, while 24 hours after insonation both adherent and in suspension cells were collected for analysis (Exp. 16). Although no expression of EGFP was detected during these experiments, viability of cells in suspension following insonation was observed to be lower than that of adherent cells (figure 9.32). Statistical analysis (student's t-test, $p=0.0002$, $n=4$) of the data confirmed a significant difference between adherent cells and cells in suspension.

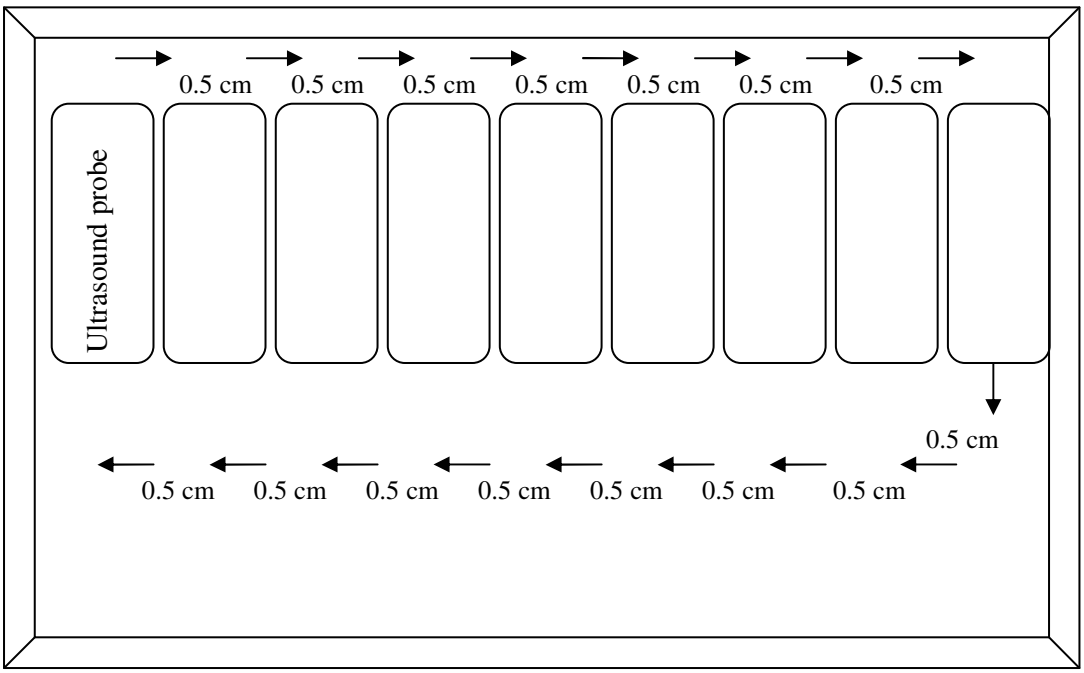

Figure 9.31 **Representation of movement of ultrasound transducer P4-2 during sonoporation experiments in the presence of pCS2 plasmid.** Sonoporation experiments were conducted with the ultrasound scanner HDI 3500. The probe of the P4-2 transducer was held at a 37º angle, while being moved 0.5 cm across the OptiCell™ and then moved 0.5 cm downwards and again 0.5 cm across, thus swiping the entire surface of the OptiCell™. Cells were insonated for 10 secs at each position (image not to scale).

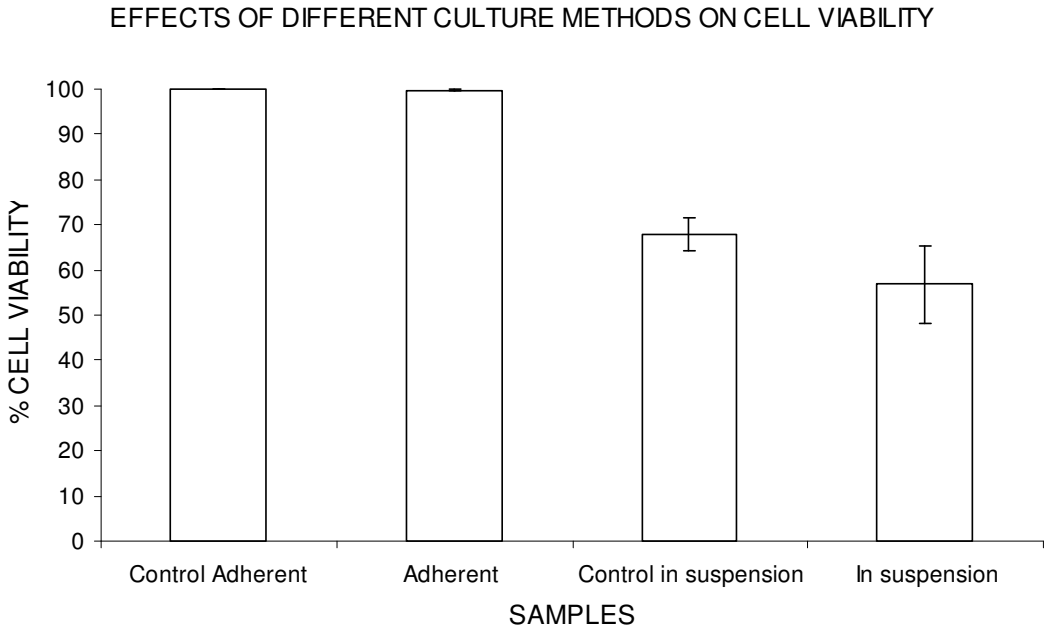

Figure 9.32 **Effects of different culture methods on cell viability**. SK Hep-1 cells were grown both in a monolayer fashion and in suspension. Each culturing method was then insonated under identical acoustic conditions in order to determine any differences in cell viability. Ultrasound was applied at an MI=1.3 for 10 secs, in the presence of 300 µl of (1.2×10^{10} / ml) Definity® microbubbles (n=4).

9.2.3.2 Cell impermeable Calcein

Although the experiments described in the previous section, did not reveal any EGFP expression that did not eliminate the possibility of sonoporation taking place. It was thus, hypothesised that if under the specific acoustic parameters used in the experiments with the ultrasound scanner sonoporation efficiency was very low, then EGFP expression, which depends largely on passage of the DNA plasmid through the plasma membrane, would also be compromised. In order to test this hypothesis, experiments investigating sonoporation in the presence of cell impermeable Calcein were carried out (Exp. 17). Cells were insonated with ultrasound wave of MI=1.3 in the presence of a range of Definity® microbubble concentrations, identical to those used during similar experiments with the use of "physiotherapy machine "(section 9.2.2.3.1). Statistical analysis (student's t test, p=0.07 (5 μl), p=0.0006 (300μl), p=0.06 (600μl), n=3) for the data collected revealed that there is no significant difference between control samples and samples containing 5 μl or 600 μl of Definity® microbubbles, yet there is a significant difference between control samples and 300 μl microbubble sample. Thus it can be deduced that with the experimental conditions used, sonoporation was achieved in the presence of Definity® microbubbles (figure 9.33). As can be seen from figure 9.34 the maximum sonoporation efficiency obtained was 1.13 %. This was much lower to that obtained with the use of the "physiotherapy machine "under similar conditions (8.37 %).

(a)

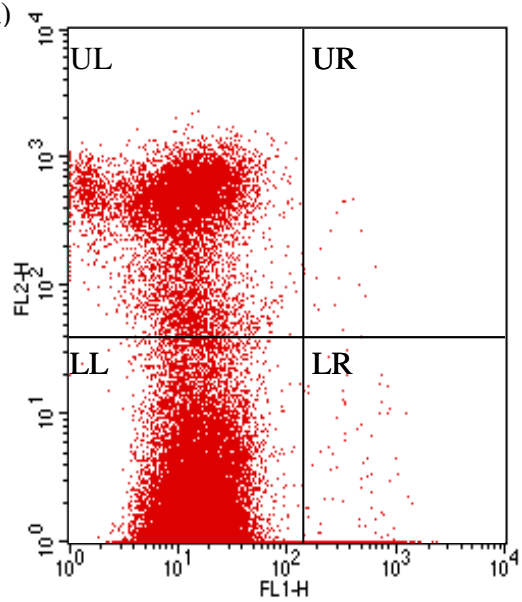

(b)

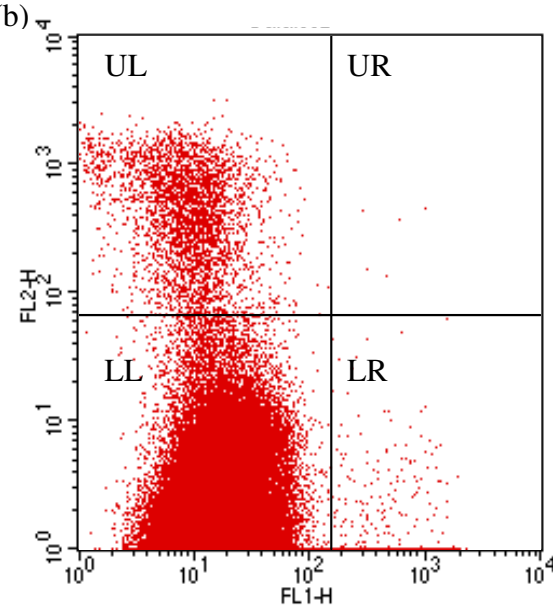

(c)

Sample ID:
Gate: G1
Gated Events: 50000
Total Events: 52696

Quad	Events	% Gatec	% Tota
UL	8104	16.21	15.38
UR	18	0.04	0.03
LL	41337	82.67	78.44
LR	541	1.08	1.03

(d)

Sample ID:
Gate: G1
Gated Events: 100000
Total Events: 106197

Quad	Events	% Gated	% Total
UL	3466	3.47	3.26
UR	5	0.01	0.00
LL	95399	95.40	89.83
LR	1130	1.13	1.06

Figure 9.33 **Sonoporation of SK Hep-1 cells with the aid of an ultrasound scanner in the presence of Definity® microbubbles.** Representation of data collected via flow cytometry, during application of ultrasound (a) & (b). Cells were fed through a flow cytometer and emission of Calcein (green) and PI (red) fluorescence were detected. A 2D histogram was plotted with the x- axis (FL1-H) representing the Calcein fluorescence and the y-axis (FL2-H) representing the PI fluorescence. The histogram can thus be divided into 4 quadrants with 4 distinct populations. The lower left (LL) quad is Calcein and PI negative, i.e. cells are alive but have not been sonoporated. The Upper left (UL) quad is Calcein negative and PI positive, i.e. cells are dead and were not sonoporated. The lower right (LR) quad is Calcein positive and PI negative, i.e. cells were sonoporated and are still alive. The upper right (UR) quad is Calcein and PI positive, i.e. cells were sonoporated but died. A total of 100,000 cells were examined per sample and the statistics for each histogram is shown in (c) and (d).

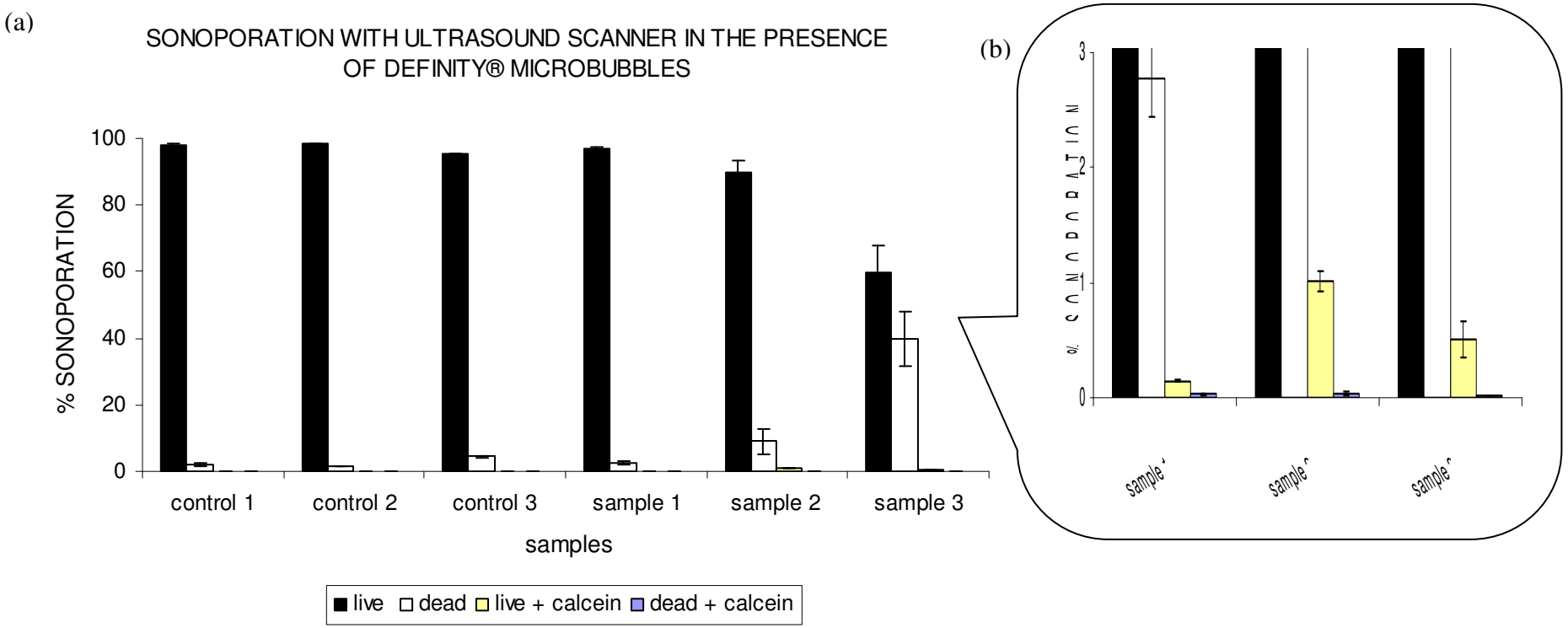

Figure 9.34 **Sonoporation of SK Hep-1 cells with the aid of an ultrasound scanner in the presence of Definity® microbubbles.** Ultrasound was applied for 2-3 secs, in the presence of 5 µl (sample 1), 300 µl (sample 2), & 600 µl (sample 3) of (1.2 x 10^{10} / ml) Definity® microbubbles, in order to detect attainment of sonoporation. After sonoporation cells underwent flow cytometry, where the presence of Calcein and viability of cells were assessed. Successful sonoporation should lead to transport of Calcein into the cytoplasm of a viable cell (yellow bars). Control 1= no treatment, control 2 = only Calcein, control 3 = ultrasound and Calcein. Samples 1-3 have been magnified (b) so as to be able to see all 4 columns corresponding to each sample.

9.3 Discussion

9.3.1 Measurements of the ultrasound field

This section of the study focused on the investigation of ultrasound induced sonoporation. Initial experiments involved determining the exact acoustic field applied on the cells of interest. As mentioned previously, the nominal and actual values of an ultrasound apparatus can different significantly. In addition, it is vital to verify the elimination of any secondary acoustic forces, such as backscattering and standard waves, since they are not present in vivo (Kinoshita and Hynynen 2007). While examining the acoustical output of the "physiotherapy machine", it was concluded that the nominal and actual values of this machine differ significantly (figure 9.4). Therefore, at 1 MHz for nominal intensity of 0.5 W / cm^2, the actual intensity of the ultrasound wave is 0.97 W / cm^2, while for nominal intensity of 2.5 W / cm^2, the actual intensity is 4.20 W / cm^2, which is almost double the nominal value. It is therefore necessary to take into consideration the discrepancies between nominal and actual values when carrying out experiments with this machine, in order to be able to accurately define the ultrasound wave received by the samples. In addition, such measurements are valuable when required to replicate experiments performed with this machine, with other ultrasound apparatuses.

The use of different sonoporation apparatuses necessitated the investigation of the acoustic field created by each apparatus. Thus, experiments were conducted to accurately calibrate the acoustic pressure and intensity of the ultrasound wave emitted towards the cells of interest. The results confirmed that (a) the experimental set up used (OptiCells™) are acoustically transparent, thus eliminating the possibility of any backscatter or standing waves (figure 9.6) and (b) the acoustic parameters used with the ultrasound scanner, which correspond to the mechanical index (MI), did not

affect cell viability (figure 9.10). These results, suggest that the likelihood of any adverse bioeffects on cells is minimal.

9.3.2 "Physiotherapy machine" experiments

9.3.2.1 Investigation of non acoustic parameters

Investigation of ultrasound induced sonoporation was initially conducted with the aid of a "physiotherapy machine". Non acoustic parameters such as optimal cell concentration and potential microbubble toxicity were investigated. The optimal cell concentration was established at 2×10^5 cells / ml (figure 9.11). In addition, it was shown that the presence of in-house microbubbles, regardless of the solution used (saline or PBS), was not toxic to cells.

9.3.2.2 Investigation of acoustic parameters

Further experiments were geared towards designing a set up that would allow sonication of cells with negligible interference. Cell viability was examined upon sonication of cells seeded on Petri dishes. The results suggest that cell viability is inversely proportional to intensity of ultrasound (figure 9.14). Although previous reports claim that the use of a Petri dish allows for most of the ultrasound wave to pass through (Wu, Ross et al. 2002; Zhou, Shi et al. 2008), the large extent of cell death observed in this experiment was believed to be due to the presence of backscatter waves. When the transmitted ultrasound wave passed through the base of the Petri dish, a fraction of this wave would be reflected back towards the cells, due to the large discrepancy between the acoustic impedances of the Petri dish and the air. In addition, because of the proximity of the transducer to the cells (~0.5 cm), the ultrasound wave would not have travelled enough distance to

become attenuated, thus the possibility of the formation of strong backscatter was high.

In order to minimise the formation of such strong backscatter, a new setup was devised, that involved seeding cells in OptiCells™ and placing them in a specially designed ultrasound tank. The setup was designed is such a way so as to eliminate any backscatter, by adding an acoustic absorber at the bottom of the tank. In addition, the ultrasound transducer was held at an angle so that any backscatter still present was redirected away from the cells (figure 9.17). Application of under these experimental conditions showed reduced bioeffects compared to those observed with the use of Petri dishes (figure 9.15). It was thus concluded that backscatter waves present at the Petri dish set up were eliminated with the use of OptiCells™ and the ultrasound tank. Since no bioeffects were observed under these conditions, further experiments were conducted with increased levels of ultrasound intensity. Ultrasound was applied for different time periods in the presence of different Definity® concentrations (figures 9.19-9.20). The results suggested that there was no significant difference between the difference concentrations of microbubbles or the amount of time ultrasound was applied. Although it is anticipated that longer periods of ultrasound application would lead to higher sonoporation efficiency rates, the possibility of adverse bioeffects would also be great (Pan, Zhou et al. 2005). The duration of ultrasound in studies that have reported sonoporation varies immensely as do so many other parameters. There are studies that have reported sonoporation with application of ultrasound as little as 0.5 sec (Deng, Sieling et al. 2004), while other studies have insonated their samples for up to 7 min (Wu, Ross et al. 2002). A study investigating the effect of increasing times of insonation on sonoporation efficiency, reported an initial

increase in transfection efficiency followed by a decrease for longer exposure of up to 16 sec (Zarnitsyn and Prausnitz 2004). Since several studies have reported sonoporation with short insonation periods, and in order to minimise the likelihood of any bioeffects, ultrasound application in sonoporation experiments was kept to a minimum of 2-3 sec in the presence of 100 μl of Definity® microbubbles (Liang, Lu et al. 2004; Rahim, Taylor et al. 2006a; Van Wamel, Kooiman et al. 2006b).

9.3.2.3 Sonoporation in the presence of Definity® microbubbles

Once the initial parameters for sonoporation were established, further experiments were conducted in order to achieve ultrasound induced sonoporation and the subsequent expression of EGFP fluorescent protein. Cells were sonicated in the presence of Definity® microbubbles and pCS2 plasmid. Successful sonoporation would lead to diffusion of the DNA molecule into the cells, following expression of the EGFP. Initial results suggested that EGFP had not been expressed. However, this did not exclude the incidence of sonoporation. Two possibilities existed: (a) the pores formed during sonoporation were too small for the DNA molecule to pass through or (b) the amount of DNA used for not sufficient to exhibit detectable amounts of EGFP.

9.3.2.3.1 Cell impermeable Calcein

In order to eliminate the second possibility, similar quantities of DNA were used to transfect SK Hep-1 cells with a transfection agent (ExGen 500). Although the mechanism underlying such a transfection is different to that of sonoporation, this experiment was performed purely to demonstrate that the amounts of DNA used during sonoporation experiments could potentially express detectable levels of EGFP. Results from this experiment suggested

that the amounts used during sonoporation experiments were able to express detectable levels of EGFP (figure 9.22). Having eliminated one of the two possibilities, it was deduced that the lack of EGFP expression was due to the small size of perforations formed during sonoporation. This possibility was then examined by applying the same sonication parameters in the presence of a small fluorescent molecule (Calcein). Since Calcein is impermeable to plasma membranes, its transport into the cytoplasm would be a direct effect of sonoporation. Results suggested that sonoporation in the presence of cell impermeable Calcein was achieved with maximum sonoporation efficiency at 8.37 % (figure 9.24).

Comparing sonoporation efficiencies between studies is complex, since acoustic parameters and contrast agents used vary significantly from one study to another (Kinoshita and Hynynen 2007). There are studies that claim sonoporation was achieved at an efficiency of 4 % (Rahim, Taylor et al. 2006b) and others at an efficiency of 67 % (Van Wamel, Kooiman et al. 2006b). A large discrepancy in the cell viability documented, can also be identified (Kinoshita and Hynynen 2007). Such inconsistencies in the efficiency rates of sonoporation are anticipated, since sonoporation is dependent on several factors, both acoustic and non-acoustic. Non-acoustic parameters include the cell to bubble ratio, the culture method of cells (monolayer or suspension), whereas acoustic parameters include the power, frequency and duration of the ultrasound beam and the transmittance of the beam through the sample cells with minimum reflective effects (i.e. backscatter and standing waves).

A study investigating the importance of standing waves in sonoporation, reported that in the absence of standing waves, sonoporation efficiency rates were decreased in comparison to set ups where standing waves were present (Kinoshita and Hynynen 2007). The efficiency rates of

sonoporation in the absence of standing waves are similar to those achieved in this study. In the same study, cell viability was reported to be higher in the absence of standing waves. A possible explanation for the low sonoporation efficiency rate observed can be due to the elimination of standing waves. Although Kinoshita et al. (2007), suggest that standing waves are necessary for achieving "a satisfactory amount" of sonoporation, it can be argued that standing waves rarely occur in the human body, therefore experimental set ups that minimise the possibility of standing waves, such as in this study, are more realistic and valuable for clinical use.

9.3.2.3.2 EGFP expression in SK Hep-1 cells

As mentioned earlier, successful sonoporation in the presence of Calcein signified that EGFP had not been previously expressed due to the small size of the pores formed during sonoporation. It was thus linearisation of the DNA plasmid further validate this theory. In addition, serum free medium was used, as reports have suggested that serum can inhibit DNA-cell interactions (Nchinda, Überla et al. 2002). Indeed, EGFP was detected upon sonication of SK Hep-1 cells in the presence of Definity® microbubbles and pCS2 plasmid (figure 9.26).

Although sonoporation was achieved, the efficiency was lower (2 %) compared to that observed with the use of Calcein under the same conditions (4.97 %) (figures 9.24 & 9.26 respectively). Zarnitsyn et al. (2004) also reported similar findings, where under identical conditions; sonoporation efficiency was lower when measuring gene expression of DNA plasmid than when adding fluorescent molecules. A possible explanation could be the number of obstacles that DNA plasmid has to endure once it enters the cell cytoplasm until it reaches the nucleus, where it can initiate expression of the proteins it encodes. Once in the cytoplasm the plasmid would be taken up by

lysosomes for degradation (Khalil, Kogure et al. 2006). The next hurdle it has to overcome is the nuclear membrane, which contains nuclear pores, which in turn allow for passive diffusion of molecules up to 70 kDa (Khalil, Kogure et al. 2006). It is believed that DNA plasmid, which would not normally be able to pass through the nuclear pores, passes through it during mitosis, when permeability of nuclear membrane is compromised (Khalil, Kogure et al. 2006). However, under normal conditions, the cycles of cells within a cell culture are not synchronized, thus not all cells would have compromised nuclear membranes that would allow the DNA plasmid to be expressed. Another possible explanation for the difference in sonoporation efficiencies observed could be the degradation of DNA during insonation (Zarnitsyn and Prausnitz 2004). Miller et al. (2009) demonstrated that sonoporation activates apoptotic pathways, thus altering gene expression levels. This could provide a third possible explanation for the observations seen in this study. Therefore, although EGFP expression is an established method of accessing sonoporation efficiency, there are additional factors which may affect its expression which are not directly related to sonoporation.

9.3.2.3.3 Pore size formation during sonoporation

Although sonoporation and EGFP expression was achieved, the issue of pore size had come to the surface. The experiments conducted so far suggested that EGFP was too large to pass through the pores from during sonoporation, whereas Calcein and linearised DNA were small enough to passively diffuse through. An attempt was made to determine the upper size limit of the pores formed during sonoporation, by sonicating SK Hep-1 cells in the presence of EGFP. As EGFP was not detected in the cytoplasm of sonoporated cells, this suggests that the pores formed during sonoporation have an upper size limit of 2.4 nm. However this was much smaller than that

previously reported (Mehier-Humbert, Bettinger et al. 2005a). There are several possible explanations for such a finding. Firstly, since sonoporation has been shown to occur due to the mechanical stress applied by the microbubbles on to the cell membrane (Van Wamel, Kooiman et al. 2006b), then it can be hypothesised that microbubbles of different physical parameters, such as size and compressibility, would exert different amounts of mechanical pressure. The pore size in the presence of Definity® microbubbles has not been investigated until now. Secondly, cell viability during insonation is different for distinct cell lines, i.e. there is a discrepancy amongst levels of cell toxicity during sonoporation by ultrasound among cell types (Kinoshita and Hynynen 2007). Although not proven in this study, it can be postulated, that the cell line used in this study (SK Hep-1) can only repair small sized perforations, whereas larger ones lead to cell death. This would explain, the passage / transport of smaller but not larger molecules through the plasma membrane, during this study.

9.3.2.3.4 Sonoporation of different cell lines

An important part of this investigation was to construct a setup that would achieve ultrasound induced sonoporation. Ideally, one would be able to use this setup to achieve sonoporation across a range of different cell lines. An attempt was therefore made to demonstrate the usability of this setup across a range of cell lines, by performing sonoporation experiments with ACHN and HUH7 cell lines. The results from these experiments suggest that sonoporation did not take place (figure 9.27). Nevertheless, they provide useful information. Careful comparison between all three cell lines used in this study (SK Hep-1, ACHN and HUH7) illustrates a significant difference in cell viability during insonation between each cell line used (figure 9.29). A possible explanation for this outcome is the fact that each distinct cell type is

portrayed by different characteristics, such as cell size and cell membrane structure, thus increasing the possibility of different response to cavitational effects and hence sonoporation efficiencies (Wang, Liu et al. 2009).

9.3.2.3.5 Sonoporation in the presence of in-house microbubbles

Further experiments were directed towards establishing sonoporation in the presence of in-house microbubbles. Since sonoporation was established in the presence of Definity® microbubbles, it should be possible to achieve sonoporation in the presence of in-house microbubbles. However, the data collected suggest that sonoporation was not achieved under these experimental conditions (figure 9.30). The only difference between this experiment and previous ones where successful sonoporation was reported with the aid of the physiotherapy machine was the presence of different ultrasound contrast agent. As mentioned earlier in this chapter, sonoporation has been shown to be a result of cavitation and that in turn is dependent on a number of acoustical parameters, including the physical properties of the microbubbles. Since all acoustic parameters remained the same apart from the type of microbubbles employed, it can be deduced that the difference in the properties of the in-house microbubbles compared to those of the Definity® microbubbles are responsible for the lack of sonoporation. The mode of oscillation of microbubbles and thus their ability to cause sonoporation under specific ultrasonic conditions, is determined by a number of variables, including their size, contents and shell compressibility (Dawson 1999). Although it was shown earlier in this study that the size distribution of in-house microbubbles is comparable to that of commercially available ultrasound contrast agents, including Definity® (chapter 8), the contents of the in-house microbubbles differ to those of Definity®. While the former are most probably filled with aqueous solution (section 8.1.1), the

latter are filled with gas. In addition, only a limited amount of information is available on the characteristics of the Definity® microbubbles, while valuable information such as the composition of their shell are not been disclosed. Differences in the shell constituents of the microbubbles, could lead to differences in their compressibility, which could also explain the lack of sonoporation (Dawson 1999).

In conclusion, several of the microbubble physical properties contribute to sonoporation. Although a number of possible explanations can be hypothesized, it was not possible to determine the basis for lack of sonoporation in the presence of in-house microbubbles. This was mainly because comparison between Definity® and in-house microbubble experiments was not feasible due to insufficient information of the commercial contrast agent used in this study. Further investigation of the parameters necessary to achieve sonoporation in the presence of in-house microbubbles would be required.

9.3.3 Ultrasound scanner experiments

9.3.3.1 EGFP expression in SK Hep-1 cells

In contrast to physiotherapy machines that are used for therapeutic purposes, ultrasound scanners are used for diagnostic purposes. The latter operate at higher frequencies in order to provide an image with good axial resolution with minimal bioeffects (Miller 2007b). Thus ultrasound scanners are employed more frequently in clinics. As a result, further experiments in this study were performed with an ultrasound scanner as this became available for use. Ultrasound induced sonoporation in the presence of Definity® microbubbles was investigated. However, since the acoustic parameters emitted from the ultrasound scanner differ immensely to those of the "physiotherapy machine", further adjustments where necessary in order

to achieve sonoporation and subsequent EGFP expression. Several parameters were examined, including pCS2 and Definity® concentration. In retrospect, it was thought that increased amounts of microbubbles could attenuate the ultrasound beam, thus decreasing the likelihood of sonoporation. Indeed, it has been shown that high microbubble concentrations, reduce the microbubbles' capacity to act upon adjacent cells, thus decreasing the likelihood of sonoporation (Guzmán, McNamara et al. 2003). In addition, cells were allowed to recover for prolonged periods of time (24 & 48 hours), thus allowing sufficient time for expression of EGFP to take place. The data collected, however, suggested that sonoporation had not taken place.

9.3.3.2 Effect of different culturing methods on sonoporation

Another parameter that differs between studies investigating sonoporation is the culture method of cells. Most studies use cells in suspension (Brayman, Coppage et al. 1999; Ward, Wu et al. 1999; Deng, Sieling et al. 2004; Mehier-Humbert, Bettinger et al. 2005a; Wu, Pepe et al. 2006), while only a handful of studies, culture cells in a monolayer fashion (Duvshani-Eshet, Baruch et al. 2005; Rahim, Taylor et al. 2006b; Van Wamel, Kooiman et al. 2006b). In addition, it has been reported that sonoporation efficiency rates are the same, regardless of the cell culture method (Kinoshita and Hynynen 2007). Furthermore, cell viability was observed to be higher when cells were grown in a monolayer fashion (Kinoshita and Hynynen 2007). Experiments conducted in this study with either culturing method (monolayer fashion or in suspension) did not result in sonoporation. These results agree with the findings of Kinoshita et al (2007), where under identical ultrasonic conditions, adherent cells have higher viability rates than cells in suspension (figure 9.32).

9.3.3.3 Cell impermeable Calcein

Ultrasound contrast agents are known to oscillate in distinct modes depending on the frequency and the acoustic pressure applied (Dawson 1999; Chen, Zagzebski et al. 2002; Tang, Eckersley et al. 2005). In addition, a direct dependence between acoustic pressure and sonoporation has been demonstrated (Han, Ikegami et al. 2007). Such a large discrepancy among sonoporation efficiencies are therefore thought to be a consequence of the different parameters of the ultrasound beams generated by the ultrasound scanner and the "physiotherapy machine". The acoustic parameters of the scanner differ significantly from those of the "physiotherapy machine", leading to a different mode of oscillation of the Definity® microbubbles, thus effecting sonoporation efficiency rates. Due to this fact, it is possible that during insonation with the ultrasound scanner, EGFP expression is lower than that observed during insonation with the "physiotherapy machine". Since experiments conducted with the "physiotherapy machine" in the presence of Calcein, resulted in sonoporation efficiency of 8.37 %, it was hypothesized that "under similar conditions", employment of the ultrasound scanner might result in lower yet detectable sonoporation efficiencies. Indeed, the data collected show that during insonation from the ultrasound scanner, maximum sonoporation efficiency in the presence of Calcein was 1.13 % (figure 9.34), which is much lower to that obtained with the use of the "physiotherapy machine "under similar conditions (8.37 %).

9.4 Conclusion

A vast number of experiments were conducted in this section in order to establish all the acoustic and non acoustic parameters necessary for achieving sonoporation. An experimental set up was developed where the acoustic field formed was accurately described by measuring all the acoustic

parameters involved. In addition, factors such as backscattering and standing waves were also taken into consideration. This is of particular importance as the majority of research performed in this area fails to accurately measure the acoustic field produced, thus providing inaccurate information and making it impossible to reproduce their results (Kinoshita and Hynynen 2007).

Initial experiments in this study, were performed with a "physiotherapy machine". A range of parameters were examined prior to achieving sonoporation, including cell and microbubble concentration, ultrasound time exposure and, acoustic pressure and intensity of ultrasound, different cell lines, different culturing methods, upper size limit of pores formed, transport of small molecules and DNA across plasma membrane and expression of the latter. Successful sonoporation was achieved in the presence of Definity® microbubbles under specific ultrasound conditions with the aid of the "physiotherapy machine". Attempts were made to demonstrate sonoporation in the presence of in-house microbubbles under identical conditions, yet they were not successful. Although Definity® and in-house microbubbles are of similar composition and size; they also have other characteristics that can affect their ability to achieve sonoporation, such as their core contents.

Further experiments involved investigating sonoporation with the aid of an ultrasound scanner as this is more clinically relevant. Successful sonoporation was accomplished in the presence of Definity® microbubbles under specific ultrasound conditions with the aid of the ultrasound scanner HDI 3500. While the results obtained demonstrate the achievement of sonoporation, they do not provide an explanation as to why under identical experimental conditions, EGFP expression was no detected. It was, however, hypothesized that ultrasound application might act as a stressful stimulus

and thus affect gene expression in cells. Therefore, subsequent research focused on investigation of the cellular responses following ultrasound application. Upregulation of specific genes that reveal stressful conditions for the cells, were investigated, following insonation of identical parameters to those used for achieving sonoporation. Such information would assist in gaining a better understanding of the effects ultrasound has on cells and thus help establish the parameters for achieving sonoporation and determine any potential bioeffects.

Chapter 10

Investigation of ultrasound mediated cellular responses

10.0 Introduction

10.1 Cell responses during insonation

Heat shock proteins are involved in a multitude of vital cellular functions (Horvath, Multhoff et al. 2008). It is therefore not surprising that they contribute in the development of several human disorders. Heat shock proteins implement a protective role against stress stimuli that would otherwise lead to apoptosis (Santoro 2000).

Application of ultrasound can result in a number of bioeffects, depending on the pressure and frequency of the ultrasound waves. Ultrasound bioeffects can be separated into two categories, mechanical and thermal (Cheng-Huang, Yeh et al. 2008). Insonation at low intensities exerts a mechanical stress on cells that brings about formation of perforations on the cell membrane (Blomley, Cooke et al. 2001; Sontag and Kruglikov 2009). However, certain ultrasonic conditions can induce irreparable damage to the cell membrane and therefore lead to instant cell death (Miyake and McNeil 1995; Ferrara, Pollard et al. 2007). Miller et al. reported that in addition to initial cell death, sonoporated cells experience damages that eventually lead to apoptosis (Miller and Dou 2009). Once the apoptotic pathway has been activated, the capacity of cells to express genes is altered. This could provide a possible explanation for the observations seen both in this study and by Zarnitsyn (2004), where under identical conditions; sonoporation efficiency was lower when measuring gene expression of a DNA plasmid than when adding fluorescent molecules.

The aim of this section was to validate this hypothesis by investigating expression of heat shock proteins, such as Hsp70 and HO-1. Variations in expression of these proteins, resulting from insonation, will provide vital information as to the degree of stress the cells are experiencing and whether the apoptotic pathway has been instigated. This in turn can assist in

adjusting the parameters involved in sonoporation so as to achieve maximum sonoporation with minimal bioeffects.

10.2 Results

10.2.1 Heat shock protein 70

SK Hep-1 cells were insonated under identical conditions to those used for achieving sonoporation with the aid of the physiotherapy machine. Expression of Hsp70 was examined prior to and following insonation, in the presence (300 μl) and absence of Definity® microbubbles. Upregulation of Hsp70 protein during insonation would indicate that cells were experiencing stressful conditions.

Subsequently samples insonated in the presence and absence of ultrasound contrast agents were probed against GAPDH and actin antibodies. Results shown in figure 10.2 revealed that expression of both GAPDH and actin was upregulated in the absence of ultrasound contrast agents. In addition, the total amount of protein loaded was examined for insonated samples in the absence of ultrasound contrast agents and for non-treated samples. Careful observation of figure 10.3 revealed that insonated samples have less high molecular mass bands and additional lower molecular mass bands.

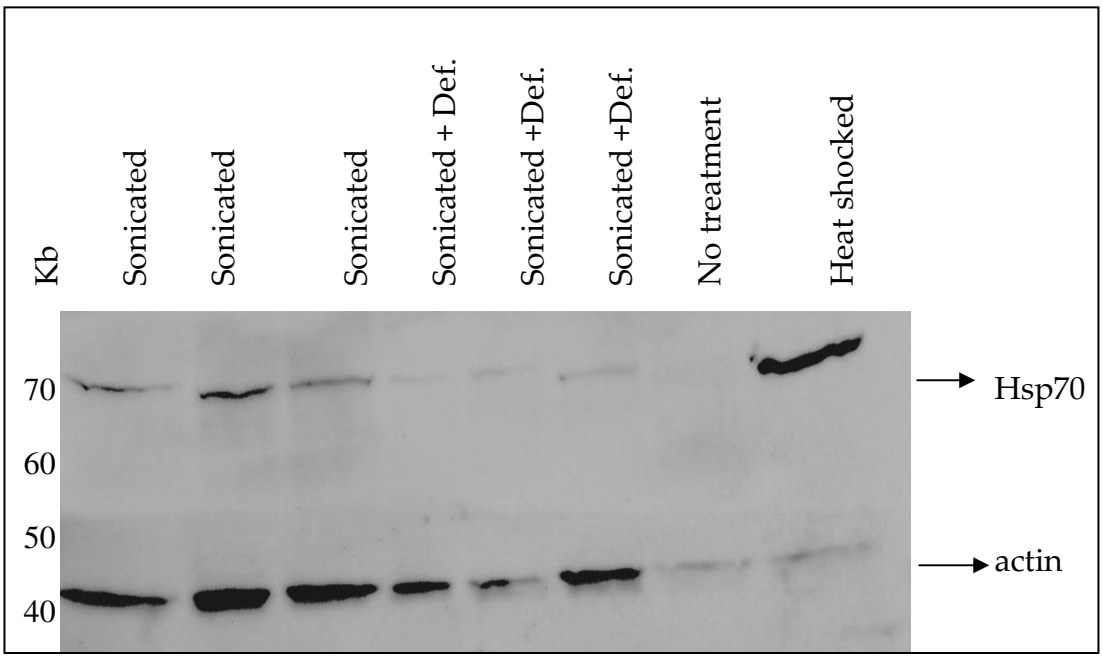

Figure 10.1 **Effects of sonication on Hsp70**. SK Hep-1 cells were sonicated in the presence and absence of Definity® microbubbles under identical ultrasound conditions as those used to achieve sonoporation. Following sonication, samples were collected and examined for increased stress levels. As heat shock protein 70 (Hsp70) is upregulated during stressful conditions, this provided a direct measurement of the stress exerted on cells. Immunoblotting shows increased levels of actin and Hsp70 to a lesser extend for sonicated samples. In addition, both proteins examined show a lower level upregulation in the presence of Definity® microbubbles than in the absence of Definity® microbubbles. A negative (non sonicated) and a positive (heat shocked) sample were used as controls.

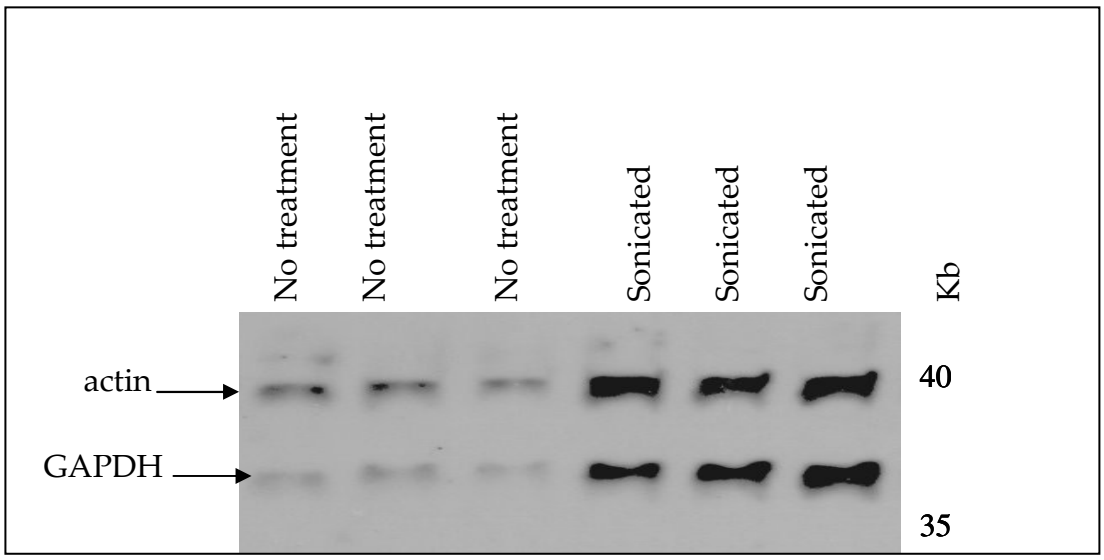

Figure 10.2 **Effects of sonication on actin and GAPDH**. Cells were sonicated in the absence of Definity® microbubbles under identical ultrasound conditions as those used to achieve sonoporation. Sonicated and non sonicated samples were collected and examined in order to detect any changes in levels of expression of actin and/or GAPDH. Immunoblot analysis reveals that both actin and GAPDH expression is upregulated in sonicated samples compared to those that were not sonicated.

(a)

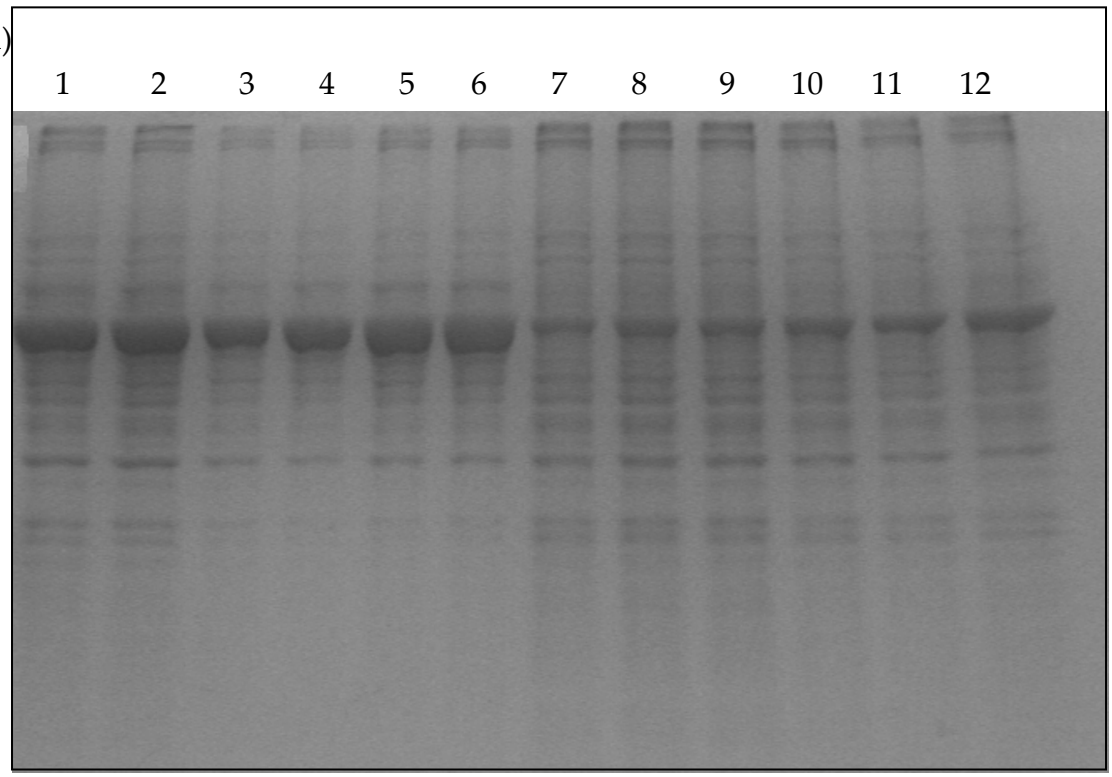

(b)

Sonicated	no treatment
(1) 80357	(7) 85063
(2) 81544	(8) 87803
(3) 78177	(9) 89499
(4) 74167	(10) 87835
(5) 73979	(12) 73037
(6) 78553	(12) 70525

Figure 10.3 **Effects of sonication on all proteins.** Since both actin and GAPDH which are normally used as loading controls were previously shown to be upregulated in sonicated samples, it was thought that examination of the total amount of protein within cells could also serve as a loading control. The same samples as those used in previous experiment (figure 10.2) were loaded on a gel and examined for total amount of protein. a) Although Immunoblot analysis shows that the total amount of protein loaded was similar across the samples, the level of expression of certain proteins changes between sonicated and non sonicated samples. Samples 1-6 = sonicated, samples 7-12 no treatment. (b) Intensity of total protein of each sample (pixels), measured by image J 1.41 software (National Institute of Health, USA), shows that the total amount of protein is similar between all samples (Numbers is brackets correspond to sample lanes from immunoblot).

10.2.2 Heme oxygenase-1

HO-1 expression is associated with oxidative stress (Morse and Choi 2005; Sontag and Kruglikov 2009). Expression of HO-1 following insonation was also investigated in order to assess whether cells are experiencing stressful conditions. Furthermore, HO-1 expression was not detected in the presence of microbubbles. It can thus be proposed that the presence of microbubbles provides a protection for cells from the effects of ultrasound waves.

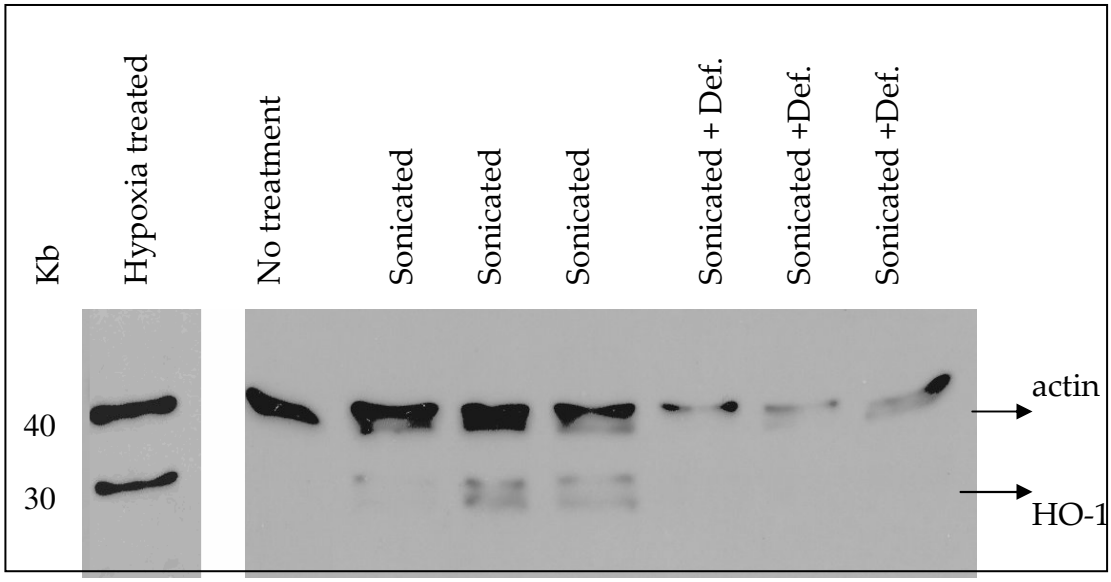

Figure 10.4 **Effects of sonication on HO-1**. SK Hep-1 cells were sonicated in the presence and absence of Definity® microbubbles under identical ultrasound conditions as those used to achieve sonoporation. Following sonication, samples were collected and examined for increased stress levels. As heme oxygenase (HO-1) is upregulated during stressful conditions, this provided a direct measurement of the stress exerted on cells. Immunoblotting shows increased levels of actin and HO-1 to a lesser extend for sonicated samples. In addition, actin shows a lower level upregulation in the presence of Definity® microbubbles than in the absence of Definity® microbubbles, while HO-1 expression is undetectable in the presence of Definity® microbubbles. A negative (non sonicated) and a positive (hypoxia treated) sample were used as controls. Hypoxia treated sample was taken from a different immunoblot experiment.

10.3 Discussion

10.3.1 Heat Shock protein 70

The aim of this section was to examine whether insonation of cells in the presence of ultrasound contrast agents exerts a stress on cells. Indeed, stress responses were revealed to take place with upregulation of stress proteins, such as Hsp70 and HO-1 (figure 10.1 & 10.4). From the data shown in figure 10.1 three observations can be made. First, the amount of actin was much lower when cells were insonated in the presence of Definity® microbubbles that when cells were simply insonated. Actin is a cytoskeletal protein used regularly as a control, since its expression is thought to be unaffected by stressful stimuli. Therefore, addition of actin can provide an assurance that similar amounts of cellular proteins have been loaded during Western blotting. However Dittmer et al. (2006) demonstrated that actin is not a very reliable loading control as it cannot distinguish amongst different concentrations of protein. Furthermore, Dittmer et al. (2006) reported that a number of other proteins such as glyceraldehydes-3-phosphate dehydrogenase (GAPDH), were more suitable for serving as loading controls.

The unusual upregulation of both actin and GAPDH during insonation also strengthens the notion that cells are experiencing stressful conditions during insonation (figure 10.2). In addition, an increase in GAPDH expression during oxidative stress and apoptosis has been previously reported (Darstoor and Dreyer 2001; Hara, Cascio et al. 2006). It can therefore be suggested that application of ultrasound via a "physiotherapy machine" creates stressful conditions for cells, thus altering expression of a multitude of proteins, including actin and GAPDH.

Coomassie assay staining reveals the amounts of all proteins present in a loaded sample, which are separated according to their molecular mass. Therefore, such an assay would further indicate whether equal amounts of

cellular proteins were loaded during Western blotting. Careful observation of figure 10.3 revealed that insonated samples have less high molecular mass bands and additional lower molecular mass bands. Since the possibility of protein degradation by proteases was eliminated with the addition of protease inhibitors in the samples during the assay preparation, it was not possible to explain such a difference between smaller and larger proteins. Nevertheless, measurement of the total amount of proteins in each sample revealed that all samples contained similar amounts of total protein (figure 10.3). Although stressful conditions have not been previously associated with upregulation of actin, a recent study demonstrated upregulation of over 200 genes during application of low intensity pulsed ultrasound (Tabuchi, Takasaki et al. 2008).

Taking into account that the amount of total protein loaded was similar for all samples examined, as demonstrated by the Coomassie assay, then the second observation that can be made from figure 10.1 is that Hsp70 expression is upregulated following insonation in the absence of ultrasound contrast agents. Application of pulsed wave ultrasound has been previously shown to increase expression of other heat shock proteins, such as Hsp32, Hsp40 and Hsp90 (Ando, Feril et al. 2006). It can therefore be concluded that ultrasound causes a stressful environment to the cells, upon which expression of several heat shock proteins, including Hsp70, is upregulated.

A third observation that can be made from figure 10.1 is that although Hsp70 is also expressed following insonation in the presence of microbubbles, its levels of expression are lower than those observed in the absence of microbubbles. These results are in conflict with other studies, which have shown that the presence of ultrasound contrast agents lowers the ultrasound pressure required to induce apoptosis (Tran, Jongbum et al. 2002; Ando, Feril

et al. 2006). Thus under identical sonication conditions one would expect to observe higher levels of Hsp70 expression in the presence of microbubbles. A possible hypothesis could be that the presence of microbubbles attenuates the ultrasound affect to the cells, thus minimising their stress response compared to sonication in the absence of microbubbles. Finally, it can be concluded that application of ultrasound both in the presence and absence of microbubbles, acts as a stress stimuli to cells, which in turn respond by expressing Hsp70.

10.3.2 Heme oxygenase 1

Results from figure 10.4 suggest that HO-1 expression is upregulated following insonation in the absence of microbubbles. Previous reports have also demonstrated induction of HO-1 following application of continuous wave ultrasound (Kagiya, Ogawa et al. 2006). Furthermore, HO-1 expression was not detected in the presence of microbubbles. Similarly to the observations made for Hsp-70 expression, it can be proposed that the presence of microbubbles provides a protection for cells from the effects of ultrasound waves. HO-1 expression has been associated with several human disorders; therefore such findings could potentially serve as indicators of potential bioeffects of gene therapy.

10.4 Conclusions

It can therefore be hypothesized from the alterations observed in protein expression that ultrasound cannot only lead to sonoporation but it can potentially lead to several other bioeffects. Stress proteins are upregulated in an attempt to promote cell survival through stressful conditions. Upregulation of stress related genes could therefore also be coupled with downregulation of other non stress related genes, which could

serve as a possible explanation to the low efficiencies observed in EGFP expression during sonoporation experiments. Therefore, establishing the effects of ultrasound on cell survival is of great importance since it can facilitate in adjusting acoustic parameters so as to achieve maximum sonoporation with minimal bioeffects.

Chapter 11

Conclusions and future aims

11.0 Conclusions and future aims

11.1 Conclusions

Several commercial microbubbles have been shown to induce sonoporation under specific ultrasonic conditions. The purpose of this study was to develop techniques for successful sonoporation and delivery of therapeutic agents. Therefore, it is necessary to quantify the composition and physical characteristics of microbubbles in order to be able to determine how these affect the sonoporation process as required. Since the components of the shell of the commercially available microbubbles have not been disclosed, experimental in-house microbubbles were used.

Characterisation of the in-house microbubbles was necessary prior to any attempts to use them as delivery vehicles *in vitro*, or indeed, *in vivo*. Confocal imaging and 3-D reconstruction of in-house microbubbles indicated the structure, morphology and size-distribution of these membrane-bound microbodies. Microbubbles were later separated according to size using a density gradient. It was concluded that the size distribution of the in-house microbubbles was comparable to that of commercial microbubbles that have been previously shown to induce sonoporation.

The majority of studies provide insufficient amount of information for the acoustic parameters used (transmit frequency, acoustic pressure, pulse period), making it difficult to obtain a specific protocol for achieving sonoporation (Sboros, Moran et al. 2004). Therefore, this study focused firstly on establishing the parameters necessary for achieving sonoporation. It was decided that the use of a commercial ultrasound contrast agent that have previously been shown to induce sonoporation, would be a good starting point. Initial experiments were conducted with the aid of a "physiotherapy machine" and in the presence of Definity® microbubbles. Ultrasound parameters were optimised in order to increase delivery of target molecules

into the cells. Both acoustic and non-acoustic parameters necessary for achieving *in vitro* sonoporation were established. Greatest sonoporation efficiency (8 %) was observed with the aid of cell impermeable Calcein during insonation in the presence of Definity® microbubbles. In addition, the exact acoustic field applied was determined, thus providing information on the precise characteristics of the ultrasound field (pressure, frequency) experienced by the cells. This in turn provides useful information for investigating potential bioeffects under such acoustic conditions. Microbubble mediated gene delivery (EGFP) was also accomplished in SK Hep-1 cells with the aid of the physiotherapy machine. Although sonoporation efficiency was half of that observed in the presence of cell impermeable Calcein, the achievement in itself brings us a step closer to establishing the parameters for regulated and consistent gene therapy. In addition, lack of delivery of EGFP protein into the cells during insonation revealed that the upper size limit of the perforations formed during sonoporation was 2.4 nm, thus providing essential information on the size limitations of molecules that can be delivered to the cells. Furthermore, examination of several distinct cell lines revealed that under identical sonication conditions, sonoporation efficiency was dependent on the cell type used. This finding is of particular importance as it suggests that acoustic parameters need to be adjusted in order to achieve sonoporation in different cell types.

Subsequent experiments were performed with the aid of an ultrasound scanner as this is more clinically relevant. Sonoporation efficiencies were negligible in the presence of Calcein while no sonoporation was observed with the use of a DNA plasmid. Nevertheless, the conditions used in these experiments can serve as a starting point for future experiments,

in order to adjust the parameters so as to establish sonoporation with an ultrasound scanner.

Since sufficient sonoporation was achieved with the aid of the physiotherapy machine, experiments were also conducted with the "physiotherapy machine" in order to investigate sonoporation in the presence of in-house microbubbles. Investigation of sonoporation in the presence of in-house microbubbles revealed that the acoustic parameters for achieving sonoporation are different to those in the presence of Definity® microbubbles. The mode of oscillation of an ultrasound contrast agent under specific ultrasonic conditions, is dependent on a number of variables such as its contents, size and constituents (Dawson 1999). The degree of oscillation of the ultrasound contrast agents will affect the degree of stress exerted on to the cell membranes, thus regulating the possibility of sonoporation. Although certain parameters of the in-house microbubbles were comparable to Definity® microbubbles (size distribution), other parameters were either most probably different (contents) or unknown (constituents). Thus further investigation is required in order to establish the parameters necessary for achieving sonoporation in the presence of in-house microbubbles.

During insonation a fraction of the cells were instantly killed (necrosis), another fraction was filled with molecules from the extracellular environment (sonoporation), such as Calcein and plasmid DNA, and some were impervious (Zarnitsyn and Prausnitz 2004). Furthermore, it was observed that the sonoporated fraction was smaller in the presence of plasmid DNA than in the presence of marker molecules such as Calcein. Such discrepancies in sonoporation efficiencies can be challenging for attaining high gene expression via sonoporation. It was therefore important to examine the cause of this discrepancy. A possible explanation could be

that during insonation cells are experiencing stressful conditions and are initiating apoptotic pathways thus upregulating expression of selective genes that have a protective role. In order to validate this hypothesis, cells were insonated under identical conditions to those used for achieving sonoporation. Cellular stress response was detected by examining upregulation of stress proteins such as Hsp70 and HO-1. Both Hsp70 and HO-1 expression were found to be elevated. It can thus be concluded that sonication creates a stressful environment for cells and induces activation of apoptotic processes. These results can also explain the discrepancy between sonoporation efficiencies in the presence of a DNA plasmid and marker molecules. Identifying the cellular mechanisms in response to ultrasound, could assist in establishing the parameters for attaining maximal sonoporation and gene expression (Zarnitsyn and Prausnitz 2004).

11.2 Future aims

The principal aim for gene therapy is to develop a method where expression of a therapeutic gene is achieved in target cells (Gao 2007). The use of ultrasound in the presence of ultrasound contrast agents is one of the leading candidate methods for use in gene therapy. The mechanical stress exerted on cells by oscillating microbubbles during insonation, results in the formation of transient perforations on the cell membrane thus allowing delivery of therapeutic molecules into the intracellular compartment of the cells. Successful delivery of therapeutic molecules, such as drugs or genes, into cells will open the road for curing a broad range of human diseases (Verma and Weitzman 2005). However, obstacles such as innate immune response, non-specific uptake by cells, degradation of genes by enzymes in the blood, interaction with blood components and rapid clearance, are yet to be conquered (Sakurai, Kawabata et al. 2008; Shigeru Kawakami 2008). In

addition, efficiency levels of ultrasound mediated gene delivery are still much lower than those achieved by viral methods, especially for *in vivo* delivery (Gao 2007). Therefore, considerable amount of research has yet to be performed before ultrasound mediated gene delivery can be fit for clinical use (Shigeru Kawakami 2008).

In this study the acoustic parameters were established for achieving sonoporation with the aid of a clinically relevant scanner in the presence of commercially available Definity® microbubbles. All the field parameters affecting cell responses, such as standing waves, reflective waves and pressure of the ultrasound beam applied, were taken into consideration, in order to be able to specify the precise acoustic parameters necessary for inducing sonoporation. Being able to induce sonoporation in the presence of in-house microbubbles would be of immense benefit for future work as it would allow for modifications in the microbubble design in order to improve sonoporation efficiencies (Shigeru Kawakami 2008). In-house microbubbles could also be modified in order to interact efficiently with DNA load (Shigeru Kawakami 2008). Furthermore, in-house microbubbles could be targeted for delivery to specific cells / tissues thus eliminating non-specific uptake (Shigeru Kawakami 2008). A better understanding of the fate of DNA following delivery into the cell, would allow for improvement of the ultrasound mediated gene delivery system (Gao 2007). Finally, patient safety is of utmost importance. Future work should therefore, involve further investigation into the cellular responses triggered during sonoporation, which would allow adjustment of the field parameters in order to achieve maximum gene transfer with minimal tissue damage.

Appendix 1 Solutions

RIPA buffer

1 x PBS

1 % NONIDET P-40 (v/v)

0.5 % Sodium deoxycholate (w/v)

0.1 % SDS (w/v)

D-PBS (Ca and Mg free)

1 g KCl

1 g KH_2PO_4

40 g NaCl

5.75 g Na_2HPO_4 (anhydrous)

Dissolve in 5 l of H_2O

50 x TAE

242 g Tris base

57.1 ml glacial acetic acid

100 ml 0.5 M EDTA (pH 8.0)

Dissolve in 1 l of H_2O adjust to pH 8.5

10 x TBS

121 g Tris

438.5 g NaCl

Dissolve up to 5 l with H_2O, adjust pH 7.4

TBST

1x TBS

0.5 % Tween 20 (v/v)

SDS-PAGE 10 % separating gel (2 gels)

3.96 ml distilled H_2O

2.5 ml 0.375 M Tris, pH 8.8

100 µl 10 % SDS (w/v)

3.33 ml Acrylamide / Bis (30 % stock) (Biorad)

100 µl 10 % AMPS Ammonium persulphate (v/v)

10 µl TEMED

SDS-PAGE 4 % Stacking gel (2 gels)

3 ml distilled H_2O

1.25 ml 0.5 M Tris-HCl, pH 6.8

50 µl 10 % SDS (w/v)

0.6 ml Acrylamide / Bis (30 % stock) (Biorad)

50 µl 10 % AMPS Ammonium persulphate (v/v)

10 µl TEMED

Sample loading buffer (x5)

0.5 ml distilled H_2O

2.5 ml 1 M Tris-HCl, pH 6.8

4 ml glycerol

0.8 g 10 % SDS (w/v)

2 ml 2-β-mercaptoethanol

1 ml 0.05 % bromophenol blue (v/v)

Running buffer (5x)

30 g Tris

144 g Glycine

10 g SDS

Dissolve in 1800 ml of H_2O, adjust pH to 8.3

Make up to 2 l with H_2O

Transfer buffer

5.86 g Glycine

11.65 g Tris

0.75 g SDS

400 ml Methanol

Dissolve up to 2 l with H_2O

Molecular Marker

Kaleidoscope Prestained standards (BioRad)

L Broth

5 g Tryptone

2.5 g yeast extract

5 g NaCl

Dissolve in 500 ml of H_20, adjust to pH 7 with NaOH

LB agar plates

7.5 g Bacto agar in 500 ml of L Broth

Terrific Broth

12 g Tryptone

24 g Yeast extract

4 ml glycerol

Dissolve in 900 ml of H_20. Add 100 ml sterile 0.17 M KH_2PO_4

Antibody dilutions

Hsp70	1 in 5000 (diluted in TBST)
Anti-Heme-oxygenase-1	1 in 5000 (diluted in TBST)
Actin b	1 in 10,000 (diluted in TBST)
GAPDH	1 in 10,000 (diluted in TBST)

0.1 % Coomassie blue R250 stain

40 % MeOH (v/v)

10 % acetic acid (v/v)

50 % H_20 (v/v)

Coomassie blue R250 destain

5 % MeOH (v/v)

7.5 % acetic acid (v/v)

87.5 % to 100 % H_20 (v/v)

Appendix 2 Summary of studies investigating sonoporation *in vitro*

Frequency	Wave type	MI	negative peak Pressure	Intensity	Time	Microbubble amounts	DNA amount	Type of culture / material of chamber	Reference
2.25 MHz	CW		0.2 MPa-0.6 MPa		1 min	Definity® 0.1 % (v/v)	40 μg/ml	SR / PE	(Miller and Dou 2009)
2.2 MHz	PW	1.1		80 W/cm^2		Optison® 4.5x10^{7}ml		SR / CT	(Wu, Ross et al. 2002)
1.75 MHz	PW		0.3 MPa			In-house liposomes 10^9/ml Definity® 0.1 % (v/v)		A / PS	(Zhou, Shi et al. 2008)
1.98 MHz	PW		0.2 MPa		5 min	Optison® 120 μl/ml		SR / CT	(Ward, Wu et al. 2000)
100 kHz	CW		0.1 MPa-5 MPa		10 sec-10 min		0.66 μg/ml	S	(Huber and Pfisterer 2000)
255 kHz	CW			0.4 W/cm^2	30 sec			S	(Tachibana, Uchida et al. 1999)

*acoustic power, *peak to peak pressure, *** peak positive pressure, CW=continuous wave, PW=pulsed wave, S=cells cultured in suspension, SR= cells cultured in suspension and rotating, A=cells cultured in monolayer fashion, Pl=plastic, PE=polyethylene, PS=polystyrene, OC=OptiCell™, P=6, 12, 48 well plate, CT=culture tube, CF=copolymer foil, ATM=acoustically transparent membrane.

Frequency	Wave type	MI	negative peak Pressure	Intensity	Time	Microbubble amounts	DNA amount	Type of culture / material of chamber	Reference
1 MHz	PW				60 sec	Sonovue® $2x10^8$-$5x10^8$/ml	5 μg/ml	A / OC	(Rahim, Taylor et al. 2006a)
2.25 MHz	CW		570 kPa		10 sec	Soft-shelled UCA (1A009) 25-30 / cell		SR / PS	(Mehier-Humbert, Bettinger et al. 2005a)
21.4 kHz	CW		0.4 MPa-4.1 MPa		1-7 min	hard-shelled UCA (BG1766) 25-30 / cell		S / CT	(Wu, Ross et al. 2002)
1.7 MHz	CW			0-4 W/cm^{2*}	15-120 sec	Optison® 5, 10 % (v/v)		AS / P	(Kinoshita and Hynynen 2007)
24 kHz	PW				2 sec			S	(Schlicher, Radhakrishna et al. 2006)

*acoustic power, *peak to peak pressure, *** peak positive pressure, CW=continuous wave, PW=pulsed wave, S=cells cultured in suspension, SR= cells cultured in suspension and rotating, A=cells cultured in monolayer fashion, Pl=plastic, PE=polyethylene, PS=polystyrene, OC=OptiCell™, P=6, 12, 48 well plate, CT=culture tube, CF=copolymer foil, ATM=acoustically transparent membrane.

Frequency	Wave type	MI	negative peak Pressure	Intensity	Time	Microbubble amounts	DNA amount	Type of culture / material of chamber	Reference
500 KHz	CW		0-570 kPa		60 sec	Definity® 3.3 % (v/v)		S	(Karshafian, Bevan et al. 2009)
2.5 MHz			0kPa-2320 kPa		2 min				
5 MHz			0kPa-3500 kPa						
3.5 MHz	PW		0.39 MPa	6.9 W/cm^2		Optison® variable amounts		A / ATM	(Miller 2000)
0.98 MHz	PW		0.4 MPa		10 sec	Optison® 10 % (v/v)		A / ATM	(Pan, Zhou et al. 2005)
1 MHz	PW		0.35 MPa-1.4 MPa **		10 sec	Optison® 2×10^8-5×10^8/ml		A / OC	(Rahim, Taylor et al. 2006b)
1 MHz	PW	0.159		2 W/cm^2	30 min	Optison® 10 % (v/v)	0.5-7.5 mg/ml	A / Pl	(Duvshani-Eshet, Baruch et al. 2005)

*acoustic power, *peak to peak pressure, *** peak positive pressure, CW=continuous wave, PW=pulsed wave, S=cells cultured in suspension, SR= cells cultured in suspension and rotating, A=cells cultured in monolayer fashion, Pl=plastic, PE=polyethylene, PS=polystyrene, OC=OptiCell™, P=6, 12, 48 well plate, CT=culture tube, CF=copolymer foil, ATM=acoustically transparent membrane.

Frequency	Wave type	MI	negative peak Pressure	Intensity	Time	Microbubble amounts	DNA amount	Type of culture / material of chamber	Reference
2.25 MHz	CW		0.1 MPa		1 min	Albunex® 10 % (v/v)	20 μg/ml	SR / PE	(Bao, Thrall et al. 1997)
1.8 MHz	CW	0.1-0.5			50 sec	Sonovue® 10 μl/ml		A / OC	(Juffermans, Dijkmans et al. 2006)
1 MHz	PW	0.1-0.5							
1 MHz	CW		0.5 MPa		30 sec			SR / PS	(Brayman, Coppage et al. 1999)
1 MHz	CW			0.4 W/cm^2	60 sec		7.5 mg/ml	A / P	(Lawrie, Brisken et al. 1999)
1.7 MHz	PW	1.15-1.8	195kPa-2350 kPa		50 sec	Optison® 2 x10^6/ml		A / CF	(Kirosoglou, Hardt et al. 2006)
0.96 MHz	PW		1 MPa		1 sec	Sonovue® 2x10^7/ml Optison® 0.05- 5 % (v/v)		S / ATM	(Deng, Sieling et al. 2004)

*acoustic power, *peak to peak pressure, *** peak positive pressure, CW=continuous wave, PW=pulsed wave, S=cells cultured in suspension, SR= cells cultured in suspension and rotating, A=cells cultured in monolayer fashion, Pl=plastic, PE=polyethylene, PS=polystyrene, OC=OptiCell™, P=6, 12, 48 well plate, CT=culture tube, CF=copolymer foil, ATM=acoustically transparent membrane.

Frequency	Wave type	MI	negative peak Pressure	Intensity	Time	Microbubble amounts	DNA amount	Type of culture / material of chamber	Reference
2 MHz	CW / PW		0.2 MPa		5-10 min	Albunex® 12 % (v/v)		SR / CT	(Ward, Wu et al. 1999)
2.25 MHz	PW		200 kPa		10 sec	Optison® 6.5 % (v/v) BR14 $3x10^7$/ml	10 μg/ml	S / PS	(Mehier-Humbert, Yan et al. 2007)
500 KHz	PW		0.6MPa-3 MPa		2-34 sec 12-2000 ms	Sonovue® Optison® 1.7 % (v/v)		S / PE	(Guzmán, Nguyen et al. 2001a)
2.25 MHz	PW	0.38	570 MPa		10 sec	UCA by Bracco $25-30x10^6$/ml		S / PS	(Mehier-Humbert, Bettinger et al. 2005b)
20 KHz	CW				0.5-30 sec		0.5, 20 μg/ml	A / P	(Fischer, Stanke et al. 2006)
1 MHz	PW		0.4 MPa		5 sec	lipid shell $1-2x10^5$/ml		A / OC	(Van Wamel, Kooiman et al. 2006a)

*acoustic power, *peak to peak pressure, *** peak positive pressure, CW=continuous wave, PW=pulsed wave, S=cells cultured in suspension, SR= cells cultured in suspension and rotating, A=cells cultured in monolayer fashion, Pl=plastic, PE=polyethylene, PS=polystyrene, OC=OptiCell™, P=6, 12, 48 well plate, CT=culture tube, CF=copolymer foil, ATM=acoustically transparent membrane.

Frequency	Wave type	MI	negative peak Pressure	Intensity	Time	Microbubble amounts	DNA amount	Type of culture / material of chamber	Reference
1 MHz	PW	0.4	0.4 MPa		5 sec	BR14 $1\text{-}2x10^5$/ml Definity®		A / OC	(Van Wamel, Kooiman et al. 2006b)
1 MHz	PW		0.5 MPa***		30 sec	30 % (v/v)		A / Pl	(Han, Ikegami et al. 2007)
1 MHz	PW		0.31 MPa-0.74 MPa	0.25-4 W/cm^2	1-60 sec		50 µg/ml	A / P	(Liang, Lu et al. 2004)
500 kHz	PW	0.7	0.5 MPa-2 MPa		60-480 ms	Optison® $1.1x10^7$/ml Levovist®	20 µg/ml	S / PE	(Zarnitsyn and Prausnitz 2004)
1 MHz	PW			2 W/cm^2	20 sec	10-40 mg/ml Optison® 5-20 % (v/v) Albunex® 5-20% (v/v)	20 µg/ml	S / P	(Li, Tachibana et al. 2003)
1.5 MHz	PW		2.09 MPa		34-200 ms	Definity® 0.1 % (v/v)		S / PE	(Zhou, Cui et al. 2008)

*acoustic power, *peak to peak pressure, *** peak positive pressure, CW=continuous wave, PW=pulsed wave, S=cells cultured in suspension, SR= cells cultured in suspension and rotating, A=cells cultured in monolayer fashion, Pl=plastic, PE=polyethylene, PS=polystyrene, OC=OptiCell™, P=6, 12, 48 well plate, CT=culture tube, CF=copolymer foil, ATM=acoustically transparent membrane.

Frequency	Wave type	MI	negative peak Pressure	Intensity	Time	Microbubble amounts	DNA amount	Type of culture / material of chamber	Reference
500 kHz	PW		0.64MPa-2.96 MPa		120-2000 ms	Optison® 3.6x 10^4-9.3x10^7/ml		S	(Guzmán, McNamara et al. 2003)
1 MHz	PW			0.1-2 W/cm^2	1 min			A / P	(Feril, Ogawa et al. 2005)
1 MHz	CW		0.41 MPa***		20 sec	Albunex® 50x10^6/ml	40 μg/ ml	A / Pl	(Greenleaf, Bolander et al. 1998)

*acoustic power, *peak to peak pressure, *** peak positive pressure, CW=continuous wave, PW=pulsed wave, S=cells cultured in suspension, SR= cells cultured in suspension and rotating, A=cells cultured in monolayer fashion, Pl=plastic, PE=polyethylene, PS=polystyrene, OC=OptiCell™, P=6, 12, 48 well plate, CT=culture tube, CF=copolymer foil, ATM=acoustically transparent membrane.

Appendix 3 List of parameters used in sonoporation experiments

Experiment 1 (n=9)

Chamber: Petri dish

Place: bench

Cells: SK Hep-1

Angle: 90°

Type of microbubbles: Definity®

Amount of microbubbles: 12.5 μl, 25 μl, 50 μl, 75 μl

Temperature: room temperature

Machine: physiotherapy machine

US duration: 1 min

Intensity: 0.1-0.2-0.3-0.4-0.6-0.8 W / cm^2

Examine by: electron microscopy

Experiment 2 (n=3)

Chamber: OptiCell™

Place: tank

Cells: SK Hep-1

Angle: 90°

Type of microbubbles: Definity®

Amount of microbubbles: 12.5 μl, 25 μl, 50 μl, 75 μl

Temperature: room temperature

Machine: physiotherapy machine

US duration: 1 min

Intensity: 0.1-0.2-0.3-0.4-0.6-0.8 W / cm^2

Examine by: electron microscopy

Experiment 3 (n=3)

Chamber: OptiCell™

Place: tank

Cells: SK Hep-1

Angle: 90°

Type of microbubbles: Definity®

Amount of microbubbles: 100, 300 μl

Temperature: room temperature

Machine: physiotherapy machine

US duration: 1-3 min

Intensity: 2.54 W / cm^2

Examine by: electron microscopy

Experiment 4 (n=3)

Chamber: OptiCell™

Place: tank, acoustic absorber

Cells: SK Hep-1

Angle: 37°

Type of microbubbles: Definity®

Amount of microbubbles: 100μl, 300 μl

Temperature: 37 °C

Machine: physiotherapy machine

US duration: 1-3 min

Intensity: 2.54 W / cm^2

Examine by: electron microscopy

Experiment 5 (n=3)

Chamber: OptiCell™

Place: tank, acoustic absorber

Cells: SK Hep-1

Angle: 37°

Type of microbubbles: Definity®

Amount of microbubbles: 100μl

Temperature: 37 °C

Machine: physiotherapy machine

US duration: 2-3 sec

Intensity: 2.54 W / cm^2

DNA: 0.1, 0.3 μg / ml

Examine by: electron microscopy, 24 hours after insonation

Experiment 6 (n=3)

Chamber: OptiCell™

Place: tank, acoustic absorber

Cells: SK Hep-1

Angle: 37°

Type of microbubbles: Definity®

Amount of microbubbles: 5 μl, 300 μl, 600 μl, 900 μl

Temperature: 37 °C

Machine: physiotherapy machine

US duration: 2-3 sec

Intensity: 2.54 W / cm^2

Calcein: 10 μM

Examine by: flow cytometry

Experiment 7 (n=3)

Chamber: OptiCell™

Place: tank, acoustic absorber

Cells: SK Hep-1

Angle: 37°

Type of microbubbles: Definity®

Amount of microbubbles: 300 μl

Temperature: 37 °C

Machine: physiotherapy machine

US duration: 2-3 sec

Intensity: 2.54 W / cm^2

DNA: linearised, 0.3 μg / ml

Examine by: flow cytometry, 24 hours after insonation

Experiment 8 (n=3)

Chamber: OptiCell™

Place: tank, acoustic absorber

Cells: SK Hep-1 (no serum in medium)

Angle: 37°

Type of microbubbles: Definity®

Amount of microbubbles: 300 µl

Temperature: 37 °C

Machine: physiotherapy machine

US duration: 2-3 sec

Intensity: 2.54 W / cm^2

DNA: linearised, 0.3 µg / ml

Examine by: flow cytometry, 24 hours after insonation

Experiment 9 (n=3)

Chamber: OptiCell™

Place: tank, acoustic absorber

Cells: SK Hep-1

Angle: 37°

Type of microbubbles: Definity®

Amount of microbubbles: 300 µl

Temperature: 37 °C

Machine: physiotherapy machine

US duration: 2-3 sec

Intensity: 2.54 W / cm^2

EGFP: 70mM, 700mM, 2.1M

Examine by: flow cytometry

Experiment 10 (n=3)

Chamber: OptiCell™

Place: tank, acoustic absorber

Cells: ACHN, HUH7

Angle: 37°

Type of microbubbles: Definity®

Amount of microbubbles: 300 µl

Temperature: 37 °C

Machine: physiotherapy machine

US duration: 2-3 sec

Intensity: 2.54 W / cm^2

DNA: linearised, 0.3 mg / ml

Examine by: flow cytometry, 24 hours after insonation

Experiment 11 (n=3)

Chamber: OptiCell™

Place: tank, acoustic absorber

Cells: SK Hep-1

Angle: 37°

Type of microbubbles: in-house microbubbles

Amount of microbubbles: 0.9 ml, 1.8 ml, 3 ml, 5 ml

Temperature: 37 °C

Machine: physiotherapy machine

US duration: 2-3 sec

Intensity: 2.54 W / cm^2

Calcein: 10 μM

Examine by: flow cytometry

Experiment 12 (n=3)

Chamber: OptiCell™

Place: tank, acoustic absorber

Cells: SK Hep-1 (± serum in medium)

Angle: 90°

Type of microbubbles: Definity®

Amount of microbubbles: 100 μl, 300 μl

Temperature: 37 °C

Machine: scanner

US duration: 10 sec

MI: 0.2-0.5-1.1

DNA: linearised, 0.1, 1, 5 μg / ml

Examine by: flow cytometry, 24 hours after insonation

Experiment 13 (n=3)

Chamber: OptiCell™

Place: tank, acoustic absorber

Cells: SK Hep-1 (no serum in medium)

Angle: 90°

Type of microbubbles: Definity®

Amount of microbubbles: 100 μl, 300 μl

Temperature: 37 °C

Machine: scanner

US duration: 10 sec

MI: 0.2-0.5-1.1

DNA: linearised, 0.1, 1, 5 μg / ml

Examine by: flow cytometry, 48 hours after insonation

Experiment 14 (n=3)

Chamber: OptiCell™

Place: tank, acoustic absorber

Cells: SK Hep-1 (no serum in medium)

Angle: 90°

Type of microbubbles: Definity®

Amount of microbubbles: 300 μl

Temperature: 37 °C

Machine: scanner

US duration: 10 sec

MI: 1.3

DNA: linearised, 20, 30 μg / ml

Examine by: flow cytometry, 24, 48 hours after insonation

Experiment 15 (n=3)

Chamber: OptiCell™

Place: tank, acoustic absorber

Cells: SK Hep-1 (no serum in medium)

Angle: 90°

Type of microbubbles: Definity®

Amount of microbubbles: 1 ml

Temperature: 37 °C

Machine: scanner

US duration: 10 sec

MI: 1.3

DNA: linearised, 20 μg / ml

Examine by: flow cytometry, 24 hours after insonation

Experiment 16 (n=4)

Chamber: OptiCell™

Place: tank, acoustic absorber

Cells: SK Hep-1 (no serum in medium)

Angle: 90°

Type of microbubbles: Definity®

Amount of microbubbles: 300 µl

Temperature: 37 °C

Machine: scanner

US duration: 10 sec

MI: 1.3

DNA: linearised, 20 µg / ml

Cell culture method: suspension and adherent

Examine by: flow cytometry, 24 hours after insonation

Experiment 17 (n=3)

Chamber: OptiCell™

Place: tank, acoustic absorber

Cells: SK Hep-1

Angle: 90°

Type of microbubbles: Definity®

Amount of microbubbles: 5 μl, 300 μl, 600 μl

Temperature: 37 °C

Machine: scanner

US duration: 10 sec

MI: 1.3

Calcein: 10 μM

Examine by: flow cytometry

Bibliography

Agosto, L. M., J. J. Yu, et al. (2007). "HIV-1 integrates into resting CD4+ T cells even at low inoculums as demonstrated with an improved assay for HIV-1 integration." Virology **368**(1): 60-72.

Akiyama, M., T. Ishibashi, et al. (1998). "Low-frequency ultrasound penetrates the cranium and enhances thrombolysis in vitro." Neurosurgery **43**(4): 828-832.

Alkan-Onyuksel, H., S. M. Demos, et al. (1996). "Development of inherently echogenic liposomes as an ultrasonic contrast agent." Journal of Pharmaceutical Sciences **85**(5): 486-490.

Allocca, M., M. Doria, et al. (2008). "Serotype-dependent packaging of large genes in adeno-associated viral vectors results in effective gene delivery in mice." J Clin Invest. **118**(5): 1995-1964.

Ando, H., L. B. J. Feril, et al. (2006). "An echo-contrast agent, Levovist, lowers the ultrasound intensity required to induce apoptosis of human leukemia cells." Cancer Letters **242**(1): 37-45.

Apfel, R. E. and C. K. Holland (1991). "Gauging the likelihood of cavitation from short-pulse, low-duty cycle diagnostic ultrasound." Ultrasound in Medicine & Biology **17**(2): 179-185.

Bachor, R., H. W. Gottfried, et al. (1995). "Minimal invasive therapy of prostatic abscess by transrectal ultrasound-guided perineal drainage." Eur Urol **28**(4): 320-324.

Bao, S., B. D. Thrall, et al. (1997). "Transfection of a reporter plasmid into cultured cells by sonoporation in vitro." Ultrasound in Medicine & Biology **23**(6): 953-959.

Barnett, S. B., ter Haar, G. R., Ziskin, M. C., Nyborg, W. L., Maeda, K., Bang, J. (1994). "Current status of research on biophysical effects of ultrasound." Ultrasound in Med. & Biol. **20**(3): 205-218.

Barrack, T. and E. Stride (2009). "Microbubble Destruction During Intravenous Administration: A Preliminary Study." Ultrasound in Medicine & Biology **35**(3): 515-522.

Becker, J. and E. A. Craig (1994). "Heat-shock proteins as molecular chaperones." European Journal of Biochemistry **219**(1-2): 11-23.

Behr, J. P. (1994). "Gene transfer with synthetic cationic amphiphiles: prospects for gene therapy." Bioconj Chem **5**: 382-389.

Bekeredjian, R., S. Chen, et al. (2005). "Augmentation of cardiac protein delivery using ultrasound targeted microbubble destruction." Ultrasound in Medicine & Biology **31**(5): 687-691.

Bekeredjian, R., P. A. Grayburn, et al. (2005). "Use of ultrasound contrast agents for gene or drug delivery in cardiovascular medicine." Journal of the American College of Cardiology **45**(3): 329-335.

Benjamin, I. J. and D. R. McMillan (1998). "Stress (Heat Shock) Proteins : Molecular Chaperones in Cardiovascular Biology and Disease." Circ Res **83**(2): 117-132.

Berkowitz, R. D., Lives, H., Plavec, I., Veres, G. (2001). "Gene transfer systems derived from Visna virus: Analysis of virus production and infectivity." Virology **279**: 116-129.

Bett, A. J., L. Prevec, et al. (1993). "Packaging capacity and stability of human adenovirus type 5 vectors." J. Virol. **67**(10): 5911-5921.

Bigey, P., Bureau, M. F., Scherman, D. (2002). "In vivo plasmid DNA electrotransfer." Curr Opin Biotechnol **13**: 443-447.

Blomley, M. J. K., J. C. Cooke, et al. (2001). "Science, medicine, and the future: Microbubble contrast agents: a new era in ultrasound." BMJ **322**(7296): 1222-1225.

Bloquel, C., Fabre, E., Bureau, M. F., Scherman, D. (2004). "Plasmid DNA electrotransfer for intracellular and secreted proteins expression: new methodological developments and applications." J Gene Med **6**(Suppl 1): S11-S23.

BMUS. (2007). "Statement on the safe use and potential hazards of diagnostic ultrasound." from http://www.bmus.org/policies-guides/pg-safety04.asp.

Boretti, F. S., C. M. Leutenegger, et al. (2000). "Protection against FIV challenge infection by genetic vaccination using minimalistic DNA constructs for FIV env gene and feline IL-12 expression." AIDS **14**(12): 1749-1757.

Bottega, R. and R. M. Epand (2002). "Inhibition of protein kinase C by cationic amphiphiles." Biochemistry **31**(37): 9025-9030.

Boussif, O., M. A. Zanta, et al. (1996). "Optimized galenics improve in vitro gene transfer with cationic molecules up to a thousandfold." Gene Ther **3**(12): 1074-1080.

Brayman, A. A., M. L. Coppage, et al. (1999). "Transient poration and cell surface receptor removal from human lymphocytes in vitro by 1 MHz ultrasound." Ultrasound in Medicine & Biology **25**(6): 999-1008.

Broadley, S. A. and F. U. Hartl (2009). "The role of molecular chaperones in human misfolding diseases." FEBS Letters **In Press, Uncorrected Proof**.

Brooks, A. I., Stein, C. S., Hughes, S. M., Heth, J., McCray, P.M., Sauter, S. L., Johnston, J. C., Cory-Slechta, D. A., Federoff, H. J., Davidson, B. L. (2002). "Functional correction of established central nervous system deficits in an animal model oflysosomal storage disease with feline

immunodeficiency virus-based vectors " Proc Natl Acad Sci U S A **99**(9): 6216-6221.

Bukrinsky, M. I., Haggerty, S., Dempsey, M. P., Sharova, N., Adzhubel, A., Spitz, L., Lewis, P., Goldfarb, D., Emerman, M., Stevenson, M. (1993). "A nuclear localization signal within HIV-1 matrix protein that governs infection of non-dividing cells." Nature **365**(6447): 366-369.

Cahalan, M. D., I. Parker, et al. (2002). "Two-photon tissue imaging: seeing the immune system in a fresh light." Nat Rev Immunol **2**(11): 872-880.

Calliada, F., R. Campani, et al. (1998). "Ultrasound contrast agents: Basic principles." European Journal of Radiology **27**(Supplement 2): S157-S160.

Carter, P. J. S., R. J. (2000). " Adeno-associated viral vectors as gene delivery vehicles." Int. J. Mol. Med. **6**(1): 17-27.

Chen, Q., J. Zagzebski, et al. (2002). "Pressure-dependent attenuation in ultrasound contrast agents." Ultrasound in Medicine & Biology **28**(8): 1041-1051.

Cheng-Huang, S., H.-I. Yeh, et al. (2008). "non viral technologies for gene therapy in cardiovascular therapy." International Journal of Gerontology **2**(2): 35-47.

Chiorini, J. A., Kim, F., Yang, L., Kotin, R. M. (1999). "Cloning and characterization of adeno-associated virus type 5." J Virol **73**: 1309-1319.

Church, C. C. (2005). "Frequency, pulse length, and the mechanical index." Acoustics Research Letters Online **6**(3): 162-168.

Claudon, M., D. Cosgrove, et al. (2008). "Guidelines and Good Clinical Practice Recommendations for Contrast Enhanced Ultrasound (CEUS) - Update 2008." Ultraschall in Med **29**(01): 28-44.

Cockrell AS, K. T. (2007). "Gene delivery by lentivirus vectors." Mol Biotechnol **36**(3).

Cosgrove, D. (2006). "Ultrasound contrast agents: An overview." European Journal of Radiology **60**(3): 324-330.

Crum, H. (1982). "Growth of air bubbles in tissue by rectified diffusion." J Physics in Medicine and Biology **27**(3): 413-417.

Curran, M. A., Kaiser, S. M., Achacoso, P. L., Nolan, G. P. (2000). "Efficient transduction of nondividing cells by optimized feline immunodeficiency virus vectors." Mol Ther **1**(1): 31-38.

Dalecki, D. (2004). "Mechanical bioeffects of ultrasound." Annual Review of Biomedical Engineering **6**(1): 229-248.

Darstoor, Z. and J.-L. Dreyer (2001). "Potential role of nuclear translocation of glyceraldehyde-3-phosphate dehydrogenase in apoptosis and oxidative stress." Journal of Cell Science **14**(9): 1643-1653.

David, G., M. Marie-Laure, et al. (2002). "Cationic lipids derived from glycine betaine promote efficient and non-toxic gene transfection in cultured hepatocytes." The Journal of Gene Medicine **4**(4): 415-427.

Dawson, P. C., David. O.Granger, Ronald. G. (1999). Textbook of Contrast Media. Oxford, ISIS medical media.

Dayton, P., A. Klibanov, et al. (1999). "Acoustic radiation force in vivo: a mechanism to assist targeting of microbubbles." Ultrasound in Medicine & Biology **25**(8): 1195-1201.

de Jong, N., P. J. A. Frinking, et al. (2000). "Detection procedures of ultrasound contrast agents." Ultrasonics **38**(1-8): 87-92.

Deichmann, A., S. Hacein-Bey-Abina, et al. (2007). "Vector integration is nonrandom and clustered and influences the fate of lymphopoiesis in SCID-X1 gene therapy." J Clin Invest. **117**(8): 2225-2232.

Deng, C. X., F. Sieling, et al. (2004). "Ultrasound-induced cell membrane porosity." Ultrasound in Medicine & Biology **30**(4): 519-526.

Desser, T. S., R. B. Jeffrey, et al. (1999). "Pictorial essay: Utility of tissue harmonic imaging in abdominal and pelvic ultrasonography." J Clin Ultrasound **27**: 135-141.

Dijkmans, P. A., L. J. M. Juffermans, et al. (2004). "Microbubbles and ultrasound: from diagnosis to therapy." Eur J Echocardiogr **5**(4): 245-246.

Dittmer, A. and J. Dittmer (2006). "beta-Actin is not a reliable loading control in Western blot analysis." ELECTROPHORESIS **27**(14): 2844-2845.

Doetsch, F., I. Caillı, et al. (1999). "Subventricular Zone Astrocytes Are Neural Stem Cells in the Adult Mammalian Brain." Cell **97**(6): 703-716.

Douglas, J. T., Rogers, B. E., Rosenfeld, M. E., Micheal, S. I., Feng, M., Curiel, D. T. (1996). "Targeted gene delivery by tropism-modified adenoviral vectors." Nat Biotech **14**: 1574-1578.

Durieux, A. C., R. Bonnefoy, et al. (2004). "In vivo gene electrotransfer into skeletal muscle: effects of plasmid DNA on the occurrence and extent of muscle damage. ." J Gene Med **6**(7): 809-816.

Durieux, A. C., Bonnefoy, R., Busso, T., Freyssenet, D. (2004). " In vivo gene electrotransfer into skeletal muscle: effects of plasmid DNA on the occurrence and extent of muscle damage." J Gene Med **6**: 809-816.

Duvshani-Eshet, M., L. Baruch, et al. (2005). "Therapeutic ultrasound-mediated DNA to cell and nucleus: bioeffects revealed by confocal and atomic force microscopy." Gene Ther **13**(2): 163-172.

ECMUS. (2008). "Clinical Safety Statement for Diagnostic Ultrasound ", from http://www.efsumb.org/guidelines/2008safstat.pdf.

Edelstein. (2008). "Gene Therapy Clinical Trials Worldwide." Journal of Gene Medicine, from http://www.wiley.co.uk/genetherapy/clinical.

Everbach, E. C. and C. W. Francis (2000). "Cavitational mechanisms in ultrasound-accelerated thrombolysis at 1 MHz." Ultrasound in Medicine & Biology **26**(7): 1153-1160.

Fattori, E., La Monica, N., Ciliberto, G., Toniatti, C. (2002). "Electrogene-transfer: a new approach for muscle gene delivery." Somat Cell Mol Genet. **27**: 75-83.

FDA. (2008). "Micro-bubble Contrast Agents (marketed as Definity (Perflutren Lipid Microsphere) Injectable Suspension and Optison (Perflutren Protein-Type A Microspheres for Injection)." from http://www.fda.gov/cder/drug/infopage/microbubble/default.htm.

Felgner, J. H., R. Kumar, et al. (1994). "Enhanced gene delivery and mechanism studies with a novel series of cationic lipid formulations." Journal of Biological Chemistry **269**(4): 2550-2561.

Felgner, P. L., T. R. Gadek, et al. (1987). "Lipofection: a highly efficient, lipid-mediated DNA-transfection procedure." Proceedings of the National Academy of Sciences of the United States of America **84**(21): 7413-7417.

Felice, B., C. Cattoglio, et al. (2009). "Transcription factor binding sites are genetic determinants of retroviral integration in the human genome." PLoS One **4**(2): e4571.

Feril, J. L. B., R. Ogawa, et al. (2005). "Ultrasound enhances liposome-mediated gene transfection." Ultrasonics Sonochemistry **12**(6): 489-493.

Ferrara, K., R. Pollard, et al. (2007). "Ultrasound Microbubble Contrast Agents: Fundamentals and Application to Gene and Drug Delivery." Annual Review of Biomedical Engineering **9**(1): 415-447.

Fields, B. N., D. M. Knipe, et al. (1996). Fields Virology, Lippincott–Raven, Philadelphia.

Fields, P. A., Kowalczyk, D. W., Arruda, V.R., Armstrong, E., McCleland, M. L., Hagstrom, J. N., Pasi, K. J., Ertl, H. C., Herzog, R. W., High, K. A. (2000). "Role of vector in activation of T cell subsets in immune responses against the secreted transgene product factor IX." Mol. Ther. **1**(3): 225-235.

Fischer, A. J., J. J. Stanke, et al. (2006). "Ultrasound-mediated gene transfer into neuronal cells." Journal of Biotechnology **122**: 393-411.

Fischetti, A. J. and R. C. Scott (2007). "Basic Ultrasound Beam Formation and Instrumentation." Clinical Techniques in Small Animal Practice **22**(3): 90-92.

Follenzi, A., Ailles, L. E., Bakovic, S., Geuna, M. & Naldini, L. (2000). "Gene transfer by lentiviral vectors is limited by nuclear translocation and rescued by HIV-1 pol sequences." Nature Genet. **25**: 217-222.

Friedman, T. (1999). The Development of Human Gene Therapy. New York, Cold Spring Harbor Lab. Press.

Gao, X. K., K-S. Liu, D. (2007). "Nonviral Gene Delivery: What We Know and What Is Next." AAPS Journal **9**(1): E92-E104.

Gehl, J. (2003). "Electroporation: theory and methods, perspectives for drug delivery, gene therapy and research." Acta Physiol Scand **177**: 437–447.

Gerard, G. and W. Junru (1998). "Observation of acoustic streaming near Albunex® spheres." The Journal of the Acoustical Society of America **104**(5): 3115-3118.

Gissel, H., Clausen, T. (2001). "Excitation-induced Ca 2+ infl ux and skeletalmuscle cell damage " Acta Physiol Scand **171**: 327-334.

Goldberg, B. B., J.-B. Liu, et al. (1994). "Ultrasound contrast agents: A review." Ultrasound in Medicine & Biology **20**(4): 319-333.

Goppert-Mayer, M. (1931, German). "Elementary acts with two quantum jumps." Annalen der Physik **9**(2): 273-294.

Gramiak, R. and P. M. Shah (1968). "Echocardiography of the aortic root." Invest. Radiol. **3**: 356-466.

Greenleaf, W. J., M. E. Bolander, et al. (1998). "Artificial Cavitation Nuclei Significantly Enhance Acoustically Induced Cell Transfection." Ultrasound in Medicine & Biology **24**(4): 587-595.

Griffin, S. D. C., Allen, J. F., Lever, A. M. L. (2001). "The major HIV-2 packaging signal is present on all HIV-2 RNA species: Co-translational RNA encapsidation and limiting Gag protein confer specificity." J Viro **175**(24): 12058-12069.

Guzmán, H. R., A. J. McNamara, et al. (2003). "Bioeffects caused by changes in acoustic cavitation bubble density and cell concentration: a unified explanation based on cell-to-bubble ratio and blast radius." Ultrasound in Medicine & Biology **29**(8): 1211-1222.

Guzmán, H. R., D. X. Nguyen, et al. (2001a). "Ultrasound-mediated disruption of cell membranes. I. Quantification of molecular uptake and cell viability." The Journal of the Acoustical Society of America **110**(1): 588-596.

Han, Y. W., A. Ikegami, et al. (2007). "Sonoporation Is an Efficient Tool for Intracellular Fluorescent Dextran Delivery and One-Step Double-Crossover Mutant Construction in Fusobacterium nucleatum " Appl Environ Microbiol. **73**(11): 3677-3683.

Hangiandreou (2003). "AAPM/RSNA Physics Tutorial for Residents: Topics in US. B-mode US: Basic Concepts and New Technology." Radiographics **23**(4): 1019-1033.

Hara, M. R., M. B. Cascio, et al. (2006). "GAPDH as a sensor of NO stress." Biochimica et Biophysica Acta (BBA) - Molecular Basis of Disease **1762**(5): 502-509.

Harrison, G. H., E. K. Balcer-Kubiczek, et al. (1996). "In vitro mechanisms of chemopotentiation by tone-burst ultrasound." Ultrasound in Med. & Biol. **22**: 355-362.

Herbener, T. E. (1996). "Ultrasound physics: principles of ultrasonography." Gastrointestinal Endoscopy **43**(2, Part 2): S4-S5.

Hernot, S. and A. L. Klibanov (2008). "Microbubbles in ultrasound-triggered drug and gene delivery." Advanced Drug Delivery Reviews **60**: 1153-1166.

Horvath, I., G. Multhoff, et al. (2008). "Membrane-associated stress proteins: More than simply chaperones." Biochimica et Biophysica Acta (BBA) - Biomembranes **1778**(7-8): 1653-1664.

Huang, S. L. (2008). "Liposomes in ultrasonic drug and gene delivery." Advanced Drug Delivery Reviews **60**(10): 1167-1176.

Huber, P. E., Jenne, J., Debus, J., Wannenmacher, M. F., Pfisterer, P. (1999). "A comparison of shock wave and sinusoidal-focused ultrasound-induced localized transfection of HeLa cells." Ultrasound Med Biol **25**(9): 1451 - 1457.

Huber, P. E. and P. Pfisterer (2000). "In vitro and in vivo transfection of plasmid DNA in the Dunning prostate tumor R3327-AT1 is enhanced by focused ultrasound." Gene Therapy **7**: 1516-1525.

Hui, S. W., M. Langner, et al. (1996). "The role of helper lipids in cationic liposome-mediated gene transfer." Biophysical Journal **71**(2): 590-599.

Humphrey, V. F. (2007). "Ultrasound and matter--Physical interactions." Progress in Biophysics and Molecular Biology **93**(1-3): 195-211.

Inoue, N., Hirata, R. K. & Russell, D. W. (1999). "High-fidelity correction of mutations at multiple chromosomal positions by adeno-associated virus vectors." J. Virol. **73**(9): 7376–7380.

Jans, D. A., Xiao, C. Y. & Lam, M. H. (2000). "Nuclear targeting signal recognition: a key control point in nuclear transport?" bioessays **22**(6): 532-544.

Jaroszeski, M. J., R. Gilbert, et al. (1999). "In vivo gene delivery by electroporation." Advanced Drug Delivery Reviews **35**(1): 131-137.

Johnston, J. C., Gasmi, M., Lira, L. E., Elder, J. H., Yee, J. K., Jolly, D. J., Campbell, K. P., Davidson, B. L., Sauter, S. L. (1999). "Minimum requirements for efficient transduction of dividing and nondividing cells by feline immunodeficiency virus vectors." J Virol **73**(6): 4991-5000.

Joyner, C. R., J. M. Reid, et al. (1963). "Reflected ultrasound in the assessment of mitral valve disease." Circulation **27**(4 Pt 1): 503-511.

Juffermans, L. J. M., P. A. Dijkmans, et al. (2006). "Transient permeabilization of cell membranes by ultrasound-exposed microbubbles is related to formation of hydrogen peroxide." Am J Physiol Heart Circ Physiol **291**(4): H1595-1601.

Junru, W. and W. L. Nyborg (2008). "Ultrasound, cavitation bubbles and their interaction with cells." Advanced Drug Delivery Reviews **60**: 1103-1116.

Kafri, T., Blomer, U., Peterson, D. A., Gage, F. H. & Verma, I. M. (1997). "Sustained expression of genes delivered directly into liver and muscle by lentiviral vectors." Nature Genet. **17**: 314-317.

Kagiya, G., R. Ogawa, et al. (2006). "Expression of heme oxygenase-1 due to intracellular reactive oxygen species induced by ultrasound." Ultrasonics Sonochemistry **13**(5): 388-396.

Kaminski, J. M., M. R. Huber, et al. (2002). "Design of a nonviral vector for site-selective, efficient integration into the human genome." FASEB J. **16**(10): 1242-1247.

Karshafian, R., P. D. Bevan, et al. (2009). "Sonoporation by Ultrasound-Activated Microbubble Contrast Agents: Effect of Acoustic Exposure

Parameters on Cell Membrane Permeability and Cell Viability." Ultrasound in Medicine & Biology **In Press, Corrected Proof**.

Kavic, M. (1996). "Three-dimensional ultrasound." Surgical Endoscopy **10**(1): 74-76.

Khalil, I. A., K. Kogure, et al. (2006). "Uptake Pathways and Subsequent Intracellular Trafficking in Nonviral Gene Delivery." Pharmacol Rev **58**(1): 32-45.

Kiang, J. G. and G. C. Tsokos (1998). "Heat Shock Protein 70 kDa: Molecular Biology, Biochemistry, and Physiology." Pharmacology & Therapeutics **80**(2): 183-201.

Kim, Y. H., J. H. Park, et al. (2005). "Polyethylenimine with acid-labile linkages as a biodegradable gene carrier." Journal of Controlled Release **103**(1): 209-219.

Kinoshita, M. and K. Hynynen (2007). "Key factors that affect sonoporation efficiency in in vitro settings: The importance of standing wave in sonoporation." Biochemical and Biophysical Research Communications **359**: 860-865.

Kircheis, R., L. Wightman, et al. (2001). "Polyethylenimine/DNA complexes shielded by transferrin target gene expression to tumors after systemic application." Gene Ther **8**(1): 28-40.

Kirosoglou, G., S. Hardt, E., et al. (2006). "Ultrasound exposure can increase the membrane permeability of human neutrophil granulocytes containing microbubbles without causing complete cell destruction." Ultrasound in Med. & Biol. **32**(2): 297-303.

Klibanov, A. L. (2005). "Ligand-Carrying Gas-Filled Microbubbles: Ultrasound Contrast Agents for Targeted Molecular Imaging." Bioconjugate Chemistry **16**(1): 9-17.

Kobayashi, M., Iida, A., Ueda, Y., Hasegawa, M. (2003). "Pseudotyped lentivirus vectors derived from simian immunodeficiency virus SIVagm with envelope glycoproteins from paramyxovirus." J. Virology **77**(4): 2607-2614.

Kornbluth, M., D. H. Liang, et al. (1998). "Native Tissue Harmonic Imaging Improves Endocardial Border Definition and Visualization of Cardiac Structures." Journal of the American Society of Echocardiography **11**(7): 693-701.

Kotin, R. M., M. Siniscalco, et al. (1990). "Site-Specific Integration by Adeno-Associated Virus." Proceedings of the National Academy of Sciences of the United States of America **87**(6): 2211-2215.

Kremkau, F. W., J. S. Kaufmann, et al. (1976). "Ultrasonic enhancment of nitrogen mustard cytotoxicity in mouse leukemia." Cancer **37**: 1643-1647.

Laemmli, U. K. (1970). "Cleavage of Structural Proteins during the Assembly of the Head of Bacteriophage T4." Nature **227**(5259): 680-685.

Laird, W. R. E. and A. D. Walmsley (1991). "Ultrasound in dentistry. Part 1--biophysical interactions." Journal of Dentistry **19**(1): 14-17.

Larsen, S. S., M. Krasnik, et al. (2002). "Endoscopic ultrasound guided biopsy of mediastinal lesions has a major impact on patient management." Thorax **57**(2): 98-103.

Lawrie, A., A. F. Brisken, et al. (2000). "Microbubble-enhanced ultrasound for vascular gene delivery." Gene Ther **7**: 2023-2027.

Lawrie, A., A. F. Brisken, et al. (1999). "Ultrasound Enhances Reporter Gene Expression After Transfection of Vascular Cells In Vitro." Circulation **99**(20): 2617-2620.

Ledley, F. D. (1994). "Non viral gene therapy." Current Opinion in Biotechnology **5**: 626-636.

Leighton, T. G. (2007b). "What is ultrasound?" Progress in Biophysics and Molecular Biology **93**(1-3): 3-83.

Lentacker, I., S. C. De Smedt, et al. (2006). "Microbubbles which bind and protect DNA against nucleases." Journal of Controlled Release **116**(2): e73-e75.

Lever, A., P. Strappe, et al. (2004). "Lentiviral vectors." Journal of Biomedical Science **11**(4): 439-449.

Lewis, P., Hensel, M. & Emerman, M. (1992). "Human immunodeficiency virus infection of cells arrested in the cell cycle." EMBO J. **11**(8): 3053-3058.

Li, P., L. Q. Cao, et al. (2003). "Impact of myocardial contrast echocardiography on vascular permeability: an in vivo dose response study of delivery mode, pressure amplitude and contrast dose." Ultrasound in Medicine & Biology **29**(9): 1341-1349.

Li, S. and L. Huang (2000). "Nonviral gene therapy: promises and challenges." Gene Therapy **7**(1): 31-34.

Li, T., K. Tachibana, et al. (2003). "Gene Transfer with Echo-enhanced Contrast Agents: Comparison between Albunex, Optison, and Levovist in Mice--Initial Results." Radiology: 2292020500.

Li, T., K. Tachibana, et al. (2003). "Gene Transfer with Echo-enhanced Contrast Agents: Comparison between Albunex, Optison, and Levovist in Miceβ€"Initial Results1." Radiology **229**(2): 423-428.

Liang, H. D., Q. L. Lu, et al. (2004). "Optimisation of ultrasound-mediated gene transfer (sonoporation) in skeletal muscle cells." Ultrasound in Medicine & Biology **30**(11): 1523-1529.

Lieber, A., D. S. Steinwaerder, et al. (1999). "Integrating Adenovirus-Adeno-Associated Virus Hybrid Vectors Devoid of All Viral Genes." J. Virol. **73**(11): 9314-9324.

Linda, J. L., C. P. Niels, et al. (1986). "Seroepidemiologic survey of captive old-world primates for antibodies to human and simian retroviruses, and isolation of a lentivirus from sooty mangabeys <I>(Cercocebus atys)</I>." International Journal of Cancer **38**(4): 563-574.

Lindner, J. R. and S. Sanjiv Kaul (2001). "Delivery of Drugs with Ultrasound." ECHOCARDIOGRAPHY, Volume 18, No. 4, May 2001 **18**(4): 329-337.

Lindquist, S. (1986). "The Heat-Shock Response." Annual Review of Biochemistry **55**(1): 1151-1191.

Liu, F., S. Heston, et al. (2006). "Mechanism of in vivo DNA transport into cells by electroporation: electrophoresis across the plasma membrane may not be involved." J Gene Med **8**: 353–361.

Liu, F., Huang, L., (2002). "Development of non-viral vectors for systemic gene delivery." J. Control. Release **78**: 259-266.

Loewen, N., Leske, D. A., Chen, Y., Teo, W. L., Saenz, D. T., Peretz, M., Holmes, J. M., Poeschla, E. M. (2003). "Comparison of wild-type and class I integrase mutant-FIV vectors in retina demonstrates sustained expression of integrated transgenes in retinal pigment epithelium." J Gene Med **5**(12): 1009-1917.

Loisel, S., Le Gall, C., Doucet, L., Ferec, C., Floch, V. (2001). "Contribution of plasmid DNA to hepatotoxicity after systemic administration of lipoplexes." Hum. Gene. Ther. **12**(6): 685-696.

Lv, H., S. Zhang, et al. (2006). "Toxicity of cationic lipids and cationic polymers in gene delivery." Journal of Controlled Release **114**(1): 100-109.

Lyman, S. K., Guan, T., Bednenko, J., Wodrich, H. & Gerace, L. (2002). "Influence of cargo size on Ran and energy requirements for nuclear protein import." J. Cell Biol. **159**(1): 55-67.

Lynch, C. M., Hara, P. S., Leonard, J. C., Williams, J. K., Dean, R. H., Geary, R. L. (1997). "Adenc-associated virus vectors for vascular gene delivery." Circ Res **80**: 497-505.

Madersbacher, S., K. Kratzik, et al. (1995). "Minimally invasive therapy of benign prostatic hyperplasia with focused ultrasound." Urology **34**: 98-104.

Madersbacher, S., M. Padevilla, et al. (1995). "Effect of high intensity focused ultrasound on human prostate cancer in vivo " Cancer Res **55**: 3346-3351.

Madersbacher, S., M. Pedevilla, et al. (1995). "Effect of High-Intensity Focused Ultrasound on Human Prostate Cancer in Vivo." Cancer Res **55**(15): 3346-3351.

Makiya Nishikawa, L. H. (2001). "Nonviral Vectors in the New Millennium: Delivery Barriers in Gene Transfer." Human Gene Therapy **12**(8): 861-870.

Mangeot, P. E., Negre, D., Dubois, B., Winter, A. J., Leissner, P., Mehtali, M., Kaiserlian, D., Cosset, F. L., Darlix, J. L. (2000). "Development of minimal lentivirus vectors derived from simian immunodeficiency virus (SIVmac251) and their use for gene transfer into human dendritic cells." J Virol **74**(18): 8307-8315.

Marcel, R. B., L. K. Alexander, et al. (2009). "Ultrasound triggered image-guided drug delivery." European Journal of Radiology(In Press).

Mason, J. P. L. a. T. J. (1987). "Sonochemistry. Part 1—The physical aspects." Chem. Soc. Rev. **16**: 239-274.

McCarty, D. M., P. E. Monahan, et al. (2001). "Self-complementary recombinant adeno-associated virus (scAAV) vectors promote efficient transduction independently of DNA synthesis." Gene Ther. **8**(16): 1248-1254.

McMahon, J. M., Wells, D. J. (2004). "Electroporation for gene transfer to skeletal muscles: current status." BioDrugs **18**: 155-165.

McNally, J. G., T. Karpova, et al. (1999). "Three-Dimensional Imaging by Deconvolution Microscopy." Methods **19**(3): 373-385.

Mehier-Humbert, S., T. Bettinger, et al. (2005a). "Plasma membrane poration induced by ultrasound exposure: Implication for drug delivery." Journal of Controlled Release **104**(1): 213-222.

Mehier-Humbert, S., T. Bettinger, et al. (2005b). "Ultrasound-mediated gene delivery: Kinetics of plasmid internalization and gene expression." Journal of Controlled Release **104**(1): 203-211.

Mehier-Humbert, S., F. Yan, et al. (2007). "Ultrasound-Mediated Gene Delivery: Influence of Contrast Agent on Transfection." Bioconjugate Chemistry **18**(3): 652-662.

Miller, A. P. and N. C. Nanda (2004). "Contrast echocardiography: new agents." Ultrasound in Medicine & Biology **30**(4): 425-434.

Miller, D. L. (2007a). Cavitation Biology and the Safety of Contrast-Aided Diagnostic Ultrasound. 19th International congress on acoustics. Madrid.

Miller, D. L. (2007b). "Overview of experimental studies of biological effects of medical ultrasound caused by gas body activation and inertial cavitation." Progress in Biophysics and Molecular Biology **93**(1-3): 314-330.

Miller, D. L., M. A. Averkiou, et al. (2008). "Bioeffects Considerations for Diagnostic Ultrasound Contrast Agents." J Ultrasound Med **27**(4): 611-632.

Miller, D. L. and C. Y. Dou (2009). "Induction of apoptosis in sonoporation and ultrasonic gene transfer " Ultrasound in Med. & Biol. **35**(1): 144-145.

Miller, D. L., S. V. Pislaru, et al. (2002). "Sonoporation: mechanical DNA delivery by ultrasonic cavitation." Somat Cell Mol Genet. **27**(1-6): 115-134.

Miller, D. L. and J. Quddus (2000). "Sonoporation of monolayer cells by diagnostic ultrasound activation of contrast-agent gas bodies." Ultrasound in Medicine & Biology **26**(4): 661-667.

Miller, M. W. (2000). "Gene transfection and drug delivery." Ultrasound in Medicine & Biology **26**(Supplement 1): S59-S62.

Mir, L. M., Bureau, M. F., Gehl, J., Rangara, R., Rouy, D., Caillaud, J. M. et al (1999). "High-efficiency gene transfer into skeletal muscle mediated by electric pulses." Proc Natl Acad Sci U S A **96**: 4264-4267.

Mitragotri, S. (2005). "Healing sound: the use of ultrasound in drug delivery and other therapeutic applications." Nat Rev Drug Discov **4**(3): 255-260.

Mitrophanous, K., Yoon, S., Rohll, J., Patil, D., Wilkes, F., Kim, V., Kingsman, S., Kingsman, A., Mazarakis, N. (1999). "Stable gene transfer to the nervous system using a non-primate lentiviral vector." Gene Ther **6**(11): 1808-1818.

Miyake, K. and P. L. McNeil (1995). "Vesicle accumulation and exocytosis at sites of plasma membrane disruption." J. Cell Biol. **131**(6): 1737-1745.

Monse, H., S. Laufs, et al. (2006). "Viral determinants of integration site preferences of simian immunodeficiency virus-based vectors." J Virol. **80**(16): 8145-8150.

Montini, E., D. Cesana, et al. (2009). "The genotoxic potential of retroviral vectors is strongly modulated by vector design and integration site selection in a mouse model of HSC gene therapy." J Clin Invest. **119**(4): 964-975.

Morse, D. and A. M. K. Choi (2005). "Heme Oxygenase-1: From Bench to Bedside." Am. J. Respir. Crit. Care Med. **172**(6): 660-670.

Moseley, P. (2000). "Stress proteins and the immune response." Immunopharmacology **48**(3): 299-302.

Mousnier, A., N. Kubat, et al. (2007). "von Hippel Lindau binding protein 1-mediated degradation of integrase affects HIV-1 gene expression at a postintegration step." Proc Natl Acad Sci U S A. **104**(34): 13615-13620.

Mselli-Lakhal, L., Favier, C., Da Silva Teixeira, M. F., Chettab, K., Legras, C., Ronfort, C., Verdier, G., Mornex, J. F., Cheblounе, Y. (1998). "Defective RNA packaging is responsible for low transduction efficiency of CAEV-based vectors." Arch Virol **143**: 681-695.

Multhoff, G. (2007). "Heat shock protein 70 (Hsp70): Membrane location, export and immunological relevance." Methods **43**(3): 229-237.

Nabel, E. G., Nabel, G. J. (1994). "Complex models for the study of gene function in cardiovascular biology." Annu Rev Physiol. **56**: 741-761.

Nchinda, G., K. Überla, et al. (2002). "Characterization of cationic lipid DNA transfection complexes differing in susceptability to serum inhibition." BMC Biotechnol. **2**(12).

Nelson, R. J., S. Perry, et al. (1990). "Transcranial Doppler ultrasound studies of cerebral autoregulation and subarachnoid hemorrhage in the rabbit." Journal of Neurosurgery **73**(4): 601-610.

Nico de Jong, P. D., Ayache Bouakaz, Ph.D., Peter Frinking, Ph.D. (2002). "Basic Acoustic Properties of Microbubbles." Echocardiography 2013 Jnl Cardiovascular Ultrasound & Allied Techniques **19**(3): 229-240.

Nozaki, T., Ogawa, R., Feril, L. B., Kagiya, G., Fuse, H., Kondo, T. (2003). "Enhancement of ultrasound-mediated gene transfection by membrane modification." J Gene Med **5**(12): 1046-1055.

Nyborg, W. L. and D. L. Miller (1982). "Biophysical implications of bubble dynamics." Applied Scientific Research **38**(1): 17-24.

O'Brien, J. W. D. (2007). "Ultrasound-biophysics mechanisms." Progress in Biophysics and Molecular Biology **93**(1-3): 212-255.

Oehen, S., T. Junt, et al. (2000). "Antiviral protection after DNA vaccination is short lived and not enhanced by CpG DNA." Immunology **99**(2): 163–169.

Ogawa, R., Kagiya, G., Feril, L. B., Nakaya, N., Nozaki, T., Fuse, H., Kondo, T. (2004). "Ultrasound mediated intravesical transfection enhanced by treatment with lidocaine or heat." J Urol **172**(4 Pt1): 1469 - 1473.

Olsen, J. C. (1998). "Gene transfer vectors derived from equine infectious anemia virus." Gene Ther **5**(11): 1481-1487.

Olsen, J. C. (2001). "EIAV,CAEV and other lentivirus vector systems." Somat Cell Mol Genet. **26**: 131-145.

Otterbein, L. E. and A. M. K. Choi (2000). "Heme oxygenase: colors of defense against cellular stress." Am J Physiol Lung Cell Mol Physiol **279**(6): L1029-1037.

Paliwal, S. and S. Mitragotri (2009). "Therapeutic opportunities in biological responses of ultrasound." Ultrasonics **In Press, Corrected Proof**.

Palma, L. D. and M. Bertolotto (1999). "Section V: New microbubble contrast agents: Introduction to ultrasound contrast agents: physics overview." Eur. Radiol. **9 (Suppl. 3)**(S338-S342).

Pan, H., Y. Zhou, et al. (2005). "Study of sonoporation dynamics affected by ultrasound duty cycle." Ultrasound in Medicine & Biology **31**(6): 849-856.

Patil, M. N. and A. B. Pandit (2007). "Cavitation - A novel technique for making stable nano-suspensions." Ultrasonics Sonochemistry **14**(5): 519-530.

Pawley, J. B. (2006). Handbook of biological confocal microscopy. New York, Springer.

Piston, D. W. (1999). "Imaging living cells and tissues by two-photon excitation microscopy." Trends in Cell Biology **9**(2): 66-69.

Pomper, M. G. and J. G. Gelovani (2008). Molecular Imaging in Oncology, Informa Health Care.

Preston, R. C., D. R. Bacon, et al. (1983). "PVDF membrane hydrophone performance properties and their relevance to the measurement of the acoustic output of medical ultrasound equipment." J Phys E: Sci Instrum **16**: 786-796.

Qin, L., Ding, Y., Pahud, D.R., Chang, E., Imperiale, M.J., Bromberg, J.S., (1997). "Promoter attenuation in gene therapy: interferon-gamma and tumor necrosis factor-alpha inhibit transgene expression." Hum. Gene. Ther. **8**(17): 2019-2029.

Quaia, E. (2007). "Microbubble ultrasound contrast agents: an update." Eur Radiol **17**(8): 1995-2008.

Rahim, A., S. L. Taylor, et al. (2006a). "Physical parameters affecting ultrasound/microbubble-mediated gene delivery efficiency in vitro." Ultrasound in Medicine & Biology **32**(8): 1269-1279.

Rahim, A. A., S. L. Taylor, et al. (2006b). "Spatial and acoustic pressure dependence of microbubble-mediated gene delivery targeted using focused ultrasound." J Gene Med. **8**(11): 1347-1357.

Raisinghani, A. and A. N. DeMaria (2002). "Physical principles of microbubble ultrasound contrast agents." The American Journal of Cardiology **90**(10, Supplement 1): 3-7.

Rajotte D., A., W., Hagedorn, M., Koivunen, E., Pasqualini, R., Ruoslahti, E. (1998). "Molecular heterogeneity of the vascular endothelium revealed by in vivo phage display." J Clin Invest. **102**(2): 430-437.

Raper, S. E., N. Chirmule, et al. (2003). "Fatal systemic inflammatory response syndrome in a ornithine transcarbamylase deficient patient following adenoviral gene transfer." Molecular Genetics and Metabolism **80**(1-2): 148-158.

Ritossa, F. (1962). "A new puffing pattern induced by temperature shock and DNP in Drosophila." Experientia **18**: 571-573.

Rizvi, T. A., Panganiban, A. T. (1992). "Propagation of SIV vectors by genetic complementation with a heterologous env gene." AIDS Res Hum Retroviruses **8**(1): 89-95.

Rizzuto, G., Cappelletti, M., Maione, D., Savino, R., Lazzaro, D., Costa, P., et al. (1999). "Efficient and regulated erythropoietin production by naked

DNA injection and muscle electroporation." Proc Natl Acad Sci U S A **96**: 6417-6422.

Robbins, P. D. and S. C. Ghivizzani (1998). "Viral Vectors for Gene Therapy." Pharmacology & Therapeutics **80**(1): 35-47.

Robert, J. (2003). "Evolution of heat shock protein and immunity." Developmental & Comparative Immunology **27**(6-7): 449-464.

Rose, J. K., Buonocore, L., Whitt, M. A. (1991). "A new cationic liposome reagent mediating nearly quantitative transfection of animal cells." Biotechniques **10**(4): 520-525.

Rubanyi, G. M. (2001). "The future of human gene therapy." Molecular Aspects of Medicine **22**(3): 113-142.

Rubin, J. M. (2004). "Do Microbubbles Interact Differently with Leukocytes?" Radiology **230**(3): 604-605.

Sadaie, M. R., Zamani, M., Whang, S., Sistron, N., Arya, S. K. (1998). "Towards developing HIV-2 lentivirus-based retroviral vectors for gene therapy: Dual gene expression in the context of HIV-2 LTR and Tat." J Med Virol **54**(2): 118-128.

Sakurai, H., K. Kawabata, et al. (2008). "Innate immune response induced by gene delivery vectors." International Journal of Pharmaceutics **354**(1-2): 9-15.

Sandrin, V., S. J. Russell, et al. (2003). "Targeting retroviral and lentiviral vectors." Curr Top Microbiol Immunol. **281**(1): 137-178.

Santoro, M. G. (2000). "Heat shock factors and the control of the stress response." Biochemical Pharmacology **59**(1): 55-63.

Sboros, V. (2008). "Response of contrast agents to ultrasound." Advanced Drug Delivery Reviews **60**(10): 1117-1136.

Sboros, V., C. M. Moran, et al. (2004). "An in vitro study of a microbubble contrast agent using a clinical ultrasound imaging system." Phys. Med. Biol. **49**: 159-173.

Schlicher, R. K., H. Radhakrishna, et al. (2006). "Mechanism of intracellular delivery by acoustic cavitation." Ultrasound in Med. & Biol. **32**(6): 915-924.

Schneider, M. (1999). "SonoVue, a new ultrasound contrast agent." Eur. Radiol. **9 (Suppl. 3)**: S347-S348.

Schnell, T., Foley, P., Wirth, M., Munch, J., Uberla, K. (2000). "Development of self-inactivating, minimal lentivirus vector based on simian immunodeficiency virus." Hum Gene Ther **11**(3): 439-337.

Sellins, K., Fradkin, L., Liggitt, D., Dow, S. (2005). "Type I interferons potently suppress gene expression following gene delivery using liposome(−)DNA complexes." Mol. Ther. **12**(3): 451-459.

Setoguchi, Y., H. A. Jaffe, et al. (1994). "Intra-peritoneal in vivo gene therapy to deliver alpha 1-antitrypsin to the systemic circulation." Am. J. Resp. Cell Mol. Biol. **10**(4): 369-377.

Shigeru Kawakami, Y. H. M. H. (2008). "Nonviral approaches for targeted delivery of plasmid DNA and oligonucleotide." Journal of Pharmaceutical Sciences **97**(2): 726-745.

Shohet, R. V., S. Y. Chen, et al. (2000). "Echocardiographic destruction of albumin microbubbles directs gene delivery to the myocardium." Circulation **101**(22): 2554-2556.

Singer, S. J. and G. L. Nicolson (1971). "The Structure and Chemistry of Mammalian Cell Membranes." American Journal of Pathology **65**(2): 427-435.

Smith, T. A., M. G. Mehaffey, et al. (1993). "Adenovirus gene mediated expression of therapeutic plasma levels of human therapeutic applicable for cancer or any other disease factor IX in mice." Nature Genet **5**(4): 397-402.

Somia, N. and I. M. Verma (2000). "Gene therapy: trials and tribulations." Nat Rev Genet **1**(2): 91-99.

Sontag, W. and I. L. Kruglikov (2009). "Expression Of Heat Shock Proteins After Ultrasound Exposure In Hl-60 Cells." Ultrasound in Medicine & Biology **In Press, Corrected Proof**.

Stitz, J., Muhlebach, M. D., Blomer, U., Scherr, M., Selbert, M., Wehner, P., Steidl, S., Schmitt, I., Konig, R., Schweizer, M., Cichutek, K. (2001). "A novel lentivirus vector derived from apathogenic simian immunodeficiency virus." Virology **291**(2): 191-197.

Swanstrom, R., Wills, J. W., Coffin, J.M., Hughes, S. H., Varmus, H. E, (1997). Synthesis, assembly and processing of viral protein. New York, Cold Spring Harbor Press.

Tabuchi, Y., I. Takasaki, et al. (2008). "Genetic networks responsive to low-intensity pulsed ultrasound in human lymphoma U937 cells." Cancer Letters **270**: 286-294.

Tachibana, K., T. Uchida, et al. (1999). "Induction of cell-membrane porosity by ultrasound." The Lancet **353**(9162): 1409-1409.

Takahashi, K., Luo, T., Saishin, Y., Sung, J., Hackett, S., Brazzell, R. K., Kaleko, M., Campochiaro, P. A. (2002). "Sustained transduction of ocular cells with a bovine immunodeficiency viral vector." Hum Gene Ther **13**(11): 1305-1316.

Tang, M. X., R. J. Eckersley, et al. (2005). "Pressure-dependent attenuation with microbubbles at low mechanical index." Ultrasound in Medicine & Biology **31**(3): 377-384.

ter Haar, G. (2007). "Therapeutic applications of ultrasound." Progress in Biophysics and Molecular Biology **93**(1-3): 111-129.

ter Haar, G. R. (2002). "Ultrasonic contrast agents: safety considerations reviewed." European Journal of Radiology **41**(3): 217-221.

Terence, R. F. (2007). "Gene therapy: The first two decades and the current state-of-the-art." Journal of Cellular Physiology **213**(2): 301-305.

Toelen, J., C. M. Deroose, et al. (2007). "Fetal gene transfer with lentiviral vectors: long-term in vivo follow-up evaluation in a rat model." American Journal of Obstetrics and Gynecology **196**(4): 352.e1-352.e6.

Towbin, H., T. Staehelin, et al. (1979). "Electrophoretic transfer of proteins from polyacrylamide gels to nitrocellolose sheets: procedure and some applications." Proc.Nat.Acad.Sci.USA **76**: 4350-4354.

Tran, B. C., S. Jongbum, et al. (2002). "The effect of microbubble concentration on thresholds for tissue damage produced by single bursts of high intensity ultrasound during continuous Optison® infusion." Ultrasonics Symposium **2**: 1411-1414.

Unger, E. C., T. O. Matsunaga, et al. (2002). "Therapeutic applications of microbubbles." European Journal of Radiology **42**(2): 160-168.

Van Wamel, A., K. Kooiman, et al. (2006a). "Ultrasound microbubble induced endothelial cell permeability." Journal of Controlled Release **116**(2): e100-e102.

Van Wamel, A., K. Kooiman, et al. (2006b). "Vibrating microbubbles poking individual cells: Drug transfer into cells via sonoporation." Journal of Controlled Release **112**(2): 149-155.

Vanbever, R., N. Lecouturier, et al. (1994). "Transdermal Delivery of Metoprolol by Electroporation." Pharmaceutical Research **11**(11): 1657-1662.

Verma, I. M. and M. D. Weitzman (2005). "GENE THERAPY: Twenty-First Century Medicine." Annual Review of Biochemistry **74**(1): 711-738.

Vigneron, J. P., N. Oudrhiri, et al. (1996). "Guanidinium-cholesterol cationic lipids: efficient vectors for the transfection of eukaryotic cells." Proceedings of the National Academy of Sciences of the United States of America **93**(18): 9682-9686.

Wade, G. (2000). "Human uses of ultrasound: ancient and modern." Ultrasonics **38**(1-8): 1-5.

Walther, W. and U. Stein (2009). "Heat-responsive gene expression for gene therapy." Advanced Drug Delivery Reviews **In Press, Accepted Manuscript**.

Wang, G., Slepushkin, V., Zabner, J., Keshavjee, S., Johnston, J. C., Sauter, S. L., Jolly, D. J., Dubensky, T .W., Davidson, B. L., McCray, P. B. (1999). "Feline immunodeficiency virus vectors persistently transduce

nondividing airway epithelia and correct the cystic fibrosis defect." J Clin Invest **104**(11): R55-R62.

Wang, X., H.-D. Liang, et al. (2005). "Gene Transfer with Microbubble Ultrasound and Plasmid DNA into Skeletal Muscle of Mice: Comparison between Commercially Available Microbubble Contrast Agents1." Radiology **237**(1): 224-229.

Wang, X., Q. Liu, et al. (2009). "Comparisons among sensitivities of different tumor cells to focused ultrasound in vitro." Ultrasonics **In Press, Corrected Proof**.

Ward, M., J. Wu, et al. (1999). "Ultrasound-induced cell lysis and sonoporation enhanced by contrast agents." The Journal of the Acoustical Society of America **105**(5): 2951-2957.

Ward, M., J. Wu, et al. (2000). "Experimental study of the effects of optison® concentration on sonoporation in vitro." Ultrasound in Medicine & Biology **26**(7): 1169-1175.

White, N. S. and R. J. Errington (2005). "Fluorescence techniques for drug delivery research: theory and practise." Advanced Drug Delivery Reviews **57**(17).

Whittingham, T. A. (2007). "Medical diagnostic applications and sources." Progress in Biophysics and Molecular Biology **93**(1-3): 84-110.

Wickham, T. J., Roelvink, P. W., Brough, D. E., Kovesdi, I. (1996). "Adenovirus targeted to heparin-containing receptors increases its gene delivery efficiency to multiple cell types." Nat Biotech **14**: 1570-1573.

Williams. R. S., J., S. A., Riedy, M., Devit, M .J., MCelligott, S. G., Sanford, J. C. (1991). "Introduction of nonvrial vectors in the new millennium: 869 foreign genes into tissues of living mice by DNA-coated microprojectiles." Proc Natl Acad Sci U S A **88**: 2726–2730.

Winkelmann, J. W., M. D. Kenner, et al. (1994). "Contrast echocardiography." Ultrasound in Medicine & Biology **20**(6): 507-515.

Wu, J., D. Chen, et al. (2006). "Application of liposomes to sonoporation." Ultrasound in Med. & Biol. **32**(3): 429-437.

Wu, J. and W. L. Nyborg (2008). "Ultrasound, cavitation bubbles and their interaction with cells." Advanced Drug Delivery Reviews **60**(10): 1103-1116.

Wu, J., J. Pepe, et al. (2006). "Sonoporation, anti-cancer drug and antibody delivery using ultrasound." Ultrasonics **44**: e21–e25.

Wu, J., J. P. Ross, et al. (2002). "Reparable sonoporation generated by microstreaming." The Journal of the Acoustical Society of America **111**(3): 1460-1464.

Xiao, W., Chirmule, N., Berta, S. C., McCullough, B., Gao, G., Wilson, J. M. (1999). "Gene therapy vectors based on adeno-associated virus type 1." J Virol **73**: 3994-4003.

Xu, Y. and F. C. Szoka (1996). "Mechanism of DNA Release from Cationic Liposome/DNA Complexes Used in Cell Transfectionβ€ ,β€¨." Biochemistry **35**(18): 5616-5623.

Yang, N. S., J. Burkholder, et al. (1990). "In vivo and in vitro gene transfer to mammalian somatic cells by particle bombardment." Proc Natl Acad Sci U S A **87**(24): 9568-9572.

Yang, N. S., Burkholder, J. , Roberts, B. , Martinell, B. , McCabe, D . (1990). "In vivo and in vitro gene transfer to mammalian somatic cells by particle bombardment." Proc Natl Acad Sci U S A **87**: 9568-9572.

Yang, N. S., Burkholder, J., Roberts, B., Martinell, B., McCabe, D. (1990). "In vivo and in vitro gene transfer to mammalian somatic cells by particle bombardment." Proc Natl Acad Sci U S A **87**: 9568–9572.

Yang, Y., Q. Li, et al. (1995). "Cellular and humoral immune responses to viral antigens create barriers to lung-directed gene therapy with recombinant adenoviruses." J. Virol. **69**(4): 2001-2015.

Yang, Y., F. A. Nunes, et al. (1995). "Cellular immunity to viral antigens limits E1-deleted adenoviruses for gene therapy." Proc. Natl. Acad. Sci. USA **91**(10): 4402-4411.

Zagzebski (1996). Essentials of Ultrasound Physics. Missouri, Mosby, Inc.

Zarnitsyn, V. G. and M. R. Prausnitz (2004). "Physical parameters influencing optimization of ultrasound-mediated DNA transfection." Ultrasound in Medicine & Biology **30**(4): 527-538.

Zelenin, A. V., Kolesnikov, V. A., Tarasenko, O. A., Shafei, R. A., Zelenina, I. A., Mikhalov, V. V., Semenova, M. L., Kovalenko, D. V., Artemyeva, O. V., Ivaschenko, T. E., Evgrafov, O. V., Dickson, G. (1997). "Bacterial b-galactosidase and human dystrophin genes are expressed in mouse skeletal fibers after ballistic transfection." FEBS Letters **414**: 319-322.

Zennou, V., C. Petit, et al. (2000). "HIV-1 genome nuclear import is mediated by a central DNA flap." Cell **101**: 173-185.

Zeqiri, B. (2007). "Metrology for ultrasonic applications." Progress in Biophysics and Molecular Biology **93**(1-3): 138-152.

Zhang, L., Nolan, E., Kreitschitz, S., Rabussay, D. P. (2002). "Enhanced delivery of naked DNA to the skin by non-invasive in vivo electroporation." Biochim Biophys Acta **1572**: 1-9.

Zhou, Y., J. Cui, et al. (2008). "Dynamics of Sonoporation Correlated with Acoustic Cavitation Activities." Biophys J. **94**(7): L51-L53.

Zhou, Y., J. Cui, et al. (2008). "Dynamics of Sonoporation Correlated with Acoustic Cavitation Activities." Biophysical Journal **94**(7): L51-L53.

Zhou, Y., J. Shi, et al. (2008). "Effects of extracellular calcium on cell membrane resealing in sonoporation." Journal of Controlled Release **126**.

Zufferey, R., Nagy, D., Mandel, R. J., Naldini, L. & Trono, D. (1997). "Multiply attenuated lentiviral vector achieves efficient gene delivery in vivo." Nature Biotechnol. **15**: 871-875.

Zufferey, R., Nagy, D., Mandel, R. J., Naldini, L. & Trono, D. (1997). "Multiply attenuated lentiviral vector achieves efficient gene delivery in vivo." Nature Biotechnol. **15**: 871-875.

Zufferey. R, T. Dull, et al. (1998). "Self-Inactivating Lentivirus Vector for Safe and Efficient In Vivo Gene Delivery." J virol **72**(12): 9873-9880.